GDAŃSK UNIVERSITY OF TECHNOLOGY
FACULTY OF CHEMISTRY

The author of the PhD dissertation: Wioletta Brankiewicz
Scientific discipline: Chemistry

DOCTORAL DISSERTATION

Title of PhD dissertation: Evaluation and cellular responses of modulators of TRF1/TRF2 protein's function as potential anticancer drugs interfering with telomeric shelterin's function

Title of PhD dissertation (in Polish): Ewaluacja i badanie odpowiedzi komórkowej nowych modulatorów funkcji białek TRF1/TRF2 jako potencjalnych leków przeciwnowotworowych zaburzających funkcję telomerowych szelteryn

Supervisor *signature*	Second supervisor  *signature*
Professor Maciej Bagiński, PhD DSc	Marek Drab, PhD DSc
Auxiliary supervisor *signature*	Cosupervisor *signature*
<Title, degree, first name and surname>	<Title, degree, first name and surname>

Gdańsk, year 2023

GDAŃSK UNIVERSITY OF TECHNOLOGY
FACULTY OF CHEMISTRY

STATEMENT

The author of the PhD dissertation: Wioletta Brankiewicz

I, the undersigned, agree that my PhD dissertation entitled:

Evaluation and cellular responses of modulators of TRF1/TRF2 protein's function as potential anticancer drugs interfering with telomeric shelterin's function

may be used for scientific or didactic purposes.[1]

Gdańsk,.....20.06.2023..... Wioletta Brankiewicz

signature of the PhD student

Aware of criminal liability for violations of the Act of 4th February 1994 on Copyright and Related Rights (Journal of Laws 2006, No. 90, item 631) and disciplinary actions set out in the Law on Higher Education (Journal of Laws 2012, item 572 with later amendments),[2] as well as civil liability, I declare, that the submitted PhD dissertation is my own work.

I declare, that the submitted PhD dissertation is my own work performed under and in cooperation with the supervision of Professor Maciej Bagiński, PhD DSc, the second supervision of Marek Drab, PhD, DSc.

This submitted PhD dissertation has never before been the basis of an official procedure associated with the awarding of a PhD degree.

All the information contained in the above thesis which is derived from written and electronic sources is documented in a list of relevant literature in accordance with art. 34 of the Copyright and Related Rights Act.

I confirm that this PhD dissertation is identical to the attached electronic version.

Gdańsk, ...20.06.2023..... Wioletta Brankiewicz

signature of the PhD student

I, the undersigned, agree to include an electronic version of the above PhD dissertation in the open, institutional, digital repository of Gdańsk University of Technology, Pomeranian Digital Library, and for it to be submitted to the processes of verification and protection against misappropriation of authorship.

Gdańsk, ...20.06.2023..... Wioletta Brankiewicz

signature of the PhD student

[1] Decree of Rector of Gdansk University of Technology No. 34/2009 of 9th November 2009, TUG archive instruction addendum No. 8.

[2] Act of 27th July 2005, Law on Higher Education: Chapter 7, Criminal responsibility of PhD students, Article 226.

GDAŃSK UNIVERSITY OF TECHNOLOGY
FACULTY OF CHEMISTRY

DESCRIPTION OF DOCTORAL DISSERTATION

The Author of the PhD dissertation: Wioletta Brankiewicz

Title of PhD dissertation: Evaluation and cellular responses of modulators of TRF1/TRF2 protein's function as potential anticancer drugs interfering with telomeric shelterin's function

Title of PhD dissertation in Polish: Ewaluacja i badanie odpowiedzi komórkowej nowych modulatorów funkcji białek TRF1/TRF2 jako potencjalnych leków przeciwnowotworowych zaburzających funkcję telomerowych szelteryn

Language of PhD dissertation: English

Supervision: Professor Maciej Bagiński, PhD DSc

Second supervision: Marek Drab, PhD, DSc

Date of doctoral defense:

Keywords of PhD dissertation in Polish: complex shelterin, telomery, rozwój leków, odkrywanie leków, rak piersi

Keywords of PhD dissertation in English: shelterin complex, telomere, drug development, drug discovery, breast cancer

Summary of PhD dissertation in Polish: W ludzkich komórkach zlokalizowano szereg białek oddziałujących z telomerami, co wskazuje na dużą plastyczność organizacji ludzkich kompleksów nukleoproteinowych. Najważniejszym kompleksem jest kompleks „shelterin", który składa się z sześciu białek: TRF1, TRF2, TIN2, POT1, TPP1. TRF1 oraz TRF2 łączą się bezpośrednio z telomerowym dwuniciowym DNA oraz białkiem TIN2. Białko TIN2 łączy się ponadto z białkiem TPP1, stabilizując w ten sposób strukturę całego kompleksu „shelterin".
W przedstawionej dystertacji został scharakteryzowany wpływ jedenastu małocząsteczkowych związków (B070, B087, B176, B280, B327, A822, A378, A670, A628, ST50, ST2S), które zostały zaprojektowane metodami *in silico*, jako potencjalne inhibitory odziaływań pomiędzy białkami TRF1-TIN2 oraz TRF2-TIN2. Do badań wykorzystano linie nowotworowe ludzkiego raka piersi: MDA-MB-231 (ER/PR-; HER2/Neu-), BT-20 (ER/PR-; HER2/Neu-), SK-BR-3 (ER/PR-; HER2/Neu+), BT-474 (ER/PR+; HER2/Neu+), MCF-7 (ER/PR+; HER2/Neu-) i T47D (ER/PR+; HER2/Neu), które reprezentują podstawowe podtypy molekularne nowotworów piersi. Eksperymenty przeprowadzono również na komórkach pierwotnych HMEC, i materiale pochodzącym od pacjentów (inwazyjny przewodowym rakiem piersi, ER/PR+; HER2/Neu-). Na podstawie wyników uzyskanych metodami biologii molekularnej - począwszy od testów toksyczności, poprzez zawansowanie metody barwienia fluorescencyjnego z wykorzystaniem mikroskopii konfokalnej oraz technikę SPR wyłoniono dwa związki (A822 oraz B327) jako obiecujące, które zostały objęte zgłoszeniem patentowym.

Summary of PhD dissertation in English: A number of proteins that interact with telomeres have been identified in human cells, indicating the high plasticity of human nucleoprotein complex organization. The most important complex is the "shelterin" complex, which consists of six proteins: TRF1, TRF2, TIN2, POT1, TPP1. The TRF1 and TRF2 directly bind to telomeric double-stranded DNA and the TIN2 protein. The TIN2 protein also binds to the TPP1 protein, stabilizing the structure of the entire "shelterin" complex.

The PhD thesis presents the characterization of the effect of eleven small molecule compounds (B070, B087, B176, B280, B327, A822, A378, A670, A628, ST50, ST2S), which were designed *in silico* as potential inhibitors of interactions between TRF1-TIN2 and TRF2-TIN2 proteins. Human breast cancer cell lines were used for the studies: MDA-MB-231 (ER/PR-; HER2/Neu-), BT-20 (ER/PR-; HER2/Neu-), SK-BR-3 (ER/PR-; HER2/Neu+), BT-474 (ER/PR+; HER2/Neu+), MCF-7 (ER/PR+; HER2/Neu-) and T47D (ER/PR+; HER2/Neu), which represent the basic molecular subtypes of breast cancer. Experiments were also carried out on primary HMEC cells and material from patients (invasive ductal breast cancer, ER/PR+; HER2/Neu-). Based on the results obtained using molecular biology methods - starting from toxicity tests, through the advanced technique of fluorescent staining using confocal microscopy and SPR technique - two compounds (A822 and B327) were identified as promising, which were included in a patent application.

I would like to express my deepest gratitude to my supervisors, Professor Maciej Baginski and Marek Drab, PhD DSc, for their guidance, encouragement, and unwavering support throughout my doctoral studies. Their expertise, insights, and mentorship were invaluable in shaping my research and academic career.

I am also grateful to my colleagues, Katarzyna Węgrzyn, PhD and Mariusz Szajewski, PhD, for their collaboration, valuable input, and constructive feedback, which greatly contributed to the quality of my research.

Finally, I would like to thank my family and friends for their love, encouragement, and support, which sustained me during the ups and downs of my doctoral journey.

Nothing in life is to be feared, it is only to be understood. Now is the time to understand more, so that we may fear less.

Maria Skłodowska-Curie

To all Women,

who with strength and resilience,

face the challenges that life presents them.

This work was supported by a grant from the National Center for Research and Development Program under contract Strategmed3/306853/9/NCBR/2017 (TARGETTELO), Warsaw, Poland.

Table of Contents

Abbreviations

3'UTR	3' Untranslated Region
7-ADD	7-Amino-Actinomycin
Akt1	Protein Kinase B Alpha
ALT	Alternative Lengthening Of Telomeres
APC/C	Anaphase-Promoting Complex; Also Known As The Cyclosome
ATM	Ataxia Telangiectasia Mutated Protein
ATP	Adenosine Triphosphate
ATR	Ataxia-Telangiectasia Rad3-Related Protein
BC	Breast Cancer
BCR-ABL	Breakpoint Cluster Region-Abelson Murine Leukemia Viral Oncogene Homolog 1 Fusion Protein
BT20	Breast Cancer Cell Line 20
BT474	Breast Cancer Cell Line 474
C33A	Cervical Carcinoma Cell Line
CAMK1D	Calcium/Calmodulin-Dependent Protein Kinase Id
CDK9	Cyclin-Dependent Kinase
CDKs	Cyclin-Dependent Kinases
CIN	Chromosomal Instability
CLK3	Cdc-Like Kinase 3
CTX	Cyclophosphamide
DC	Dendritic Cell
DCIS	Ductal Carcinoma In Situ
DMSO	Dimethyl Sulfoxide
DNA	Deoxyribonucleic Acid
DSB	Double-Strand Break
dsDNA	Double-Stranded DNA
ELISA	Enzyme-Linked Immunosorbent Assay
EMT	Epithelial-Mesenchymal Transition

ER	Estrogen Receptor
ERBB2	Receptor Tyrosine-Protein Kinase Erbb-2 (Also Known As HER2)
ERK	Extracellular Signal-Regulated Kinase
G1	Gap 1 Phase Of The Cell Cycle
G2	Gap 2 Phase Of The Cell Cycle
GALT	Gut-Associated Lymphoid Tissue;
GMB	Glioblastoma Multiforme
GSK-3β	Glycogen Synthase Kinase-3 Beta
HDR	Homology-Directed Repair
hEGF	Human Epidermal Growth Factor
HER2	Human Epidermal Growth Factor Receptor 2
HMEC	Human Mammary Epithelial Cell
HMT-3522	Non-Tumorigenic Human Breast Epithelial Cell Line
HPV	Human Papillomavirus
HR	Homologous Recombination
HSCT	Hematopoietic Stem Cell Transplantation
HT1080	Human Fibrosarcoma Cell Line
HTB9	Bladder Carcinoma Cell Line
IFN-I	Interferon Type I
IOM	Immuno-Oncology-Microbiome
Ki67	Ki-67 Antigene
KIFC1	Requires Kinesin-Like Protein
MAMPs	Microbe-Associated Molecular Pattern;
MAP2K3	Mitogen-Activated Protein Kinase Kinase 3
MAP4K2	Mitogen-Activated Protein Kinase Kinase Kinase Kinase 2
MAPK12	Mitogen-Activated Protein Kinase 12
MCF 10A	Non-Tumor Human Breast Epithelial Cell Line
MCF7	Breast Cancer Cell Line
MCF7/Adr	Adriamycin-Resistant MCF7 Breast Cancer Cell Line
MDA-452	Breast Cancer Cell Line

MDA-MB-231	Metastatic Breast Adenocarcinoma Cell Line-231
MDSCs	Myeloid-Derived Suppressor Cells
MEK	Mitogen-Activated Protein Kinase Kinase
mLN	Mesenteric Lymph Node
MN	Micronuclei
MOMP	Mitochondrial Outer Membrane Permeabilization
mRNA	Messenger RNA
mtDNA	Mitochondrial DNA
mTOR	Mechanistic Target Of Rapamycin
MTT	3-(4,5-Dimethylthiazol-2-Yl)-2,5-Diphenyltetrazolium Bromide
ncRNA	Non-Coding RNA
NHEJ	Non-Homologous End Joining
NK	Natural Killer Cell;
OMVs	Bacterial Outer Membrane Vesicles;
PAK4	P21-Activated Kinase 4
PAM50	Prediction Analysis Of Microarray 50
PARP1	Poly-ADP-Ribose Polymerase 1
PBS	Phosphate-Buffered Saline
PHPT1	Phosphohistidine Phosphatase 1
PI	Propidium Iodide
PLK1	Polo-Like Kinase 1
POT1	Protection Of Telomeres Protein-1
PPM1G	Protein Phosphatase 1g
PPP1R2	Protein Phosphatase 1 Regulatory Subunit 2
PR	Progesterone-Receptor (PR)
PRR	Pattern Recognition Receptor
PRR	Pattern Recognition Receptor;
PTPN5	Protein Tyrosine Phosphatase Non-Receptor Type 5
RAP1	Human Repressor Activator Protein 1
RNA	Ribonucleic Acid

ROS	Reactive Oxygen Species
S	Synthesis Phase Of The Cell Cycle
SAPS3	Sin3a-Associated Protein
SCFAs	Short-Chain Fatty Acids
shRNA	Short Hairpin RNA
SK-BR-3	Human Breast Cancer Cell Line
SPR	Surface Plasmon Resonance
ssDNA	Single-Stranded DNA
subG1	Fraction Of Cells With Less Than 2N DNA Content In Cell Cycle Analysis
SULF2	Sulfatase 2
T47	Human Breast Cancer Cell Line
TAMs	Tumor-Associated Macrophages
TCA	Tricarboxylic Acid
TERC	Telomerase RNA Component
TERT	Telomerase Reverse Transcriptase
TIL	Tumor-Infiltrating Lymphocytes
TIN2	Trf1 Interacting Nuclear Protein 2
TME	Tumor Microenvironment
TNM	A Tumor (T) , Node (N), Metastasis (M) Staging System
TPP1	Pot1-Tin2 Organizing Protein
TRF1	Telomeric Repeat-Binding Factor 1
TRF2	Telomeric Repeat-Binding Factor 2
U2OS	Bone Osteosarcoma Epithelial Cell Line
UICC	Union For International Cancer Control
UPR^{mt}	Mitochondrial Unfolded Protein Response
WHO	World Health Organization
WI-38	Fibroblast-Like Fetal Lung Cell Line
XPF	Xeroderma Pigmentosum Group F Endonuclease
ZO1	Zonula Occludens-1

List of Figures

List of Tables

Abstract

A number of proteins that interact with telomeres have been identified in human cells, indicating the high plasticity of human nucleoprotein complex organization. The most important complex is the "shelterin" complex, which consists of six proteins: TRF1, TRF2, TIN2, POT1, TPP1. The TRF1 and TRF2 directly bind to telomeric double-stranded DNA and the TIN2 protein. The TIN2 protein also binds to the TPP1 protein, stabilizing the structure of the entire "shelterin" complex.

The PhD thesis presents the characterization of the effect of eleven small molecule compounds (B070, B087, B176, B280, B327, A822, A378, A670, A628, ST50, ST2S), which were designed *in silico* as potential inhibitors of interactions between TRF1-TIN2 and TRF2-TIN2 proteins. Human breast cancer cell lines were used for the studies: MDA-MB-231 (ER/PR-; HER2/Neu-), BT-20 (ER/PR-; HER2/Neu-), SK-BR-3 (ER/PR-; HER2/Neu+), BT-474 (ER/PR+; HER2/Neu+), MCF-7 (ER/PR+; HER2/Neu-) and T47D (ER/PR+; HER2/Neu), which represent the basic molecular subtypes of breast cancer. Experiments were also carried out on primary HMEC cells and material from patients (invasive ductal breast cancer, ER/PR+; HER2/Neu-). Based on the results obtained using molecular biology methods - starting from toxicity tests, through the advanced technique of fluorescent staining using confocal microscopy and SPR technique - two compounds (A822 and B327) were identified as promising, which were included in a patent application.

Streszczenie

W ludzkich komórkach zlokalizowano szereg białek oddziałujących z telomerami, co wskazuje na dużą plastyczność organizacji ludzkich kompleksów nukleoproteinowych. Najważniejszym kompleksem jest kompleks „shelterin", który składa się z sześciu białek: TRF1, TRF2, TIN2, POT1, TPP1. TRF1 oraz TRF2 łączą się bezpośrednio z telomerowym dwuniciowym DNA oraz białkiem TIN2. Białko TIN2 łączy się ponadto z białkiem TPP1, stabilizując w ten sposób strukturę całego kompleksu „shelterin".

W przedstawionej dystertacji został scharakteryzowany wpływ jedenastu małocząsteczkowych związków (B070, B087, B176, B280, B327, A822, A378, A670, A628, ST50, ST2S), które zostały zaprojektowane metodami *in silico*, jako potencjalne inhibitory odziaływań pomiędzy białkami TRF1-TIN2 oraz TRF2-TIN2. Do badań wykorzystano linie nowotworowe ludzkiego raka piersi: MDA-MB-231 (ER/PR-; HER2/Neu-), BT-20 (ER/PR-;HER2/Neu-), SK-BR-3 (ER/PR-; HER2/Neu+), BT-474 (ER/PR+; HER2/Neu+), MCF-7 (ER/PR+; HER2/Neu-) i T47D (ER/PR+; HER2/Neu), które reprezentują podstawowe podtypy molekularne nowotworów piersi. Eksperymenty przeprowadzono również na komórkach pierwotnych HMEC, i materiale pochodzącym od pacjentów (inwazyjny przewodowym rakiem piersi, ER/PR+; HER2/Neu-). Na podstawie wyników uzyskanych metodami biologii molekularnej - począwszy od testów toksyczności, poprzez zawansowanie metody barwienia fluorescencyjnego z wykorzystaniem mikroskopii konfokalnej oraz technikę SPR wyłoniono dwa związki (A822 oraz B327) jako obiecujące, które zostały objęte zgłoszeniem patentowym.

Introduction

Cancer ranks as a leading cause of death and a critical barrier for increasing life expectancy in most countries [1,2]. This is due to the aging of the population, as well as changes in the prevalence and distribution of the main risk factors for cancer, several of which are associated with socio-economic development [3,4]. General risk factors for cancer include older age, a personal or family history of cancer, smoking, obesity, alcohol abuse, some types of viral infections, such as human papillomavirus (HPV), specific chemicals, exposure to radiation, including ultraviolet radiation from the sun [2]. The estimations indicate that 19.3 million new cases and 10 million cancer deaths worldwide were recorded in 2020 (the data from International Agency for Research on Cancer). According to their data, Europe accounts for 22.8% of the total cancer cases and 19.6% of cancer deaths. Prostate cancer is the most frequently occurring cancer in men in Europe, followed by lung and colorectal cancer for incidence, and lung, colorectal and prostate cancer for mortality. In women, breast cancer is the most commonly diagnosed cancer and the leading cause of cancer death, followed by colorectal and lung cancer for incidence, and vice versa for mortality [2]. Among the challenges to cure the cancer there are the complexity and variability of its manifestations. On one end of the spectrum, the disease can be mild and curable within a short time span and, following treatment, the patient may continue life largely as before. On the other end of the spectrum, cancer can be aggressive and non-responsive to therapy, spreading and quickly killing its host. Although medical science has come a long way with cancer treatments, and physicians now have sophisticated therapy options, cancer remains a leading cause of death in the developed countries. Therefore, it is still necessary to search for new therapeutic options. In this thesis, I focus on female breast cancer and a novel approach to strategy of treatment based on compounds interfering function of telomeres.

Tumorigenesis and the Basic Principles of Cancer

The Hallmarks of Cancer were proposed as a set of functional capabilities acquired by human cells as they make their way from normal to neoplastic growth states, more specifically capabilities that are crucial for their ability to form malignant tumors (a process called tumorigenesis) [5,6]. In 2000, Hanahan and Weinberg published their seminal article Hallmarks of Cancer, describing six key biological functions or changes that cells acquire in the multistep process of becoming cancerous. In 2011, two additional hallmarks were proposed, and two enabling characteristics were added [6]. In the most recent elaboration of this concept, unlocking phenotypic plasticity and senescent cells were segregated as new emerging hallmarks. Furthermore, two enabling characteristics were added: nonmutational epigenetic reprogramming, and polymorphic microbiome [7]. These 14 traits are briefly introduced here (Figure 1).

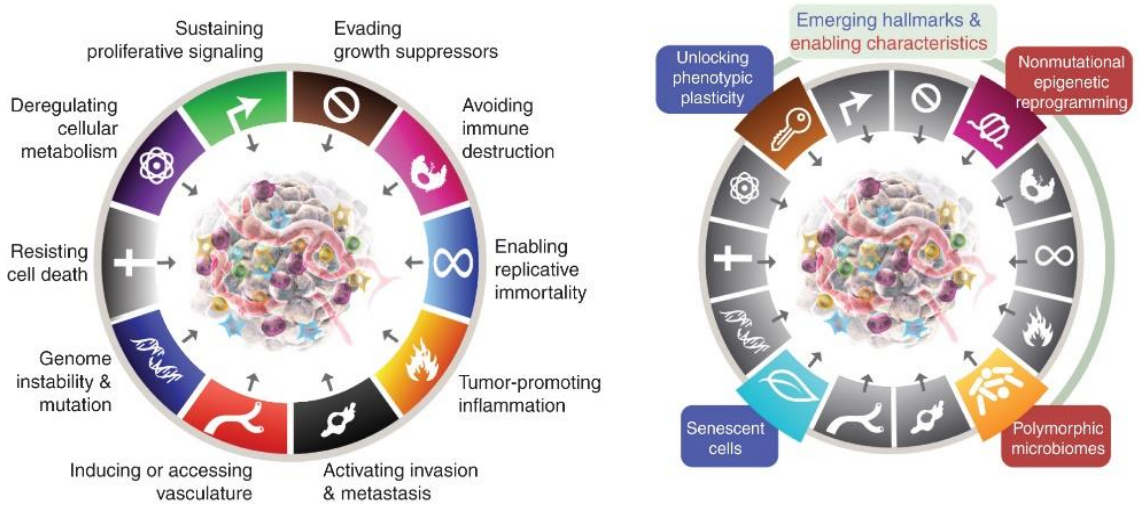

Figure 1. Hallmarks of Cancer, circa 2022. Left, the Hallmarks of Cancer currently embody eight hallmark capabilities and two enabling characteristics introduced in 2011. Right, this review incorporates additional proposed emerging hallmarks and enabling characteristics involving “unlocking phenotypic plasticity,” “nonmutational epigenetic reprogramming,” “polymorphic microbiomes,” and “senescent cells ” [7].

Sustaining proliferative signaling, evading growth suppressors, and resisting cell death

In normal tissue, growth signals are carefully orchestrated to maintain a steady balance between the healthy, functioning cells that grow and divide continuously and the old or malfunctioning cells. This carefully controlled process ensures homeostasis. Tissue homeostasis requires coordinated cell death, cell proliferation and cell differentiation. Cell proliferation is a process of increasing cell numbers that occurs naturally under healthy conditions, such as during childhood growth and pregnancy. However, the continual unregulated proliferation of cells is a fundamental abnormality resulting in the development of cancer. Cancer can result from abnormal proliferation of any of the different kinds of cells in the body, so there are more than a hundred distinct types of cancer, which can vary substantially in their nature and response to treatment. The most important issue in cancer pathology is the distinction between benign (noncancerous) tumors - not invading nearby tissue or spreading to other parts of the body and malignant (cancerous) tumors - the cells can grow and spread to other parts of the body (Figure 2) [8,9].

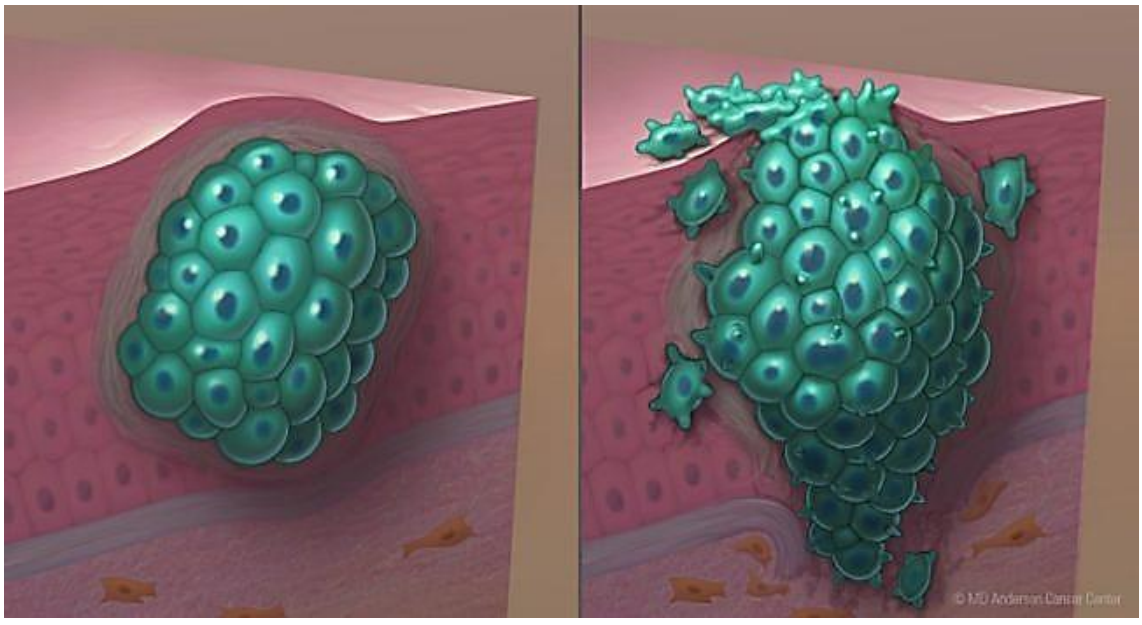

Figure 2. Benign vs malignant tumor. Left - benign tumor cells. Right – a malignant tumor [9].

Cell senescence and enabling replicative immortality

Normal cells have a limited ability to grow and undergo limited number of cell division. In other words, normal cells “grow old”, and cell division eventually ceases. Senescence is broadly defined as a viable growth arrest characterised by the inability of affected cells to resume proliferation in the presence of appropriate mitogenic factors. In the absence of externally or oncogenically induced stresses, telomerase repression (an enzyme maintaining the length of telomeric DNA) may be the only physiological impediment to indefinite replication. Telomerase is composed of protein and RNA components; the major being the reverse transcriptase TERT and its RNA partner TERC (telomerase RNA component), which provides a template for TERT; together they constitute the telomerase reverse transcriptase activity [10]. Telomerase activity is prominent in highly proliferative cells such as stem cells and germ cells, as well as in > 85% of all human cancers [11,12], the remaining 10–15% of tumors are telomerase-negative and utilize the ALT (Alternative Lengthening of Telomeres) mechanism of telomere maintenance [13–15]. ALT activation is prevalent in certain cancer types, including sarcomas, glioblastoma, and neuroendocrine pancreatic cancer [16–18]. While the precise trigger for ALT activation remains unclear, the underlying pathway of ALT-mediated telomere extension has been well characterized and involves DNA repair synthesis mechanisms that are analogous to break-induced replication [19–21]. Specifically, telomere extension events initiate from DSBs that originate from exacerbated and unresolved replication stress and collapsed forks that are particularly prevalent in ALT telomeres [21].

Replicative senescence, as originally described by Hayflick in cultures of cells from non-malignant tissues, is due to natural repression of telomerase and the resulting DNA damage response that occurs when the number of telomeric TTAGGG repeat sequences on the ends of chromosomes becomes too few to support the assembly of stable telomere complexes [22–24]. Structures formed through interactions of TTAGGG repeat sequences with a protein complex referred to as shelterin, function to “cap” the chromosome ends, protecting against DNA degradation, recombination, and chromosome fusion [25]. However, the vast majority of cancer cells expresses the enzyme telomerase, which counteracts this process by adding telomere repeat segments. In this way, cancer

cells may acquire the potential for unlimited replication and continue to divide and give rise to even more cancer cells [8].

Senescence can be also induced in cells by a variety of conditions, including microenvironmental stresses such as nutrient deprivation and DNA damage, as well as damage to organelles and cellular infrastructure, and imbalances in cellular signalling networks [26,27]. Most of the aforementioned instigators of the senescent program are associated with malignancy, in particular DNA damage as a consequence of aberrant hyperproliferation, so-called oncogene-induced senescence due to hyperactivated signaling, and therapy-induced senescence consequent to cellular and genomic damage caused by chemotherapy and radiotherapy. In different experimental systems, senescent cancer cells have been shown to variously contribute to proliferative signaling, avoiding apoptosis, inducing angiogenesis, stimulating invasion and metastasis, and suppressing tumor immunity [7,28,29].

Genome instability and mutation

Maintenance of genome stability is crucial for cell survival and relies on accurate DNA replication. However, replication fork progression is under constant attack from different exogenous and endogenous factors that can give rise to replication stress, a source of genomic instability [30]. 'Genomic instability' can involve both, structural and numerical alterations to the genome. Structural abnormalities include mutations and chromosomal rearrangements, whereas numerical abnormalities involve the gain or loss of entire chromosomes, is also referred to as 'chromosomal instability' and results in aneuploidy. Genomic instability in cancer can be caused by various mechanisms, including germline or somatic defects in DNA repair [31], oncogene-induced replication stress [6], defective mitotic chromosome segregation [32], collisions between the replication and transcription machinery [33] or genotoxic anti-cancer treatment [34]. Importantly, genomic instability facilitates the acquisition of oncogenic features that allow tumors to proliferate and metastasise [35–39].

DNA damage

DNA damage can alter nucleotide sequences and lead to expression of dysfunctional proteins that impact normal cellular physiology [40]. Sources of DNA damage can be endogenous or exogenous and include reactive oxygen species (ROS) or ionizing radiation [41]. DNA damaging agents can broadly be classified into two different categories: clastogens and aneugens. Clastogens cause chromosomal breaks and induce micronuclei (MN) due to generation of acentric chromosomal fragments. In contrast, aneugens lead to the incorporation of whole chromosomes in MN by generation of aneuploidy that affects cell proliferation and the mitotic spindle apparatus [40,42].

Chromosomal instability

Chromosomal instability (CIN) results in the accumulation of large-scale losses, gains and rearrangements of DNA[43] , which causes intratumoral heterogeneity. Furthermore, CIN enables cancer cells to rapidly explore complex genetic makeups by potentially causing the simultaneous acquisition of whole-chromosome or segmental aneuploidy, structural chromosomal aberrations, and the acquisition of mutations [44] .

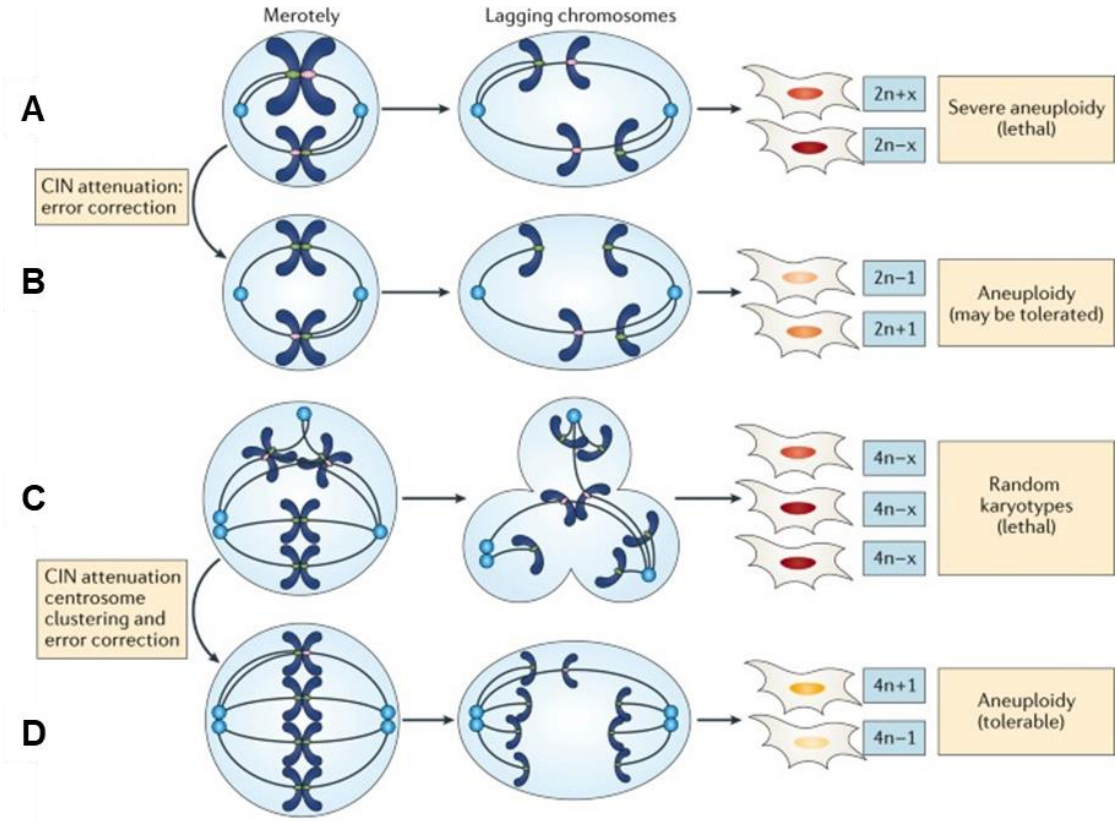

Figure 3. Merotely, tetraploidy, and chromosomal instability attenuation. A - several types of mitotic defects can lead to aberrant chromosome segregation. Those illustrated herein are merotelic attachments, whereby one of the sister chromatids (magenta) is attached to opposite poles. These errors are not detected by the mitotic checkpoint, hence, mitosis proceeds without delay, resulting in a lagging chromosome that can undergo aberrant segregation, leading to aneuploid daughter cells. Severe defects (excessive chromosomal instability (CIN)) generate a high frequency of daughter cells with an unviable aneuploid karyotype that deviates greatly from a 2n diploid content (2n±x) owing to the loss or gain of too many chromosomes (dark red daughter cells). B - infrequent segregation errors involving fewer chromosomes likely generate viable progeny (orange daughter cells), whose proliferation will then depend on the various mechanisms of aneuploidy tolerance. The frequency of segregation errors can be attenuated by acquiring secondary alterations that improve mitotic fidelity. APC/C (anaphase-promoting complex; also known as the cyclosome) dysfunction is one mechanism that leads to CIN attenuation by delaying mitosis, thus providing more time for endogenous mechanisms to correct attachment errors. C - supernumerary centrosomes in tetraploid cells (4n) frequently generate multipolar spindles and merotelic attachments. Failure to cluster these extra centrosomes into two poles will lead to a multipolar division (resulting in 3 or 4 daughter cells, as shown), often with severe and random chromosome losses (4n–x). The presence of extra centrosomes also greatly increases the risk of merotely. D - tetraploid cells avoid multipolar divisions through centrosome clustering, which requires kinesin-like protein KIFC1. Tetraploid cells are believed to be more tolerant of segregation errors than diploid cells because such errors have a milder effect on overall protein stoichiometry. Delaying mitotic progression provides more time to achieve centrosome clustering and reduces the frequency of segregation errors, thus improving tetraploid cell fitness and the propagation of a sustainable rate of CIN (yellow daughter cells) [44].

Mitochondrial genomic instability

Similar to nuclear DNA, the integrity of mitochondrial DNA (mtDNA) also requires maintenance, and an inability to do so has been linked to carcinogenesis [45]. Damage to mtDNA leads to less efficient mitochondrial function, resulting in excessive ROS production and further accumulation of damage to mtDNA, as well as damage to nuclear DNA [39,46,47].

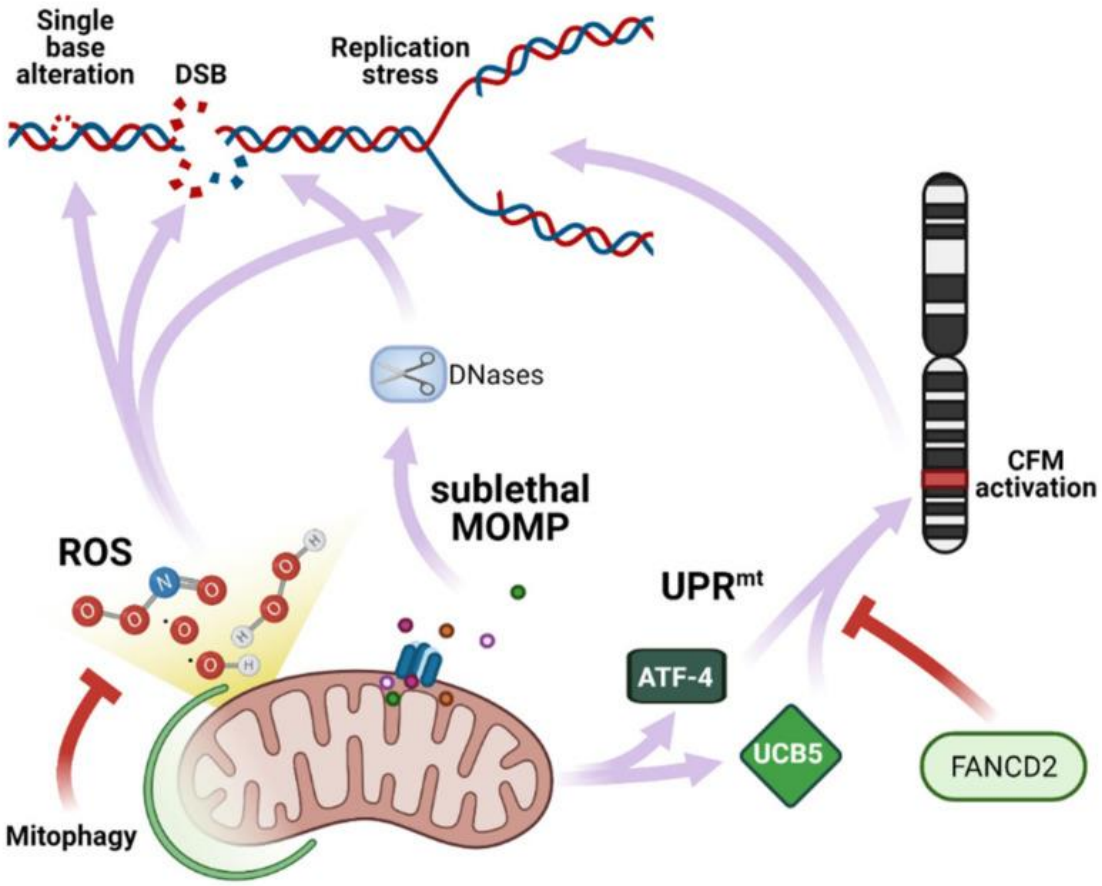

Figure 4. Mitochondrial response to DNA damage. Mitochondria directly induces DNA damage via ROS production, the activation of DNase during sublethal MOMP (mitochondrial outer membrane permeabilization) or activation of CFM mediated by UPR^{mt} (mitochondrial unfolded protein response) [47].

Inducing or accessing vasculature

Angiogenesis is a term that describes the formation of new blood and lymphatic vessels from a pre-existing vasculature [48]. The formation of new blood vessels is regulated by the activity of proangiogenic and antiangiogenic factors (Figure 5) [49]. Angiogenesis is crucial in embryogenesis, wound healing and the menstrual cycle [50]. Deregulation of the balance between proangiogenic and antiangiogenic factors causes pathologic conditions such as cancer development [51]. Angiogenesis in tumor cells enables provision of nutrients and oxygen to the tumor and the removal of metabolic waste. Furthermore, new vessel formation enables cancer cells to metastasize and proliferate to distant sites through entry into the newly formed blood and lymphatic system and subsequent extravasation [52]. On the other hand, a lack of adequate blood supply could halt tumor growth, leading to tumor shrinkage and sometimes cancer cell death [48,53].

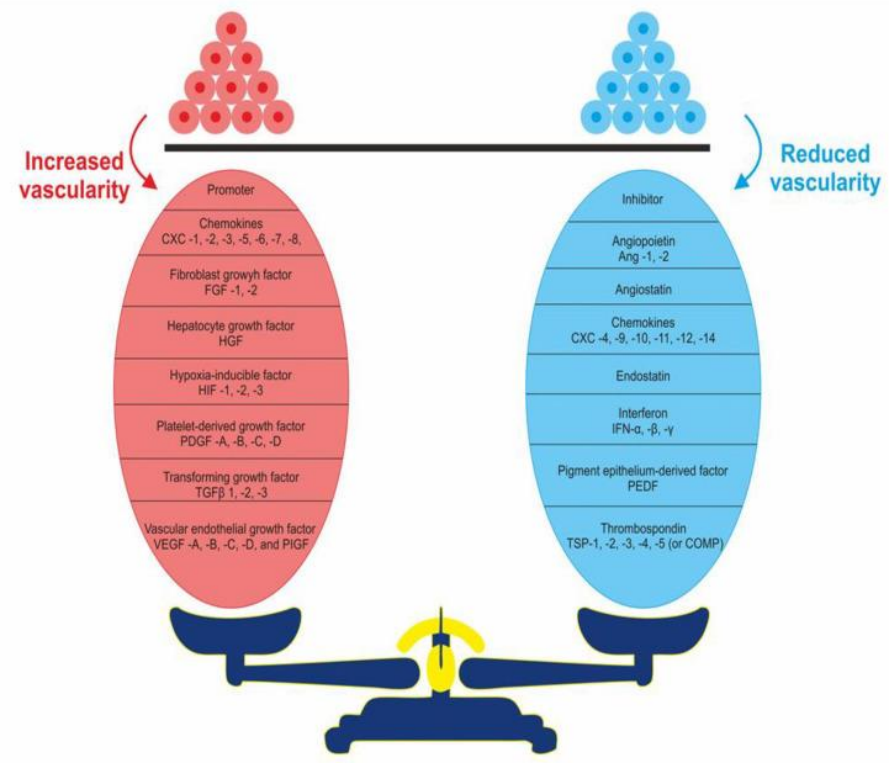

Figure 5. Maintaining homeostasis results from an equilibrium between promotors and inhibitors of angiogenesis [48].

Deregulating cellular metabolism

Metabolic processes are altered in cancer cells, which obtain advantages from this metabolic reprogramming in terms of energy production and synthesis of biomolecules that sustain their uncontrolled proliferation[54] . Fast-growing, poorly differentiated tumor cells typically exhibit increased aerobic glycolysis, even in the presence of replete oxygen, by converting a majority of glucose-derived pyruvate to lactate, a phenomenon known as the Warburg effect [55] . Initially, it was thought that this Warburg effect was a cause of cancer, but it was later established that this shift to glycolytic metabolism was an effect of cancer cell transformation. Due to this, tumor cells depend on glutamine anaplerosis to replenish the tricarboxylic acid (TCA) cycle intermediates for macromolecular biosynthesis and nicotinamide adenine dinucleotide phosphate production (Figure 6) [56,57]. But aerobic glycolysis and glutamine anaplerosis cannot explain all the metabolic changes that are necessary to support the requirements of cell growth. Moreover, cancer cells acquire alterations to the metabolism of all four major classes of macromolecules: carbohydrates, proteins, lipids, and nucleic acids, which act in concert to support cellular biomass synthesis, and energy storage for uncontrolled proliferation and growth [58,59]. Furthermore, metabolic reprogramming frequently cooperates with genomic instability, chronic inflammation, and immune escape to promote tumor progression [6].

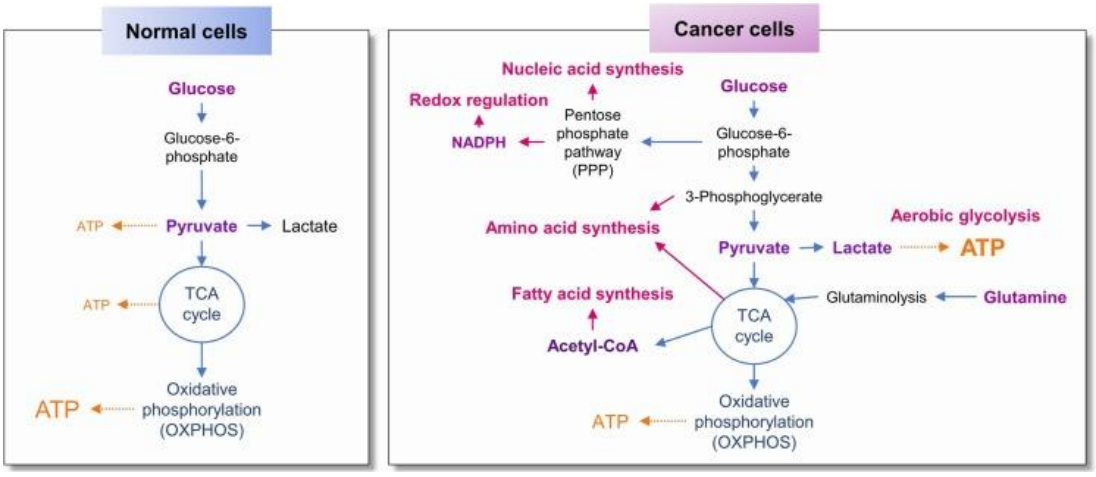

Figure 6. Metabolic reprogramming in cancer cells compared with a normal cell [57].

Activating tissue invasion and metastasis

Cancer metastasis represents an advanced stage of malignancy and is the leading cause of cancer-related deaths [60]. Metastasis is a multistep process that includes migration and invasion of cancer cells to other regions of the organism (Figure 7) [61]. The loss of cell-cell adhesion capacity allows malignant tumor cells to dissociate from the primary tumor mass and changes in cell-matrix interaction enable the cells to invade the surrounding stroma. This involves the secretion of substances to degrade the basement membrane and extracellular matrix and also the expression/suppression of proteins involved in the control of motility and migration [62]. The blood vessel within the tumor's vicinity can then provide a route for the detached cells to enter the circulatory system and metastasize to distant sites [63,64]. Once the tumor cell has arrived at a likely point of intravasation, it interacts with the endothelial cells by undergoing biochemical interactions. The new tumor can then proliferate at this secondary focus [62].

The process through which epithelial cells undergo a series of morphological and biochemical changes to take on a more mesenchymal phenotype is known as epithelial–mesenchymal transition (ETM). EMT involves the loss of cell-cell adhesion and the polarized epithelial morphology through the characteristic loss of epithelial cell junctional proteins such as E-cadherin, claudins and ZO-1, and a subsequent increase in mesenchymal markers such as N-cadherin, vimentin and fibronectin and cytoskeletal reorganization [65].

Thus, diagnosis and treatment of metastatic disease are vital areas in the constant battle many patients face against cancer, yet effective treatments are limited and substantial morbidity and mortality are still associated with metastatic disease [66].

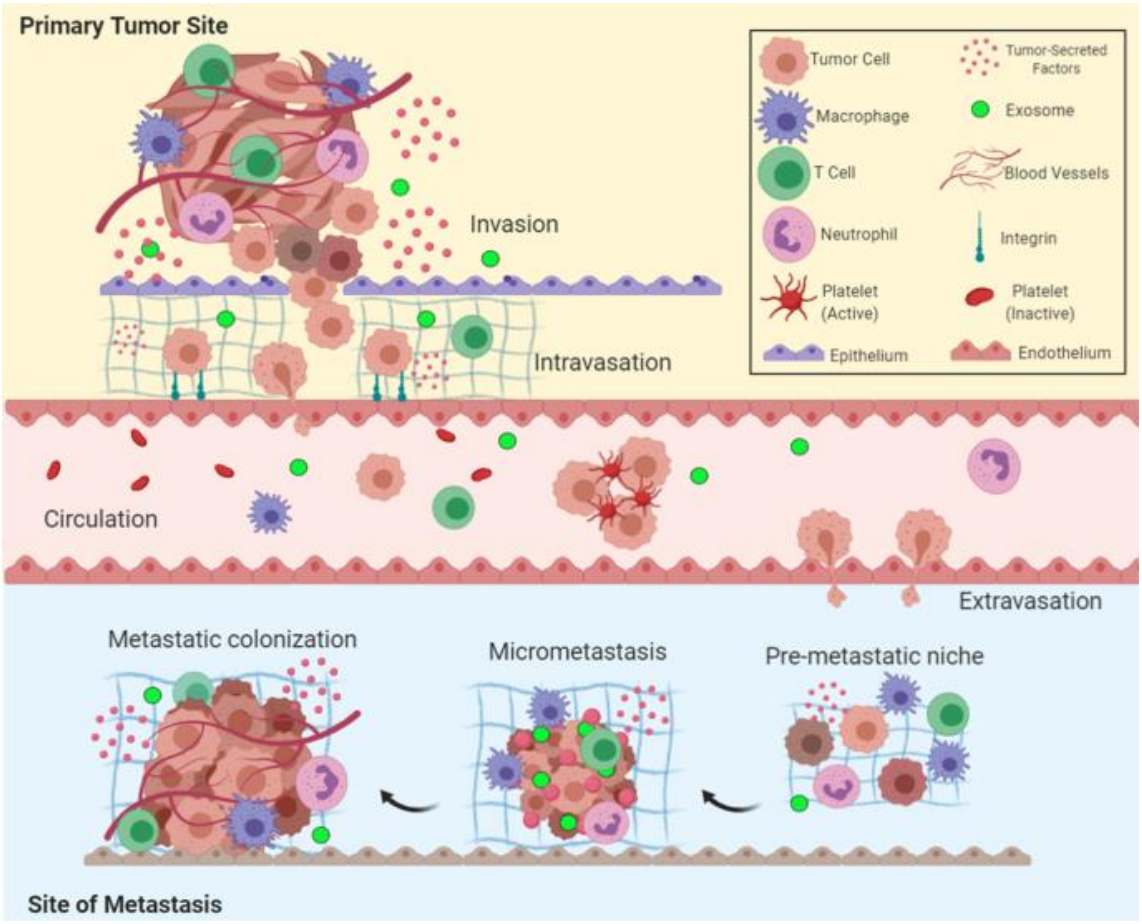

Figure 7. Overview of the metastatic cascade: The five key steps of metastasis include invasion, intravasation, circulation, extravasation, and colonization [60].

Tumor-promoting inflammation and avoiding immune destruction

Inflammation is an ancient evolved process that involves the activation, recruitment and action of cells of innate and adaptive immunity [67]. Initially highlighted for its essential role in host defense against pathogens, inflammation is equally important for tissue repair, regeneration and remodeling and subtle forms of inflammation are essential for the regulation of tissue homeostasis [68]. A role for inflammation in tumorigenesis is now generally accepted, and it has become evident that an inflammatory microenvironment is an essential component of all tumors, including some in which a direct causal relationship with inflammation is not yet proven [68]. Only a minority of all cancers are caused by germline mutations, whereas the vast majority (90%) are linked to somatic mutations and environmental factors [69]. Along with its pro-tumorigenic effects, inflammation also influences the host immune response to tumors [70]. While innate

immune cells, such as neutrophils, monocytes, and macrophages, are critical mediators for sterile and nonsterile inflammation, persistent inflammation, such as that which occurs in cancer, is known to disturb normal myelopoiesis [71]. This disturbance leads to the generation of immunosuppressive myeloid cells, such as myeloid-derived suppressor cells (MDSCs) and tumor-associated macrophages (TAMs). Due to their potent suppressive activities against effector lymphocytes and their abundance in the tumor microenvironment, immunosuppressive myeloid cells act as a major barrier to cancer immunotherapy [71].

Polymorphic microbiomes

The inclusion of polymorphic microbes to the hallmarks of cancer reflects increasing appreciation that the complex microbial ecosystems (or 'microbiome') – including bacteria, fungi, and viruses, which symbiotically associate with the human body – have a profound impact on cancer pathogenesis [72]. Evidence now demonstrates that the microbiome plays a substantial role in tumorigenesis, cancer differentiation, and malignant progression [7,73]. Furthermore, the microbiome directly interacts, both positively and negatively, with other established cancer hallmarks, such as tumor inflammation, avoiding immune destruction, genome instability, and resistance to anticancer therapies (Figure 8) [7,74].

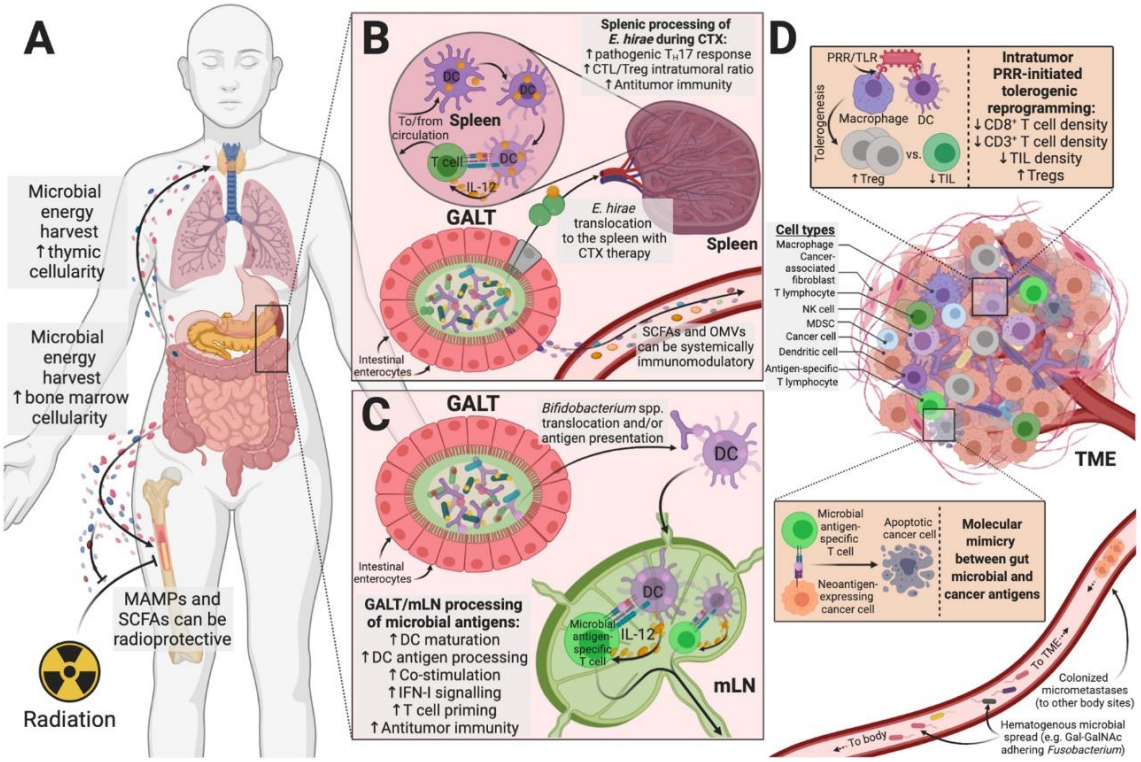

Figure 8. Defining the immuno-oncology-microbiome (IOM) axis. Gut and TME microbiota regulate host metabolism and immunity, which ultimately influence antitumor immunity. A - gut microbial metabolites and byproducts influence host lympho- and myelopoiesis, including during allogeneic HSCT and radiotherapy. B - cyclophosphamide (CTX)-derived gut epithelial damage enables *E. hirae* translocation and antitumor immunity. C - gut translocation of *Bifidobacterium* species or its antigens can increase IFN-I signaling and antitumor immunity. D - microbes within the tumor microenvironment (TME) can be either immunosuppressive (often PRR-mediated) or immunogenic, including shaping response to immunotherapy. Cancer (neo)antigens may share epitopes with microbes through molecular mimicry. Microbial hematogenous spread or colonized micrometastases may complete this feedback loop that originated in the gut. Abbreviations: MAMPs=microbe-associated molecular pattern; SCFAs=short-chain fatty acids; GALT=gut-associated lymphoid tissue; mLN=mesenteric lymph node; DC=dendritic cell; OMVs=bacterial outer membrane vesicles; NK=natural killer cell; PRR=pattern recognition receptor; TIL=tumor-infiltrating lymphocytes [73].

Nonmutational epigenetic reprogramming

Historically cancer was mostly considered a genetic disease, however, the “somatic mutation theory” did not explain the origin of most cancers [75] . Tumor cells are mostly characterized by abnormalities in responding to internal and external signals, cellular identity, and deregulation of gene expression [76–78]. In fact, epigenetic mechanisms are tightly controlled and regulate embryonic development and adult life and their deregulation has been involved in many

disorders including cancer [79]. Epigenetics is “defined as the study of mitotically and meiotically heritable changes in gene function that are not dependent on DNA sequence” [80]. External and internal signals may enhance or reduce chromatin resistance leading to a “restrictive state that blocks differentiation programs” or epigenetic plasticity, respectively [81]. Epigenetic plasticity in turn provides a permissive environment for premalignant and malignant cells to stimulate different gene regulatory pathways resulting in abnormal cell fates. These driver epigenetic conditions may be fixed during cell proliferation by various mechanisms including DNA methylation, histone modifications, and ncRNA contributions resulting in tumor suppressor gene inhibition and oncogene activation [7,82] .

Unlocking phenotypic plasticity

Phenotype plasticity means that genotypes produce different phenotypes under different environmental conditions and is a crucial mechanism to adapt to environmental heterogeneity [83]. Traditionally, phenotype plasticity is considered to be decentralized and differentiated during tissue regeneration or wound healing [83]. Although the degeneration process is the main link of the organization, the decentralization itself has the risk of cancer. Therefore, phenotype plasticity provides a new paradigm to understand the occurrence, development of cancer, and resistance to treatment [83].

Thus, nascent cancer cells originating from a normal cell that had advanced down a pathway approaching or assuming a fully differentiated state may reverse their course by dedifferentiating back to progenitor-like cell states [7]. Conversely, neoplastic cells arising from a progenitor cell that is destined to follow a pathway leading to end-stage differentiation may short-circuit the process, maintaining the expanding cancer cells in a partially differentiated, progenitor-like state [7]. Alternatively, transdifferentiation may operate, in which cells that were initially committed into one differentiation pathway switch to an entirely different developmental program, thereby acquiring tissue-specific traits that were not preordained by their normal cells-of-origin (Figure 9) [7].

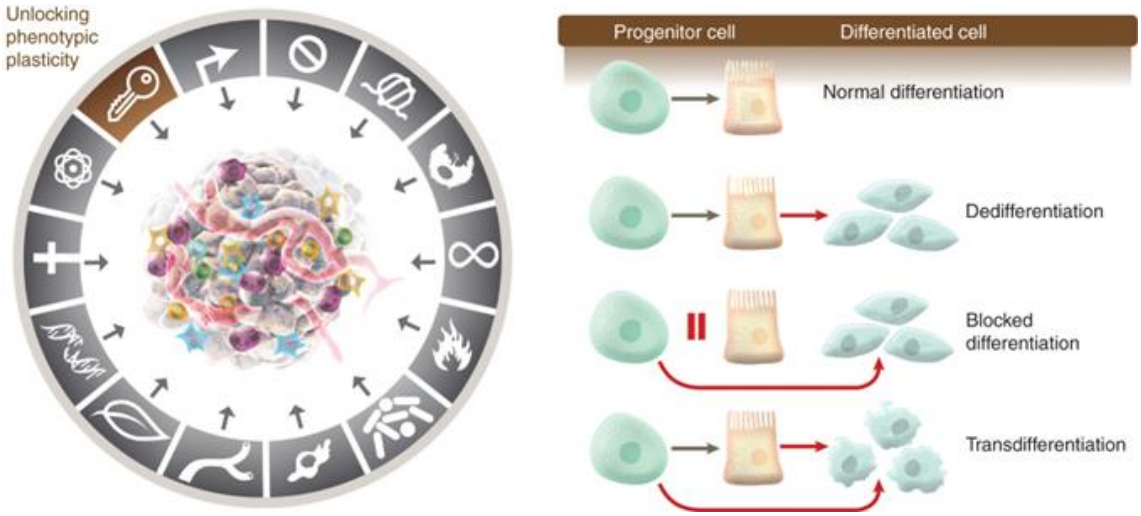

Figure 9. Unlocking phenotypic plasticity. Left, phenotypic plasticity is arguably an acquired hallmark capability that enables various disruptions of cellular differentiation, including (i) dedifferentiation from mature to progenitor states, (ii) blocked (terminal) differentiation from progenitor cell states, and (iii) transdifferentiation into different cell lineages. Right, depicted are three prominent modes of disrupted differentiation integral to cancer pathogenesis. By variously corrupting the normal differentiation of progenitor cells into mature cells in developmental lineages, tumorigenesis and malignant progression arising from cells of origin in such pathways is facilitated [7].

Breast cancer biology and classification

Breast cancer is one of the oldest described cancers in human history, with the first evidence dating back to ancient Egypt. The Edwin Smith Surgical Papyrus, dating back to 3,000–2,500 B.C., and possibly attributable to Imhotep (the Egyptian physician-architect), provides authentic accounts of breast cancer [84]. In ancient Greece, a divinity was exhorted to offer relief from breast maladies, as evidenced by votive offerings in the shape of breasts in Greek temples that housed Asclepius, the god of medicine [85]. The different stages of breast cancer were described by Hippocrates as early as 400 B.C.E. Thereafter in A.D. 200, Galen described cancer as well, he postulated that some tumors were more dangerous than others. He suggested medications like opium, castor oil, licorice, sulfur, salves, etc. for medicinal therapy of breast cancers [84]. By the mid-nineteenth century, William Halstead from New York made radical breast surgery the gold standard for the next 100 years. In XX and XXI centuries, with the advent of modern medicine, one can see the development of novel therapies for breast cancer including hormone treatments, surgeries and biological therapies.

Breast cancer in Poland

Worldwide, breast cancer is the most frequent female malignancy, with more than 2 million new cases annually. In Poland, breast cancer accounted for as many as 24 644 cases and 8 805 deaths in 2020 [86]. Regarding incidence time trends, in the last 15 years, observed for breast cancer incidence has been increasing since 2009, around + 1.2% per year. According to age-standardized in every age group, the most common cancer sites were breast: young women (20-44 years of age) - 28% of cases, 27% of deaths, middle-aged women (45-64 years of age) - 29% of cases, 18% of deaths, the oldest age-group (> 65 years of age) - 19% of cases, 14% of deaths [86].

Anatomy and physiology of the breast

The female breasts are a visual and important part of women's physiology, they have strong symbolic associations with beauty, fertility and femininity, and motherhood. The human breast is composed of skin, adipose tissue, connective tissues, and mammary glands [87]. The skin, adipose tissue, and mammary glands are fixed to the chest wall by connective tissues, known as Cooper's ligaments in the human breast. The mammary glands, immersed in surrounding adipose tissue, are composed of a cluster of radial epithelial ducts arranged in 15 to 20 lobes [87]. The lobes comprise a number of lobules that terminate in glandular alveoli, in which milk is produced. In addition to the lobes, ducts, connective tissues and adipose tissue, the breast also contains blood and lymph vessels, lymph nodes and nerves (Figure 10) [87].

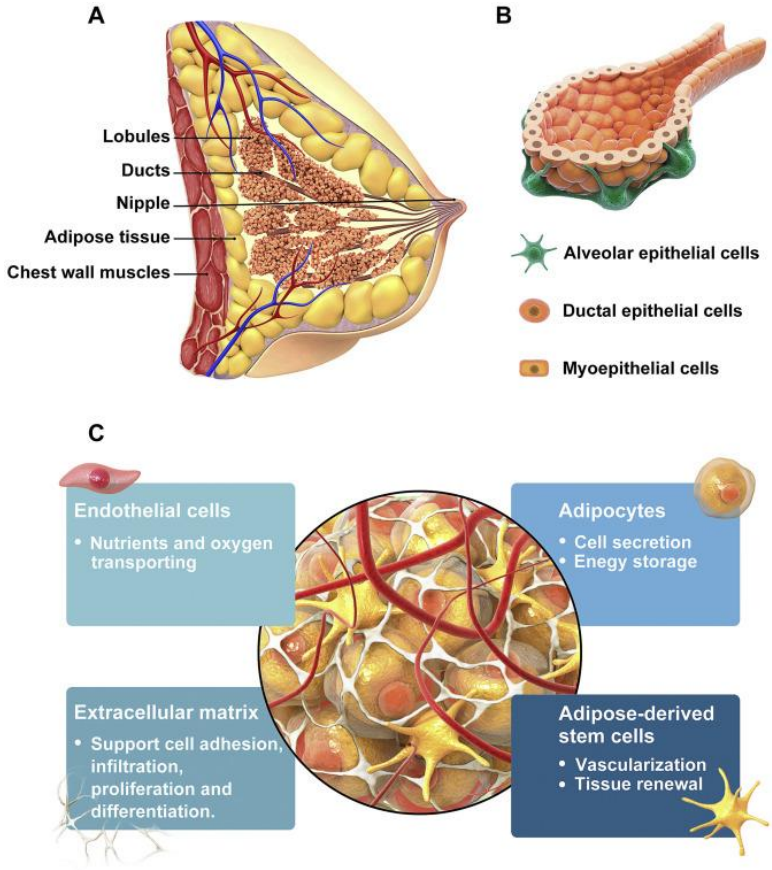

Figure 10. Anatomy and main components of the human female breast. A - anatomy of the female human breast is composed of skin, adipose tissue, the connective tissues, and the mammary glands. The skin, adipose tissue, and glands are fixed to the chest wall by connective tissues. B - glandular alveola and ducts are mainly made up with epithelial cells. C - main component of adipose tissue illustrating adipocytes, extracellular matrix, endothelial cells and adipose-derived stem cells [87].

Terminology and classification of breast cancer

Breast cancer (BC) comprises a heterogeneous group of tumors that displays marked variation in clinical presentation, morphology, molecular features, biological behavior, and response to therapy [88]. The significant categories of breast cancer classification are the histopathological type, the grade of the tumor, the stage of the tumor, and the expression of proteins and genes. The purpose of classification is to select the best treatment.

Histopathologic classification

Histopathologic classification is based on characteristics seen upon light microscopy of biopsy specimens. They can broadly be classified into:

- Carcinoma in situ

There are 2 types of breast carcinoma in situ: ductal carcinoma in situ (DCIS) and Paget disease of the nipple. DCIS is a condition in which the abnormal cells are found in the lining of a breast duct. The abnormal cells have not spread outside the duct to other tissues in the breast. Paget disease of the nipple is a condition in which abnormal cells are found in the skin cells of the nipple and may spread to the areola. Patients with Paget disease of the nipple may also have DCIS or invasive breast cancer in the same breast. Also called stage 0 breast carcinoma in situ [58].

- Invasive carcinoma

Breast cancers that have spread into surrounding breast tissue are known as invasive breast cancers. Most breast cancers are invasive, but there are different types of invasive breast cancer. The two most common are invasive ductal carcinoma and invasive lobular carcinoma [89].

WHO classification

The 2019 World Health Organization (WHO) classification of breast tumors which includes benign (generally harmless) tumors and malignant (cancerous) tumors, recommends the following pathological types [90]:

1. **Epithelial tumors of the breast**

Benign epithelial proliferations and precursors

- Usual ductal hyperplasia
- Columnar cell lesions, including flat epithelial atypia
- Atypical ductal hyperplasia

Adenosis and benign sclerosing lesions

- Sclerosing adenosis
- 8401/0 Apocrine adenoma
- Microglandular adenosis
- Radial scar/complex sclerosing lesion

Adenomas

- 8211/0 Tubular adenoma NOS
- 8204/0 Lactating adenoma
- 8503/0 Duct adenoma NOS

Epithelial-myoepithelial tumors

- 8940/0 Pleomorphic adenoma
- 8983/0 Adenomyoepithelioma NOS
- 8983/3 Adenomyoepithelioma with carcinoma
- 8562/3 Epithelial-myoepithelial carcinoma

Papillary neoplasms

- 8503/0 Intraductal papilloma
- 8503/2 Ductal carcinoma in situ, papillary
- 8504/2 Encapsulated papillary carcinoma
- 8504/3 Encapsulated papillary carcinoma with invasion
- 8509/2 Solid papillary carcinoma in situ
- 8509/3 Solid papillary carcinoma with invasion
- 8503/3 Intraductal papillary adenocarcinoma with invasion

Non-invasive lobular neoplasia

- Atypical lobular hyperplasia
- 8520/2 Lobular carcinoma in situ NOS
- Classic lobular carcinoma in situ
- Florid lobular carcinoma in situ
- 8519/2 Lobular carcinoma in situ, pleomorphic

Ductal carcinoma in situ (DCIS)

- 8500/2 Intraductal carcinoma, non-infiltrating, NOS
- DCIS of low nuclear grade
- DCIS of intermediate nuclear grade
- DCIS of high nuclear grade

Invasive breast carcinoma

- 8500/3 Infiltrating duct carcinoma NOS
- 8290/3 Oncocytic carcinoma
- 8314/3 Lipid-rich carcinoma
- 8315/3 Glycogen-rich carcinoma
- 8410/3 Sebaceous carcinoma
- 8520/3 Lobular carcinoma NOS
- 8211/3 Tubular carcinoma
- 8201/3 Cribriform carcinoma NOS
- 8480/3 Mucinous adenocarcinoma
- 8470/3 Mucinous cystadenocarcinoma NOS
- 8507/3 Invasive micropapillary carcinoma of breast
- 8401/3 Apocrine adenocarcinoma
- 8575/3 Metaplastic carcinoma NOS

Rare and salivary gland-type tumors

- 8550/3 Acinar cell carcinoma
- 8200/3 Adenoid cystic carcinoma

Classic adenoid cystic carcinoma

Solid-basaloid adenoid cystic carcinoma

- Adenoid cystic carcinoma with high-grade transformation
- 8502/3 Secretory carcinoma
- 8430/3 Mucoepidermoid carcinoma

- 8525/3 Polymorphous adenocarcinoma
- 8509/3 Tall cell carcinoma with reversed polarity

Neuroendocrine neoplasms

- 8240/3 Neuroendocrine tumor NOS
- 8240/3 Neuroendocrine tumor, grade 1
- 8249/3 Neuroendocrine tumor, grade 2
- 8246/3 Neuroendocrine carcinoma NOS
- 8041/3 Neuroendocrine carcinoma, small cell
- 8013/3 Neuroendocrine carcinoma, large cell

2. Fibroepithelial tumors and hamartomas of the breast

Hamartoma

9010/0 FlbroadenomaNOS

9020/1 Phyllodes tumourNOS

Periductal stromal tumor

9020/0 Phyllodes tumour, benign

9020/1 Phyllodes tumour, borderline

9020/3 Phyllodes tumor, malignant

3. Tumors of the nipple

Epithelial tumors

- 8407/0 Syringoma NOS
- 8506/0 Adenoma of nipple
- 8540/3 Paget disease of breast

4. Mesenchymal tumors of the breast

Vascular tumors

- 9120/0 Haemangioma NOS

Perilobular haemangioma

Venous haemangioma

Cavernous haemangioma

Capillary haemangioma

Angiomatosis

Usual angiomatosis

Capillary angiomatosis

* 9126/0 Atypical vascular lesion

Lymphatic atypical vascular lesion, resembling lymphangioma

Vascular atypical vascular lesion, resembling haemangioma or hobnail haemangioma

* 9120/3 Post-radiation angiosarcoma

Epithelioid angiosarcoma

* 9120/3 Angiosarcoma

Epithelioid angiosarcoma

Fibroblastic and myofibroblastic tumors

* 8828/0 Nodular fasciitis
* 8825/0 Myofibroblastoma
* 8821/1 Desmoid-type fibromatosis
* 8825/1 Inflammatory myofibroblastic tumor

Epithelioid inflammatory myofibroblastic sarcoma

Peripheral nerve sheath tumors

* 9560/0 Schwannoma NOS

Cellular schwannoma

Epithelioid schwannoma

Plexiform schwannoma

Melanotic schwannoma

* 9540/0 Neurofibroma NOS

Diffuse neurofibroma

Atypical neurofibroma

Plexiform neurofibroma

* 9580/0 Granular cell tumor NOS
* 9580/3 Granular cell tumor, malignant

Smooth muscle tumors

* 8890/0 Leiomyoma NOS

Cutaneous (pilar) leiomyoma

Leiomyoma of the nipple/areola (muscularis mamillae and areolae)

Leiomyoma of the breast parenchyma

8890/3 Leiomyosarcoma NOS

Adipocytic tumors

- 8850/0 Lipoma NOS
- 8861/0 Angiolipoma NOS
- 8850/3 Liposarcoma NOS

Other mesenchymal tumors and tumor-like conditions

- Pseudoangiomatous stromal hyperplasia

5. Haematolymphoid tumors of the breast

Lymphoma

- 9699/3 Mucosa-associated lymphoid tissue lymphoma
- 9690/3 Follicular lymphoma NOS
- 9680/3 Diffuse large B-cell lymphoma NOS
- 9687/3 Burkitt lymphoma NOS/Acute leukaemia, Burkitttype

Endemic Burkitt lymphoma

Sporadic Burkitt lymphoma

lmmunodeficiency-associated Burkitt lymphoma

- 9715/3 Breast implant-associated anaplastic large cell lymphoma

Breast cancer staging system

The breast cancer staging system, called the tumor, node, metastasis (TNM) staging system (Table 1). This system relies on a set standardized criteria developed by the Union for International Cancer Control (UICC) [91], and is based on the size of the tumor (T), involvement of regional lymph nodes (N), and whether the cancer has metastasized (M). Each category is assigned a number to describe the extent of tumor load [92].

Table 1. TNM Staging System. Simplified summary of the UICC TNM staging system for breast cancer [92].

Category	Description
TX	Primary tumor cannot be evaluated
T0	No evidence of primary tumor
Tis (DCIS)	Carcinoma *in situ*
Tis (Paget's)	Paget's disease of nipple NOT associated with invasive carcinoma and/or carcinoma in situ (DCIS) in underlying breast parenchyma. Carcinomas in breast parenchyma associated with Paget disease are categorized based on size and characteristics of parenchymal disease, although presence of Paget disease should still be noted
T1-T4	Size and/or extent of the primary tumor
T1	Tumor ≤ 2 cm in greatest dimension
T1mi	Tumor ≤ 1 mm in greatest dimension
T1a	Tumor > 1 mm but ≤ 5 mm in greatest dimension (round any measurement 1.0–1.9 mm to 2 mm)
T1b	Tumor > 5 mm but ≤ 10 mm in greatest dimension
T1c	Tumor > 10 mm but ≤ 20 mm in greatest dimension
T2	Tumor > 2.0 ≤ 5.0 cm in greatest diameter
T3	Tumor > 5.0 cm in greatest diameter
T4	Tumor independent of size, but with direct extension to chest wall and/o to skin (ulceration or macroscopic nodules)
T4a	Extension to chest wall, not including only pectoralis muscle adherence/invasion
T4b	Ulceration and/or ipsilateral macroscopic satellite nodules and/or edema (including peau d'orange) of skin, which do not meet criteria for inflammatory carcinoma
T4c	Both T4a and T4b
T4d	Inflammatory carcinoma
pNX	Regional lymph nodes cannot be evaluated
pN0	No regional lymph node involvement (no cancer found in the lymph nodes)
pN1-N3	Involvement of regional lymph nodes (number and/or extent of spread)
pN1	Micrometastases; or metastases in 1–3 axillary lymph nodes; and/or clinically negative mammaria interna lymph nodes with micro- or macrometastases by SLN biopsy
pN1mi	Micrometastases (approximately 200 cells, larger than 0.2 mm, but none larger than 2.0 mm)
pN1a	Metastases in 1–3 axillary lymph nodes, at least one metastasis larger than 2.0 mm

pN1b	Metastases in ipsilateral internal mammary sentinel lymph nodes, excluding ITCs
pN1c	pN1a and pN1b combined
pN2	Metastases in 4–9 axillary lymph nodes; or positive (by imaging) ipsilateral mammaria interna lymph nodes(s) in absence of axillary lymph node metastases
pN2a	Metastases in 4–9 axillary lymph nodes (at least one tumor deposit larger than 2.0 mm)
pN2b	Metastases in clinically detected internal mammary lymph nodes with or without microscopic confirmation; with pathologically negative axillary lymph nodes
pN3	Metastases in i. ≥10 axillary lymph nodes; or infraclavicular lymph nodes, or ii. Positive ipsilateral mammaria interna lymph nodes by imaging in presence of positive axillary lymph node (s); or iii. >3 axillary lymph nodes and micro- or macrometastases by SLN biopsy in clinically negative ipsilateral mammaria interna lymph nodes; or in ipsilateral supraclavicular lymph nodes
pN3a	Metastases in 10 or more axillary lymph nodes (at least one tumor deposit larger than 2.0 mm); or metastases to infraclavicular (level III axillary lymph) nodes
pN3b	pN1a or pN2a in presence of cN2b (positive internal mammary lymph nodes by imaging); or pN2a in presence of pN1b
pN3c	Metastases in ipsilateral supraclavicular lymph nodes
MX	Distant metastasis cannot be evaluated
M0	No distant metastasis (cancer has not spread to other parts of the body)
M1	Distant metastasis (cancer has spread to distant parts of the body)

The grade of breast cancer

The grade of cancer describes what the cancer cells look like compared to normal cells. The histological grade is based on the quantification of the following morphologic features: mitotic count (0–7, 8–15, >16), degree of tubular formation (>75%, 10%–75%, <10%), and nuclear pleomorphism (uniform, moderate, high) [93,94]. Microscopic investigation of these characteristics results in an overall score of one, two, or three, correlating with increasingly worse outcomes, as depicted in Figure 11 [95] .

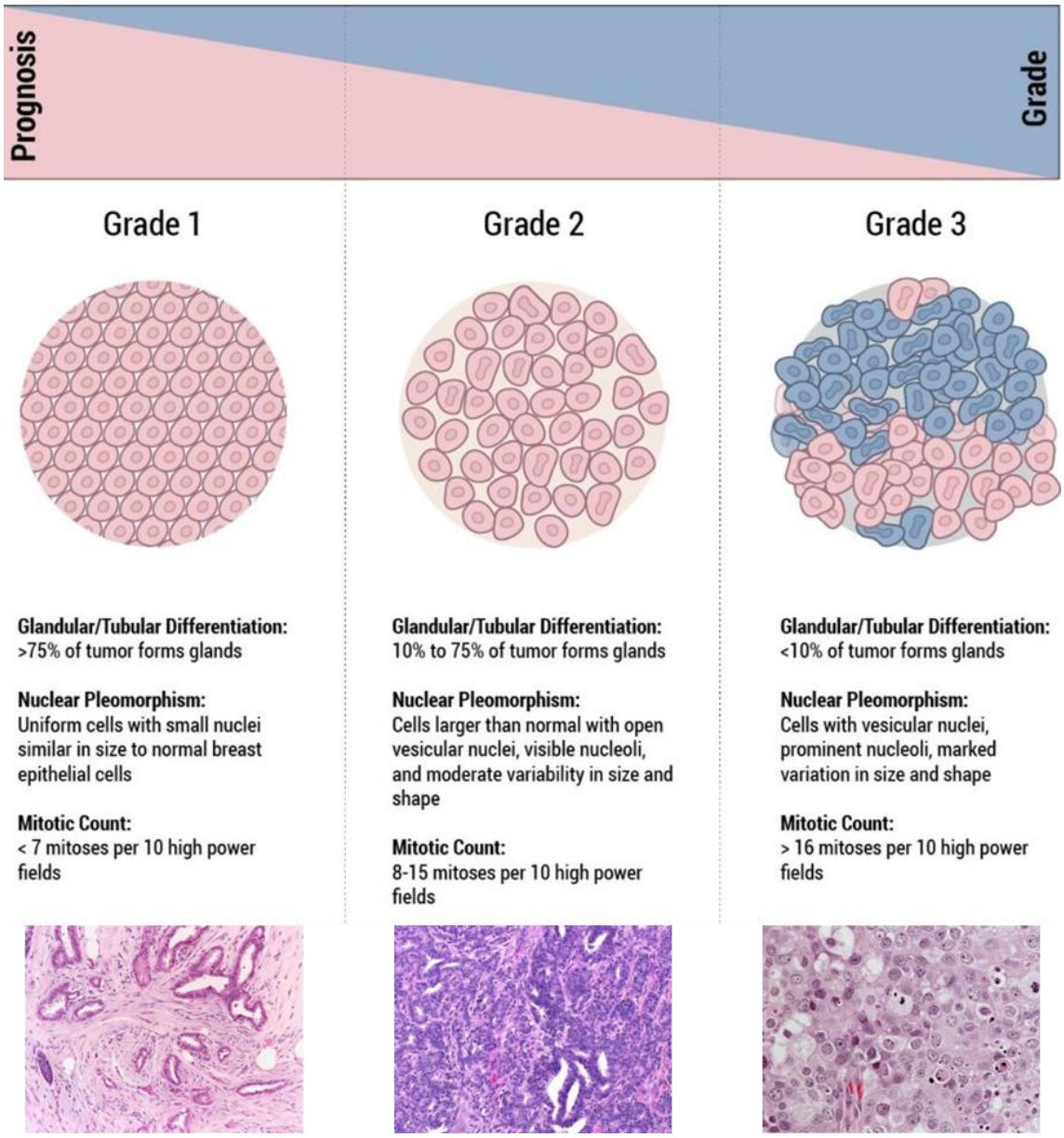

Figure 11. Histological Grade in Breast Cancer [95].

Expression of proteins and genes

Receptor status

Breast cancer receptor status, most commonly defined by estrogen-receptor (ER), progesterone-receptor (PR), and human epidermal growth factor receptor 2 (HER2) status in the clinical setting, has major implications for breast cancer prevention strategies and patient management [96–98]. Estrogen receptor (ER) is an important diagnostic determinant, as approximately 70–75% of invasive breast carcinomas are characterized by significantly high ER expression [99,100]. The progesterone receptor (PR) is expressed in more than 50% of ER-positive patients, and very rarely in those with ER-negative breast cancer. PR expression is regulated by ER [101]; therefore, physiological PR values inform about the functional ER pathway. Human epidermal growth factor receptor 2 (HER2) expression accounts for approximately 15–25% of breast cancers and its status is mainly relevant in the choice of appropriate treatment [102,103]. HER2 overexpression is one of the earliest events during breast carcinogenesis [103]. HER2 increases the detection rate of metastatic or recurrent breast cancers by 50% and even 80%. HER2 overexpression also correlates with a significantly shorter disease-free period [104]. The Ki67 antigen is a cellular marker of proliferation and is an excellent marker for providing information on cell proliferation. The proliferative activities determined by Ki67 reflect the aggressiveness of the cancer along with response to treatment and time to recurrence [105,106].

Gene expression

Breast tumors have been classified in molecular subtypes with distinctive clinical characteristics and a recognizable gene expression signature [107]. Such signature has been reduced to 50 genes that achieve the best separation of subtypes, attaining the PAM50 classifier [50,97]. PAM50 classifies breast cancer into five molecular intrinsic subtypes: Luminal A, Luminal A, Luminal B, human epidermal growth factor receptor 2 (HER2)-enriched, Basal-like and Normal-like [108,109]. Each of the five molecular subtypes vary by their biological properties and prognoses

[110–112] . Luminal A generally has the best prognosis; HER2-enriched and Basal-like are considered more aggressive diseases. Less common subtypes, such as Claudin-low, Interferon-rich and Molecular Apocrine, have also been identified using other gene expression profiling assays [113–116]. The molecular classification of breast cancer was shown in Figure 12.

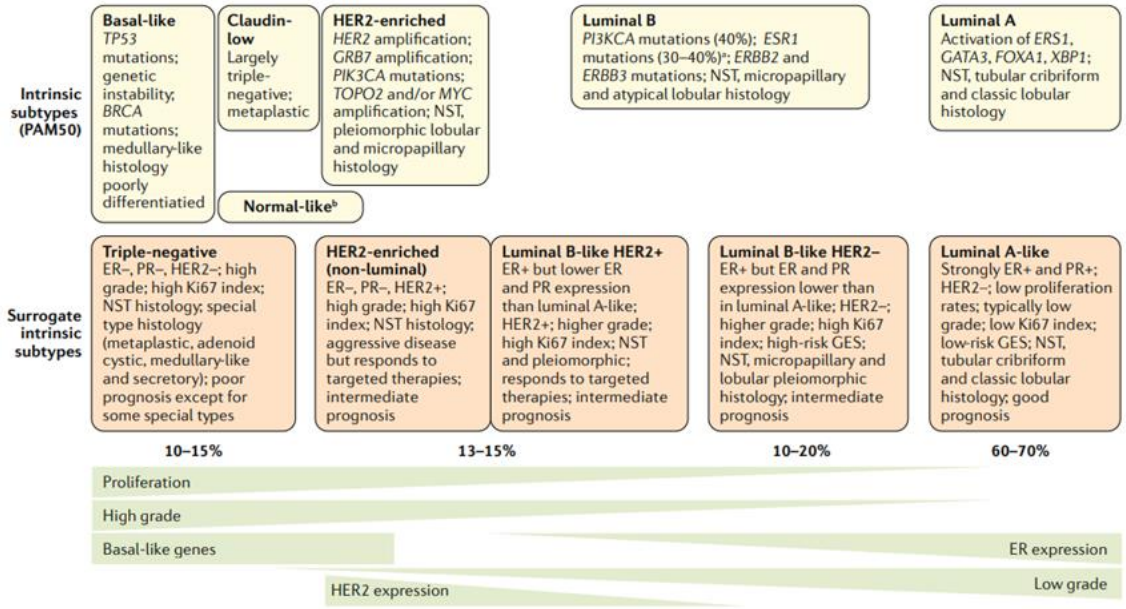

Figure 12. Molecular classification of breast cancer. The intrinsic subtypes of Perou and Sorlie are based on a 50-gene expression signature (PAM50). The surrogate intrinsic subtypes are typically used clinically and are based on histology and immunohistochemistry expression of key proteins: estrogen receptor (ER), progesterone receptor (PR), human epidermal growth factor receptor 2 (HER2) and the proliferation marker Ki67 [88].

Breast cancer treatment

Breast cancer prognosis and treatment options are based on tumor-node-metastasis staging [117]. Lymphovascular spread, histologic grade, hormone receptor status, ERBB2 (formerly HER2 or HER2/neu) overexpression, comorbidities, and patient menopausal status and age are also important factors [118]. One of the therapy options is neoadjuvant combination therapy, often including targeted agents, which is a standard of care (especially in ERBB2-positive and triple-negative breast cancer), and the basis for de-escalation of surgery in the breast and axilla and for risk-adapted post-neoadjuvant strategies [119]. Despite ERBB2 is proposed in a new nomenclature, to facilitate integration of

large datasets accumulated for the last decades, within this manuscript the HER2 synonym will be used. Radiotherapy still remains a cornerstone of breast cancer therapy, but de-escalation schemes have become the standard of care. ER-positive tumors are treated with 5–10 years of endocrine therapy and chemotherapy, based on an individual risk assessment. For metastatic breast cancer, standard therapy options include targeted approaches such as CDK4 and CDK6 inhibitors, PI3K inhibitors, PARP inhibitors, and anti-PD-L1 immunotherapy, depending on tumor type and molecular profile [119]. Below, there are presented important drugs used in the treatment of breast cancer (based on the list from National Cancer Institute).

- Tamoxifen (Nolvadex), Anastrozole (Arimidex), Letrozole (Femara), Exemestane (Aromasin), and Fulvestrant (Faslodex) are hormonal therapy drugs that target the hormone receptors in breast cancer cells to prevent the growth and spread of cancer cells.

- Palbociclib (Ibrance), Ribociclib (Kisqali), and Abemaciclib (Verzenio) are CDK4/6 inhibitors, which means they block a type of enzymes, cyclin-dependent kinases, that promote cell division. These drugs are typically used in combination with hormonal therapy.

- Trastuzumab (Herceptin), Pertuzumab (Perjeta), Lapatinib (Tykerb), Neratinib (Nerlynx), and T-DM1 (Kadcyla) are drugs that specifically target HER2-positive breast cancer cells, which have a higher number of HER2 receptors than normal cells.

- Bevacizumab (Avastin) is a monoclonal antibody that targets a protein called vascular endothelial growth factor (VEGF), which helps cancer cells to attract new blood vessels to grow and spread - angiogenesis. This drug is used to treat certain types of advanced or metastatic breast cancer.

- Capecitabine (Xeloda), Docetaxel (Taxotere), Doxorubicin (Adriamycin), Epirubicin (Ellence), Cyclophosphamide (Cytoxan), Paclitaxel (Taxol), Nab-paclitaxel (Abraxane), Gemcitabine (Gemzar), Vinorelbine

(Navelbine), Eribulin (Halaven), Ixabepilone (Ixempra), and Mitoxantrone (Novantrone) are chemotherapy drugs that work by killing rapidly dividing cancer cells.

- Methotrexate (Rheumatrex), Carboplatin (Paraplatin), and Cisplatin (Platinol) are also chemotherapy drugs used to treat breast cancer.

- Olaparib (Lynparza) and Talazoparib (Talzenna) are PARP inhibitors that are used to treat certain types of advanced or metastatic breast cancer with BRCA mutations.

- Ribociclib/letrozole (Kisqali Femara Co-Pack) and Abemaciclib/fulvestrant (Verzenio) are combination therapies that include a CDK4/6 inhibitor with hormonal therapy to treat hormone receptor-positive, HER2-negative advanced or metastatic breast cancer.

Although there are many available therapies for breast cancer, new therapies are constantly being developed to improve outcomes and reduce side effects.

Shelterin complex at telomeres

Telomeres are the genomic portions containing DNA and proteins at the ends of linear chromosomes [120]. Telomeric DNA in vertebrates is made of a hexameric nucleotide repeat sequence (TTAGGG) that is initially double-stranded DNA (dsDNA) but ends with single-stranded DNA (ssDNA) called overhang (G'-overhang) [121]. The extended 5′ to 3′ DNA strand contains the G-rich telomeric repeats and is referred to as the G-strand, while the 3′ to 5′ strand is defined as the C-strand [122]. Telomere repeats are lost with each cycle of DNA replication [123,124]. This is because RNA primers attach at the lagging strand during the synthesis of Okazaki fragments, and the resulting shedding RNA leads to telomere shortening [125]. This so-called "end replication problem" results in eventual apoptosis, cellular senescence, and cell cycle arrest [121,126,127]. Furthermore, telomeric DNA is are associated with specific proteins composed of six subunits (TRF1, TRF2, RAP1, TPP1, TIN2, and POT1) that compose shelterin (Figure 13) [128,129]. The shelterin complex constitutes the so-called capping end of the telomeres, which is essential for their protection, preventing telomeres from fusion to other chromosome ends, reducing telomere fragility, and protecting from degradation [130]. Also, the shelterin complex allows DNA to form a lasso-like structure with a telomeric loop (T-loop) and a displacement loop (D-loop) that then shields the 3′-end from DNA damage and blocks the activation of the DNA repair mechanisms, such as ataxia-telangiectasia Rad3-related (ATR)-mediated DNA damage kinase signaling and ataxia-telangiectasia mutation (ATM) kinase cascades, as well as unwanted repair reactions [131]. However, in cancers, mutations in the shelterin complex that cause telomere dysfunction and dysregulation are very common [132].

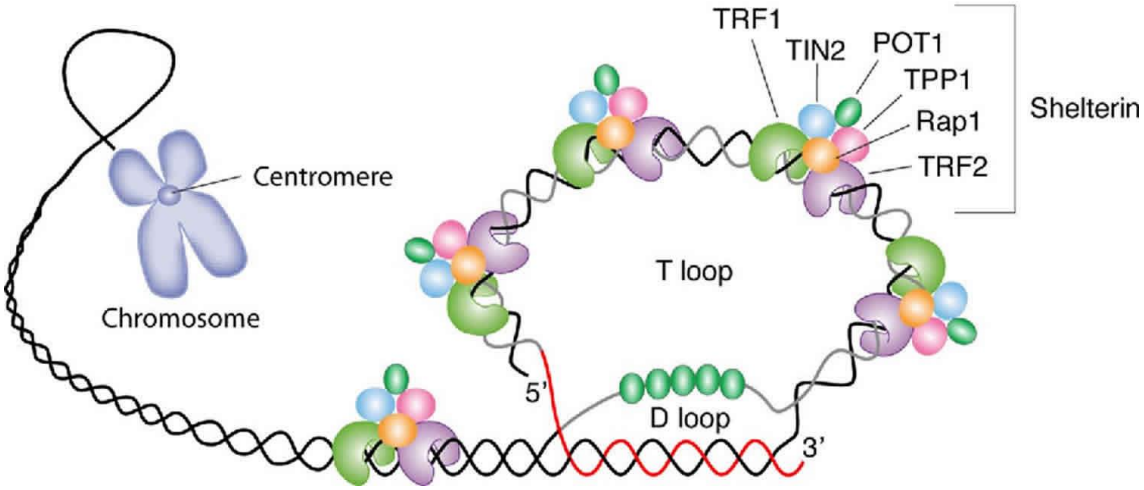

Figure 13. Schematic representation of Telomere structure [129].

TRF1 (Telomeric Repeat Binding Factor 1)

The TRF1 protein consists of 439 amino acids. The TRF1 protein exists in two isoforms (based on Uniprot.org).

TRF1

Length 439 aa

Mass 50.246 kDa

MAEDVSSAAPSPRGCADGRDADPTEEQMAETERNDEEQFECQELLECQVQV
GAPEEEEEEEEDAGLVAEAEAVAAGWMLDFLCLSLCRAFRDGRSEDFRRTR
NSAEAIIHGLSSLTACQLRTIYICQFLTRIAAGKTLDAQFENDERITPLESALMIW
GSIEKEHDKLHEEIQNLIKIQAIAVCMENGNFKEAEEVFERIFGDPNSHMPFKSK
LLMIISQKDTFHSFFQHFSYNHMMEKIKSYVNYVLSEKSSTFLMKAAAKVVESK
RTRTITSQDKPSGNDVEMETEANLDTRKSVSDKQSAVTESSEGTVSLLRSHK
NLFLSKLQHGTQQQDLNKKERRVGTPQSTKKKKESRRATESRIPVSKSQPVT
PEKHRARKRQAWLWEEDKNLRSGVRKYGEGNWSKILLHYKFNNRTSVMLKD
RWRTMKKLKLISSDSED

Pin2

Length 419 aa

Mass 48.239 kDa

MAEDVSSAAPSPRGCADGRDADPTEEQMAETERNDEEQFECQELLECQVQV
GAPEEEEEEEEDAGLVAEAEAVAAGWMLDFLCLSLCRAFRDGRSEDFRRTR
NSAEAIIHGLSSLTACQLRTIYICQFLTRIAAGKTLDAQFENDERITPLESALMIW
GSIEKEHDKLHEEIQNLIKIQAIAVCMENGNFKEAEEVFERIFGDPNSHMPFKSK
LLMIISQKDTFHSFFQHFSYNHMMEKIKSYVNYVLSEKSSTFLMKAAAKVVESK
RTRTITSQDKPSGNDVEMETEANLDTRKRSHKNLFLSKLQHGTQQQDLNKKE
RRVGTPQSTKKKKESRRATESRIPVSKSQPVTPEKHRARKRQAWLWEEDKN
LRSGVRKYGEGNWSKILLHYKFNNRTSVMLKDRWRTMKKLKLISSDSED

It is involved in binding to the duplex array of TTAGGG repeats at the telomeres [133,134]. It has specific conserved domains which assist in the formation of a stable TRF1-TRF1 homodimeric structure along with the two myb-like domains of the homodimer which help in a stable interaction with the duplex DNA at the telomere by binding to it at a specific bending angle of approximately 120^{o} [135]. The TRF1 binds to Telomere Repeat Binding Factor 2 (TRF2) via TRF-1 Interacting Nuclear Protein-2 (TIN2), which holds two homodimers of TRF1 and TRF2 together (Figure 14) [135–137].

The major function of TRF1 is to negatively regulate the telomere length by suppressing the telomerase activity [138]. It is also known to interact with the telomere during interphase and mitosis [139,140]. Accessibility of TRF1 is essential for the maintenance of telomeres, and downregulation of TRF1 can activate the ATR kinase and consequently induce fragile site phenotypes at the telomere [128]. Besides chromosome protection, TRF1 also plays a critical role in sister telomere cohesion [141,142], DNA damage responses [143,144], telomere transcription, and replication [145,146]. Replication machinery encounters significant challenges at telomeres due to the TTAGGG repeats, which resemble fragile sites [147]. TRF1 is essential for efficient replication by recruiting helicase and a shelterin repressor to solve TTAGGG repeat-associated replication issues [148,149].

TRF1 is overexpressed in several cancer types, such as renal cell carcinoma [150] and gastrointestinal tumors [151], and is upregulated in glioblastoma multiforme (GBM). Brain-specific TRF1 genetic deletion in GBM mouse models inhibits tumor initiation and progression, increasing mice survival. In addition, deleted TRF1 increases telomeric DNA damage and reduces proliferation and stemness.

TRF1 chemical inhibitors of its function mimicked these effects in human GBM cells and also blocked tumor sphere formation in vitro [121,152].

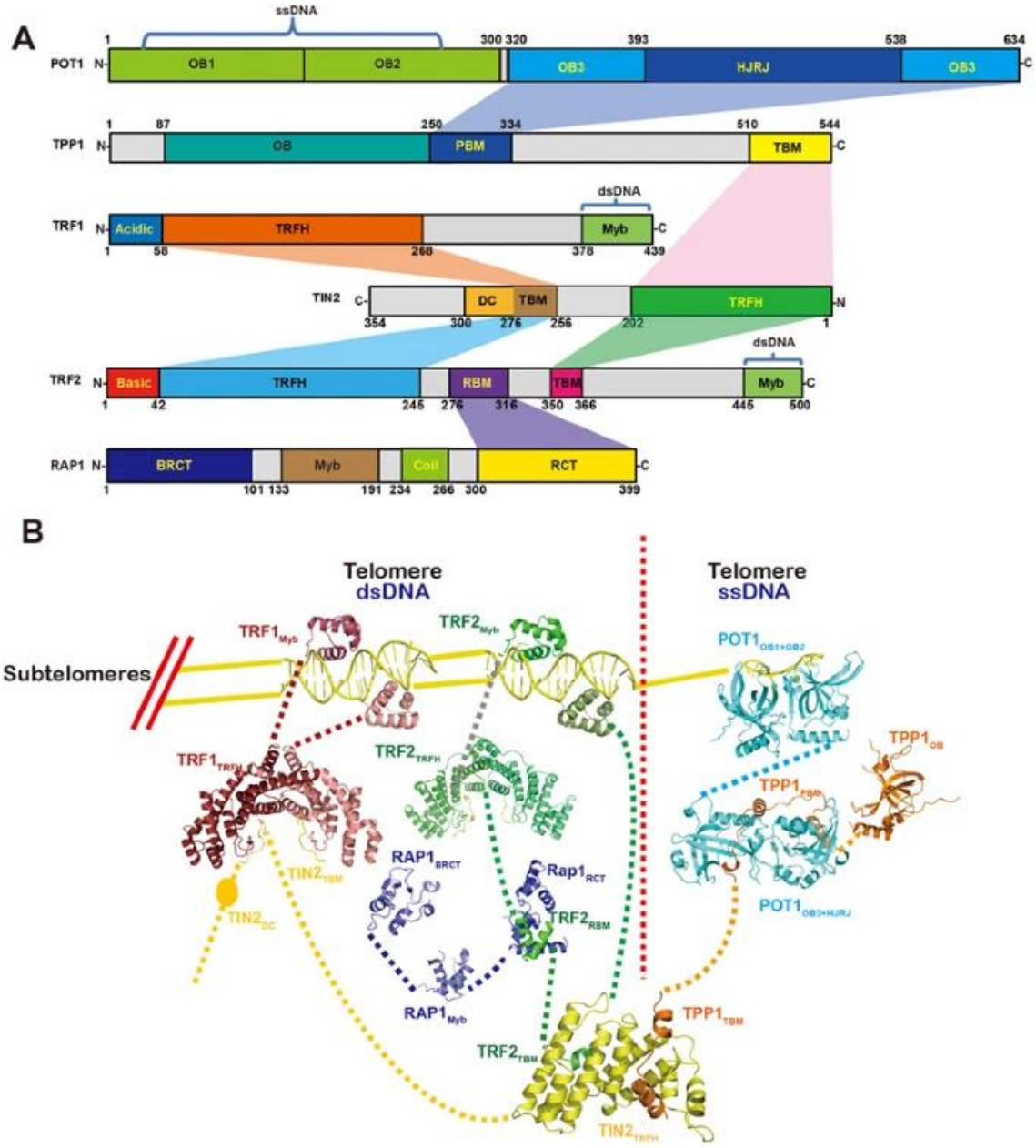

Figure 14. The structure of human shelterin complex. A - domain organization of the shelterin components. B - The structural model of human shelterin complex based on currently available structures, including $TRF1_{Myb}$-dsDNA (PDB: 1W0T), $TRF2_{Myb}$-dsDNA (PDB: 1W0U), $POT1_{OB1+OB2}$-ssDNA (PDB: 1XJV), $TRF1_{TRFH}$ in complex with $TIN2_{TBM}$ (PDB: 3BQO), $TRF2_{TRFH}$ in complex with $TIN2_{TBM}$ (PDB: 3BU8), $RAP1_{BRCT}$ (modeled from PDB 2L42), $RAP1_{Myb}$(PDB: 1FEX), $RAP1_{RCT}$ in complex with $TRF2_{RBM}$ (PDB: 3K6G), $TPP1_{OB}$ (PDB: 2I46), $POT1_{OB3+HJRJ}$ in complex with $TPP1_{PBM}$ (PDB: 5H65), and $TIN2_{TRFH}$ in complex with $TPP1_{TBM}$ and $TRF2_{TBM}$. All DNAs are shown in yellow. Dashed lines indicate the flexible linkers connecting these structural modules. For clear illustration purpose, only one RAP1 and TIN2 are presented, and only one $TRF2_{TBM}$ and $TRF2_{RBM}$ from a TRF2 monomer are shown [137].

TRF2 (Telomeric Repeat Binding Factor 2)

Telomeric Repeat Binding Factor 2 (TRF2) comprises 542 amino acid residues. TRF2 protein exists in two isoforms (based on Uniprot.org).

TRF2

Length 542 aa

Mass 59.594 kDa

MAAGAGTAGPASGPGVVRDPAASQPRKRPGREGGEGARRSDTMAGGGGS
SDGSGRAAGRRASRSSGRARRGRHEPGLGGPAERGAGEARLEEAVNRWVL
KFYFHEALRAFRGSRYGDFRQIRDIMQALLVRPLGKEHTVSRLLRVMQCLSRI
EEGENLDCSFDMEAELTPLESAINVLEMIKTEFTLTEAVVESSRKLVKEAAVIICI
KNKEFEKASKILKKHMSKDPTTQKLRNDLLNIIREKNLAHPVIQNFSYETFQQK
MLRFLESHLDDAEPYLLTMAKKALKSESAASSTGKEDKQPAPGPVEKPPREP
ARQLRNPPTTIGMMTLKAAFKTLSGAQDSEAAFAKLDQKDLVLPTQALPASPA
LKNKRPRKDENESSAPADGEGGSELQPKNKRMTISRLVLEEDSQSTEPSAGL
NSSQEAASAPPSKPTVLNQPLPGEKNPKVPKGKWNSSNGVEEKETWVEEDE
LFQVQAAPDEDSTTNITKKQKWTVEESEWVKAGVQKYGEGNWAAISKNYPFV
NRTAVMIKDRWRTMKRLGMN

Length 293 aa

Mass 32.298 kDa

MAAGAGTAGPASGPGVVRDPAASQPRKRPGREGGEGARRSDTMAGGGGS
SDGSGRAAGRRASRSSGRARRGRHEPGLGGPAERGAGEARLEEAVNRWVL
KFYFHEALRAFRGSRYGDFRQIRDIMQALLVRPLGKEHTVSRLLRVMQCLSRI
EEGENLDCSFDMEAELTPLESAINVLEMIKTEFTLTEAVVESSRKLVKEAAVIICI
KNKEFEKASKILKKHMSKDPTTQKLRNDLLNIIREKNLAHPVIQNFSYETFQQK
MLRFLESHLDDAEPYLLTVRLGPSPITMVCP

It is involved in binding to the duplex array of TTAGGG repeats at the telomeres. TRF2 binds to the double stranded/single stranded DNA junction [153,154]. Like TRF1, it is also a homodimer with C-terminal myb-like domains for binding directly to the DNA. It is ubiquitously expressed, bound specifically to duplex TTAGGG repeats also *in vitro* and localized to all human telomeres in metaphase chromosomes. TRF2 shares an architectural similarity with TRF1 but it still differs from TRF1 in that its N-terminus is basic rather than acidic and is much more conserved than TRF1 [155]. TRF2 binds to component RAP1 which contains a myb domain [132] (Figure 14).

TRF2 suppresses an ATM-dependent DDR (DNA damage response) at chromosome ends and inhibits end-to-end chromosome fusions and classical NHEJ (Non-homologous end joining) by folding telomeric DNA into a t-loop. Moreover, TRF2 and RAP1 are essential to prevent t-loop cleavage by repressing the activation of PARP1 (poly-ADP-ribose polymerase 1) to protect telomeres from HR-mediated repair in mammals [156].

As with the TRF1-knockout mice, TRF2-knockout mice are lethal at embryo stage [157]. TRF2 over-expressing mice under the 5′-regulatory region of the keratin 5 (K5) gene have increased vulnerability to spontaneous skin tumors and are sensitive to UV-induced carcinogenesis [158–160]. TRF2 production is often raised in human skin carcinomas [158]. Patients with xeroderma pigmentosum who have XPF, a nuclease associated with UV-damage repair, specific mutations are susceptible to TRF2-associated telomere shortening and chromosomal instability [121,158].

TIN2 (TRF1- Interacting Nuclear Protein 2)

TRF1-interacting protein 2 (TIN2) comprises 451 amino acids. TIN2 protein exists in three isoforms (based on Uniprot.org) .

TIN2L

Length 451 aa

Mass 50.023 kDa

MATPLVAGPAALRFAAAASWQVVRGRCVEHFPRVLEFLRSLRAVAPGLVRYR
HHERLCMGLKAKVVVELILQGRPWAQVLKALNHHFPESGPIVRDPKATKQDL
RKILEAQETFYQQVKQLSEAPVDLASKLQELEQEYGEPFLAAMEKLLFEYLCQ
LEKALPTPQAQQLQDVLSWMQPGVSITSSLAWRQYGVDMGWLLPECSVTDS
VNLAEPMEQNPPQQQRLALHNPLPKAKPGTHLPQGPSSRTHPEPLAGRHFNL
APLGRRRVQSQWASTRGGHKERPTVMLFPFRNLGSPTQVISKPESKEEHAIY
TADLAMGTRAASTGKSKSPCQTLGGRALKENPVDLPATEQKENCLDCYMDPL
RLSLLPPRARKPVCPPSLCSSVITIGDLVLDSDEEENGQGEGKESLENYQKTK
FDTLIPTLCEYLPPSGHGAIPVSSCDCRDSSRPL

TIN2S

Length 354 aa

Mass 39.444 kDa

MATPLVAGPAALRFAAAASWQVVRGRCVEHFPRVLEFLRSLRAVAPGLVRYR
HHERLCMGLKAKVVVELILQGRPWAQVLKALNHHFPESGPIVRDPKATKQDL
RKILEAQETFYQQVKQLSEAPVDLASKLQELEQEYGEPFLAAMEKLLFEYLCQ
LEKALPTPQAQQLQDVLSWMQPGVSITSSLAWRQYGVDMGWLLPECSVTDS
VNLAEPMEQNPPQQQRLALHNPLPKAKPGTHLPQGPSSRTHPEPLAGRHFNL
APLGRRRVQSQWASTRGGHKERPTVMLFPFRNLGSPTQVISKPESKEEHAIY
TADLAMGTRAASTGKSKSPCQTLGGRALKENPVDLPATEQKE

Length 137 aa

Mass 15.434 kDa

MATPLVAGPAALRFAAAASWQVVRGRCVEHFPRVLEFLRSLRAVAPGLVRYR
HHERLCMGLKAKVVVELILQGRPWAQVLKALNHHFPESGPIVRDPKATKQDL
RKILEAQETFYQQVKQLSEAPVDLASKLQVRLV

The 196 residues at the N-terminal of TIN2 are responsible for mitochondrial localization and also for interaction with TPP1 in both cytoplasm and nucleus [131,161]. Localization of TIN2 in mitochondria is responsible for bringing down the ATP production and increasing reactive oxygen species (ROS) in case of aging, whereas the absence of TIN2 in mitochondria will increase the ATP production and bring down ROS which could lead to the increased metabolic proliferation of the cell and in the long run can lead to uncontrolled proliferation and instability in cells [162]. Disruption of this region can reduce the localization of TIN2 towards nuclear/telomeric while promoting its cytoplasmic/mitochondrial targeting [132].

As an adaptor protein, TIN2 plays a linking role at the shelterin complex. Also, this vital protein can bind TRF1 and TPP1-POT1 complex (Figure 14), which constructs the bridge between different shelterin components [153]. Furthermore, the attachment of TIN2 to TRF1 induces changes in TRF1 conformation and stabilizes the telomeric structure, and these changes inhibit telomerase access to telomeres [163,164].

The over-expression of TIN2 has been shown to prevent telomere elongation in several human cell lines, such as HT1080 (human fibrosarcoma cell line), WI-38 (fibroblast-like fetal lung cell line), U2OS (bone osteosarcoma epithelial cell line), HTB9 (bladder carcinoma cell line), C33A (cervical carcinoma cell line), MDA-452 (breast cancer cell line), and HMT-3522 (non-tumorigenic human breast

epithelial cell line) [121]. In contrast, the expression of a dominant-negative TIN2 results in uncontrolled telomere elongation [165] . Chiang et al. [166] have observed that early embryonic lethality occurs in mice with TIN2 deletion, similar to the findings of TRF1- and TRF2-deficient mice [157,167]. Low expression of TRF1, TRF2, and TIN2 have been detected in human gastric carcinoma [151], and down-regulation of TRF1, TRF2, and TIN2 gene expression may be vital to maintain telomeres in gastric cancers [168]. Low expression of TRF1, TRF2, and TIN2 have also been found in patients with adult T-cell leukemia [169]. Increased expression of TRF1, TRF2, and TIN2 is linked to telomere shortening during multi-step hepatocarcinogenesis [170].

RAP1 (Human Repressor Activator Protein 1)

Human Repressor Activator Protein 1 *(*RAP1), also known as TRF2 interacting protein of the shelterin complex, is composed of 399 amino acids (based on Uniprot.org).

RAP1

Length 399 aa

Mass 44.260 kDa

MAEAMDLGKDPNGPTHSSTLFVRDDGSSMSFYVRPSPAKRRLSTLILHGGGT
VCRVQEPGAVLLAQPGEALAEASGDFISTQYILDCVERNERLELEAYRLGPAS
AADTGSEAKPGALAEGAAEPEPQRHAGRIAFTDADDVAILTYVKENARSPSSV
TGNALWKAMEKSSLTQHSWQSLKDRYLKHLRGQEHKYLLGDAPVSPSSQKL
KRKAEEDPEAADSGEPQNKRTPDLPEEEYVKEEIQENEEAVKKMLVEATREF
EEVVVDESPPDFEIHITMCDDDPPTPEEDSETQPDEEEEEEEEKVSQPEVGAA
IKIIRQLMEKFNLDLSTVTQAFLKNSGELEATSAFLASGQRADGYPIWSRQDDI
DLQKDDEDTREALVKKFGAQNVARRIEFRKK

RAP1 forms a complex with TRF2 and is enlisted to telomeres to control telomere length (Figure 14) [171]. RAP1 improves the selective binding of TRF2 to telomeric DNA [172]. Mammalian RAP1 can shield telomeres from NHEJ activities in vitro and the context severe telomere uncapping induced by TRF2 dysfunction [173]. Loss of RAP1 function in human cells does not result in NHEJ, homology-directed repair (HDR), or a DNA damage response [174]. At the same time, mouse RAP1 has been shown to shield telomere ends by repressing HDR and preventing sister telomere

recombination [174]. RAP1 binds also to extra-telomeric DNA and acts as a transcriptional regulator [174,175]. RAP1 has also been reported to associate with I kappa B (IκB) kinases and activate nuclear factor kappa B (NF-κB) [176]. The expression of RAP1 has been shown to be significantly higher in breast tumor tissues than in the adjacent non-tumor tissues [176], suggesting that RAP1 could be involved in cancer progression. Moreover, RAP1 is reported to be highly expressed in colorectal cancer tissues, and the expression levels of RAP1 are significantly correlated with poor prognosis and metastasis [121,177].

TPP1 (POT1-TIN2 Organizing Protein)

The POT1-TIN2 Organizing Protein (TPP1) is composed of 458 amino acids. TPP1 protein exists in two isoforms (based on Uniprot.org).

Length 458 aa

Mass 48.976 kDa

MAGSGRLVLRPWIRELILGSETPSSPRAGQLLEVLQDAEAAVAGPSHAPDTSD
VGATLLVSDGTHSVRCLVTREALDTSDWEEKEFGFRGTEGRLLLLQDCGVHV
QVAEGGAPAEFYLQVDRFSLLPTEQPRLRVPGCNQDLDVQKKLYDCLEEHLS
ESTSSNAGLSLSQLLDEMREDQEHQGALVCLAESCLTLEGPCTAPPVTHWAA
SRCKATGEAVYTVPSSMLCISENDQLILSSLGPCQRTQGPELPPPDPALQDLS
LTLIASPPSSPSSSGTPALPGHMSSEESGTSISLLPALSLAAPDPGQRSSSQPS
PAICSAPATLTPRSPHASRTPSSPLQSCTPSLSPRSHVPSPHQALVTRPQKPS
LEFKEFVGLPCKNRPPFPRTGATRGAQEPCSVWEPPKRHRDGSAFQYEYEP
PCTSLCARVQAVRLPPQLMAWALHFLMDAQPGSEPTPM

Length 455 aa

Mass 48.627 kDa

MAGSGRLVLRPWIRELILGSETPSSPRAGQLLEDAEAAVAGPSHAPDTSDVG
ATLLVSDGTHSVRCLVTREALDTSDWEEKEFGFRGTEGRLLLLQDCGVHVQV
AEGGAPAEFYLQVDRFSLLPTEQPRLRVPGCNQDLDVQKKLYDCLEEHLSES
TSSNAGLSLSQLLDEMREDQEHQGALVCLAESCLTLEGPCTAPPVTHWAASR
CKATGEAVYTVPSSMLCISENDQLILSSLGPCQRTQGPELPPPDPALQDLSLTL
IASPPSSPSSSGTPALPGHMSSEESGTSISLLPALSLAAPDPGQRSSSQPSPAI
CSAPATLTPRSPHASRTPSSPLQSCTPSLSPRSHVPSPHQALVTRPQKPSLEF
KEFVGLPCKNRPPFPRTGATRGAQEPCSVWEPPKRHRDGSAFQYEYEPPCT
SLCARVQAVRLPPQLMAWALHFLMDAQPGSEPTPM

It links TIN2 and POT1 while chiefly interacting with POT1 [178,179] (Figure 14). Concerning the role of TPP1 in linking TIN2 and other components of shelterin complex with POT1, any mutation leads to structural alteration in TPP1 for recruiting of the shelterin complex [132,180]. One of the most critical functions of TPP1 is the regulation of telomerase recruitment to telomeres via the interaction with telomerase reverse transcriptase (TERT), as a catalytic part of the telomerase, for telomere maintenance [180,181]. Besides, through mediators of DNA damage response such as ATM and ATR, TPP1 plays a pivotal role in growth arrest [182]. Therefore, POT1 and TPP1 bind as a heterodimer to ssDNA (single-strand DNA) telomere DNA to inhibit DNA damage responses from capped telomeres [183]. On the other hand, it was shown that mouse cells lacking TPP1 exhibit an increase in chromosomal fusions with non-homologous chromosomes [128,184]. TPP1 deficiency can cause telomere dysfunction phenotypes, including widespread epithelial dysplasia, defective hair follicle morphogenesis, growth, severe skin hyperpigmentation, and peri-natal death [121,128,185,186].

POT1 (Protection of Telomeres Protein-1)

Protection of telomeres protein 1 (POT1) is a protein with a sequence length of 634 amino acids. POT1 protein exists in two isoforms (based on Uniprot.org).

Length 634 aa

Mass 71.442 kDa

MSLVPATNYIYTPLNQLKGGTIVNVYGVVKFFKPPYLSKGTDYCSVVTIVDQTN
VKLTCLLFSGNYEALPIIYKNGDIVRFHRLKIQVYKKETQGITSSGFASLTFEGTL
GAPIIPRTSSKYFNFTTEDHKMVEALRVWASTHMSPSWTLLKLCDVQPMQYF
DLTCQLLGKAEVDGASFLLKVWDGTRTPFPSWRVLIQDLVLEGDLSHIHRLQN
LTIDILVYDNHVHVARSLKVGSFLRIYSLHTKLQSMNSENQTMLSLEFHLHGGT
SYGRGIRVLPESNSDVDQLKKDLESANLTANQHSDVICQSEPDDSFPSSGSVS
LYEVERCQQLSATILTDHQYLERTPLCAILKQKAPQQYRIRAKLRSYKPRRLFQ
SVKLHCPKCHLLQEVPHEGDLDIIFQDGATKTPDVKLQNTSLYDSKIWTTKNQ
KGRKVAVHFVKNNGILPLSNECLLLIEGGTLSEICKLSNKFNSVIPVRSGHEDLE
LLDLSAPFLIQGTIHHYGCKQCSSLRSIQNLNSLVDKTSWIPSSVAEALGIVPLQ
YVFVMTFTLDDGTGVLEAYLMDSDKFFQIPASEVLMDDDLQKSVDMIMDMFC
PPGIKIDAYPWLECFIKSYNVTNGTDNQICYQIFDTTVAEDVI

Length 538 aa

Mass 60.534 kDa

MSLVPATNYIYTPLNQLKGGTIVNVYGVVKFFKPPYLSKGTDYCSVVTIVDQTN
VKLTCLLFSGNYEALPIIYKNGDIVRFHRLKIQVYKKETQGITSSGFASLTFEGTL
GAPIIPRTSSKYFNFTTEDHKMVEALRVWASTHMSPSWTLLKLCDVQPMQYF
DLTCQLLGKAEVDGASFLLKVWDGTRTPFPSWRVLIQDLVLEGDLSHIHRLQN
LTIDILVYDNHVHVARSLKVGSFLRIYSLHTKLQSMNSENQTMLSLEFHLHGGT
SYGRGIRVLPESNSDVDQLKKDLESANLTANQHSDVICQSEPDDSFPSSGSVS
LYEVERCQQLSATILTDHQYLERTPLCAILKQKAPQQYRIRAKLRSYKPRRLFQ
SVKLHCPKCHLLQEVPHEGDLDIIFQDGATKTPDVKLQNTSLYDSKIWTTKNQ
KGRKVAVHFVKNNGILPLSNECLLLIEGGTLSEICKLSNKFNSVIPVRSGHEDLE
LLDLSAPFLIQGTIHHYGCKQCSSLRSIQNLNSLVDKTSWIPSSVAEDVNSVLV

POT1 interacts with TPP1 and attaches to the ssDNA 3′ overhang (Figure 14), thereby repressing ATR-mediated DDR by stopping the recruitment of replication protein A (RPA) to the ssDNA [187]. Also, POT1 can bind to TRF1 [188] via protein-protein interactions. G-quadruplex formation (non-canonical DNA structure formed by G-rich DNA) inhibits telomere elongation; however, POT1 by displacing/replacing a G-quadruplex structure promotes telomerase activity [189]. Besides, POT1 regulates telomere length and telomere capping, and it has a vital role in the regulation of telomerase activity on telomeres. Furthermore, several functions of this protein include protection of chromosome ends from recombination, catastrophic chromosome instability, and abnormal chromosome segregation [190]. Two POT1 orthologs, POT1a and POT1b, are present in the mouse [121]. Double knockout cells for the POT1a and POT1b genes have been demonstrated to result in telomere elongation, an increase in DNA damage foci at the telomeres, endo-reduplication, and early initiation of senescence [191]. POT1 mRNA concentrations have been significantly linked with telomere length in colon and gastric cancer cells [191,192]. A known variant of POT1, with D224N mutation, disrupts POT1 binding to ssDNA telomere oligonucleotides, leading to longer and fragile telomeres, predisposing for chronic leukocyte leukemia, glioma, angiosarcoma, osteosarcoma, thyroid cancer, colorectal cancer, and cutaneous melanoma [193]. Convergently, the shelterin complex interacts with more than 300 proteins, including RING-finger- or U-box-containing proteins, functioning as ubiquitin E3 ligases or stability regulators for telomere-associated proteins, protein phosphatase catalytic and regulatory subunits (PPM1G, PHPT1, PTPN5, SAPS3, and PPP1R2), and phosphorylation-related kinases (Akt1, CAMK1D,

CLK3, MAP2K3, MAP4K2, MAPK12, and PAK4) [194] , indicating that the complex not only stabilizes the chromosomal ends and protects hosts from diseases, but also acts as a busy hub for the complex signaling net workflow [121].

Regulation of shelterin complex in cancer

Recent studies show that components of the shelterin complex display several mutations in cancer. In particular, multiple studies have reported the downregulation of TRF1 in breast cancer [195–198]. This is correlated with the overexpression of an oncomiR, miR-155, which targets a partially conserved site in the 3′UTR of TRF1. Overexpression of miR-155 has been reported in over 80% of breast cancers that were associated with TRF1 downregulation [198]. The TRF1 was far less abundant in almost all breast cancer tissues examined compared to normal tissue, implicating the maintenance of longer telomeres for the prolonged proliferation of cancer cells [196]. Moreover, it was shown that TIN2 was overexpressed in more than half of the breast cancer cell lines studied, and its silencing by shRNA caused a decrease in cell proliferation and migration [199]. Although the expression of TRF1 and TRF2 was not examined in this study, it is likely that the silencing of TIN2 would also cause the suppression of TRF1 and TRF2, at least at functional level (TIN2 is necessary for bridging TRF1 and TRF2 into functional complex). In contrast to downregulation of TRF1 in cancer, the upregulation of TRF2 in breast cancer protects critically short telomeres from being recognized as DNA damage sites, preventing apoptosis [200]. Considering other shelterin components in breast cancer, the level of RAP1 and NF-κB were highly correlated and associated with higher breast cancer grades [201].

Among other types of cancer, aberrations in shelterin complex and telomeres are frequently observed. In lung cancer, telomere attrition occurs at the earliest stage of lung carcinogenesis as an initiating event, preceding TRF1 and TRF2 overexpression for telomere stabilization [202]. Furthermore, primary endothelial cells isolated from mouse tumors have increased expression of TRF2 compared to that of normal lung endothelial cells, and this corresponds to an increase in angiogenic properties such as proliferation, migration and tube formation [203].

In colorectal cancer patients, the upregulation of TRF2 was directly correlated with SULF2 upregulation, and tumors which had higher TRF2 levels also displayed stronger angiogenesis. These oncogenic properties of TRF2 appeared independent of its effects merely on telomeres and DNA damage response [203] and therapeutic strategies could be targeted at suppressing TRF2 in this type of cancer. In a model of colon multistep carcinogenesis, the data indicate that

telomeric length and protein TRF1 and TRF2 expression levels are inversely correlated with the activation of the DDR pathway [204]. Furthermore, the elongation of telomeric overhang by telomerase, which might be regulated by POT1, may contribute to the increase of malignant potential in colorectal cancers [205]. The role of shelterin complex in other cancer types is summarized in Table 2 [206].

Table 2. Role of shelterin complex in different cancer types [206].

Cancer	**Proteins expression levels**	**Suggested functional outcome/references**
Breast cancer	Downregulation of *TRF1*	Maintenance of long telomeres [196]
	Downregulation of TRF1 mRNA as cancer grade increases	Increased telomerase access and telomere elongation [195]
	Hypermethylation and downregulation of TRF1	[197]
	Repression of TRF1 by miRNA-155	Increased genomic instability and telomere fragility [198]
	Upregulation of TRF2	Protect critically short telomeres from being recognized as DNA damage, prevent apoptosis [200]
	Upregulation of TIN2	[199]
	Upregulation of RAP1	Resistance to chemotherapy and poorer prognosis [207]
	Downregulation of POT1 mRNA	Dysregulation of telomerase activity [208]
Lung cancer	Increase in TRF1 expression as disease progresses	[208]
	Increase in TRF2 expression as disease progresses	Increased tolerance to short telomeres, prevent apoptosis [208]
Colorectal cancer	Upregulation of TRF1	[209]
	Downregulation of TRF1 mRNA	[205]

	Downregulation of TRF1 expression in early cancer stage; re-expression of TRF1 in invasive stage cancer	Disrupted telomeric homeostasis [204]
Prostate cancer	Upregulation of TRF1	[183]
	Upregulation of TIN2	[210]
Gastric cancer	Downregulation of TRF1	Increased telomerase activity, maintenance of telomere length [204]
	Upregulation of TRF1	Telomere shortening, maintenance of chromosomal end, cell immortalization [151,211]
	Upregulation of TRF2	Protect and maintain telomere ends in cells with low telomerase activity, cell immortalization [151,211]
	Increase in TIN2 expression as disease progresses	Telomere shortening [151]
	Upregulation of RAP1	Interaction with TRF2 to inhibit the expression of ATM-dependent DSB responsive genes [212]
	Downregulation of POT1 mRNA in early cancer stage	Telomere dysfunction in early-stage cancer [213]
	Downregulation of POT1; expression decreases with disease severity	[214]
Hepatocellular carcinoma (HBV- and HCV-associated)	Upregulation of TRF1 mRNA and protein	Telomere shortening, increased chromosomal instability [215,216]
	Upregulation of TRF2	Telomere shortening, increased chromosomal instability [215]
	Upregulation of TIN2	Telomere shortening, increased chromosomal instability [215]
	Upregulation of POT1 mRNA	Preserved 3′ overhang length, unlimited division of cancer cells, increased chromosomal instability [215]

Hepatocellular carcinoma	Progressive upregulation of TRF1, TRF2 and TIN2 mRNA during carcinogenesis	Telomere shortening, increased chromosomal aberrations [170,217]
	Upregulation of RAP1	[218]
	Upregulation of TPP1	Maintenance of telomere length [218,219]
Glioblastoma	Upregulation of TRF1	[152]
	Upregulation of TRF1 in early carcinogenesis; downregulation of TRF1 in late stage cancer	Telomere shortening, increased chromosomal instability; telomerase activation [220]
	Upregulation of TRF2	GSC maintained in a highly proliferative and chemotherapy-resistant state [221]
	Downregulation of POT1	Poorer prognosis [213]
Acute lymphocytic leukemia	Upregulated of TRF1	[222]
Adult T-cell leukemia	Upregulated of TRF1	Progressive telomere shortening in telomerase-positive cells, increased genetic instability [169]
	Upregulation of TRF2	Telomere shortening in telomerase-positive cells, increased [169]
	Upregulation of TIN2	Telomere shortening in telomerase-positive cells, increased chromosomal instability [169]
Chronic lymphocytic leukemia	Upregulation of TRF1 mRNA and protein	[223]
	Downregulation of TRF1 and TRF2	[224,225]
	Downregulation of TIN2 mRNA and protein	Increased telomere DNA damage-induced foci [225,226]
	Upregulation of RAP1	Telomere shortening, increased genomic instability [227]
	Upregulation of TPP1	[223]

	Downregulation of TPP1 mRNA and protein	Increased telomere DNA damage-induced foci [225,226]
Chronic myeloid leukemia	Initial upregulation in TRF1; downregulation of TRF1 as disease progresses	Telomere shortening [228]
	Initial upregulation in TRF2; downregulation of TRF2 as disease progresses	Telomere shortening in telomerase-positive cells, increased chromosomal instability [169]
Non-small cell lung cancer	Upregulation of TRF1 mRNA and protein	Telomere dysfunction, altered checkpoint controls [229]
	Downregulation of TRF1 mRNA	[230,231]
	Upregulation of TRF2 mRNA and protein	Telomere dysfunction, altered checkpoint controls [229]
	Downregulation of TRF2	[232]
Pancreatic cancer	Downregulation of TRF1	[233]
Renal cell carcinoma	Upregulation of TRF1 and TRF2 mRNA and protein	[150]
Head and neck squamous cell carcinoma	Upregulation of TRF2	Interaction with phosphorylated p38, activation of p38 MAPK pathway [234]
Classical Hodgkin lymphoma (EBV-associated)	Downregulation of TRF2	Increased telomere fusions, giant chromosomes, hyperploidy, endomitosis [235,236]
Skin cancer (basal cell carcinoma, squamous cell carcinoma	Upregulation of TRF2	Dysregulation of NER [158]
Familial papillary thyroid cancer	Downregulation of RAP1 and POT1 as compared to sporadic cancers	[237]
Splenic marginal zone lymphomas	Downregulation of POT1	Increased chromosomal instability [238]

Melanoma	Upregulation of POT1	[239]

To summarize, mutations in shelterin complex genes have been found in various types of cancer, suggesting a potential role for this complex in tumorigenesis. It's worth noting that mutations in shelterin complex genes are relatively rare in most types of cancer, and more research is needed to determine their precise role in tumorigenesis. However, the identification of these mutations highlights the importance of telomere maintenance and genomic stability in cancer development and suggests that targeting the shelterin complex may have therapeutic potential in some cases of cancer.

Shelterin complex inhibitors

There has been considerable interest in developing small molecule inhibitors or modulators of the shelterin complex as potential therapeutics for cancer and other diseases. These compounds target different components of the complex and can have various effects on telomere length and function. Here are some examples of shelterin complex inhibitors:

TRF1 protein inhibitors

Alisertib (ETP-51634) - a small molecule inhibitor of Aurora A kinase, which plays a critical role in mitosis and cell division. The studies demonstrated that treatment with Alisertib led to telomere shortening and reduced TRF1 expression in lung cancer cells, indicating that the drug can have significant effects on telomere maintenance and TRF1 function. Other studies shown that Alisertib-induced DNA damage led to activation of the ATM kinase pathway, which in turn phosphorylated and destabilized TRF1, leading to telomere dysfunction [240,241].

Dasatinib (ETP-51801) - a tyrosine kinase inhibitor that targets several oncogenic signaling pathways, including BCR-ABL, Src family kinases, and receptor tyrosine kinases. The treatment with Dasatinib led to telomere shortening and reduced TRF1 expression in chronic myeloid leukemia cells, indicating that the drug can have significant effects on telomere maintenance and

TRF1 function. Another group found that Dasatinib-induced DNA damage led to activation of the ATM kinase pathway, which in turn phosphorylated and destabilized TRF1, leading to telomere dysfunction [240,241].

Epigallocatechin-3-gallate (EGCG) - a polyphenol compound found in green tea [242]. Some studies suggest that EGCG can inhibit the growth of cancer cells and induce cell death in various types of cancer, including breast, lung, prostate, and colon cancer [242–244]. Results also suggest that EGCG inhibits the binding of TRF1 to telomeric DNA, thus the shelterin complex's function in protecting telomeres could be inhibited [245].

Flavopiridol (ETP-47306) - a small molecule inhibitor of cyclin-dependent kinases (CDKs), a group of enzymes that play a key role in the regulation of cell cycle progression and DNA replication. CDKs have been shown to interact with components of the shelterin complex, including TRF1 and TRF2 (but not known molecular mechanism), and to be involved in the regulation of telomere maintenance and function [241]. Studies have suggested that CDK inhibition can lead to telomere dysfunction and chromosomal instability in cancer cells. For example, one group found that inhibition of CDK9, a key regulator of RNA polymerase II transcription, led to telomere shortening and reduced telomerase activity in glioblastoma cells [240,241], while another group found that inhibition of CDK4/6, which play a role in the G1/S transition of the cell cycle, led to telomere attrition and increased DNA damage in breast cancer cells [246].

Geldanamycin (ETP-50853) - is a known inhibitor of the HSP90 protein. HSP90 is a molecular chaperone that is involved in the folding, stability, and function of a wide range of client proteins, including TRF1. Geldanamycin has been shown to downregulate TRF1 expression and induce telomere dysfunction and apoptosis in cancer cells [240,241].

Gemcitabine (ETP-45337) - a nucleoside analog chemotherapy drug that inhibits DNA synthesis and repair by blocking the action of ribonucleotide reductase, an enzyme that is required for the production of deoxynucleotides necessary for DNA replication. The studies demonstrated that treatment with Gemcitabine led to telomere shortening and reduced TRF1 expression in pancreatic cancer cells, indicating that the drug can have significant effects on telomere maintenance and

TRF1 function. Other studies shown that Gemcitabine-induced DNA damage led to activation of the ATR kinase pathway, which in turn phosphorylated and destabilized TRF1, leading to telomere dysfunction [240,241].

GSK461364 (ETP-51799) - a small molecule inhibitor of Polo-like kinase 1 (PLK1), a serine/threonine kinase that plays a critical role in mitotic progression and cell division. PLK1 is known to interact with several components of the telomere-associated shelterin complex, including TRF1 and TRF2 (not known molecular mechanism), and has been implicated in the regulation of telomere length and stability. Studies provided evidence that PLK1 inhibition led to telomere shortening and reduced telomerase activity in non-small cell lung cancer cells, while other studies shown that PLK1 inhibition led to increased DNA damage at telomeres in breast cancer cells [240,241].

KU-0063794 (ETP-50537) - a small molecule inhibitor of the mammalian target of rapamycin (mTOR), a serine/threonine kinase that plays a critical role in regulating cell growth, proliferation and survival. mTOR is known to interact with several components of the shelterin complex, including TRF1 and TRF2 (not known molecular mechanism), and has been implicated in the regulation of telomere length and function. Studies have suggested that mTOR inhibition can lead to telomere dysfunction and chromosomal instability in cancer cells. One study shown that mTOR inhibition led to telomere shortening and reduced telomerase activity in acute myeloid leukemia cells, while another study demonstrated that mTOR inhibition led to increased DNA damage at telomeres in prostate cancer cells [240,241].

MST-312 - a peptide inhibitor. The peptide specifically targets the TRF1 protein and inhibits its interaction with telomeric DNA, leading to telomere dysfunction and eventual cell death. MST-312 has been shown to have potent anti-cancer activity in a variety of cancer cell lines, including breast, prostate, and lung cancer [247,248]. In preclinical studies, MST-312 has been shown to inhibit tumor growth and induce tumor cell apoptosis, making it a promising candidate for the development of novel cancer therapies [249].

SCH772984 (ETP-50728) - a small molecule inhibitor of the extracellular signal-regulated kinase (ERK) pathway, a signaling cascade that plays a critical role in

cell proliferation, survival and differentiation. The ERK pathway has been shown to interact with several components of the shelterin complex, including TRF1 and TRF2 (not known molecular mechanism), and has been implicated in the regulation of telomere maintenance and function. Studies have suggested that inhibition of the ERK pathway can lead to telomere dysfunction and chromosomal instability in cancer cells. For example, ERK inhibition led to telomere shortening and reduced telomerase activity in glioblastoma cells, while another study shown that ERK inhibition led to telomere attrition and increased DNA damage in breast cancer cells [240,241].

Selumetinib (ETP-51667) - a small molecule inhibitor of the mitogen-activated protein kinase kinase (MEK) pathway, a signaling cascade that is frequently activated in cancer cells and is involved in the regulation of cell proliferation, survival, and differentiation. The MEK pathway has been shown to interact with several components of the shelterin complex, including TRF1 and TRF2 (not known molecular mechanism), and has been implicated in the regulation of telomere maintenance and function. Studies have suggested that inhibition of the MEK pathway can lead to telomere dysfunction and chromosomal instability in cancer cells. The MEK inhibition led to telomere shortening and reduced telomerase activity in melanoma cells and also MEK inhibition led to telomere attrition and increased DNA damage in lung cancer cells [240,241].

TRF2 protein inhibitors

6-ThiodG (6-thio-2'-deoxyguanosine) - a nucleoside analog that gets incorporated into the telomeric DNA and alters the structure of the telomeres, leading to the inhibition of TRF2 binding [250].

Alexidine·2HCl - a small molecule compound with broad-spectrum antimicrobial activity. In addition to its antimicrobial properties, recent studies have shown that alexidine·2HCl may have the potential as a therapeutic agent for cancer treatment. Alexidine·2HCl impaired tumor growth, neo-angiogenesis and immunosuppression by downregulating TRF2 expression [251].

APOD (Apolipoprotein D) - a glycoprotein that is involved in various biological processes, including lipid metabolism, neuronal growth and differentiation, and

immune response [252]. Recent studies have also suggested a role for APOD in telomere maintenance and cellular senescence. The study has shown that APOD interacts with the TRF2 protein and promotes the formation of the T-loop structure at telomeres, which is essential for telomere protection and stability. This study also suggested that APOD may regulate telomere length and contribute to cellular senescence through its interaction with TRF2 [253] .

AR-A014418 - a small molecule inhibitor that has been shown to inhibit the activity of glycogen synthase kinase-3β (GSK-3β), which is involved in several signaling pathways. AR-A014418 impaired tumor growth, neo-angiogenesis and immunosuppression by downregulating TRF2 [251].

Arsenic trioxide (As_2O_3) - a chemotherapeutic agent that has been reported to induce apoptosis in cancer cells through various mechanisms, including inhibition of telomerase activity and induction of telomere dysfunction. The researchers investigated the effect of As_2O_3 on telomere maintenance in cancer cells and found that treatment with As_2O_3 led to a decrease in TRF2 protein levels and telomere dysfunction [254,255] .

Curcusone C - a natural compound that has been shown to have anticancer properties. It was found to bind to the TRF2 protein and block its localization in DNA, which induces DNA damage response (DDR) and ultimately cell death in cancer cells [256].

MST-312 (3,6-bis(1-methyl-4-vinylpyridinium)carbazole diiodide) - a cationic porphyrin derivative that binds to the telomeric DNA and inhibits TRF2 binding [257].

NSC232003 - a small molecule that has been shown to inhibit the binding of TRF2 to telomeric DNA [258].

RHPS4 (3,11-Difluoro-6,8,13-trimethyl-8H-quino[4,3,2-kl]acridinium methosulfate) - a small molecule that binds to the G-quadruplex structure formed by the telomeric DNA and inhibits the binding of TRF2 to the telomeres [259,260].

Sirtinol - a small molecule inhibitor of the sirtuin family of NAD+-dependent deacetylases, which have been shown to regulate TRF2 activity [261].

POT1 protein inhibitors

Congo red (CR) - a benzidine-based diazo dye that is commonly used as a histological stain for amyloid protein deposits in tissues. Studies have shown that CR can disrupt the interaction between POT1 in vitro [262].

ZINC00005600 and ZINC00020258 - interactions with the POT1 protein of these compounds possibly interrupt the natural state binding of POT1 with telomeric ssDNA, thus probably enhancing the telomere uncapping, elongation of the telomere, and chromosomal aberration which finally leads to cell death [263].

The development of shelterin protein inhibitors encounters several challenges. One major challenge in developing shelterin inhibitors for cancer therapy is to target cancer cells only and spare normal cells. Since telomeres and shelterin complexes are also present in normal cells, it is important to develop strategies to selectively target cancer cells while minimizing toxicity to normal cells or to elaborate inhibitors which action based on the same target will be more harmful for cancer cells than normal. Another challenge is to identify which specific types of cancer would be eradicated the most from these therapies.
Overall, the future of shelterin inhibitors in cancer therapy looks promising, but more research is needed to fully understand their potential as cancer treatments and to develop strategies to minimize potential side effects. This is still developing and underexplore area of medicinal chemistry.

Aims of the Thesis

Breast cancer is one of the leading causes of cancer-related deaths in women worldwide. Telomeres play a critical role in breast cancer development and progression. Telomere-binding proteins such as TRF1, TRF2, and TIN2 are essential for maintaining telomere integrity and preventing genomic instability. Cancer cells excessively use telomerase to enter unlimited life span and avoid cell death, thus gain advantage over normal cells. Inhibiting function of these proteins could be a potential strategy for breast cancer therapy.

The aim of the PhD thesis was to evaluate the efficacy and cellular responses of inhibitors/modulators interfering with TRF1-TIN2 and TRF2-TIN2 protein complexes as potential anticancer compounds disturbing the function of telomeres in breast cancer therapy, using breast cancer cell lines (*in vitro* studies) and patient-derived tumor samples (*ex vivo* studies).

The PhD thesis was expected to provide insights into the potential of TRF1-TIN2 and TRF2-TIN2 complexes' inhibitors as novel anticancer compounds for breast cancer therapy. The obtained results may on one hand verify importance of telomeric proteins as potential anticancer targets and on the other hand may contribute to the development of new therapeutic strategies for breast cancer and promote next-generation clinical trials targeting telomeres for anticancer therapy.

Materials and Methods

Compounds

The source and characteristics of the compounds used in this study are summarized in Table 3. The compounds were designed and selected within in silico studies performed previously by Umesh Kalathiya in the project STRATEGMED.

Table 3. The source and characteristics of the compounds: B070, B087, A822, ST2S, ST50, B176, B280, B327, A628, A378, A670, Doxorubicin and Etoposide.

Potential TRF1-TIN2 protein inhibitors	
B070 **(Brains On-line, USA)**	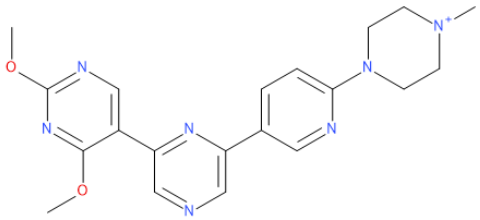 **Biofocus 035_0016_0070** Formula Weight: 394,45026 Molecular Formula: $C_{20}H_{24}N_7O_2$
B087 **(Brains On-line, USA)**	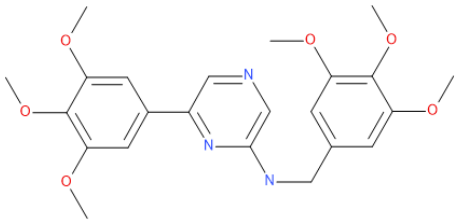 **Biofocus 035_0131_0087** Formula Weight: 441,47698 Molecular Formula: $C_{23}H_{27}N_3O_6$

A822

(Brains On-line, USA)

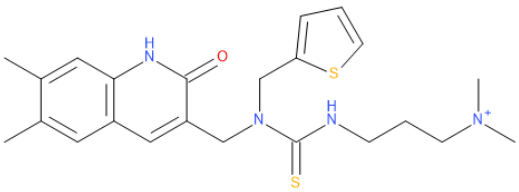

Asinex ASN 03579822

Formula Weight: 443,64844
Molecular Formula: $C_{23}H_{31}N_4OS_2$

ST2S

(Brains On-line, USA)

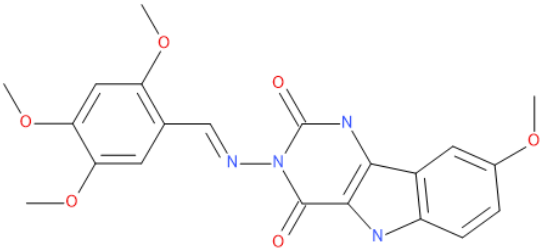

STOCK2S-09372

Formula Weight: 424,4067
Molecular Formula: $C_{21}H_{20}N_4O_6$

ST50

(Brains On-line, USA)

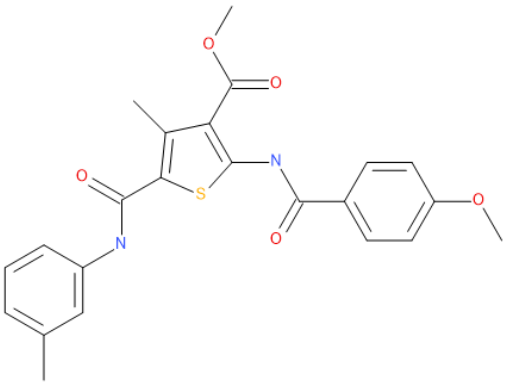

TimTec ST5013386

Formula Weight: 438,49618
Molecular Formula: $C_{23}H_{22}N_2O_5S$

Potential TRF2-TIN2 protein inhibitors

B176

(Brains On-line, USA)

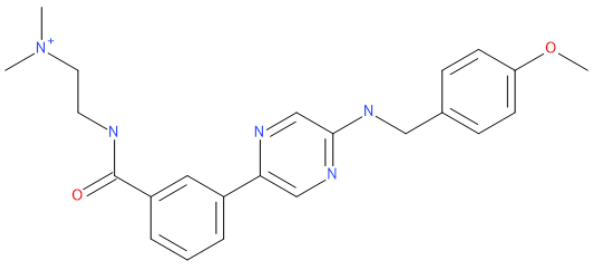

Biofocus 040_0244_0176

Formula Weight: 406,50072
Molecular Formula: $C_{23}H_{28}N_5O_2$

B280

(Brains On-line, USA)

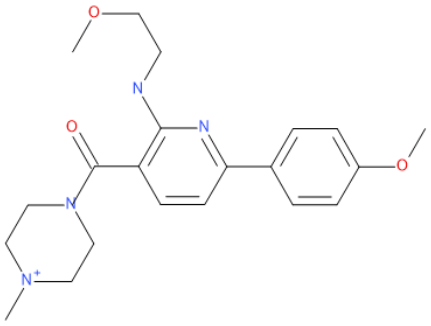

Biofocus 110_0033_0220_0280

Formula Weight: 401,52242
Molecular Formula: $C_{17}H_{20}N_2O_3.C_5H_{13}N_2$

B327

(Brains On-line, USA)

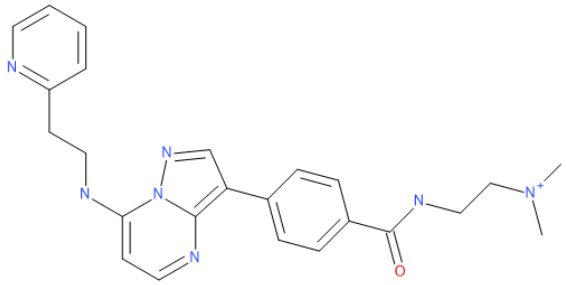

Biofocus 179_0115_0327

Formula Weight: 430,52542
Molecular Formula: $C_{24}H_{28}N_7O$

A628

(Brains On-line, USA)

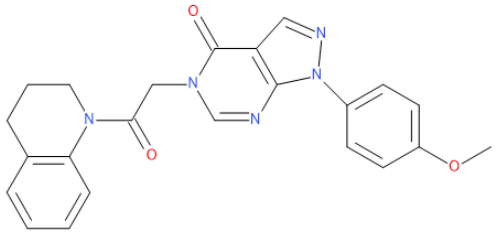

Asinex ASN 07186628

Formula Weight: 415,44454
Molecular Formula: $C_{23}H_{21}N_5O_3$

A378

(Brains On-line, USA)

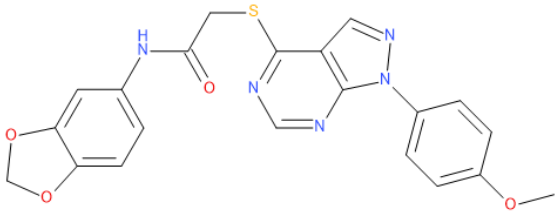

Asinex ASN 05100378

Formula Weight: 435,45578
Molecular Formula: $C_{21}H_{17}N_5O_4S$

A670

(Brains On-line, USA)

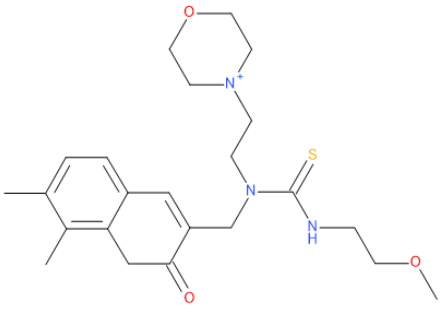

Asinex ASN 03272670

Formula Weight: 432,59936
Molecular Formula: $C_{23}H_{34}N_3O_3S$

Others

Doxorubicin

(15007, Cayman Chemical Company, USA)

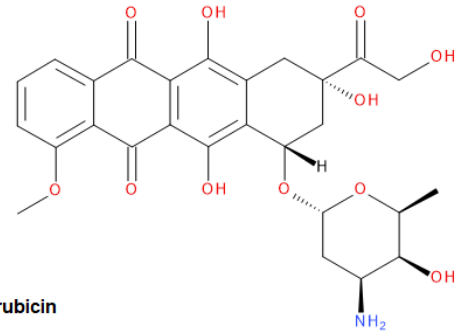

Doxorubicin

Formula Weight: 543.51926
Molecular Formula: $C_{27}H_{29}NO_{11}$

Etoposide

(12092, Cayman Chemical Company, USA)

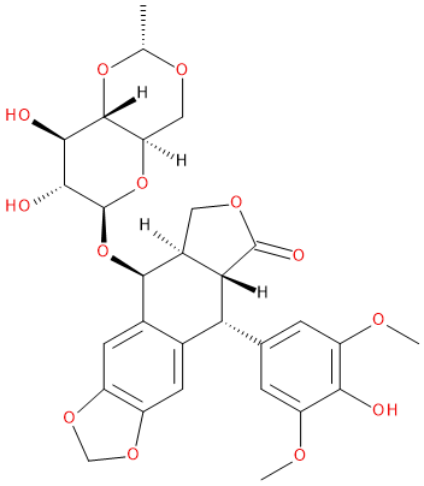

Etoposide

Formula Weight: 588.55658
Molecular Formula: $C_{29}H_{32}O_{13}$

Cell lines and culture

The source and characteristics of the breast cancer cell lines used in this study are summarized in Table 3. The MCF7, T47D, BT474, SK-BR-3, MDA-MB-231, BT20, MCF 10A cell lines were obtained from the American Tissue Culture Collection (ATCC) and the human mammary epithelial cells (HMEC) were purchased from Lonza Group AG. The MCF7, BT20 and MCF7/Adr lines were maintained in cell media consisting of Roswell Park Memorial Institute (RPMI) 1640 Medium, SK-BR-3, T47D and MDA-MB-231 in Dulbecco's modified Eagles medium (DMEM), BT474 in Minimum Essential Media (MEM) (Corning, Manassas, USA). All cell culture media were supplemented with 10% fetal bovine serum (FBS), 1% penicillin/streptomycin, and 1% L-glutamine. The MCF 10A was maintained in cell media consisting of Dulbecco's modified Eagles medium (DMEM)/Hams F-12 50/50 Mix supplemented with 5% Horse Serum, 20 ng/ml hEGF, 0.5 mg/ml Hydrocortisone, 100 ng/ml Cholera Toxin, 10 µg/ml Insulin and 1% penicillin/streptomycin. The HMEC cells were maintained in culture media consisting of a Mammary Epithelial Cell Growth Medium SingleQuots Kit. The MCF7, BT474, BT20, MCF7/Adr, MCF 10A and HMEC cell lines were cultured in an incubator at 37 °C and 5% CO_2, while the SK-BR-3, T47D and MDA-MB-

231 in an incubator at 37 °C and 10% CO_2. All cells were passaged when they reached approximately 80% confluency and media were changed every three days during growth. For trypsinization of the cells, the media were aspirated and the cells were washed with 1xPBS before adding 1ml or 4 ml of 0.025% trypsin to T25, T75 or T175 flasks, respectively. The flasks were incubated at 37 °C until the cells detached from the flask, trypsin was inactivated with 5 ml of cell specific complete media containing FBS. Cells were transferred to a 15 ml tube and pelleted by spinning at 1000 revolutions per minute (rpm) for five minutes. The media were removed and the pellet was resuspended in fresh cell specific complete media before reseeding at respective subculture ratios in new flasks containing 10-35 ml of cell specific complete media.

Materials:

- Cell culture flasks (T25) (734-0044, VWR, USA)
- Cell culture flasks (T75) (734-0046, VWR, USA)
- Cell culture flasks (T175) (734-0047, VWR, USA)
- RPMI 1640, 1X (15-040-CV, Corning, USA)
- DMEM, 1X (15-013-CV, Corning, USA)
- DMEM F-12 50/50, 1X (10-092-CV, Corning, USA)
- MEM, 1X (10-010-CV,Corning, USA)
- EGM ™ Endothelial Cell Growth Medium Bullet Kit ™ (CC-3156, Lonza, Germany)
- FBS (35-079-CV, Corning, South America)
- Horse Serum (16050122, ThermoFisher, New Zealand)
- Streptomycin (S-6501, Sigma-Aldrich, China)
- Penicillin (P-7794, Sigma-Aldrich, China)
- Insulin (I9278, Sigma-Aldrich, United Arab Emirates)
- Cholera Toxin (C8052, Sigma-Aldrich, Israel)
- hEGF (PHG0311L, Thermo Fisher Scientific, USA)
- Hydrocortisone (H0888, Sigma-Aldrich, USA)
- Trypsin solution from porcine pancreas (T4674, Sigma Aldrich, USA)
- 1xPBS (P4417, Sigma-Aldrich, USA)
- Hanks′ Balanced Salt solution (55021C, Merck, USA)

Table 4. Characterization of breast cancer cell lines used in the study. Abbreviations: TNBC = triple-negative breast cancer; NM = non-malignant.

Cell line	Primary tumor	Origin of cells	Immunoprofile	Classification	Karyotype	Morphology	Company	Catalog number	Reference
MCF7	Invasive ductal carcinoma	Metastasis (pleural effusion)	ER^+, $PR^{+/-}$, $HER2^-$	Luminal A	Hyper-triploidto hypo-tetraploid	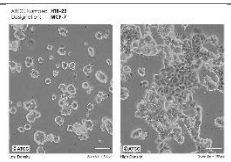	ATCC	HTB-22	https://www.cellosaurus.org/CVCL_0031
T47D	Invasive ductal carcinoma	Metastasis (pleural effusion)	ER^+, PR^+, $HER2^-$	Luminal A	Hypo-triploid	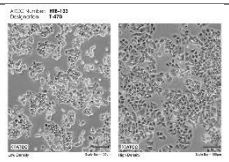	ATCC	HTB-133	https://www.cellosaurus.org/CVCL_0553
BT474	Invasive ductal carcinoma	Primary	ER^+, PR^+, $HER2^+$	Luminal B	Hyper-triploid	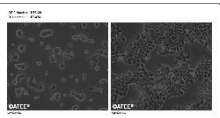	ATCC	HTB-20	https://www.cellosaurus.org/CVCL_0179
SK-BR-3	Invasive ductal carcinoma	Metastasis (pleural effusion)	ER^-, PR^-, $HER2^+$	HER2	Hyper-triploid (highly modified)	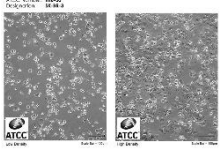	ATCC	HTB-30	https://www.cellosaurus.org/CVCL_0033
MDA-MB-231	Invasive ductal carcinoma	Metastasis (pleural effusion)	ER^-, PR^-, $HER2^-$	TNBC	Hypo-triploid	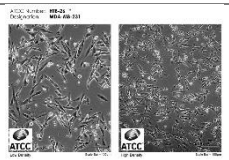	ATCC	HTB-26	https://www.cellosaurus.org/CVCL_0062
BT20	Invasive ductal carcinoma	Primary	ER^-, PR^-, $HER2^-$	TNBC	Hyper-diploid	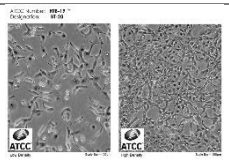	ATCC	HTB-19	https://www.cellosaurus.org/CVCL_0178

MCF7/Adr	Invasive ductal carcinoma	MCF7 cell line (genetically modified to be resistant)	ER^{+}, $PR^{+/-}$, $HER2^{-}$	Luminal A	Hyper-triploidto hypo-tetraploid	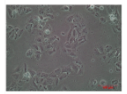	Gdansk University of Technology	-	https://www.cellosaurus.org/CVCL_1452
MCF 10A	Non-tumorigenic epithelial cell line	Benign proliferative breast tissue	ER^{-}, PR^{-}, $HER2^{-}$	NM	Near-diploid with a modal chromosome number of 46 (2n)	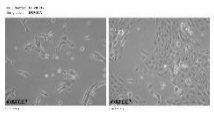	ATCC	CRL-10317	https://www.cellosaurus.org/CVCL_0598
HMEC	Human Mammary Epithelial Cells	Isolated from adult female breast tissue	ER^{-}, PR^{-}, $HER2^{-}$	Primary Mammary Epithelial Cells	Near-diploid with a modal chromosome number of 46 (2n)	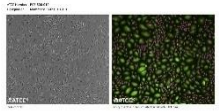	Lonza	CC-2551	-

The primary patient-derived non-tumor and tumor cell culture (PDC)

The samples consisted of tissues excised from 21 BC patients (age range at diagnosis: 33–77 years old) with infiltrating duct carcinoma [(NOS) 8500/3] G1, G2, G3 before any radiotherapy, chemotherapy or other treatment initiated (Table 5). The tissues were delivered as a post-operational material from the Gdynia Oncology Center of the Polish Red Cross Maritime Hospital, Gdynia, Poland. The human material was sampled according to local Bioethical Commission guidelines (no individualized permissions were required since the material was obtained within regular surgery operations removing carcinoma and the samples were as anonymous with regard to patient's personal data). However, according to the bioethical commission guidelines, the informed consent of the patient was necessary and was obtained from every patient (Figure 16). The obtained samples underwent identical preparative protocol. The samples were washed using phosphate buffer saline and preserved in the transfer medium consisting of DMEM/F12, + 10% Fetal Bovine Serum + 100 µg/ml Penicillin/Streptomycin + 5 µg/ml Piramycin + 50 U/ml Polymyxin B until cultivation. The samples were washed with 1xPBS in Petri dishes and then cut into small pieces using surgical scalpels. The sample fragments were washed again with 1xPBS, inserted into a 15 ml tubes containing the mixed enzyme solution (Collagenase/Hyaluronidase) and then incubated for 16 h, with gentle rotation 300 rpm, at 37 °C. After incubation with active proteolytic enzymes, the samples were filtered using 100 µm and 40 µm grid cell strainers and then centrifuged at 600×g for 5 min. For each sample, the supernatant was discarded, and the pellet containing tissue fragments was washed with 1xPBS and centrifuged at 600×g for 5 min. The pellet was resuspended with the culture initiation medium and cultivated in a 6-well plate (37 °C, 5% CO_2) for 48 hours. Afterwards, the media mix was removed and the stimulation medium was added, which was renewed every 3 days. Next, the cells were transferred into T75 flasks (75 cm^2) and cultivated in the stimulation medium until reaching a confluence of 80%. The cultured cells were then detached using trypsin solution at the working concentration of 0.025% and incubated for 1–3 min at 37 °C, and a medium containing FBS was added to neutralize trypsin. The detached cells were centrifuged at 600×g for 5 min at room temperature. The culture medium was removed and the pellet was resuspended with a fresh stimulation medium before re-seeding at

respective subculture ratios into new T75 flasks containing 20 ml of cell specific complete media as we have published before [264].

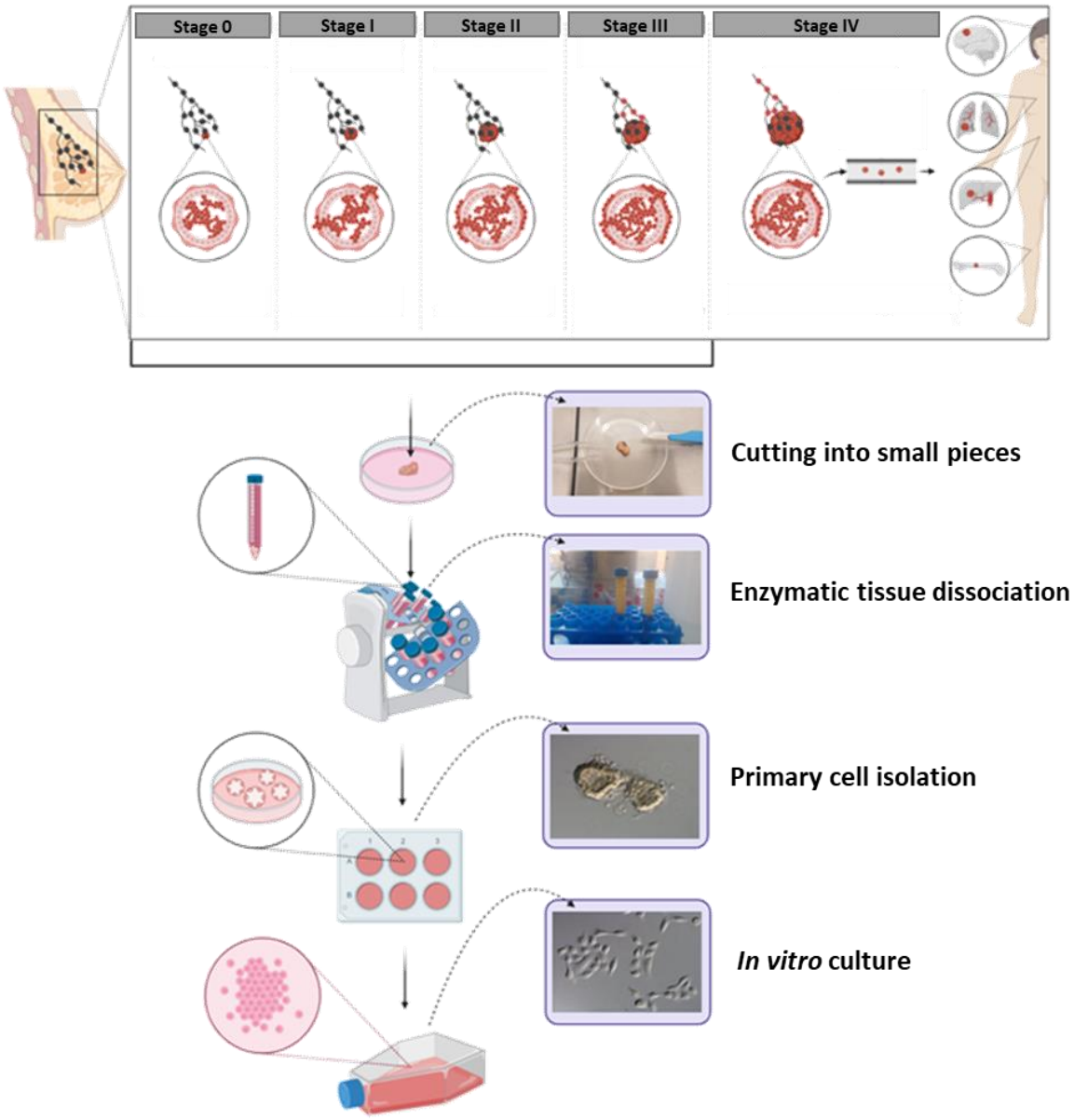

Figure 15. Schematic of derivation primary patient-derived non-tumor and tumor cell culture (PDC).

FORMULARZ ZGODY
NA UDZIAŁ W BADANIU NAUKOWYM

1. Formularz zgody na udział w badaniu

DEKLARACJA ZGODY
NA UDZIAŁ W BADANIU NAUKOWYM

Tytuł projektu:

Nowe związki o działaniu przeciwnowotworowym zaburzające funkcje telomerów.

Kierownik projektu: Prof. dr hab. inż. Maciej Bagiński

Politechnika Gdańska, Wydział Chemiczny, Katedra Technologii Leków i Biochemii

Nazwa jednostki, w której będzie realizowany projekt *(wydział/instytut/katedra/zakład): Politechnika Gdańska, Wydział Chemiczny , Katedra Technologii Leków i Biochemii oraz .....(tutaj będzie nazwa jednostki w której będzie pobierany materiał do badań ex vivo).*

Imię i nazwisko uczestnika badań (*drukowanymi literami*):

.....

Niniejszym oświadczam, że:

1. Jestem osobą pełnoletnią i nieubezwłasnowolnioną całkowicie.
2. Zostałem(am) poinformowany(a) przez
.....
(imię i nazwisko lekarza prowadzącego)
o planowanym badaniu naukowym polegającym na wykonywaniu badań ex vivo na materiale pobranym od pacjenta w ramach rutynowej operacji usunięcia nowotworu, w szczególności o jego założeniach, celach, przebiegu i sposobie przeprowadzania.

☐ TAK ☐ NIE

3. Otrzymałem(am) zadowalające odpowiedzi na wszystkie zadane przeze mnie pytania i rozumiem wszystkie przekazane mi informacje dotyczące tego badania naukowego.

☐ TAK ☐ NIE

4. Zostałem(am) poinformowany(a), że udział w badaniu naukowym jest absolutnie dobrowolny.

☐ TAK ☐ NIE

1

5. Zostałem(am) poinformowany(a), że mogę wycofać się z udziału w tym badaniu naukowym w dowolnym momencie, bez podania przyczyn, a moja decyzja nie pociągnie za sobą żadnych kar ani utraty praw, które mi przysługują z innych tytułów, w szczególności prawa do opieki zdrowotnej.

☐ TAK ☐ NIE

6. W przypadku komercjalizacji badań naukowych z wykorzystaniem pozyskanego ode mnie materiału biologicznego, nie będę rościł(a) praw do uzyskanych wyników oraz wynikających z ich ewentualnej komercjalizacji korzyści majątkowych.

☐ TAK ☐ NIE

7. **Dobrowolnie wyrażam zgodę na udział w badaniu naukowym** (należy podać tytuł projektu): Nowe związki o działaniu przeciwnowotworowym zaburzające funkcje telomerów.

☐ TAK ☐ NIE

8. **Wyrażam zgodę na przetwarzanie moich danych osobowych związanych z udziałem w niniejszym badaniu przez kierownika badania i inne osoby lub podmioty przeprowadzające to badanie w zakresie wskazanym w informacji dla uczestnika badania, zgodnie z ustawą z dnia 10 maja 2018 r. o ochronie danych osobowych (tekst jednolity Dz. U. z 2019 r. poz. 1781).**

☐ TAK ☐ NIE

8.1 Administratorem moich danych osobowych jest……...
(imię i nazwisko lekarza prowadzacego)

8.2 Podstawę prawną przetwarzania moich danych osobowych stanowi ustawa z dnia 10 maja 2018 r. o ochronie danych osobowych (tekst jednolity Dz. U. z 2019 r. poz. 1781) - dane osobowe są niezbędne do realizacji projektu: Nowe związki o działaniu przeciwnowotworowym zaburzające funkcje telomerów.

8.3 Moje dane osobowe będą przetwarzane wyłącznie w celu udzielenia wsparcia, realizacji projektu: Nowe związki o działaniu przeciwnowotworowym zaburzające funkcje telomerów.

8.4 Mam prawo dostępu do treści swoich danych i ich poprawiania.

..... ……
Miejscowość i data wpisana przez uczestnika Czytelny podpis uczestnika badań

..... ……
Miejscowość i data wpisana przez osobę odbierającą zgodę Podpis osoby odbierającej zgodę

Imię i nazwisko osoby odbierającej zgodę (drukowanymi literami):.....

2

Figure 16. Form of the informed consent of the patient.

Materials:

- Centrifuge tubes (15 ml) (734-0451, VWR, USA)
- Centrifuge tubes (50 ml) (734-0448, VWR, USA)
- 6-well plate (734-0065, VWR, USA)
- Scalpels (233-0034, VWR, USA)
- Forceps (Hurtownia Medyczna MaxiMecida, Poland)
- Cell strainers, 40 µm pore size (734-2760, VWR, USA)
- Cell strainers 40 µm pore size (734-2762. VWR, USA)
- Cell culture flasks (T75) (734-0046, VWR, USA)
- Transport medium
    - DMEM F-12 50/50, 1X (10-092-CV, Corning, USA)
    - 10% FBS (35-079-CV, Corning, South America)
    - 100 µg/ml streptomycin (S-6501, Sigma-Aldrich, China)
    - 100 U/ml penicillin (P-7794, Sigma-Aldrich, China)
    - 5 µg/ml pimaricin (1.07360**,** Milipore, Germany)
    - 50 U/ml polymyxin B (P4932, Sigma-Aldrich, Israel)
- Digestion media
    - DMEM F-12 50/50, 1X (10-092-CV, Corning, USA)
    - 100 µg/ml streptomycin (S-6501, Sigma-Aldrich, China)
    - 100 U/ml penicillin (P-7794, Sigma-Aldrich, China)
    - 5 µg/ml pimaricin (1.07360**,** Milipore, Germany)
    - 50 U/ml polymyxin B (P4932, Sigma-Aldrich, Israel)
    - 2 mg/ml BSA (A9418, Sigma-Aldrich, USA)
    - 10 µg/ml insulin (I9278, Sigma-Aldrich, United Arab Emirates)
    - 200 U/ml collagenase (17100017, ThermoFisher Scientific, USA)
    - 100 U/ml hyaluronidase (H3506, Sigma-Aldrich, USA)
- Culture initiation media
    - MM4 media (50%)
        - ✓ DMEM F-12 50/50, 1X (10-092-CV, Corning, USA)
        - ✓ 0.5% FBS (35-079-CV, Corning, South America)
        - ✓ 10 µg/ml insulin (I9278, Sigma-Aldrich, United Arab Emirates)
        - ✓ 5 ng/ml hEGF ((PHG0311L, Thermo Fisher Scientific, USA)
        - ✓ 0.1 µg/ml hydrocortisone (H0888, Sigma-Aldrich, USA)

- ✓ 10^{-8} M T3 3,3', 5-tri-iodo-L-thyronine (T6397 , Sigma-Aldrich, Germany)
- ✓ 10^{-9} M estradiol (E2758, Sigma-Aldrich, China)
- ✓ 100 µg/ml streptomycin (S-6501, Sigma-Aldrich, China)
- ✓ 100 U/ml penicillin (P-7794, Sigma-Aldrich, China)

- MCDB170+SFS media (50%)
  - ✓ Medium 171 (M171500, Thermo Fisher Scientific, USA)
  - ✓ 1% Mammary Epithelial Growth Supplement (MEGS) (S0155, Thermo Fisher Scientific, USA)
  - ✓ 5 µg/ml transferrin **(**T1147, Sigma-Aldrich, USA)
  - ✓ 10^{-5} M isoproterenol **(**I6504, Sigma-Aldrich, USA)
  - ✓ 10^{-4} M ethanolamine **(**E0135, Sigma-Aldrich, USA)
  - ✓ 10^{-4} M O-phosphoethanolamine **(**P0503, Sigma-Aldrich, Italy)
- 0.1 nM oxytocin (O3251, Sigma-Aldrich, USA)
- 0.1% AlbuMax I (11020021, Thermo Fisher Scientific, New Zealand)
- 10 µM Y-27632 dihydrochloride (Y0503, Sigma-Aldrich, USA)

- Stimulation media
  - MM4 media (50%)
  - MCDB170+SFS media (50%)
  - 0.1 nM oxytocin (O3251, Sigma-Aldrich, USA)
  - 0.1% AlbuMax I (11020021, Thermo Fisher Scientific, New Zealand)
  - 1 ng/ml cholera toxin (C8052, Sigma-Aldrich, Israel)

Table 5. Characteristics of patient sample.

No.	Age	Histological type (WHO)	Tumor dimension [cm]	Multifocality	*In situ* component	Number of nodes-lymphadenectomy (number/metastatic)	Sentinel lymph nodes (number/metastatic)	pTNM	ER	PR	HER2 IHC	HER2 FISH	Ki67	Luminal A	Luminal B HER2 negative
1.	77	Invasive ductal carcinoma (NST), G2	0.8	NO	NO	NO	4/0	T1b N0 M0	(3+) positive in 100% of cells	(3+) positive in 1% of cells	(0) negative		positive in 25% of cells		YES
2.	53	Invasive ductal carcinoma (NST), G2	1.7	NO	NO	11/5	2/2	T1c N2a M0	(3+) positive in 100% of cells	(3+) positive in 90% of cells	(2+) inconclusive	negative	positive in 20% of cells		YES
3.	52	Invasive ductal carcinoma (NST), G2	1.2	NO	NO	19/0	3/1	T1c N1a M0	(2+) positive in 95% of cells	(3+) positive in 95% of cells	(2+) inconclusive	negative	positive in 25% of cells		YES
4.	57	Invasive ductal carcinoma (NST), G3	1.7	YES	NO	18/0	3/1	T1c N1a M0	(3+) positive in 100% of cells	(2+/3+) positive in 90% of cells	(1+) negative		positive in 15% of cells		YES
5.	76	Invasive ductal carcinoma (NST), G2	2.5	NO	NO	24/0	5/1	T2 N1a M0	(3+) positive in 100% of cells	(3+) positive in 90% of cells	(1+) negative		positive in 20% of cells		YES
6.	45	Invasive ductal carcinoma (NST), G1	2.5	NO	NO	NO	5/0	T2 N0 M0	(3+) positive in 100% of cells	(3+) positive in 100% of cells	(1+) negative		positive in 20% of cells	YES	
7.	62	Invasive ductal carcinoma (NST), G1	2.2	NO	NO	20/3	NO	T2 N1a M0	(3+) positive in 100% of cells	(2+/3+) positive in 50% of cells	(1+) negative		positive in 14% of cells		YES
8.	54	Invasive ductal carcinoma (NST), G1	1.5	NO	NO	NO	3/0	T1c N0 M0	(3+) positive in 100% of cells	(2+) positive in 5% of cells	(1+) negative		positive in 30% of cells		YES

9.	59	Invasive ductal carcinoma (NST), G1	1.5	YES	YES	21/19	4/4	T4 N3a M0	(3+) positive in 95% of cells	(2+) positive in 3% of cells	(0) negative		positive in 5% of cells	YES		
10.	71	Invasive ductal carcinoma (NST), G2	2.1	NO	NO	NO	3/0	T2 N1a M0	(3+) positive in 100% of cells	(2+) positive in 95% of cells	(0) negative		positive in 10% of cells	YES		
11.	43	Invasive ductal carcinoma (NST), G1	1.1	YES	NO	21/1	2/1	T1c N1a M0	(3+) positive in 100% of cells	(3+) positive in 80% of cells	(2+) inconclusive	negative	positive in 4% of cells	YES		
12.	71	Invasive ductal carcinoma (NST), G1	1.5	NO	NO	NO	2/0	T1c N0 M0	(3+) positive in 100% of cells	(3+) positive in 30% of cells	(2+) inconclusive	negative	positive in 5% of cells	YES		
13.	33	Invasive ductal carcinoma (NST), G2	1.7	NO	NO	NO	5/1	T1c N1a M0	(3+) positive in 100% of cells	(3+) positive in 100% of cells	(1+) negative		positive in 15% of cells		YES	
14.	44	Invasive ductal carcinoma (NST), G3	2.2	NO	NO	21/3	1/1	T2 N1a M0	(3+) positive in 90% of cells	(2+) positive in 70% of cells	(2+) inconclusive	negative	positive in 10% of cells	YES		
15.	60	Invasive ductal carcinoma (NST), G2	1.4	NO	NO	NO	5/0	T1c N0 M0	(2+) positive in 90% of cells	(3+) positive in 70% of cells	(0) negative		positive in 10% of cells	YES		
16.	69	Invasive ductal carcinoma (NST), G2	1.6	NO	NO	17/1	NO	T1c N1a M0	(3+) positive in 100% of cells	(2+/3+) positive in 50% of cells	(0) negative		positive in 10% of cells	YES		
17.	40	Invasive ductal carcinoma (NST), G2	2.8	NO	NO	NO	3/0	T2 N0 M0	(2+) positive in 50% of cells	(3+) positive in 80% of cells	(0) negative		positive in 10% of cells	YES		

18.	52	Invasive ductal carcinoma (NST), G2	1.5	NO	NO	NO	4/1	T1c N1a M0	(3+) positive in 100% of cells	(3+) positive in 80% of cells	(0) negative		positive in 25% of cells		YES
19.	48	Invasive ductal carcinoma (NST), G2	1.3	NO	YES	NO	6/0	T1c N0 M0	(2+) positive in 90% of cells	(3+) positive in 95% of cells	(0) negative		positive in 10% of cells	YES	
20.	48	Invasive ductal carcinoma (NST), G2	2.2	NO	NO	19/2	3/1	T2 N1a M0	(3+) positive in 95% of cells	(3+) positive in 95% of cells	(1+) negative		positive in 5% of cells	YES	
21.	37	Invasive ductal carcinoma (NST), G3	1.4	NO	YES	NO	NO	T1c N1a M0	(2+) positive in 90% of cells	(2+) positive in 70% of cells	(2+) inconclusive	negative	positive in 90% of cells		YES

MTT assay

MTT is a colorimetric non-clonogenic assay that measures cell viability in cultures by monitoring metabolic activity (Stockert et al., 2012). MCF7, MDA-MB-231, MCF 10A, BT474, BT20, SK-BR-3, T47D, MCF7/Adr, HMEC and cell cultures from normal and cancer breast tissues were assembled and maintained as described above. Once all cell lines were about 80% confluent and since each cell line had individual proliferation rate, the cells were seeded at various densities depending on cell line characteristics. However, densities were identical within the same line. The cells were counted by a hemacytometer (Hausser Scientific, Horsham, PA, USA) and plated in 96-well microtiter plates at concentrations: 4000cells/well for MCF7 and MDA-MB-231, 3000 cells/well for MCF10A, 40 000 cells/well for BT-474, 4500 cells/well for SK-BR-3, 8000 cells/well for T47D, 6000 cells/well for BT20 and HMEC, 5000 cells/well for MCF7/Adr and 4500 cells/well for primary derived cell cultures from normal and cancer breast tissues. Cells were allowed to attach overnight at 37 °C and 5% CO_2 or 10% CO_2, conditions optimized for each cell line. All cell lines were treated with different concentrations of the tested compounds in order to determine the half-maximal inhibitory concentration (IC_{50}), which is the concentration of a drug that inhibits 50% of cell growth or viability after a specified treatment period. The range of concentrations used was 0.78-100 μM for the tested compounds and 0.01-12.5 μM for doxorubicin. The treatment period was 72 h. The final concentration of DMSO was ensured to be around 1% in all experiments. Cells were incubated with studied compounds for 72 h at 37 °C and 5% CO_2 or 10% CO_2 conditions optimized depending on cell lines. After incubation, 20 μL of MTT solution (3-[4,5-dimethylthiazol-2-yl]-2,5- diphenyltetrazolium bromide) in PBS (4 mg/ml) were added to all wells and incubated for 3 h at 37 °C. The formazan crystals formed were dissolved in 150 μL DMSO aliquots and the absorbance was measured using the Asys UVM340 multiwell plate reader at wavelength λ=540 nm. Cytotoxicity was determined for tested compounds and compared to drug-free control. All experiments were performed in triplicates. GraphPad Prism 8.0.1 was used to statistically analyze the results.

Materials:

- 96-well plate (392-0019, VWR, USA)
- 4mg/ml MTT (M2128, Sigma-Aldrich, China)
- 1xPBS (P4417, Sigma-Aldrich, USA)
- DMSO (D8418, Sigma-Aldrich, USA)

Clonogenic assay

Clonogenic assay or colony formation assay is an *in vitro* cell survival assay based on the ability of a single cell to proliferate into a multicellular colony [265,266]. MCF7 cells were seeded in triplicate at a density of 600 cells per well in six-well plates. After 3 h of incubation, cells were treated with various concentrations of B070, B087, B176, B327 (range: 1-50 μM) and A822 (range: 1-15 μM) for 3 days. The medium was changed to another one, without compounds, after 72 h and cultivated for another 9 days, until 12 days of cultivation was completed. At the end of the experiment, cells were fixed with methanol for 10 min on ice and stained with 0.5% crystal violet solution for 10 min at room temperature (RT). Stained cells were briefly rinsed with Milli-Q water and then imaged. Experiments were conducted in triplicate.

Materials:

- 6-well plate (10062-892, VWR, USA)
- Methanol (621990110, POCH, Poland)
- 0.5% crystal violet (C0775, Sigma-Aldrich, USA)

Cell cycle analysis

DNA synthesis is one of the landmark events in the cell cycle: G1 cells have one copy of the genome, S phase cells are actively engaged in DNA synthesis, and G2 cells have twice as much nuclear DNA as G1 cells. Cellular DNA content can be measured by staining with propidium iodide (PI), which binds to DNA in a stoichiometric ratio, followed by a flow cytometric readout. MCF7, MDA-MB-231 cells and primary derived cell cultures from normal and cancer breast tissues

were treated with tested compounds (Table 6) for 24 and 48 h. A negative control (growth medium without drug) was included for each assay. The cells were fixed in 75% ethanol at -20 °C overnight. Next, cell suspensions were centrifuged and pelleted cells were -resuspended in PBS containing propidium iodide and RNase A. Staining was carried out for 30 min at 24 °C in the dark. The fluorescence intensity emitted by DNA-bound propidium iodide upon excitation with UV light source was measured using a flow cytometer (Merck Millipore guava easyCyte 8, Darmstadt, Germany). GraphPad Prism 8.0.1 was used to statistically analyze the results.

Materials:

- Petri dishes (60 mm) (734-0961, VWR, USA)
- Centrifuge tubes (15 ml) (734-0451, VWR, USA)
- Eppendorf tubes (1.5 ml) (3810X, Eppendorf, UK)
- 1xPBS (P4417, Sigma-Aldrich, USA)
- 0.025% trypsin (T-4674-100ML, Sigma-Aldrich, USA)
- 75% ethanol (396420113, POCH, Poland)
- 10 µg/ml propidium iodide (P-4170, Sigma-Aldrich, USA)
- 50 µg/ml RNase A (EN0531, ThermoFisher, USA)

Table 6. Concentration of compounds used in cell cycle analysis.

Cell lines	Concentration of compounds [µM]				
	B070	B087	B176	B327	A822
MCF7	100	50	85	75	15
MDA-MB-231	60	50	90	80	15
primary derived cell cultures from normal breast tissues	50	50	40	50	10
primary derived cell cultures from cancer breast tissues	50	50	50	50	10

Annexin V/7-ADD Assay

Annexin V/7-amino-actinomycin staining is a convenient way to discriminate early apoptosis from late apoptosis and necrosis events. Early apoptotic cells expose phosphatidylserine (PS) molecules on the outer leaflet of the plasma membrane,

which is not the case in normal cells. PS can be stained by labeled annexin V. Late apoptotic cells and necrotic cells lose their cell membrane integrity and become permeable to dyes such as 7-AAD (DNA intercalator), serving as a test of lost cell vitality [267]. The MCF7 and MDA-MB-231 cells were treated by tested compounds (Table 7) for 3, 6 and 24 h. A negative control (growth medium without drug) was also included for each assay. Then, cells were harvested and suspended in 1xPBS. After centrifugation, cells were re-suspended in Annexin-binding buffer (ABB) with the addition of Annexin V-FITC and 7-AAD. Staining was carried out for 15 min in the dark. Apoptosis was assessed by flow cytometry cytometer (Merck Millipore Guava easyCyte 8, Darmstadt, Germany). Experiments were conducted in triplicate. GraphPad Prism 8.0.1 was used to statistically analyze the results.

Materials:

- Petri dishes (35 mm) (734-0005, VWR, USA)
- Centrifuge tubes (15 ml) (734-0451, VWR, USA)
- Eppendorf tubes (1.5 ml) (3810X, Eppendorf, UK)
- 1xPBS (P4417, Sigma-Aldrich, USA)
- 0.025% trypsin (T-4674-100ML, Sigma-Aldrich, USA)
- 1 µg/ml 7-AAD (A1310, ThermoFisher, USA)
- Annexin V FITC (A13199, Invitrogen, USA)
- 10X Annexin V Binding Buffer (51-66121E, BD Pharmigen, USA)

Table 7. Concentration of compounds used in apoptosis analysis.

Cell lines	Concentration of compounds [µM]				
	B070	**B087**	**B176**	**B327**	**A822**
MCF7	100	50	85	75	25
MDA-MB-231	60	50	90	80	25

Senescence-Associated-β-Galactosidase (SA-β-gal) Staining

Cellular senescence is now also considered to be a suppressive mechanism against oncogenesis [268], acting to block proliferation in cells with oncogenic mutations [269]. Detectable β-GAL activity is the most extensively used marker for senescent or aging cells whether in culture or in mammalian tissues [270 271 272]. In this study, MCF7 cells were cultured on 22 mm glass slides in a 35 mm Petri dish and treated with five different compounds: B070 (100 µM), B087 (50 µM), B176 (85 µM), B327 (75 µM) and A822 (10 µM) for 120 h. The treated and control cells were then washed in 1xPBS and fixed with 2% formaldehyde for 5 min at room temperature. Next, the cells were washed twice with 1xPBS. Following these steps, a beta-Gal staining solution was added to the cells, and the cells were incubated at 37 °C in the dark for 15 h. After incubation, a citric acid/sodium phosphate buffer was used to detect beta-Gal activity. Glass slides with cultured and stained cells were observed in the bright field mode using an Olympus BX60 microscope. GraphPad Prism 8.0.1 was used to statistically analyze the results.

Materials:

- 35 mm Petri dishes (734-0005, VWR, USA)
- Microscope slides (41-7626-2, medlab, Poland)
- 22 x 22 mm coverslips (42-2222-0, medlab, Poland)
- 2% formaldehyde (432173427, POCH, Poland)
- 1xPBS (P4417, Sigma-Aldrich, USA)
- β- Gal staining
    - 40 mM citric acide/sodium phosphate pH 6
        - ✓ 0.1 M citric acide (PHR1071, Merck, USA)
        - ✓ 0.2 M Na_2HPO_4 (1.06585, Merk, USA)
    - 5 mM potassium ferrocyanide (211095000, ThermoFisher, USA)
    - 5 mM potassium ferricyanide (223111000, ThermoFisher, USA)
    - 150 mM NaCl (S3014, Sigma-Aldrich, USA)
    - 2 mM $MgCl_2$ (M4880, Sigma-Aldrich, USA)
    - 1 mg/ml X-Gal in dimethyl-formamide (7240-90-6, Roche, UK and PHR1553, Supelco, USA)

- Mounting medium
    - DABCO (D-2522, Sigma-Aldrich, Germany)
    - Glycerol **(**443320113, POCH, Poland)
    - 1xPBS (P4417, Sigma-Aldrich, USA)

Acridine Orange Staining

Acridine Orange is a cell-permeable green fluorophore that can be protonated and trapped in acidic vesicular organelles (AVOs). Its metachromatic shift to red fluorescence is concentration-dependent and, therefore, Acridine Orange fluoresces red in AVOs, such as autolysosomes. This makes Acridine Orange staining a quick, accessible and reliable method to assess the volume of AVOs, which increases upon autophagy induction [273]. Briefly, MCF7 cells were seeded on 22 mm slides in 35 mm Petri dishes and treated with five different compounds: B070 (100 μM), B087 (50 μM), B176 (85 μM), B327 (75 μM) and A822 (10 μM) for 48 h. At the appropriate time point following compound treatment, the cells were incubated with a culture medium containing 1 mg/ml acridine orange for 15 min. Next, the cells were washed twice with PBS. Glass slides prepared were observed in the bright field mode using an Olympus BX60 microscope.

Materials:

- 35 mm Petri dishes (734-0005, VWR, USA)
- Microscope slides (41-7626-2, medlab, Poland)
- 22 x 22 mm glass coverslips (42-2222-0, medlab, Poland)
- 5 μmol/l Acridine Orange (318337, Sigma-Aldrich, USA)
- 1xPBS (P4417, Sigma-Aldrich, USA)

Lipid Droplets Detection

Lipid droplets (LDs) are dynamic cellular structures, organelles that regulate the storage and homeostasis of intracellular triglycerides and other neutral lipids. Studies show that the number, morphology, and subcellular localization of LDs are altered in a number of diseases [274]. Here, Nile Red staining was used to

detect these organelles. Briefly, MCF7 cells were grown in slides placed in a 35mm dish. After 48 h of B070 (100 μM), B087 (50 μM), B176 (85 μM), B327 (75 μM) and A822 (10 μM) exposure, Nile Red was added to the dish in order to detect lipid droplets. After 5 min of incubation with dye, the cells were washed twice with 1xPBS and observed in fluorescence mode using an Olympus BX60 microscope. Hoechst 33342 dye was used for the staining of cell nuclei. The same experiment was performed on primary derived cell cultures from normal and cancer breast tissues that were treated with tested compounds (Table 6) for 48 h.

Additionally, in this experiment a flow cytometry method was used. In this study, MCF7 cells were fixed in 4% formaldehyde. Next, cell suspensions were centrifuged and cells were re-suspended in 1xPBS containing Nile Red. Staining was carried out for 15 min at 24 °C, at RT in the dark. The fluorescence intensity was measured using a flow cytometer (Merck Millipore Guava easyCyte 8, Darmstadt, Germany). GraphPad Prism 8.0.1 was used to statistically analyze the results.

Materials:

- 35 mm Petri dishes (734-0005, VWR, USA)
- Microscope slides (41-7626-2, medlab, Poland)
- 22 x 22 mm coverslips (42-2222-0, medlab, Poland)
- 1 μg/ml Nile Red (72485, Sigma-Aldrich, Germany)
- 1 μg/ml Hoechst 333342 (14533, Sigma-Aldrich, USA)
- 1xPBS (P4417, Sigma-Aldrich, USA)
- 4% formaldehyde (432173427, POCH, Poland)

Analysis of DNA Double-Strand Breaks

It is well known that a severe cell injury after exposure to ionizing radiation or some cytotoxic compounds e.g. during cancer treatment is related to the induction of DNA double-strand breaks (DSBs) [275]. An early response to DSBs is the phosphorylation of the histone H2AX at serine 139, referred to as γ-H2AX foci. Using antibodies against phosphorylated H2AX, foci can be detected and

visualized by immunofluorescence labelling for analyses with fluorescence or confocal microscopy [276] [277]. In order to assess the DSB events after exposure to the tested compounds studied in this work, MCF7 cells were grown in slides placed in a 35mm dish. After 24 h of cell incubation with: B070 (100 μM) , B087 (50 μM), B176 (85 μM), B327 (75 μM), A822 (10 μM) and etoposide (10 μM), cells were washed with 1xPBS and fixed by 4% paraformaldehyde solution for 15 min at room temperature. After washing twice with 1xPBS, cells were permeabilized with 0.2% Triton-X-100 in 1xPBS for 10 min at room temperature and blocked in 3% (w/v) bovine serum albumin in 1xPBS overnight (4 °C). After two 1xPBS washing cycles, cells were incubated for 60 min in the incubator (37 °C), with an anti-gamma H2AX (phospho S139) antibody in a dilution buffer containing 1xPBS and 3% BSA. After washing twice in 1xPBS, DAPI was used at working concentration for the staining of cell nuclei. Digital images were captured using a confocal microscope (Zeiss LSM 800) at a magnification of 63x, applying appropriate filters and wavelengths.

Materials:

- 35 mm Petri dishes (734-0005, VWR, USA)
- Microscope slides (41-7626-2, medlab, Poland)
- Round glass coverslips (12 mm diameter) (1-6283, bionovo, Poland)
- 1xPBS (P4417, Sigma-Aldrich, USA)
- 4% paraformaldehyde (158127, Sigma-Aldrich, USA)
- Tween-20 (P1379, Sigma-Aldrich, France)
- Triton X-100 (X100, Sigma-Aldrich, USA)
- 3% BSA (A7030, Sigma-Aldrich, USA)
- Phospho-Histone H2A.X (Ser139) Monoclonal Antibody (CR55T33), Alexa Fluor™ 488 (53-9865-82, ThermoFisher, USA)
- DAPI (D9542, Sigma-Aldrich, Israel)
- Mounting medium
    - DABCO (D-2522, Sigma-Aldrich, Germany)
    - Glycerol (443320113, POCH, Poland)
    - 1xPBS (P4417, Sigma-Aldrich, USA)

Relative Human Telomere Length Quantification qPCR

Accurate and consistent quantification of telomere length is important for many aspects of cell biology such as chromosomal instability, DNA repair, senescence, apoptosis, cell disfunctions, and oncogenesis [278]. ScienCell's Relative Human Telomere Length Quantification qPCR Assay Kit (RHTLQ) was used to directly compare the average telomere length of the control sample and samples treated with compounds: B070 (50 μM), B087 (40 μM), B176 (30 μM), B327 (35 μM) and A822 (15 μM). In this study, we used MCF7 cells after 10 passages (passages every 48 hours). DNA was isolated from cultured cells using the Genomic Mini AX Tissue Kit. The difference in the mean telomere length of the tested samples was assessed using the comparative ΔΔCq (Quantification Cycle Value) method.

Materials:

- Cell culture flasks (T25) (734-0044, VWR, USA)
- Centrifuge tubes (734-0451, VWR, USA)
- 1xPBS (P4417, Sigma-Aldrich, USA)
- 0.025% trypsin (T-4674-100ML, Sigma-Aldrich, USA)
- Relative Human Telomere Length Quantification qPCR Assay Kit (8908, ScienCell, USA)
- FastStart Essential DNA Green Master (06402712001, Roche, UK)
- Genomic Mini AX Tissue Kit (056-60, A&A Biotechnology, Poland)

SDS-PAGE and Western Blotting

For protein analysis, MCF7 cells were incubated with tested compounds applied at selected concentrations (Table 6) for 48 h at 37 °C and 5% CO_2. Next, an NE-PER™ Nuclear and Cytoplasmic Extraction Reagents Kit was used and isolation was performed according to the instructions. The total protein concentration in a solution was determined by a colorimetric assay based on the protocol of DC Protein Assay. For all experiments, a normalized concentration of 25μg/ml protein was used per sample in SDS-PAGE assays.

The method of SDS-PAGE allows the separation of proteins depending on their chain length. SDS, an anionic detergent, linearizes proteins and charges them negatively thus allowing separation by size, depending on the electrophoretic mobility of the respective proteins in a polyacrylamide gel. Gels were cast in two steps, starting with the preparation of the 12% resolving gel. Components of the gel were used in amounts indicated below and mixed by vortexing before and after the addition of TEMED which initiated the polymerization of the resolving gel. The mixture was applied to a gel caster system and isopropanol was added on top of the gel in order to smoothen the surface and prevent the formation of bubbles. Secondly, the 4% stacking gel was prepared under the same conditions and poured on top of the resolving gel after the isopropanol had been discarded. Gel pockets for sample application were formed by the insertion of a comb in the gel caster system. Hardened gels were immediately used for gel electrophoresis. For sample preparation, cell pellets were dissolved in 3x β-mercaptoethanol/bromphenol-blue stock solution and heated at 98°C for 10 min for denaturation of proteins. During loading the gel with tested samples, 5 µl of a protein molecular weight marker was applied into one of the neighboring gel pockets of the same gel in order to later serve as a size standard to which sample signals could be compared. Twenty µl aliquotes of the respective samples were applied to the remaining gel pockets and the gel underwent electrophoresis at 30 mA for 70 min in a running buffer.

By using the Western blotting technique, proteins that had been separated by gel electrophoresis were then transferred onto a PDVF membrane and afterwards detected by incubation with specific antibodies. Proteins were transferred from the respective SDS gel to PDVF membranes by the semi-dry blotting procedure. Therefore, for every gel to be blotted, two stacks of four blotting papers cut to approximate gel size were soaked in blotting buffer. A PDVF membrane was cut to gel size and briefly soaked in methanol and then equilibrated in the blotting buffer. The SDS gel was transferred onto one blotting paper stack set in a semi-dry blotting chamber. The equilibrated PDVF membrane and the second blotting paper stack were piled on top and potential air bubbles were removed by gently applying pressure onto the stack using glass rods, from the middle towards the border of the pile.

Electroblotting was performed by Trans-Blot Turbo Transfer System (2.5A constant current, up to 25 V, 10 min). The efficiency of the protein transfer was controlled by subsequent staining of the PDVF membrane in Ponceau Red, a dye solution with a detection limit of protein amounts around 0.5 – 1 µg. Its water solubility enables an intense, non-permanent and unspecific protein staining with low background signal. In order to prevent unspecific antibody binding during the following incubation steps the membranes were blocked in 5% BSA dissolved in TBS-Tween buffer. Incubation was carried out under gentle agitation for 1 h at RT. For specific labeling of a given protein, the respective primary antibody was diluted in 5% BSA in TBS-Tween buffer and applied to the membrane. Samples were then incubated at RT for at 4°C overnight on a shaker?. Thereafter, membranes were washed several times in TBS-Tween buffer to remove excess unbound antibody and subsequently incubated with the respective species-specific secondary antibody diluted in 0.5% BSA in TBS-Tween buffer. After incubation at RT for 1 h at RT the blots were again rinsed 3 times 15 minutes in TBS-Tween at RT to remove excess antibody. All used secondary antibodies were labeled with the reporter enzyme horseradish peroxidase whose cleavage of a substrate chemiluminescent agent produced a luminescent signal, with intensity proportional to the amount of assayed protein. Hence, membranes were covered with SuperSignal™ West Femto Maximum Sensitivity Substrate and incubated at RT for 3 min in dark. Membranes were then photographed with ChemiDoc MP. Images were afterward analyzed and quantitated using Image Lab software. GraphPad Prism 8.0.1 was used to statistically analyze the results.

Materials:

Cell lysis

- NE-PER™ Nuclear and Cytoplasmic Extraction Reagents Kit (78833. ThermoFisher, USA)
- cOmplete™, EDTA-free Protease Inhibitor Cocktail (04693132001, Roche, Germany)
- 1xPBS (P4417, Sigma-Aldrich, USA)
- 0.025% trypsin (T-4674-100ML, Sigma-Aldrich, USA)

Resolving gel (12%)

- 4X Tris pH 8.8
    - 1.5 M Trizma base (T6066, Sigma-Aldrich, USA)
    - 1% SDS (L3771, Sigma-Aldrich, USA)
- 40% acrylamide (A3553, Sigma-Aldrich, USA)
- TEMED (1.10732, Sigma-Aldrich, USA)
- Ammonium persulfate (A3678, Sigma-Aldrich, USA)

Stacking gel (4%)

- 4X Tris pH 6.8
    - 0.5 M and 0.25 M Trizma base (T6066, Sigma-Aldrich, USA)
    - 0.2% and 0.2 SDS (L3771, Sigma-Aldrich, USA)
- 40% acrylamide (A3553, Sigma-Aldrich, USA)
- TEMED (1.10732, Sigma-Aldrich, USA)
- Ammonium persulfate (A3678, Sigma-Aldrich, USA)

Buffers

- Running buffer working solution:
    - 25 mM Trizma base (T6066, Sigma-Aldrich, USA)
    - 1, 44% glycine (527560117, POCH, Poland)
    - 0.1% SDS (L3771, Sigma-Aldrich, USA)
- Sample buffer
    - 0.25% bromophenol blue (B-8026, Sigma-Aldrich, Germany)
    - 10% glycerol (527560117, POCH, Poland)
    - 10% SDS (L3771, Sigma-Aldrich, USA)
    - 1M β-mercaptoethanol (M3148, Sigma-Aldrich, Germany)
    - 1 M Trizma base pH 6.8 (T6066, Sigma-Aldrich, USA)
- Transfer buffer
    - 25 mM Trizma base (T6066, Sigma-Aldrich, USA)
    - 192 mM glycine (527560117, POCH, Poland)
    - 20% methanol (621990110, POCH, Poland)
- Ponceau S solution
    - 0.1% Ponceau S (P3504, Sigma-Aldrich, USA)
    - 5% glacial acetic acid (64-19-7, Sigma-Aldrich, USA)
- Blocking buffer
    - 1xTBST (91414, Sigma-Aldrich, USA)

- 5% BSA (A9418, Sigma-Aldrich, USA)

Primary antibody – diluted in TBSTx1 + 5% BSA

- Anti – TRF1 antibody [TRF-78] (ab10579, Abcam, UK)
- Anti – TRF2 antibody [4A794] (ab13579, Abcam, UK)
- Anti – TIN2 antibody [EPR15319] (ab239012, Abcam, UK)
- Anti – ATP5A1 [7H10BD4F9] (459240, ThermoFisher, USA)
- Anti – β tubulin [clone AA2] (T8328, Sigma-Aldrich, USA)

Secondary antibody - diluted in TBSTx1 + 0.5% BSA

- Peroxidase AffiniPure Donkey Anti-Mouse IgG (H+L) (min X Bov, Ck, Gt, GP, Sy Hms, Hrs, Hu, Rb, Shp Sr Prot) (715-035-150, Jackson ImmunoResearch Europe Ltd, UK)
- Peroxidase AffiniPure Donkey Anti-Rabbit IgG (H+L) (min X Bov, Ck, Gt, GP, Sy Hms, Hrs, Hu, Ms, Rat, Shp Sr Prot) (711-035-152, Jackson ImmunoResearch Europe Ltd, UK)

Others:

- Petri dishes (100 mm) (734-0006, VWR, USA)
- Cell scrapers (734-0386, VWR, USA)
- DC protein assay (5000111, Bio-Rad, USA)
- PageRuler™ Plus Prestained Protein Ladder, 10 to 250 kDa (26619, ThermoFisher, USA)
- PVDF Western Blotting membranes (03010040001, Roche, UK)
- NaN_3 (71289, Sigma-Aldrich, USA)

ELISA

ELISA (enzyme-linked immunosorbent assay) is a plate-based assay technique designed for detecting and quantifying soluble substances such as peptides, proteins, antibodies, and hormones. ELISA tests were performed according to Human TRF1/TERF1 ELISA Kit, Human TRF2/TERF2 ELISA Kit, and Human TERF1 Interaction Nuclear Factor 2 ELISA Kit. In this study, MCF7 cells were

used with tested compounds in selected concentrations (Table 6) for 48 h. The absorbance was measured using the Asys UVM340 multiwell plate reader. Experiments were conducted in triplicate. GraphPad Prism 8.0.1 was used to statistically analyze the results.

Materials:

- Petri dishes (100 mm) (734-0006, VWR, USA)
- Cell scrapers (734-0386, VWR, USA)
- NE-PER™ Nuclear and Cytoplasmic Extraction Reagents Kit (78833. ThermoFisher, USA)
- cOmplete™, EDTA-free Protease Inhibitor Cocktail (04693132001, Roche, Germany)
- 1xPBS (P4417, Sigma-Aldrich, USA)
- 0.025% trypsin (T-4674-100ML, Sigma-Aldrich, USA)
- DC protein assay (5000111, Bio-Rad, USA)
- Human TRF1 / TERF1 (Sandwich ELISA) ELISA Kit (LS-F8761, LSBio, USA)
- Human TERF2 / TRF2 (Sandwich ELISA) ELISA Kit (LS-F8761, LSBio, USA)
- Human TERF1 Interacting Nuclear Factor 2 (TINF2) ELISA Kit (MBS1603839, MyBioSource.com, USA)

Co-immunofluorescence

Immunofluorescence is a technique to visualize the localization of specific molecule targets within cells using the specificity of antibodies. In this study, five different compounds were used: B070 (100 μM) , B087 (50 μM), B176 (85 μM), B327 (75 μM) and A822 (10 μM). The colocalization of the TIN2 protein with the TRF1 or TRF2 proteins before and after the MCF7 cells treatment was checked. Briefly, cells grown on coverslips were fixed for 10 min in 4% formaldehyde, 0.2% Triton X-100, 20mM Pipes (pH 6.8), 1mM $MgCl_2$ and 10mM EDTA at room temperature followed by three 5 minutes 1xPBS washes at RT. Coverslips were blocked in 2.5% BSA and 0.1% Triton X-100 in 1xPBS overnight (4 °C). Cells

were incubated with primary antibodies and after three minutes 1xPBS washes, cells were incubated with appropriate secondary antibodies followed by three 10 minutes washes in 1xPBS + 0.1% Tween-20. DNA was stained with DAPI, and digital images were captured using a confocal microscope (Zeiss LSM 800, Jena, Germany) at magnifications of 63x, applying appropriate filters and wavelengths. GraphPad Prism 8.0.1 was used to statistically analyze the results.

Materials:

- 35 mm Petri dishes (734-0005, VWR, USA)
- Microscope slides (41-7626-2, medlab, Poland)
- Circular coverslip (12 mm diameter) (1-6283, bionovo, Poland)
- 1xPBS (P4417, Sigma-Aldrich, USA)
- Tween-20 (P1379, Sigma-Aldrich, France)
- 4% formaldehyde (432173427, POCH, Poland)
- Triton X-100 (X100, Sigma-Aldrich, USA)
- 20 mM Pipes (pH 6.8) (1.10220.1000, Merck, Germany)
- 1 mM $MgCl_2$ (M-0250, Sigma-Aldrich, Germany)
- 10 mM EDTA (E5134, Sigma-Aldrich, USA)
- 2.5% BSA (A7030, Sigma-Aldrich, USA)
- Anti – TRF1 antibody [TRF-78] (ab10579, Abcam, USA)
- Anti – TRF2 antibody [4A794] (ab13579, Abcam, USA)
- Anti-TINF2 antibody (HPA059061, Sigma-Aldrich, Switzerland)
- Donkey anti-Mouse IgG (H+L) Cross-Adsorbed Secondary Antibody, DyLight 488 (SA5-10166, Thermo Fisher Scientific, USA)
- Alexa Fluor® 594 AffiniPure Donkey Anti-Rabbit IgG (H+L) (711-585-152, Jackson ImmunoResearch, UK)
- DAPI (D9542, Sigma-Aldrich, Israel)
- Mounting medium
    - DABCO (D-2522, Sigma-Aldrich, Germany)
    - Glycerol **(**443320113, POCH, Poland)
    - 1xPBS (P4417, Sigma-Aldrich, USA)

Standard surface plasmon resonance (SPR) analyses

Standard surface plasmon resonance (SPR) analyses using Biacore T200 (Cytiva) were performed as described in the manufacturer's manual. The TIN2 peptide interaction with TRF1 or TRF2 protein was analyzed using 1) TRF1 or TRF2 protein immobilized on a CM5 Sensor Chip (Cytiva) in a 10 mM sodium acetate buffer pH 4.5 or 2) biotinylated TIN2 peptide immobilized on a SA Sensor Chip (Cytiva). The serial dilutions of analytes were prepared in PBS-P buffer (Cytiva) and injected over the prepared surface of the sensor chip. In all experiments, PBS-P buffer was used as a running buffer. All analyses were performed at temp. 25°C. The sensor chips surfaces were regenerated with 1.5M NaCl and 10mM glycine pH 3. After each analysis, an additional wash with 50% DMSO solution was done. The buffer flow rate was set to 30 µl/min in all kinetics experiments. Obtained data were analyzed using Biacore T200 Evaluation Software (Cytiva). The results are presented as sensorgrams obtained after subtracting the background response signal from a reference flow cell and a control experiment with buffer injection. For all analyzed peptides, at least three kinetic experiments were performed.

The SPR (Surface Plasmon Resonance) method was developed and performed by Dr. Katarzyna Węgrzyn at the Intercollegiate Faculty of Biotechnology of the University of Gdańsk and Medical University of Gdańsk (UG and GUMed, respectively).

Materials:

- TRF1 protein
- TRF2 protein
- TIN2 peptide (256-276): RHFNLAPLGRRRVQSQWASTR

Proteins and peptide were created by MSc Maciej Prusinowski of the University of Gdańsk.

Combined Immunofluorescence and Telomere Fluorescence in situ Hybridization (FISH) on Adherent Cells

Fluorescence *in situ* hybridization (FISH) is a cytogenetic technique developed in the early 1980s. FISH uses fluorescent DNA probes to target specific chromosomal locations within the nucleus, resulting in signals that can be detected using fluorescent microscopy [279]. This study was based on combining antibody-based immunofluorescence (IF) and fluorescence in situ hybridization (FISH) with fluorescence-conjugated telomere peptide nucleic acid (PNA) probes to identify interactions between proteins of interest and telomeric DNA. Briefly, MCF7 cells were grown in slides placed in a 35 mm dish. After 48 h and 72 h cell incubation with B070 (100 μM), B087 (50 μM), B176 (85 μM), B327 (75 μM) and A822 (10 μM) the slides were subjected to the immunofluorescence protocol as indicated in materials and methods. After washing twice with 1xPBST, the cells were fixed with 2% paraformaldehyde solution for 15 min at RT. Cells were then rinsed twice with deionized water, dehydrated in cold ethanol series (70%, 90% and 100%), incubated with a denatured PNA probe at 80°C for 5 minutes and hybridized overnight at room temperature in the dark in a humidified chamber. Next, the cells were washed twice, with PNA wash A (10 min each time) and three times with PNA wash B (10 min each time) with shaking. Finally, DNA was stained with DAPI for 10 min at room temperature in the dark and the slides were visualized using a confocal microscope (Zeiss LSM 800, Jena, Germany) at a magnification of 63x, applying appropriate filters and wavelengths. GraphPad Prism 8.0.1 was used to statistically analyze the results.

Materials:

- 35 mm Petri dishes (734-0005, VWR, USA)
- Microscope slides (41-7626-2, medlab, Poland)
- Round glass coverslip (12 mm diameter) (1-6283, bionovo, Poland)
- 1xPBS (P4417, Sigma-Aldrich, USA)
- Tween-20 (P1379, Sigma-Aldrich, France)
- 4% formaldehyde (432173427, POCH, Poland)
- Triton X-100 (X100, Sigma-Aldrich, USA)

- 20 mM Pipes (pH 6.8) (1.10220.1000, Merck, Germany)
- 1 mM $MgCl_2$ (M-0250, Sigma-Aldrich, Germany)
- 10 mM EDTA (E5134, Sigma-Aldrich, USA)
- 2.5% BSA (A7030, Sigma-Aldrich, USA)
- Anti-TINF2 antibody (HPA059061**,** Sigma-Aldrich, Switzerland)
- Alexa Fluor® 594 AffiniPure Donkey Anti-Rabbit IgG (H+L) (711-585-152, Jackson ImmunoResearch, UK)
- Ethanol absolute (1.00983.1011, Merck, Germany)
- PNA (F2003, Pnagene, South Korea)
- PNA hybridization solution
    - 70% formamide (47671, Sigma-Aldrich, USA)
    - 0.25% Blocking reagent
        - ✓ 10% Blocking reagent (11096176001, Roch, Germany)
        - ✓ 100 mM maleic acid (M0375, Sigma-Aldrich, USA)
        - ✓ 150 mM NaCl (794121116, POCH, Poland)
    - 10 mM TrisCl, pH 7.5 (T6066, Sigma-Aldrich, USA)
- PNA Wash A
    - 70% formamide (47671, Sigma-Aldrich, USA)
    - 10 mM TrisHCl, pH 7.5 (T6066, Sigma-Aldrich, USA)
- PNA Wash B
    - 50 mM TrisHCl, pH 7.5 (T6066, Sigma-Aldrich, USA)
    - 150 mM NaCl (794121116, POCH, Poland)
    - 0.8% Tween-20 (P1379, Sigma-Aldrich, France)
- DAPI (D9542, Sigma-Aldrich, Israel)
- Mounting medium
    - 25 mg/ml DABCO (D-2522, Sigma-Aldrich, Germany)
    - 90% v/v glycerol (443320113, POCH, Poland**)**
    - 10% v/v 1xPBS (P4417, Sigma-Aldrich, USA)

Labeling Mitochondria with MitoTracker Dyes

Mitochondrial morphology is important for the function of this critical organelle and, accordingly, altered mitochondrial structure is exhibited in many pathologies [280]. At this point, MitoTracker Green was used to detect these organelles. A staining solution of MitoTracker Green was prepared from a 10 mM stock (prepared in DMSO) which was diluted in sterile 1xPBS to a final concentration of 20 µM (0.2% DMSO). MCF7 cells were treated with B070 (100 µM), B087 (50 µM), B176 (85 µM) and B327 (75 µM) and A822 (10 µM) for 48 h and then incubated at room temperature for 45 minutes (37 °C, in the dark). The staining solution was aspirated and cells were then washed in 1xPBS. Hoechst 33342 was used for the staining of cell nuclei. The same experiment was performed on primary derived cell cultures from normal and cancer breast tissues that were treated with tested compounds (Table 6) for 48 h. Glass slides prepared were observed in the bright field mode using an Olympus BX60 microscope.

Materials:

- 35 mm Petri dishes (734-0005, VWR, USA)
- Microscope slides (41-7626-2, medlab, Poland)
- 22 x 22 mm glass coverslips (42-2222-0, medlab, Poland)
- MitoTracker™ Green FM (M7514, Invitrogen, USA)
- 1xPBS (P4417, Sigma-Aldrich, USA)
- DMSO (D8418, Sigma-Aldrich, USA)
- 1 µg/ml Hoechst 333342 (14533, Sigma-Aldrich, USA)

Reactive Oxygen Species Generation

ROS have a dual role in cancer development; on one hand, they can promote molecular genetic alterations that are necessary for tumor initiation, growth, and progression, as well as the acquisition of treatment resistance [281]. On the other hand, permanently elevated ROS levels have cytotoxic effects, inducing activation of apoptotic pathways or inhibiting resistance to anticancer treatments [282] [283]. ROS production was measured by staining cells with 1 µM 2',7'-

dichlorodihydrofluorescein diacetate (CM-H2DCFDA) (15 min, at 37 °C and 5% CO_2 culture conditions), followed by a single 1xPBS wash and immediately analyzed with a Guava easyCyte flow cytometer (Merc, Burlington, USA). 7-AAD was used at 1 µg/ml to differentiate between live and dead cells. MCF7 cells were treated with tested compounds for 0.5, 1, 3, 6 and 24 h. A negative control (growth medium without drug) was also included at each time of testing. Concentrations used in the assay were selected according to drug potency (Table 6). The experiments were performed in triplicates. GraphPad Prism 8.0.1 was used to statistically analyze the results.

Materials:

- Petri dishes (35 mm) (734-0005, VWR, USA)
- Eppendorf tubes (1.5 ml) (3810X, Eppendorf, UK)
- 1xPBS (P4417, Sigma-Aldrich, USA)
- 0.025% trypsin (T-4674-100ML, Sigma-Aldrich, USA)
- 1 µM 2',7'- dichlorodihydrofluorescein diacetate (CM-H2DCFDA) (c6827, ThermoFischer, USA)
- 1 µg/ml 7-AAD (A1310, ThermoFisher, USA)

Telomere Fluorescent *in situ* Hybridisation (FISH) on Cytocentrifuged Chromosome Spreads (Metaphase-TIF Assay)

Telomere dysfunction-induced focus (TIF) assay allows efficient profiling of telomere disfunction in cells. In this study, primary derived cell cultures from normal and cancer breast tissue were treated (48 h) by tested compounds: B327 (50 µM) and A822 (10 µM). To prepare metaphase spreads, cells were treated with 0.3 µg/ml colcemid at 37°C for 2 h and harvested with a pre-warmed Ohnuki buffer. The cells were then fixed in methanol-acetic acid (3:1 v/v ratio) and dropped onto a clean glass slide. Cells were then dehydrated in cold ethanol series (70%, 90% and 100%), incubated with a denatured PNA probe at 80°C for 5 minutes and hybridized overnight at room temperature in the dark in a humidified chamber. After that, cells were subjected to the FISH protocol as indicated of materials and methods. Finally, the slides were visualized and

images were captured using a confocal microscope (Zeiss LSM 800) at a magnification of 63x, applying appropriate filters and wavelengths.

Materials:

- 100 mm Petri dishes (734-0006, VWR, USA)
- Microscope slides (41-7626-2, medlab, Poland)
- 24 x 50 mm glass coverslips (42-2450-0, medlab, Poland)
- Ohnuki buffer
  - KCl (P-5405, Sigma-Aldrich, Germany)
  - $NaNO_3$ (S8170, Sigma-Aldrich, USA)
  - $C_6H_5Na_3O_7$ (1.11037, Sigma-Aldrich, USA)
- Methanol (M1775, Sigma-Aldrich, USA)
- Glacial acetic (A6283, Sigma-Aldrich, USA)
- Ethanol absolute (1.00983.1011, Merck, Germany)
- PNA (F2003, Pnagene, South Korea)
- PNA hybridization solution
  - 70% formamide (47671, Sigma-Aldrich, USA)
  - 0.25% Blocking reagent
    - ✓ 10% Blocking reagent (11096176001, Roch, Germany)
    - ✓ 100 mM Maleic acid (M0375, Sigma-Aldrich, USA)
    - ✓ 150 mM NaCl (794121116, POCH, Poland)
  - 10 mM TrisHCl, pH 7.5 (T6066, Sigma-Aldrich, USA)
- PNA Wash A
  - 70% formamide (47671, Sigma-Aldrich, USA)
  - 10 mM TrisHCl, pH 7.5 (T6066, Sigma-Aldrich, USA)
- PNA Wash B
  - 50 mM TrisHCl, pH 7.5 (T6066, Sigma-Aldrich, USA)
  - 150 mM NaCl (794121116, POCH, Poland)
  - 0.8% Tween-20 (P1379, Sigma-Aldrich, France)
- DAPI (D9542, Sigma-Aldrich, Israel)
- Mounting medium
  - 25 mg/ml DABCO (D-2522, Sigma-Aldrich, Germany)
  - 90% v/v glycerol (443320113, POCH, Poland)

- 10% v/v 1xPBS (P4417, Sigma-Aldrich, USA)

Actin Cytoskeleton Evaluation by Phalloidin Staining

Phalloidin is a highly selective bicyclic peptide used for staining actin filaments (also known as F-actin). It binds to all variants of actin filaments in many different species of animals and plants [284]. In brief, primary cell cultures derived from normal and cancer breast tissues were plated onto coverslips (22x22 mm) in 35 mm Petri dishes and treated by tested compounds (Table 6) for 48 h. The cells were fixed in 4% paraformaldehyde for 15 min at room temperature, permeabilized in 0.25% Triton X-100 for 10 min at room temperature, blocked in 1xPBS containing 3% BSA overnight (4 °C) and stained with tetramethyl rhodamine isothiocyanate-phalloidin for 1h at 37 °C in the dark. The samples were washed with 1xPBS three times with 5 min intervals between each step and DNA was stained with DAPI for 10 min at room temperature in the dark. Digital images were captured using a confocal microscope (Zeiss LSM 800) at a magnifications of 63x, applying appropriate filters and wavelengths.

Materials:

- 35 mm Petri dishes (734-0005, VWR, USA)
- Microscope slides (41-7626-2, medlab, Poland)
- Round glass coverslips (12 mm diameter) (1-6283, bionovo, Poland)
- 1xPBS (P4417, Sigma-Aldrich, USA)
- 4% paraformaldehyde (158127, Sigma-Aldrich, USA)
- Tween-20 (P1379, Sigma-Aldrich, Francja)
- Alexa Fluor 647 phalloidin (A22287, ThermoFisher, USA)
- DAPI (D9542, Sigma-Aldrich, Israel)
- Mounting medium
    - DABCO (D-2522, Sigma-Aldrich, Germany)
    - Glycerol (443320113, POCH, Poland)
    - 1xPBS (P4417, Sigma-Aldrich, USA)

Results – part I

In vitro Cytotoxicity

Cell viability data using MTT assay measured the percentage reduction in activity relative to control cells. The mean of the control was standardized and defined as 100% cell activity. The difference in cell viability between the reference compound (doxorubicin) and cells after treatment with tested compounds was analyzed using one-way ANOVA corrected by Tukey's test.

The first stage of research tested 11 compounds in three mammalian cell lines including two breast cancer cell lines: MCF7 and MDA-MB-231 and one non-cancer cell line: MCF 10A. The results showed that the B070, B087, B176, B327 and A822 compounds induced the cytotoxic effect (Table 8). Based on these results, 5 compounds were selected for further deeper analysis in 7 mammalian cell lines including (i) four breast cancer cell lines: BT474, SK-BR-3, T47D and BT20; (ii) one multidrug-resistant breast cancer cell line: MCF7/Adr; (iii) human mammary epithelial cells (HMEC). All cell lines were treated with different concentrations of the tested compounds in order to determine the half-maximal inhibitory concentration (IC_{50}), which is the concentration of a drug that inhibits 50% of cell growth or viability after a specified treatment period. The range of concentrations used was 0.78-100 μM for the tested compounds and 0.01-12.5 μM for doxorubicin. The treatment period was 72 h. As demonstrated in Table 8, the strongest cytotoxic effect was obtained after the application of compounds: A822 for all cell lines (range of IC_{50}: 2-20μM) and B327 for most cell lines (range of IC_{50}: 13-35μM). Importantly, the application of A822 appeared effective in the multidrug-resistant breast cancer cell line (MCF7/Adr) towards which A822 evoked even higher cytotoxicity than doxorubicin .

Table 8. IC_{50} values for compounds: B070, B087, B176, B327, A822 (for cell lines: MCF7, MDA-MB-231, MCF 10A, BT-474, SK-BR-3, T47D,BT20 MCF7/Adr and HMEC), A822, A378, A628, A670, ST50, ST2S (for cell lines: MCF7, MDA-MB-231, MCF 10A). Doxorubicin used as a cytotoxic reference drug. The data shown are means ± SEM obtained from three independent experiments.

Compound	IC_{50} (μM)								
	Cell lines								
	MCF7	MDA-MB-231	MCF 10A	BT474	SK-BR-3	T47D	BT20	MCF7/Adr	HMEC
B070	> 50	> 50	28.35 ± 1.97	> 50	33.99 ± 0.47	30.14 ± 2.14	> 50	3.88 ± 0.56	> 50
B087	38.06 ± 1.20	35.85 ± 3.21	25.30 ± 3.56	45.07 ± 2.00	27.83 ± 3.08	14.93 ±0.74	39.97 ± 1.85	3.68 ± 0.92	31.96 ± 6.02
B176	28.37 ± 0.93	> 50	37.15 ± 1.75	> 50	37.21 ± 0.61	21.29 ± 1.57	25.13 ± 0.88	30.37 ± 1.79	> 50
B280	> 50	> 50	> 50	-	-	-	-	-	-
B327	35.84 ± 1.58	30.27 ± 1.56	16.08 ± 0.79	> 50	29.12 ± 0.89	20.25 ± 1.48	13.87 ± 0.82	> 50	26.80 ± 1.98
A822	18.21 ± 2.37	14.5 ± 1.00	12.44 ± 1.05	20.51 ± 0.24	10.35 ± 0.55	3.44 ± 0.37	8.28 ± 0.57	2.15 ± 0.18	8.16 ±2.00
A378	> 50	> 50	> 50	-	-	-	-	-	-
A628	> 50	> 50	> 50	-	-	-	-	-	-
A670	> 50	> 50	> 50	-	-	-	-	-	-
ST50	> 50	> 50	> 50	-	-	-	-	-	-
ST2S	> 50	> 50	> 50	-	-	-	-	-	-
Doxorubicin	0.12 ± 0.04	0.52 ± 0.03	0.27 ± 0.03	0.78 ± 0.02	0.72 ± 0.01	0.31 ± 0.05	0.11 ± 0.01	17.86 ± 0.18	0.17 ± 0.04

The one-way ANOVA analysis was corrected by Tukey's test to delineated the difference in cell viability between B070, B087, B176, B327 or A822 compounds and the reference compound (doxorubicin) (Figure 17). No statistically significant differences were observed between A822 treatment and doxorubicin in most of the tested cell lines, indicating strong cytotoxicity of novel compound A822. Interestingly, the difference at the level of P<0.001 was observed between efficiency A822 and doxorubicin in MCF7/Adr cells' viability. For these MCF7/Adr cells, the compound A822 demonstrated stronger cytotoxic activity than doxorubicin (IC_{50} 2.15 versus 17.86, respectively). Based on these results, five compounds were selected for the next experiments.

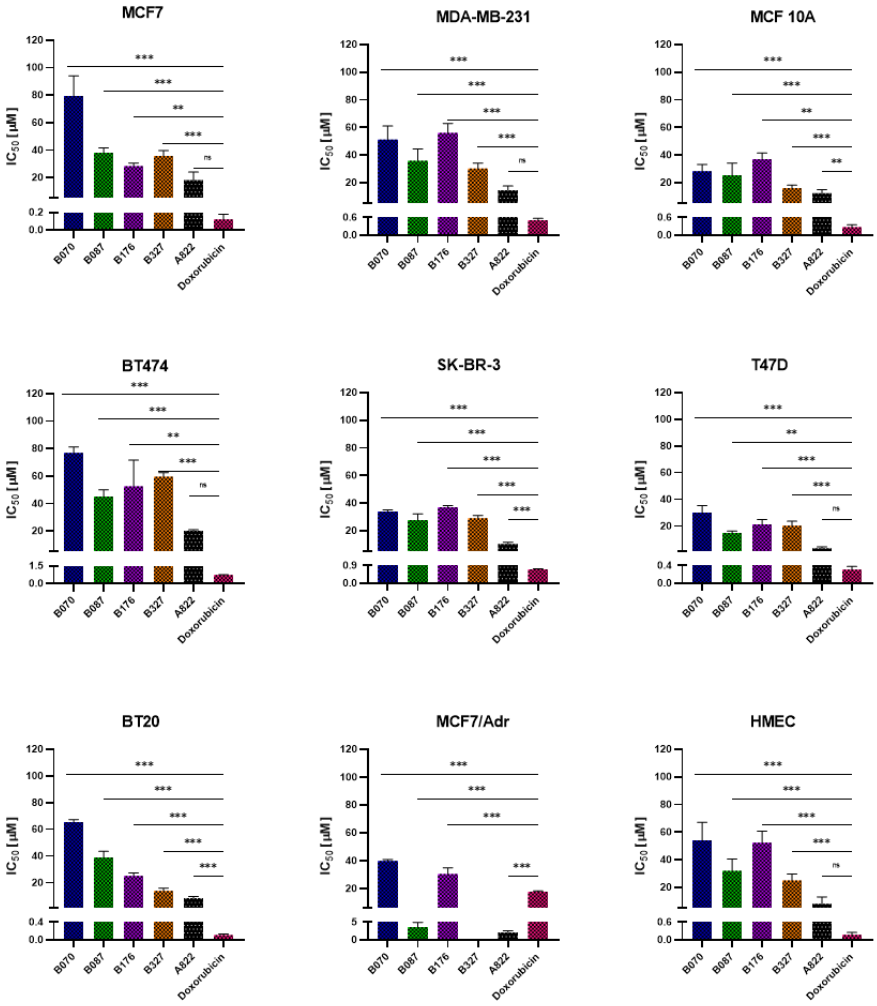

Figure 17. Comparison of the IC_{50} values of the cytotoxicity of TRF1 / TRF2-TIN2 protein interaction inhibitors and the significance of changes in IC_{50} values for inhibitors with the IC_{50} values for doxorubicin (*** - P<0.001, ** - P<0.01, * - P<0.05, ns - P>0.05, one-way ANOVA corrected by Tukey's test).

Investigation of Anticancer Effectivity by Clonogenic Survival Assay

To further confirm the anticancer efficacies of tested compounds, the clonogenic assay was employed to determine the effect of the derivatives on the survival and proliferation of MCF7 cells. Cells were grown in RPMI 1640 media for 12 days with the selected compounds. As demonstrated in our results (Figure 18), all compounds efficiently suppressed cancer cell growth from doses as low as 25μM (B176), 22.5μM (B070 and B087), 20μM (B0327) and 7.5μM (A822).

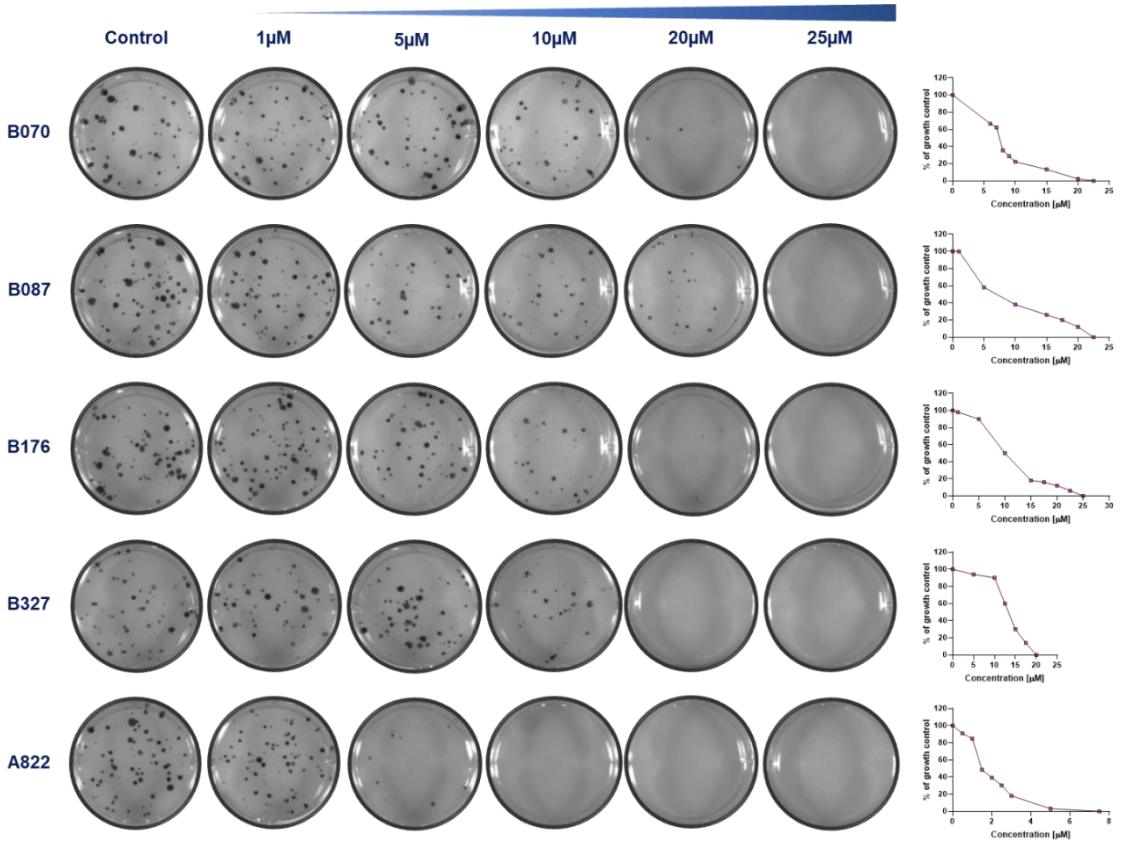

Figure 18. The effect of study compounds on colony formation in MCF7 cells line was treated with the indicated doses of B070, B087, B176, B327, and A822 for 12 days.

Effects on Cell Cycle Progression

Based on the results of the above MTT assay and clonogenic survival assay it was explored whether B070, B087, B176, B327 and A822 have interfered with cell cycle progression. MCF7, MDA-MB-231 cells were treated with tested compounds at different concentrations (Table 6) for 24 h and 48 h and then cell cycle assessed via propidium iodide (PI)/RNase staining for cell cycle staging. Figure 19 shows the increase in the sub-G1 population of treated MCF7 cells, from 2.7% in the untreated control group to 9.23% (B070), 8.35% (B087), 8.51% (B176), 9.96% (B327) and 8.31% (A822) after 24 h. Cell cycle arrest for MCF7 line occurred at the G1 phase, as indicated by a significant increase in the G1 phase populations when treated with B070, while, cell cycle arrest occurred at the G2 phase for cells after treatment with B087, B327 and A822. Furthermore, a decrease in the S-phase population of cells was observed after the treatment of all compounds. The proportion of cells in S phase decreased from 33.75% in the untreated control group to 8.63% (B070), 13.76% (B087), 8.35% (B176), 7.50% (B327) and 4.67% (A822) after 24 h. These significant statistical differences were also maintained after 48 h, proving that the tested compounds interfered with the cell cycle.

Cell cycle analysis of the MDA-MB-231 line showed an increase in the sub-G1 population of treated cells, from 1.51% in the untreated control group to 3.14% (B176), 4.00% (B327) and 4.30% (A822) after 24 h (Figure 20). However, the compounds did not induce noticeable changes in the cell cycle of this cell line.

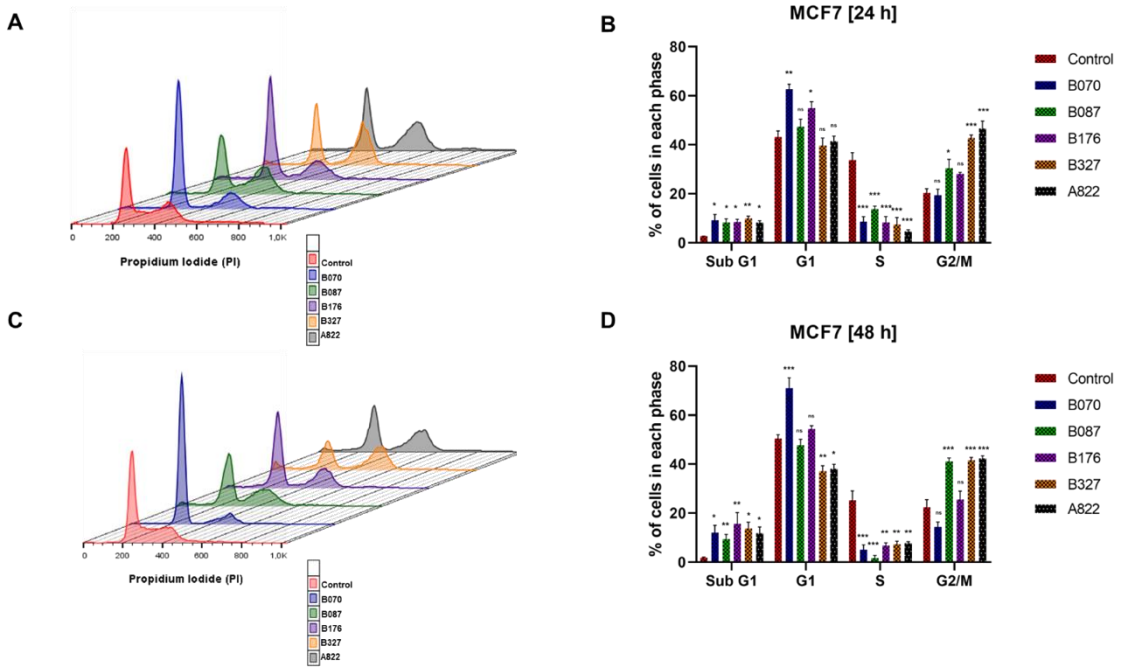

Figure 20. Flow cytometry analysis of MCF7 line cell cycle. A and C - representative flow cytometry histograms of the percentage of cells in Pre-G1, G0/G1, S and G2/M phases of the cell cycle from MCF7 cells treated with B070 (100 μM), B087 (50 μM), B176 (85 μM), B327 (75 μM), A822 (15 μM) and untreated control for 24 h and 48 h. B and D - quantification of percentage of cells in each cell cycle phase for cells treated with compounds and untreated control. Data presented as standard error of mean bar and asterisks denote statistical significance (*** - P<0.001, ** - P<0.01, * - P<0.05, ns - P>0.05) by ANOVA test.

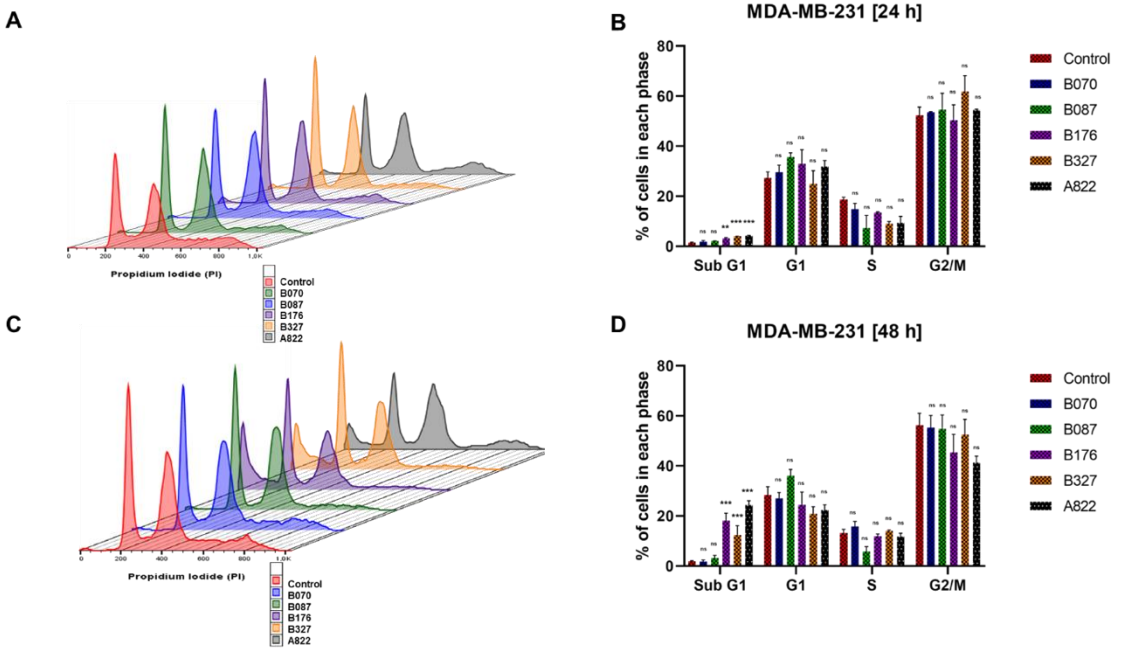

Figure 19. Flow cytometry analysis of MDA-MB-31 line cell cycle. A and C - representative flow cytometry histograms of the percentage of cells in Pre-G1, G0/G1, S and G2/M phases of the cell cycle from MDA-MB-231 cells treated with B070 (60 μM), B087 (50 μM), B176 (90 μM), B327 (80 μM), A822 (15 μM) and untreated control for 24 h and 48 h. B and D - quantification of the percentage of cells in each cell cycle phase in cells treated with compounds or untreated control. Data presented as the standard error of mean bar and asterisks denote statistical significance (*** - P<0.001, ** - P<0.01, * - P<0.05, ns - P>0.05) by ANOVA test.

Identification of Cell Death Type

The cell death mechanisms have become an important research estimate for deeper understanding of the mechanisms governing cell survival and cell proliferation in cancer. Cell death can be broadly characterized as either necrotic or apoptotic, depending on the morphological, and biochemical features of the cell itself [285]. Annexin V/7-AAD assay was performed to quantify the cells undergoing apoptosis and necrosis. MCF7, MDA-MB-231 cells were treated with testing compounds at different concentrations (Table 7) for 3 h, 6 h and 24 h, and then flow cytometry were used. As shown in Figure 21, necrosis was the major mechanism of cell death caused by all the tested compounds in MCF7 cells. Figure 22 shows that apoptosis was the major mechanism of cell death caused by the tested compounds in MDA-MB-231 cells.

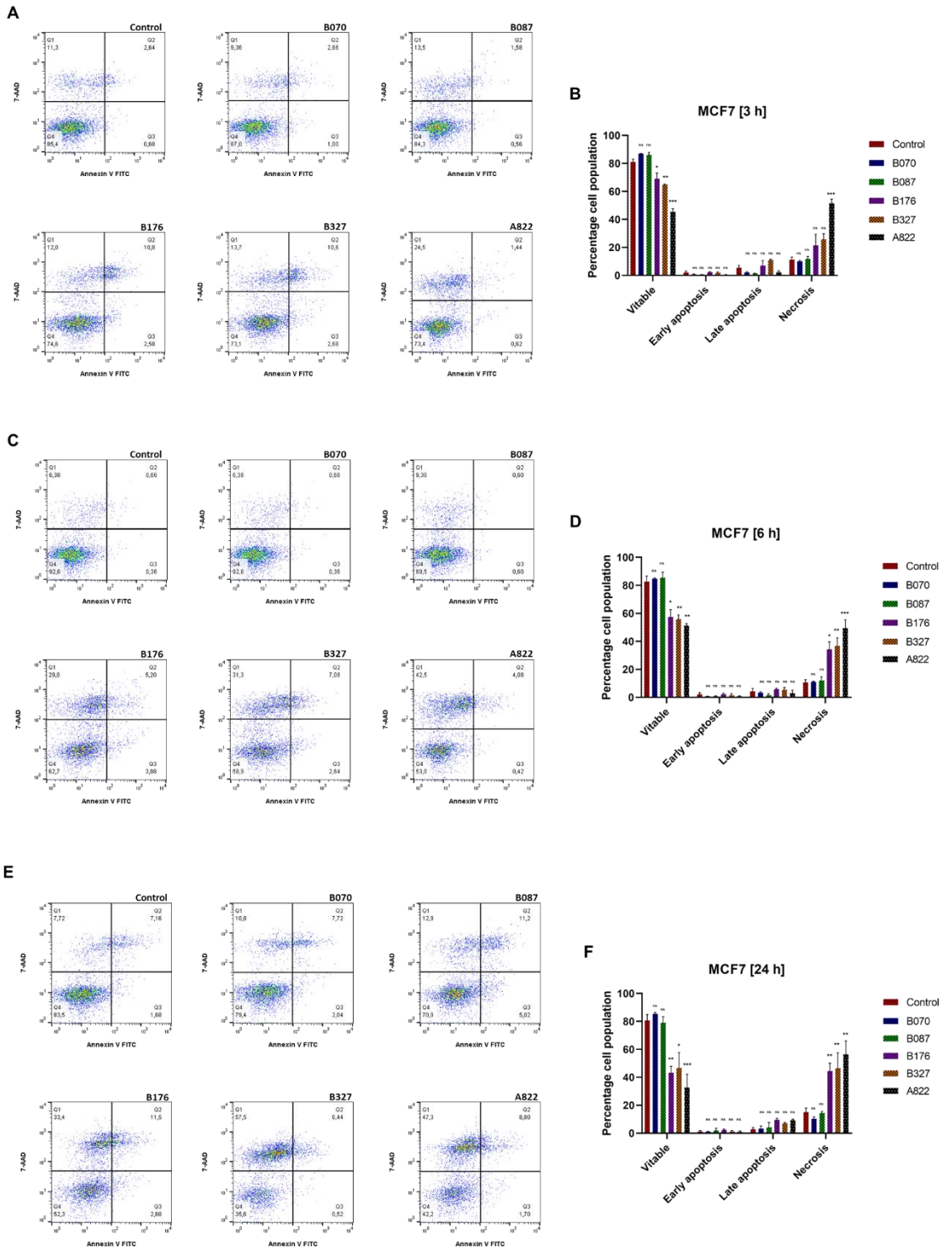

Figure 21. Apoptosis measurement of apoptosis and necrosis by flow cytometry (Q1- necrotic cells, Q2- late apoptotic/necrotic cells, Q3- early apoptotic cells, Q4- live cells). A, C, E - apoptosis and necrosis rates of MCF7 cells population treated with B070 (100 μM), B087 (50 μM), B176 (85 μM), B327 (75 μM), A822 (25 μM), and untreated control for 3 h, 6h and 24 h measured using flow cytometry with double staining of Annexin V and 7-AAD. B, D, F - quantification of % of apoptotic and necrotic in cell population treated with compounds and untreated control. Data presented as standard error mean bar and asterisks denote statistical significance (*** - P<0.001, ** - P<0.01, * - P<0.05, ns - P>0.05) by ANOVA test.

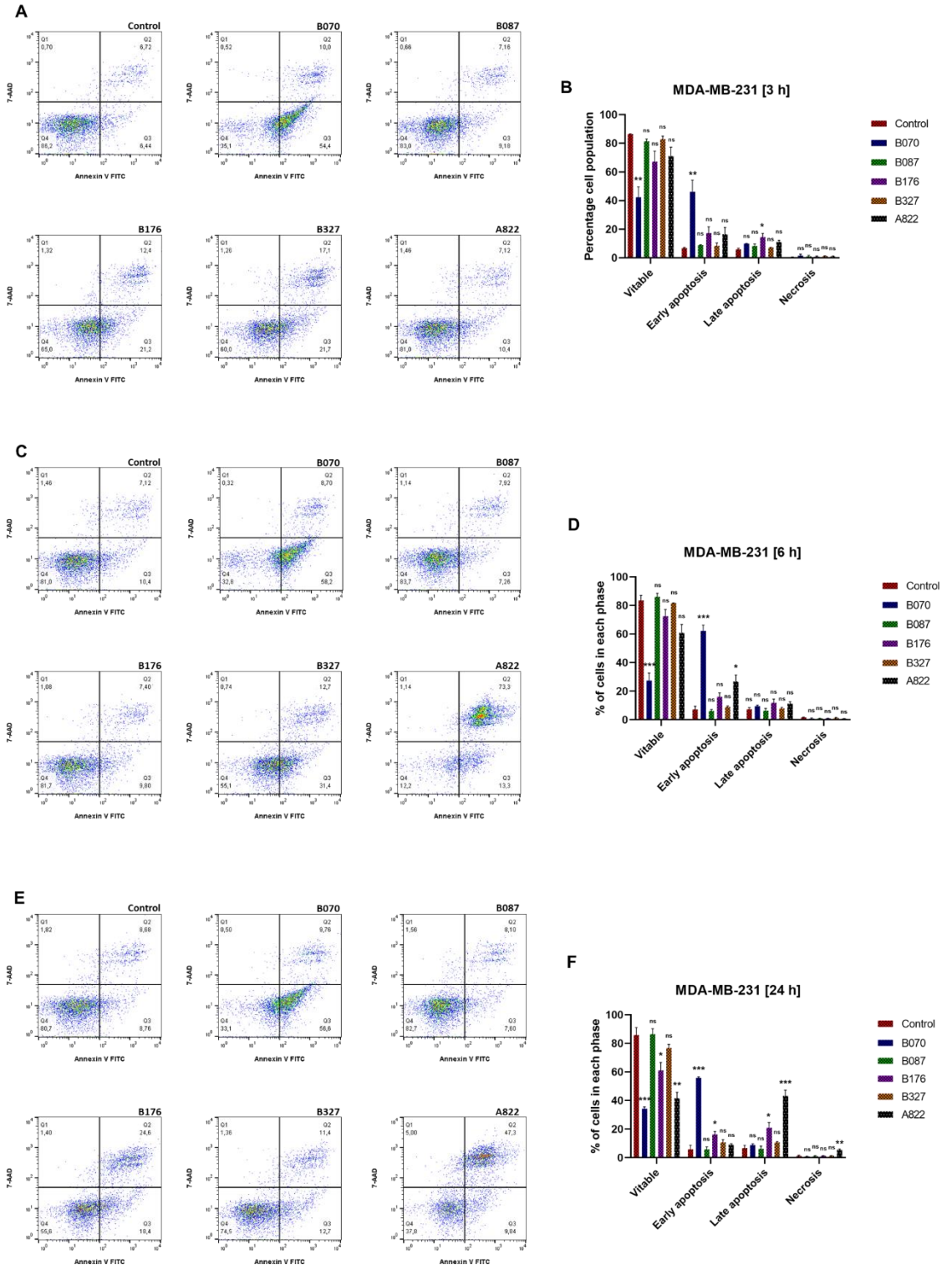

Figure 22. Apoptosis measurement of apoptosis and necrosis by flow cytometry (Q1- necrotic cells, Q2- late apoptotic/necrotic cells, Q3- early apoptotic cells, Q4- live cells). A, C, E - apoptosis and necrosis rates of MDA-MB-231 cells population treated with B070 (60 μM), B087 (50 μM), B176 (90 μM), B327 (80 μM), A822 (25 μM), and untreated control for 3 h, 6h and 24 h measured using flow cytometry with double staining of Annexin V and 7-AAD. B, D, F - quantification of % of apoptotic and necrotic in cell population treated with compounds and untreated control. Data presented as standard error mean bar and asterisks denote statistical significance (*** - P<0.001, ** - P<0.01, * - P<0.05, ns - P>0.05) by ANOVA test.

Since it has been reported that permanent growth arrest and failure to enter into S-phase are characteristics of the senescent phenotype, MCF7 cells were stained by SA-β-gal. For this purpose, cells were treated with compounds for 120 h. Interestingly, only the B327 and A822 significantly induced increased SA-β-gal in MCF7 cells (Figure 23). The received results were strongly correlated with results from cell cycle analysis. Moreover, this observation supports, the proposed mechanism of the action of the compounds consisting of the deregulation of the shelterin complex. This process contributes to telomere shortening and damage, which are recognized causes of cellular senescence and aging.

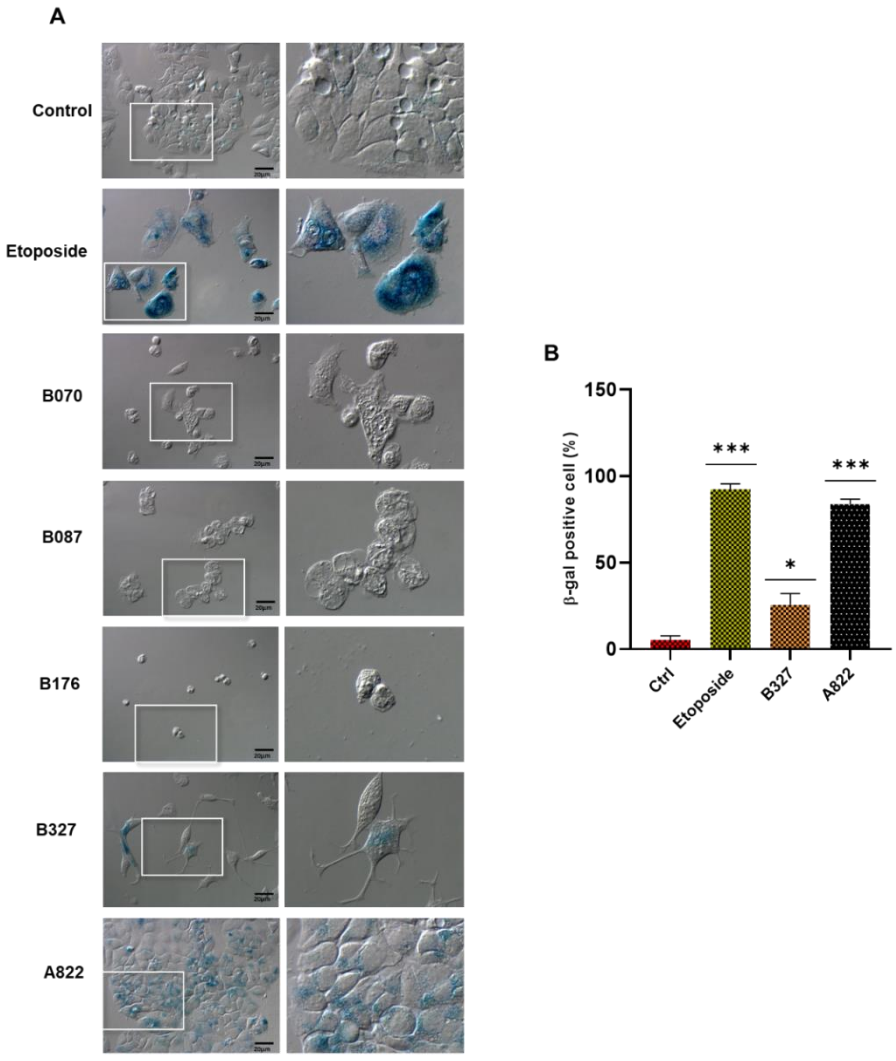

Figure 23. Senescence-associated β-galactosidase (SA-β-gal) staining. A - representative images of the MCF7 cell line after exposure to the following compounds: B070 (100 μM), B087 (50 μM), B176 (85 μM), B327 (75 μM), A822 (10 μM) and etoposide (10 μM) after 120h incubation. Control denotes reference. Scale bars correspond to 20 μm. B - quantification of SA-β-gal positive cells for quiescent control, Etoposide, B327 and A822. The percentage of SA-β-Gal positive cells as an indication of SA-β-gal activity was quantified in n = 10 images per condition. Data presented as standard error mean bar and asterisks denote statistical significance (*** - P<0.001, ** - P<0.01, * - P<0.05, ns - P>0.05) by ANOVA test.

To further elucidate the anticancer effects of testing compounds, other cell-death associated responses upon treatment of the cells with B070 (100 μM), B087 (50 μM), 0176 (85 μM), B327 (75 μM), A822 (10 μM) were examined. The acridine orange staining was used to analyze the formation of AVOs (acidic vesicular organelles), which is characteristic for autophagy. None of the compounds induced the formation of orange AVOs in the MCF7 cells (cells exhibited green fluorescence, indicating lack of AVOs) after 72 h of treatment (Figure 24). However, in contrast to the untreated control group, numerous vesicles in the cytoplasm were observed in the MCF7 cells treated with A822.

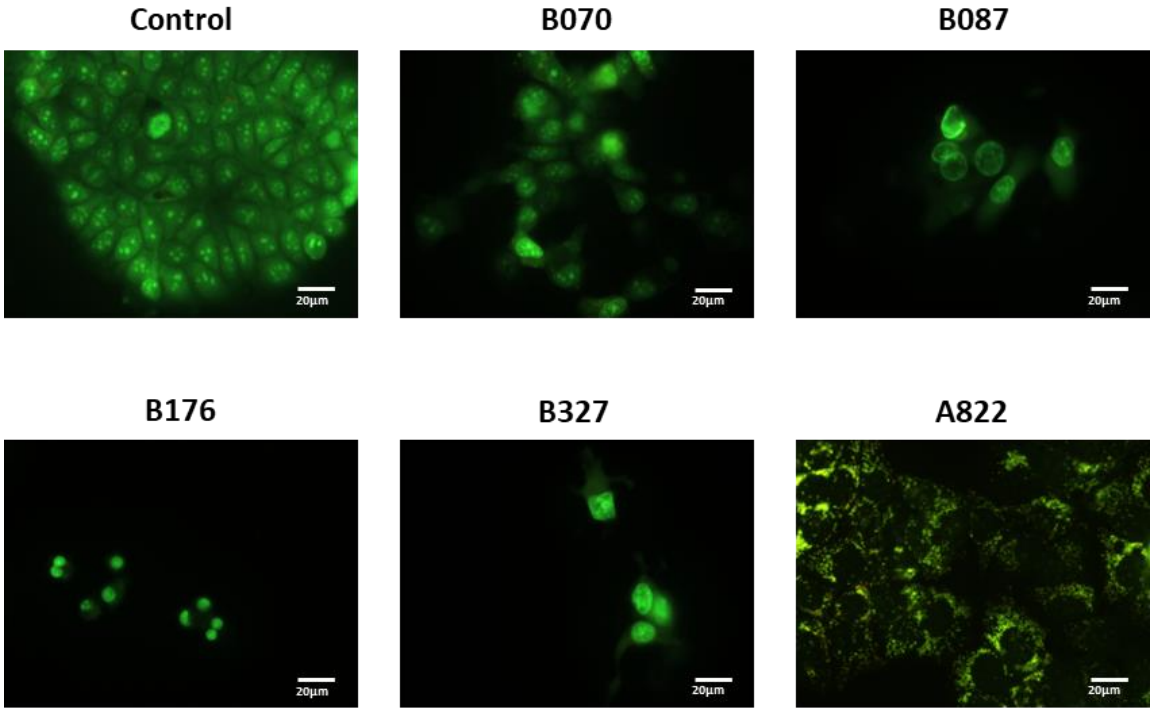

Figure 24. Representative images of acridine orange (AO) staining of MCF7 cells following treatment with B070 (100 μM), B087 (50 μM), 0176 (85 μM), B327 (75 μM), A822 (10 μM). Incubation time - 72 h. Scale bars correspond to 20 μm.

Compounds Accumulate in Lipid Droplets

Since numerous vesicles in the cytoplasm appeared in the MCF7 cells treated with A822, therefore, MCF7 cells were stained with Nile red (after 48 h incubation with compounds) to test the presence of lipid droplets. Lipid droplets (LDs) are complex organelles with multiple functions that include modulation of nuclear processes, protein trafficking, membrane trafficking, and phospholipid recycling as well as metabolic

regulation and storage of hydrophobic components [286,287]. The stain demonstrated an increase in LDs size and number in the cells for all compounds (Figure 25). The compounds-induced formation of LDs was quantified by flow cytometry after staining the cells with Nile Red. The results obtained from the flow cytometry demonstrated an increase in the percentage of cells containing LDs (Figure 25).

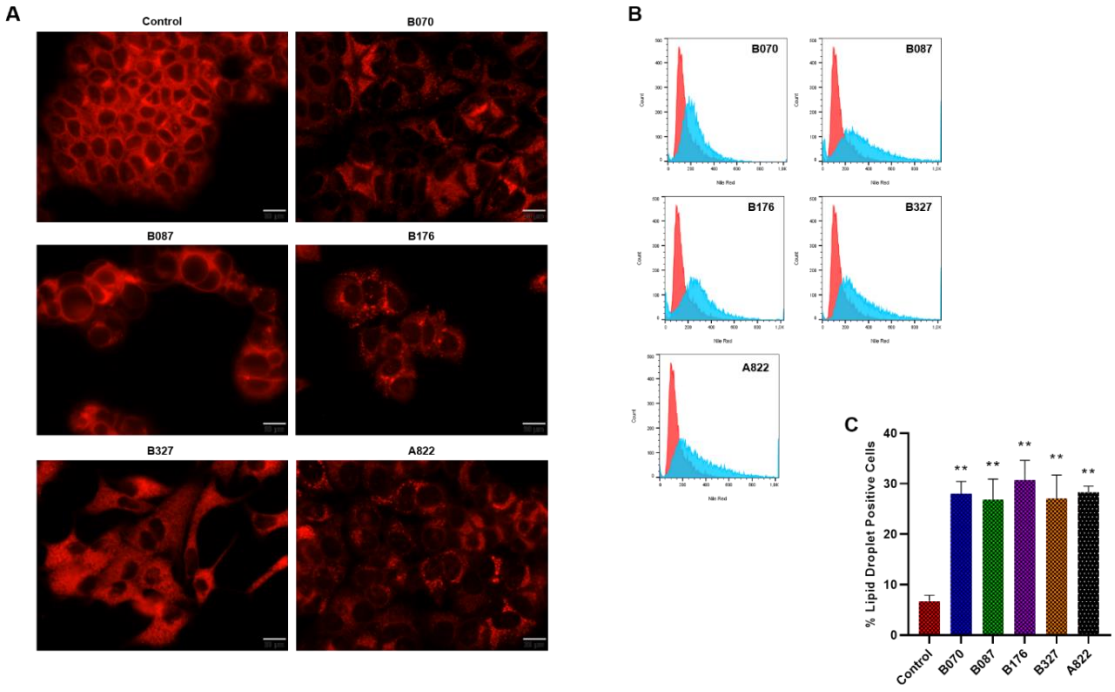

Figure 25. Detection of lipid droplets (LDs) in MCF7 cells. A - Representative images of Nile Red staining of MCF7 cells following treatment with B070 (100 µM), B087 (50 µM), 0176 (50 µM), B327 (75 µM), A822 (10 µM). Incubation time - 48 h. Scale bars correspond to 20 µm. B - Representative flow cytometry histograms of the percentage of MCF7 cells treated with compounds and untreated control. C - The percentage of LD-positive cells. Data presented as standard error mean bar, asterisks denote statistical significance (*** - P<0.001, ** - P<0.01, * - P<0.05, ns - P>0.05) by ANOVA test.

Next it was examined whether compounds accumulated in lipid droplets. In the study Nile Red was used to detect LDs and Hoechst 33342 to stain nuclei in MCF7 cells after 48 h of treatment with tested compounds. The result show, that all the compounds tended to accumulate in LDs (Figure 26).

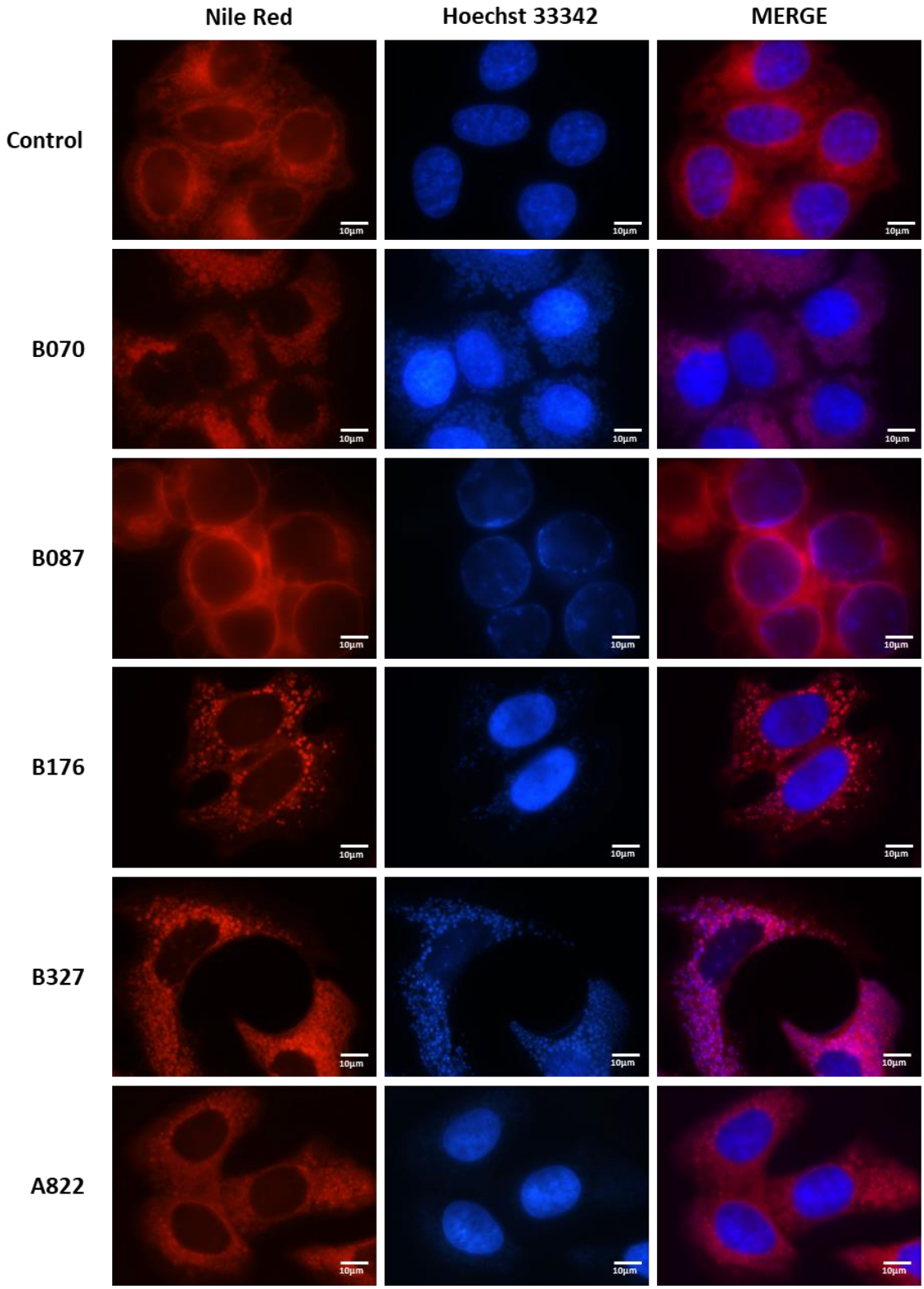

Figure 26. Representative image of compound accumulation in lipid droplets in MCF7 cells. Cell nuclei were stained with Hoechst 33342. Incubation time – 48 h. Scale bars correspond to 10 µm.

Effects of Tested Compounds on DNA Damage

The most detrimental type of DNA damage is appearance of double-strand breaks (DSBs). Unrepaired DSBs can cause senescence in proliferating cells [288]. Both TRF1 and TRF2 play a critical role in DNA damage responses (DDR), and TIN2 is key regulator of both TRFs. To determine whether perturbing TIN2's interaction with TRF1 or TRF2 after testing compounds treatment activates DDR at telomeres, the DNA damage marker γ-H2AX was used (Figure 27). In the study, MCF7 cells were treated with compounds at different concentrations for 24 h. The result showed that none of the compounds induced DSBs in treated cells.

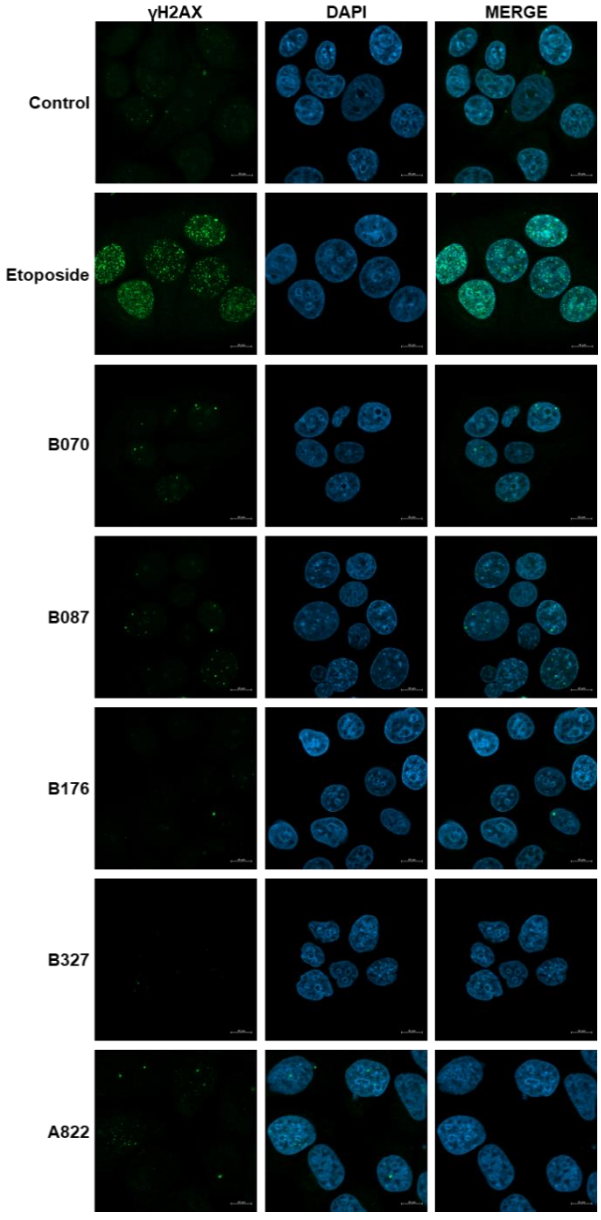

Figure 27. γ-H2AX foci formation (green) after exposure to the following compounds: MCF7 cells treated for 24 h with B070 (100 μM), B087 (50 μM), 0176 (85 μM), B327 (75 μM), A822 (10 μM) and etoposide (10 μM). DNA was stained by DAPI (blue). Scale bars correspond to 10 μm.

Telomere Length Shortening

Telomere length (TL) normally decreases with each cell division due to the incomplete replication of the lagging strand [289]. Prolonged telomere shortening or T-loop unwinding can activate the DNA damage response leading to apoptosis or replicative senescence. Cells escaping the corresponding checkpoint are prone to genomic instability, increasing the risk of tumorigenesis [289]. Telomere maintenance is primarily mediated by the ribonucleoprotein enzyme, telomerase [290]. The shelterin complex coordinates the regulation of telomerase activity at telomeres and ultimately helps define the set point for telomere length, establishing telomere length homeostasis. Based on the previous studies, the average telomere length of the samples was measured. The MCF7 cells were collected after 10 passages exposed to B070 (50 μM), B087 (50 μM), 0176 (30 μM), B327 (20 μM) and A822 (15 μM) compounds. The qPCR assay was used to directly compare the average telomere length in treated samples and untreated control. The telomere primer set recognized and amplified telomere sequences. The single copy referenced (SCR) primer set recognizes and amplifies a 100 bp-long region on human chromosome 17, and served as a reference for data normalization. The comparative ΔΔCq (Quantification Cycle Value) method demonstrated that the use of A822 and B327 compounds caused a reduction in telomere length compared to the control by 1.15 times for A822 and by 1.42 times after the application of B327 while telomere elongation in cells treated with B070 compared to the control by 1.18 times (Figure 28).

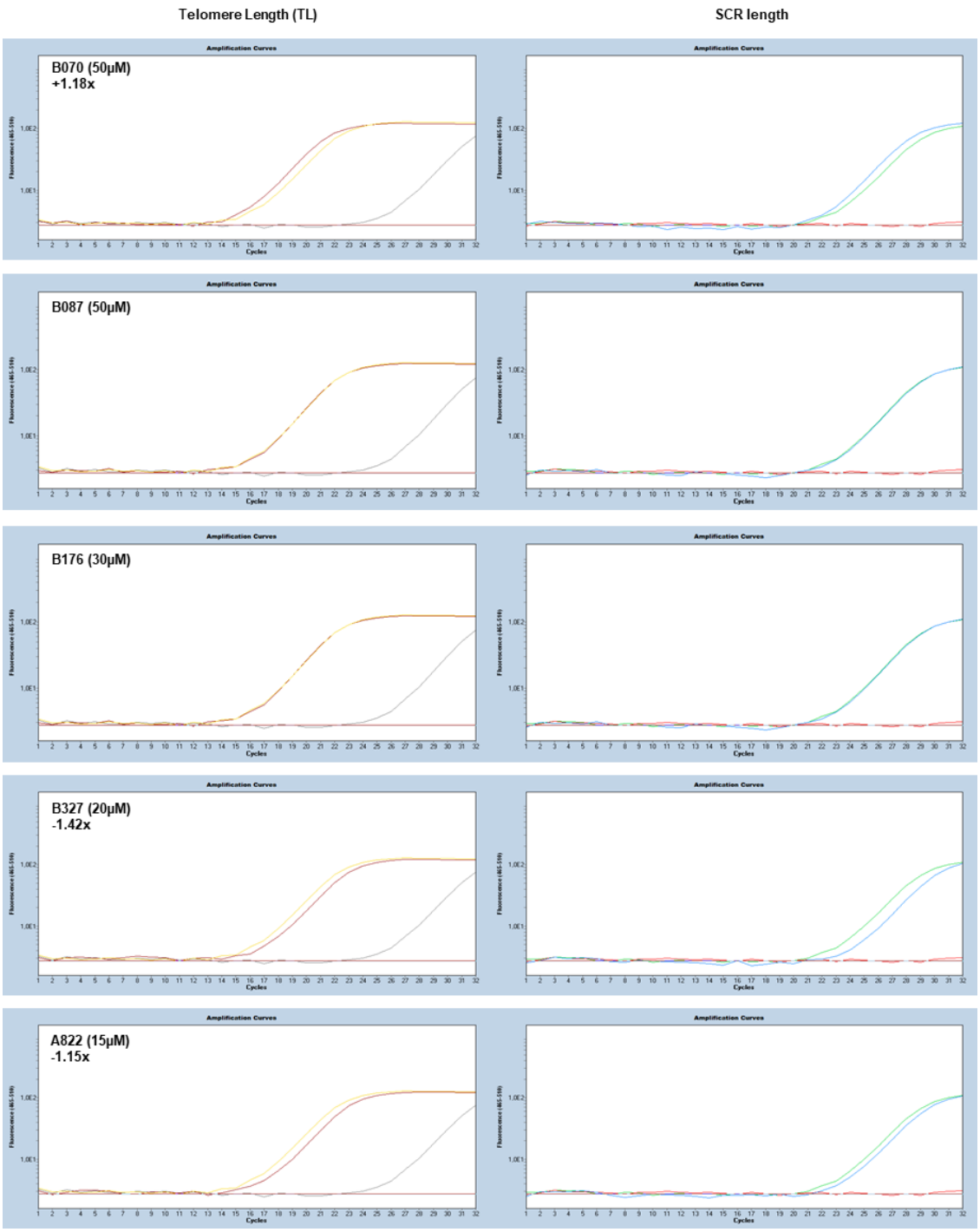

Figure 28. qPCR amplification curves using compounds. Cell lines – MCF7.
Telomere length – sampled without treatment =yellow, samples after treatment = brown, negative control =silver
SCR length – sampled without treatment =green, samples after treatment = blue, negative control = red

TRF1, TRF2 and TIN2 Proteins' Levels

To determine TRF1, TRF2 and TIN2 proteins in the nucleus and cytoplasm, Western Blot method was used. Cell extract was separately isolated from nuclei and cytoplasm of MCF7 cells. As shown in Figure 29, while TRF1 and TRF2 demonstrated nuclear localization, only TIN2 protein was located both in nuclei and cytoplasm; this is consistent with the literature data.

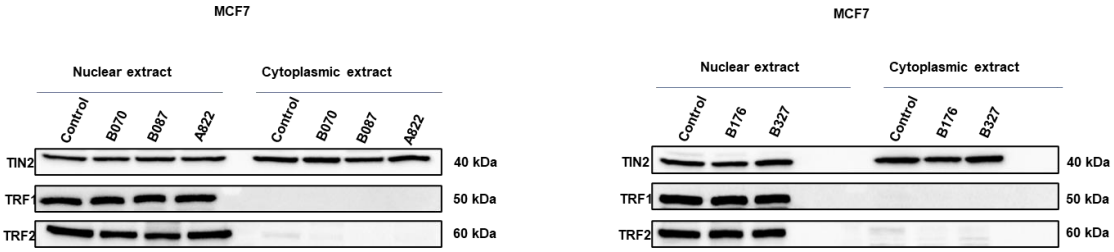

Figure 29. Detection of TRF1, TRF2 and TIN2 in MCF7 cells after 48 h incubation with B070 (100 μM), B087 (50 μM), 0176 (50 μM), B327 (75 μM), andA822 (15 μM) by Western Blot.

In order to validate the expression levels of the TRF1, TRF2 and TIN2 proteins, ELISA assays were used. MCF7 cells were incubated with B070 (100 μM), B087 (50 μM), 0176 (50 μM), B327 (75 μM), A822 (15 μM and 20 μM) compounds for 24 h and 48 h. As in the previous study, cell extracts were separately isolated from nuclei and cytoplasm. The result showed significant statistical increase in the level of TRF1 protein expression incubation with the B087 and B327 compounds already after 24 hours. Significantly increase in TRF1 protein expression level was observed after 48 h incubation with B070, B087, B176, and B327 (Figure 30). Moreover, as shown in Figure 30 significant statistical decrease in the level of TIN2 protein after 48 h incubation with the B070, B087, B327 and A822 (20 μM) was observed. The analysis of TRF2 protein level after incubation with compounds did not induce any statistically significant differences.

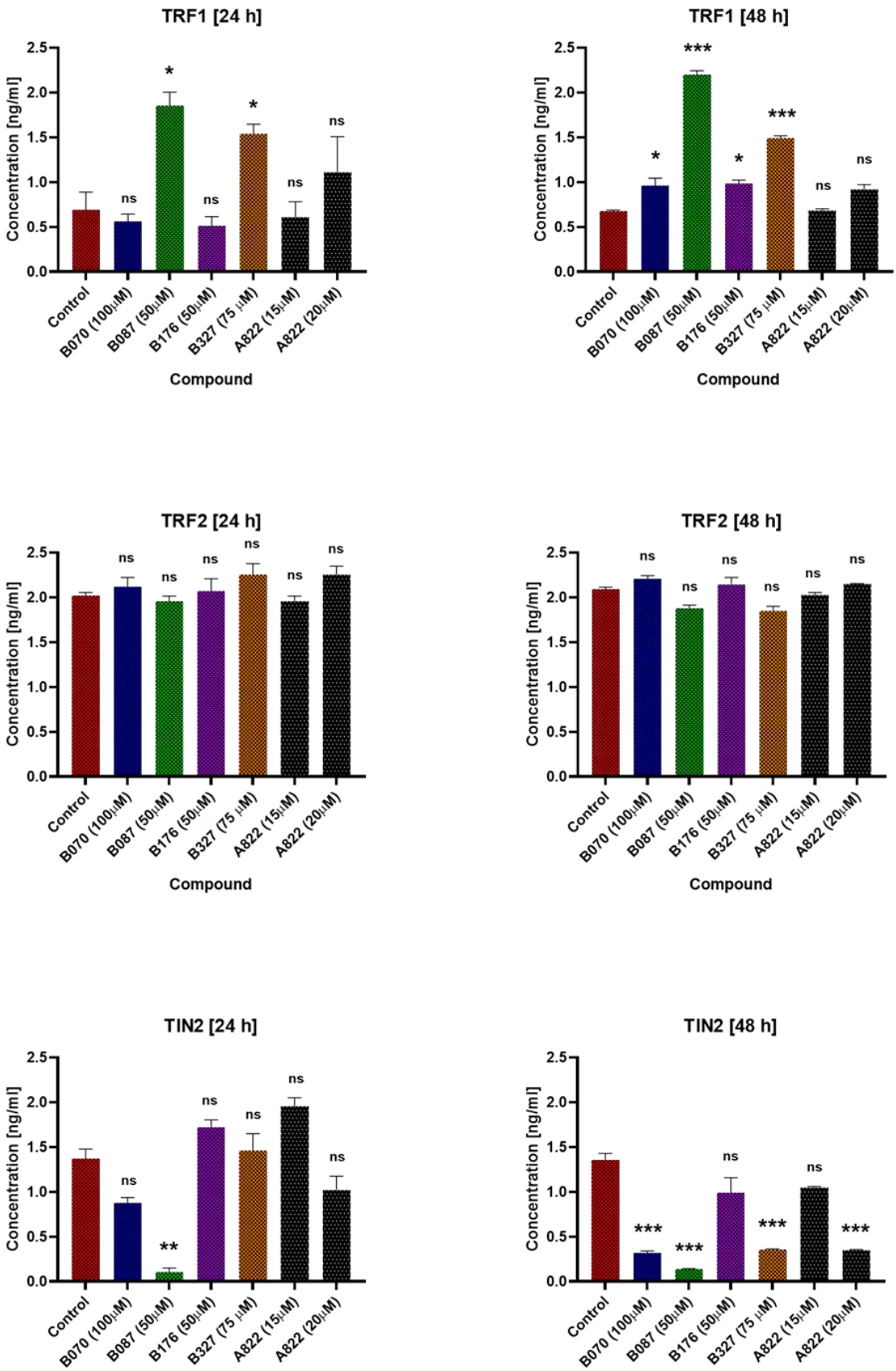

Figure 30. The expression level of TRF1, TRF2 and TIN2 proteins in MCF7 nuclei after 24 h and 48 h cell incubation with B070 (100 μM), B087 (50 μM), 0176 (50 μM), B327 (75 μM), andA822 (15 μM and 20 μM), ELISA test. Data presented as standard error mean bar and asterisks denote statistical significance (*** - P<0.001, ** - P<0.01, * - P<0.05, ns - P>0.05) by ANOVA test.

Furthermore, based on the Western Blot results, the cytoplasmic extracts were used to determine the protein expression level of TIN2 protein. The results show significant statistical increase in the level of TIN2 protein after 48 h incubation with only the B070 compound (Figure 31A) This result was further confirmed by TIN2 proteins immunostaining (Figure 31B).

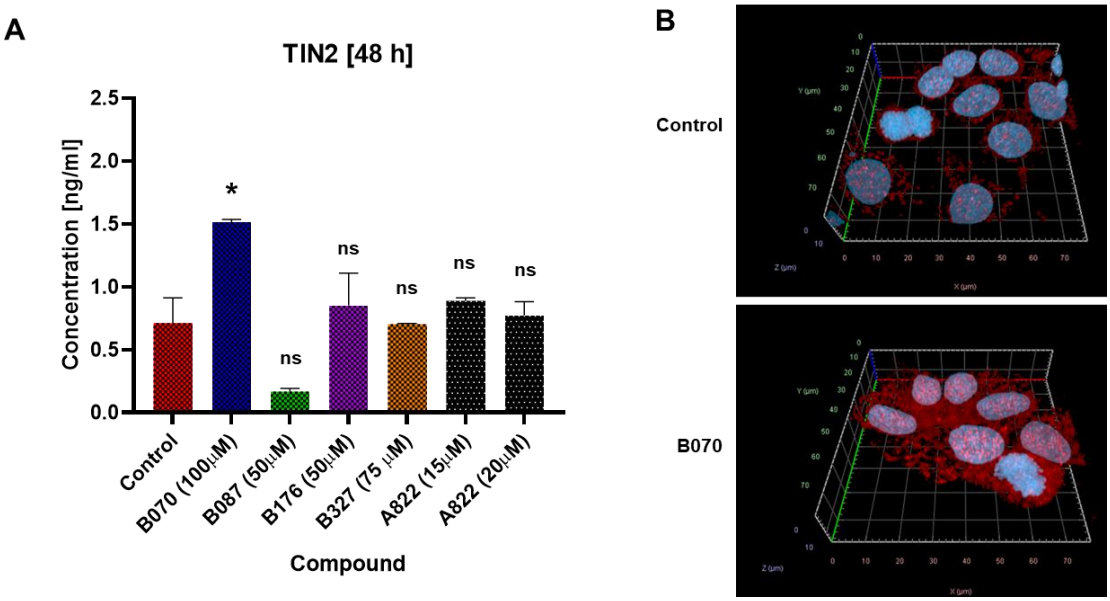

Figure 31. A - the level of TIN2 protein in MCF7 cytoplasm after 48 h cell incubation with B070 (100 μM), B087 (50 μM), 0176 (50 μM), B327 (75 μM), andA822 (15 μM and 20 μM). Western Blot. Data presented as standard error mean bar and asterisks denote statistical significance (*** - P<0.001, ** - P<0.01, * - P<0.05, ns - P>0.05) by ANOVA test. B - representative immunostaining images of MCF7 cells after exposure with B070 (100 μM) and untreated control after 48 h. Red channel - TIN2 protein, blue channel - cell nuclei.

Co-localization of TRF1/TIN2 and TRF2/ TIN2 Proteins

To evaluate the TRF1 and TIN2 protein co-localization at the cellular level, MCF7 cells were incubated with B070 (100 μM), B087 (50 μM) and A882 (10 μM) compounds for 72 h. As a control, MCF7 cells were incubated without compounds, under same conditions. To investigate the co-localization between proteins, MCF7 cells were observed by confocal microscopy, in three different laser channels, which corresponded to TRF1 proteins (green channel - AF488), TIN2 proteins (red channel - AF594) and nuclei (blue channel - DAPI). For quantification of proteins' co-localization after the treatment of compounds, Pearson's correlation coefficient (r) was used. The results showed no change in correlation between TRF1 and TIN2 after cell exposure to B070 and B087 compounds. In contrast, cell treatment with A822 resulted in a

significant reduction of correlation between TRF1 and TIN2 proteins (loss of co-localization) (Figure 32).

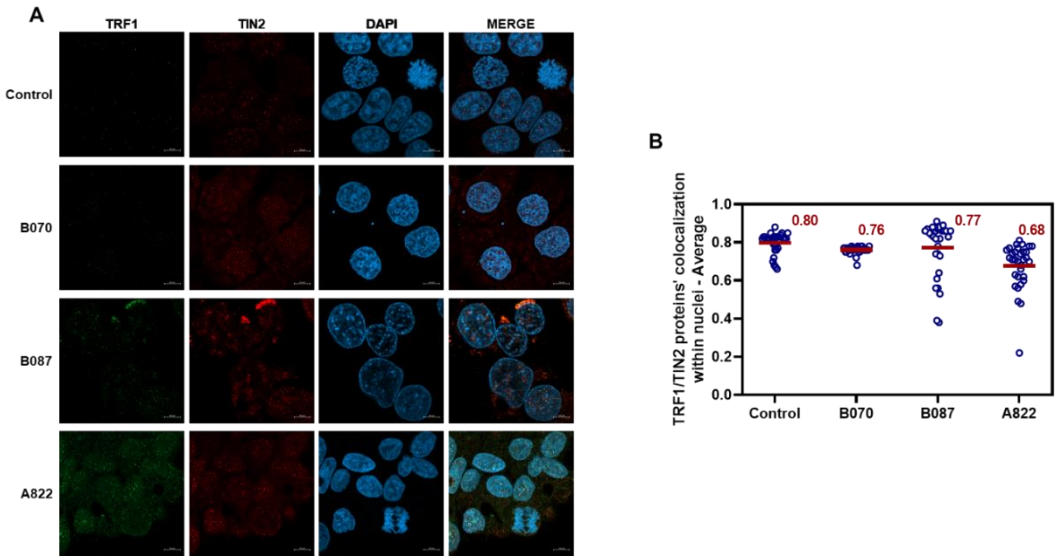

Figure 32. Co-localization of TRF1 and TIN2 proteins. A - representative immunostaining images of MCF7 cells showing co-localization between TRF1 (green) and TIN2 (red) proteins (control – untreated cells and cells after treatment with B070 (100 μM), B087 (50 μM) and A822 (10μM) compounds. Telomeres were identified by immunostaining using a mix of anti-TRF1 and anti-TIN2 antibodies. DNA was stained by DAPI (blue). Incubation time – 72 h. Scale bars correspond to 10 μm. B - quantification of TRF1 and TIN2 co-localization in MCF7 cells - control (untreated cells) and after treatment with B070 (100 μM), B087 (50 μM) and A822 (10μM) compounds with used Pearson's correlation coefficient (r). The plot shows the average number of TRF1-TIN2 co-localization per nucleus. All quantifications were carried out automatized. Each point on the plot represents a value obtained from one image (cells' nuclei). Mean values are indicated in red.

Based on the above results, the TRF1 and TIN2 protein co-localization after cell treatment with A822 in three-time points (24 h, 48 h and 72 h) was further examined. The observation indicated that significant changes in protein co-localization became evident after 72 h incubation of the cells with the compound (Figure 33).

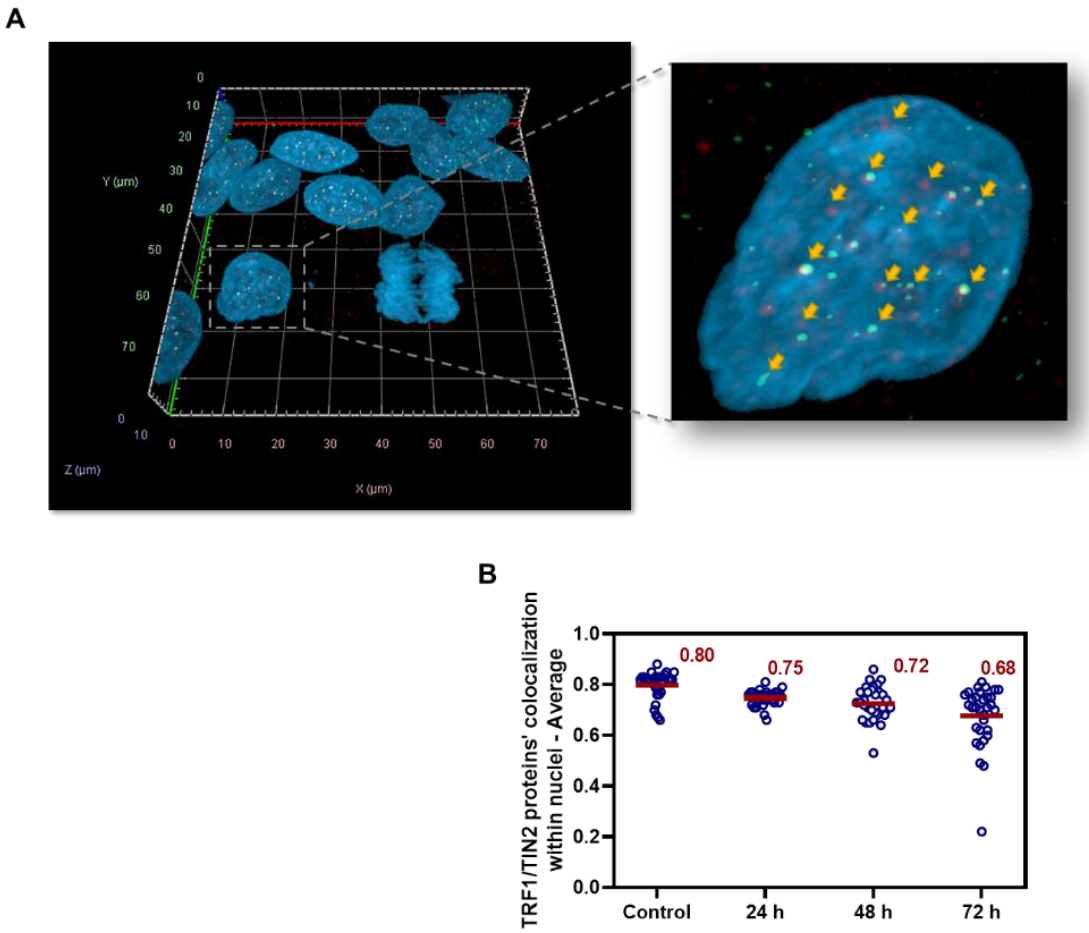

Figure 33. Co-localization of TRF1 and TIN2 proteins. A - representative 3D immunostaining images of MCF7 cells showing co-localization between TRF1 (green) and TIN2 (red) proteins in cells after treatment with A822 (10 µM) compound. Telomeres were identified by immunostaining using a mix of anti-TRF1 and anti-TIN2 antibodies. DNA was stained by DAPI (blue). Incubation time – 72 h. Yellow arrows show protein localization. B - quantification of TRF1 and TIN2 co-localization in MCF7 cells - control (untreated cells) and after treatment with A822 (10 µM) compounds with used Pearson's correlation coefficient (r). Incubation time – 24 h, 48 h, and 72 h. The plot shows the average number of TRF1-TIN2 co-localization per nucleus. All quantifications were carried out blindly. Each point on the plot represents a value obtained from one image (cells' nuclei). Mean values are indicated in red.

To evaluate the TRF2 and TIN2 protein co-localization at the cellular level, MCF7 cells were incubated with B176 and B327 compounds for 72 h. As a control, MCF7 cells were incubated without compounds under identical procedures. To investigate the co-localization between proteins, MCF7 cells were observed by confocal microscopy, in three different laser channels, which corresponded to TRF2 proteins (green channel - AF488), TIN2 proteins (red channel - AF594) and nuclei (blue channel - DAPI). As in the previous experiment, for quantification of proteins' co-localization after the treatment of compounds, Pearson's correlation coefficient (r) was used. The results

show a significant reduction of correlation between TRF2 and TIN2 proteins after cell treatment with only B327 (Figure 34).

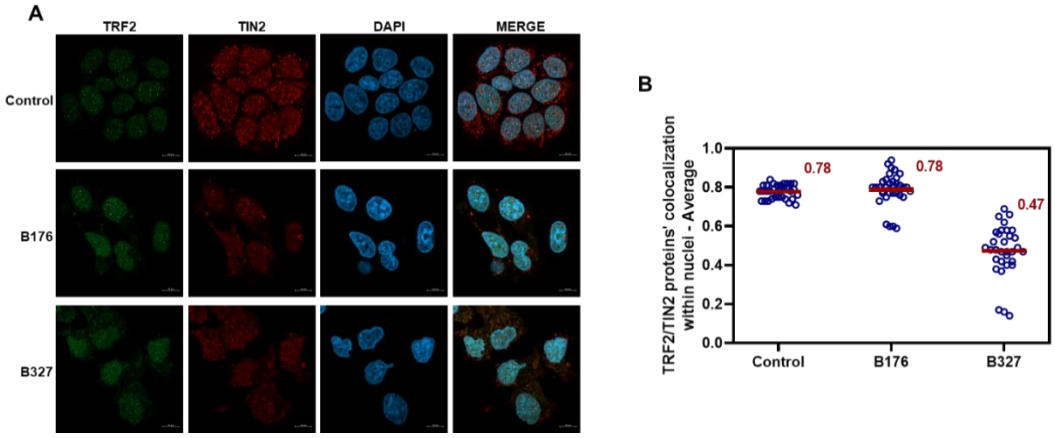

Figure 34. Co-localization of TRF2 and TIN2 proteins. A - representative immunostaining images of MCF7 cells showing co-localization between TRF2 (green) and TIN2 (red) proteins (control – untreated cells and cells after treatment with B176 (85 μM) and B327 (75 μM) compounds. Telomeres were identified by immunostaining using a mix of anti-TRF2 and anti-TIN2 antibodies. DNA was stained by DAPI (blue). Incubation time – 72 h. Scale bars correspond to 10 μm. B - quantification of TRF2 and TIN2 co-localization in MCF7 cells - control (untreated cells) and after treatment with B176 (85 μM) and B327 (75 μM) compounds with used Pearson's correlation coefficient (r). The plot shows the average number of TRF2-TIN2 co-localization per nucleus. All quantifications were carried out blindly. Each point on the plot represents a value obtained from one image (cells' nuclei). Mean values are indicated in red.

Based on the above results, the TRF2 and TIN2 protein co-localization after cell treatment with B327 at three-time points (24 h, 48 h and 72 h) was examined. The observation indicated that significant changes in protein colocalization became evident after 72 h incubation of the cells with this compound (Figure 35).

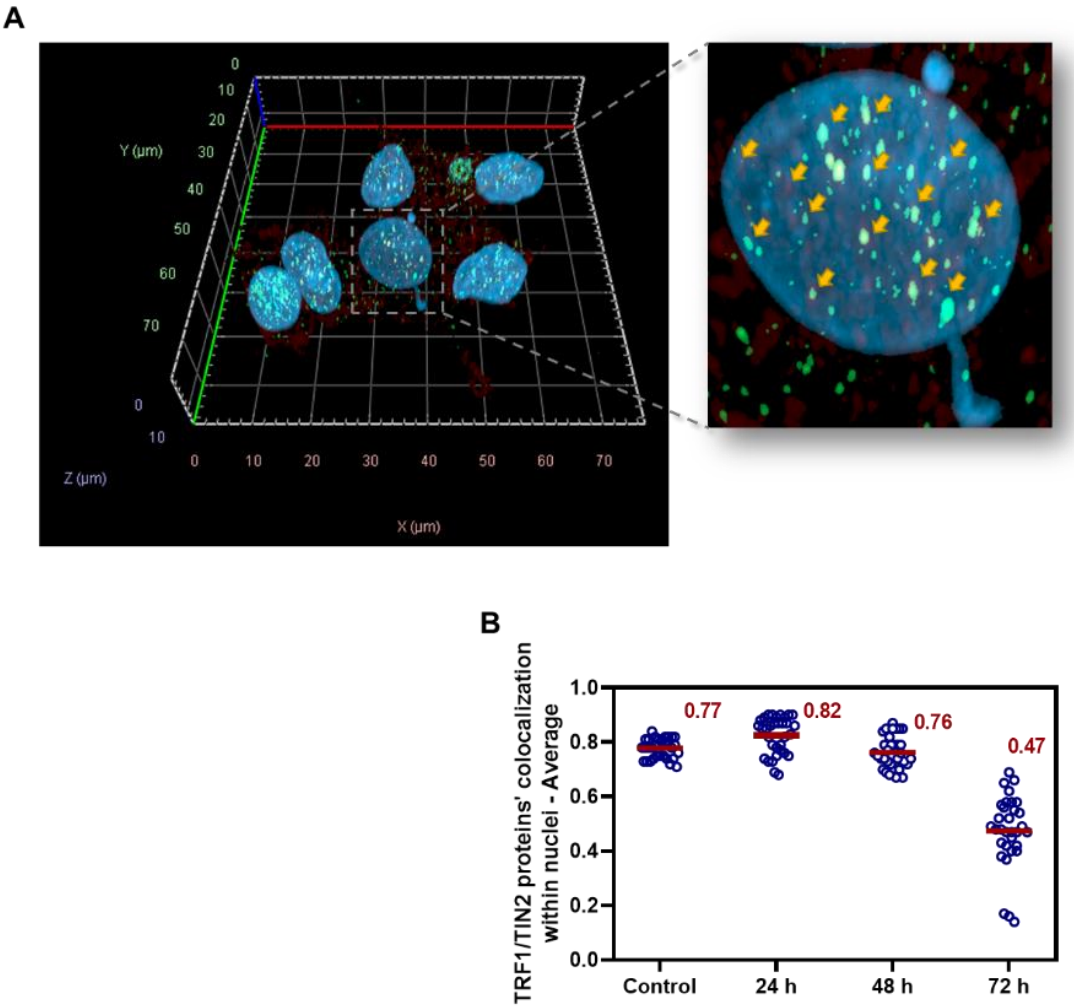

Figure 35. Co-localization of TRF2 and TIN2 proteins. A - representative 3D immunostaining images of MCF7 cells showing co-localization between TRF2 (green) and TIN2 (red) proteins in cells after treatment with B327 (75 µM) compound. Telomeres were identified by immunostaining using a mix of anti-TRF2 and anti-TIN2 antibodies. DNA was stained by DAPI (blue). Incubation time – 72 h. Yellow arrows show protein localization. B - quantification of TRF2 and TIN2 co-localization in MCF7 cells - control (untreated cells) and after treatment with B327 (75 µM) compounds with used Pearson's correlation coefficient (r). Incubation time – 24 h, 48 h, and 72 h. The plot shows the average number of TRF1-TIN2 co-localization per nucleus. All quantifications were carried out blindly. Each point on the plot represents a value obtained from one image (cells' nuclei). Mean values are indicated in red.

In vitro interactions

To check whether B070, B087 and A822 can interact with TRF1 protein directly, the compounds were injected and flowed over the surface of the sensor chip with covalently immobilized TRF1 protein and the surface plasmon resonance (SPR) changes were recorded. A significant increase in the response was detected when A822 was injected (Figure 36). In the cases of B070 and B087, only a slight increase in the response was detected. For interaction between A822 and TRF1 protein, the kinetic constants were calculated, using the 1:1 binding model. The association constant (ka) was calculated as 8.33 E+03 (± 1.6 E+03), the dissociation constant (kd) as 1.91 E-03 (± 1.68 E-04) and the equilibrium dissociation constant (KD) value was 2.36 E-07 (± 5.38 E-08). Since the interaction between B070 and B087 and TRF1 protein was very weak the calculation of kinetic constants was not feasible.

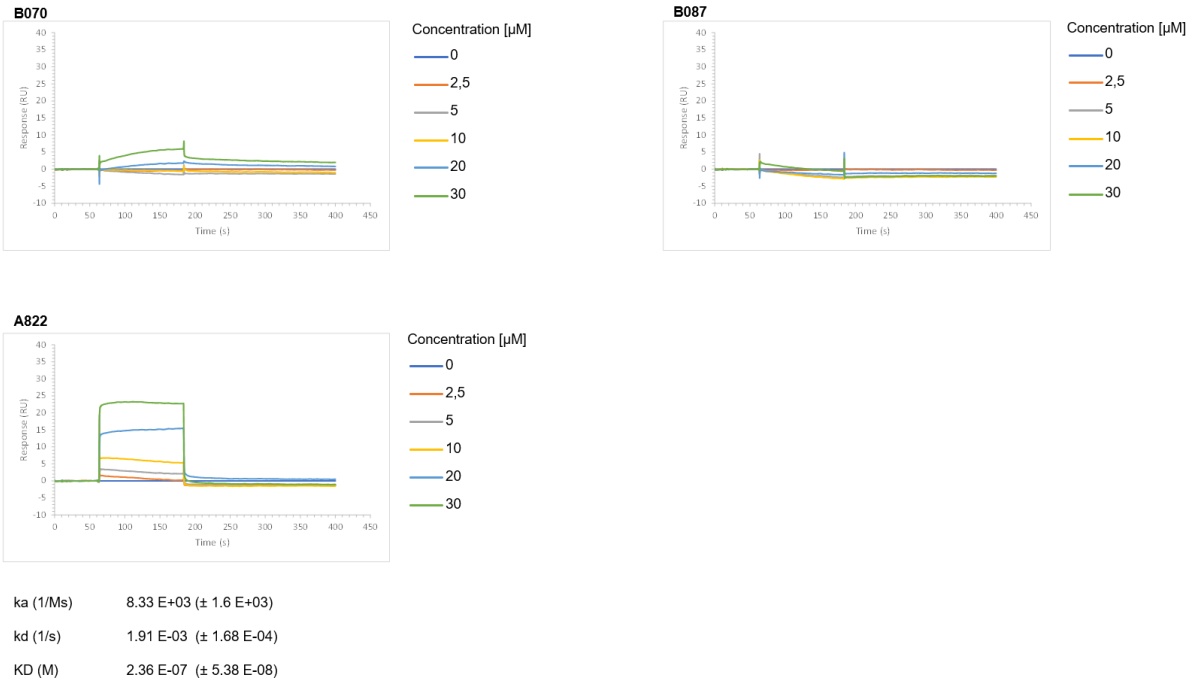

ka (1/Ms)	8.33 E+03 (± 1.6 E+03)
kd (1/s)	1.91 E-03 (± 1.68 E-04)
KD (M)	2.36 E-07 (± 5.38 E-08)

Figure 36. Analysis of B070, B087 and A822 interaction with TRF1 protein. The results are presented as sensorgrams obtained after subtracting the background response signal from a reference flow cell and a control experiment with buffer injection. For all analyzed peptides, at least six kinetic experiments were performed.

A similar experiment was performed to check whether B176 and B327 can interact with the TRF2 protein. The compounds were injected and flowed over the surface of the sensor chip with covalently immobilized TRF2 protein. A significant increase in the response was detected when B327 was injected (Figure 37). In the case of B176, the compound's precipitate was observed. Therefore, only for interaction between B327 and TRF2 protein, the kinetic constants were calculated, using the 1:1 binding model. The association constant (ka) was calculated as 8.77 E+04 (± 3.71 E+04), the dissociation constant (kd) as 9.64 E-04 (± 6.66 E-04) and the equilibrium dissociation constant (KD) value was 9.18 E-09 (± 6.38 E-09).

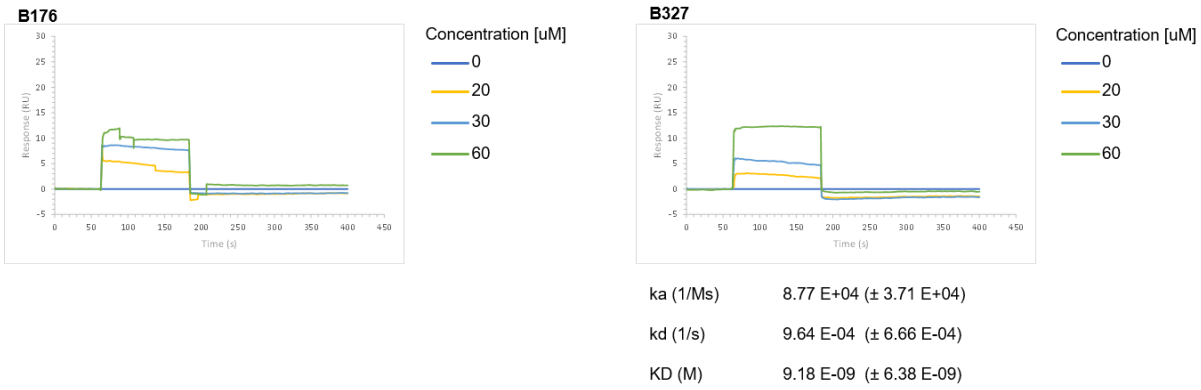

Figure 37. Analysis of B176 and B327 interaction with TRF2 protein. The results are presented as sensorgrams obtained after subtracting the background response signal from a reference flow cell and a control experiment with buffer injection. For all analyzed peptides, at least six kinetic experiments were performed.

Based on the above results, the interaction of TRF1 protein with TIN2 peptide (RHFNLAPLGRRRVQSQWASTR) was further analyzed after the immobilization of biotinylated TIN2 peptide on the surface of SA sensor chip. A mixture of both, TRF1 protein (100 nM) and A822 compound (5 μM), was injected and the responses were monitored. In all analyses, the results are presented as sensorgrams obtained after subtracting the background response signal from a reference flow cell and a control experiment with buffer injection (Figure 38). Kinetic constants calculated from SPR's data for analytes (TIN2 peptide and A822) interacting with TRF1 protein. The 1:1 binding model was applied.

To check the interaction of TRF2 protein with TIN2 peptide, a mixture of both, the TRF2 protein (100 nM) and B327 compound (5 μM) was injected and flowed over the surface of the sensor chip (SA) with covalently immobilized TIN2 peptide. As in previous analyses, the results are presented as sensorgrams obtained after subtracting the background response signal from a reference flow cell and a control experiment with buffer injection (Figure 39). Kinetic constants calculated from SPR's data for analytes (TIN2 peptide and B327) interacting with TRF2 protein. The 1:1 binding model was applied.

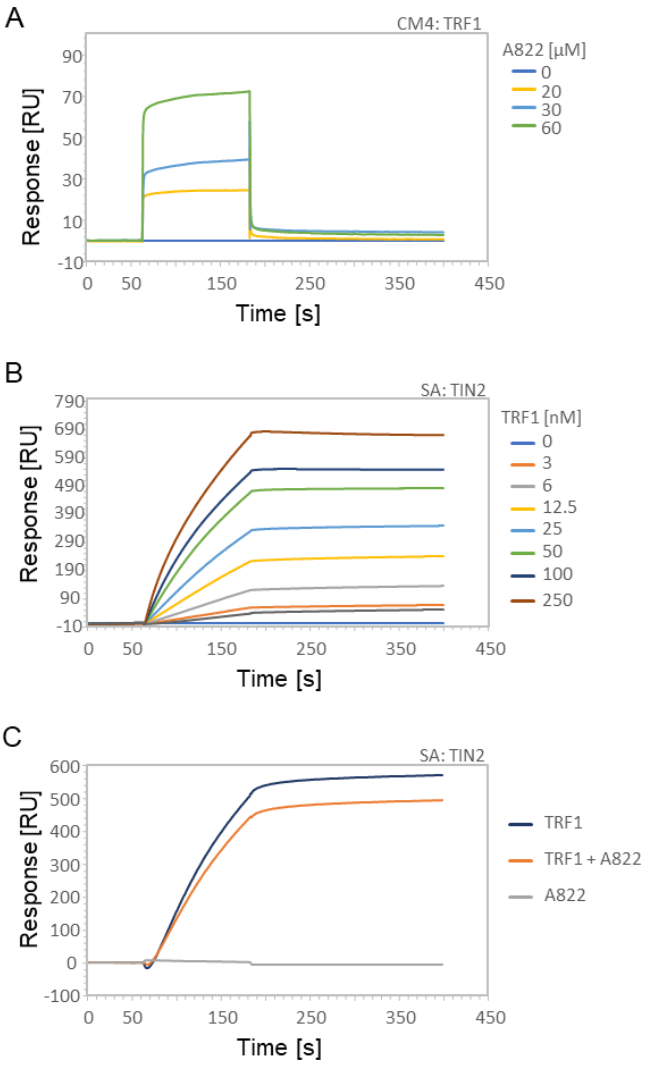

D

Analyte	ka ($M^{-1}S^{-1}$)	SD	kd (S^{-1})	SD	KD (M)	SD
TIN2	1.55 e+06	1.86 e+06	8.61 e-05	9.06 eE-05	1.11 e-10	1.63 e-10
A822	3.35 e+05	5.1 e+05	7.86 e-03	1.11 e-02	1.34 e-07	1.17 e-07

Figure 38. SPR analysis of A822 binding to TRF1 protein and its influence on TRF1-TIN2 interaction. A - the interaction of A822 with TRF1 protein was analyzed when TRF1 protein was immobilized on a surface of CM4 sensor chip using the amine coupling method. Then the increasing concentrations of A822 (20, 30, 60 µM) were run over the surface of a sensor chip with immobilized TRF1 protein. B - the interaction of TRF1 protein with TIN2 peptide was analyzed after the immobilization of biotinylated TIN2 peptide on a surface of SA sensor chip. The increasing concentrations of TRF1 protein (3, 6, 12.5, 25, 50, 100, 250, 500 nM) were run over the surface of a sensor chip with the immobilized peptide. C - the biotinylated TIN2 peptide was immobilized on the SA sensor chip surface. Next, 100 nM TRF1 protein and 5 µM A822, as a mixture of both was injected, and the obtained responses were detected. In all analyses, the results are presented as sensorgrams obtained after subtracting the background response signal from a reference flow cell and a control experiment with buffer injection. At least three kinetic experiments were performed for kinetic analysis (A and B). In C, the sensorgrams show the average from six independent experiments. D - kinetic constants calculated from SPR's data for analytes (TIN2 peptide and A822) interacting with TRF1 protein. Constants were calculated with Biacore T200 Evaluation Software using data from at least two separate titration analyzes. The 1:1 binding model was applied. SD – standard deviation.

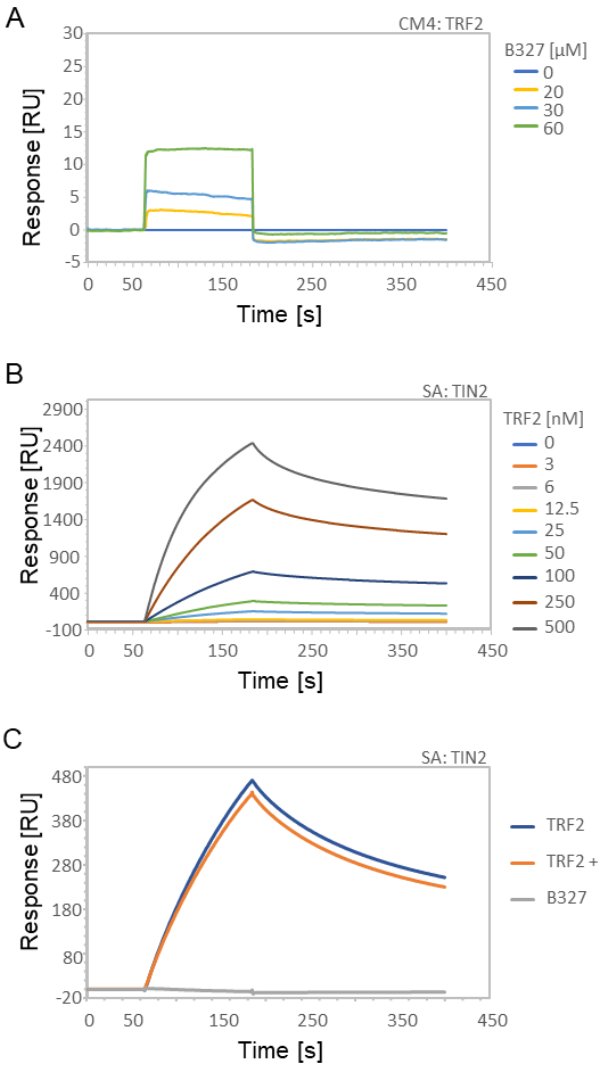

D

Analyte	ka ($M^{-1}S^{-1}$)	SD	kd (S^{-1})	SD	KD (M)	SD
TIN2	1.15 e+05	2.42 e+04	2.63 e-03	3.28 e-04	2.33 e-08	2.65 e-09
327	8.14 e+04	3.48 e+04	7.75 e-04	6.25 e-04	7.83 e-09	5.99 e-09

Figure 39. SPR analysis of B327 binding to TRF2 protein and its influence on TRF2-TIN2 interaction. A - the interaction of B327 with TRF2 protein was analyzed when TRF2 protein was immobilized on a surface of CM4 sensor chip using the amine coupling method. Then the increasing concentrations of B327 (20, 30, 60 µM) were run over the surface of a sensor chip with immobilized TRF2 protein. B - the interaction of TRF2 protein with TIN2 peptide was analyzed after the immobilization of biotinylated TIN2 peptide on a surface of SA sensor chip. Next, the increasing concentrations of TRF2 protein (3, 6, 12.5, 25, 50, 100, 250, 500 nM) were run over the surface of a sensor chip with the immobilized peptide. C - the biotinylated TIN2 peptide was immobilized on the SA sensor chip surface. Next, 100 nM TRF2 protein and 5 µM B327, as a mixture of both was injected, and the obtained responses were detected. In all analyses, the results are presented as sensorgrams obtained after subtracting the background response signal from a reference flow cell and a control experiment with buffer injection. At least three kinetic experiments were performed for kinetic analysis (A and B). In C, the sensorgrams show the average from six independent experiments. D - kinetic constants calculated from SPR's data for analytes (TIN2 peptide and B327) interacting with TRF2 protein. Constants were calculated with Biacore T200 Evaluation Software using data from at least two separate titration analyzes. The 1:1 binding model was applied. SD – standard deviation

Co-localization of TIN2 Protein and Telomeres

To determine, whether TIN2 proteins were localized to telomeres after MCF7 cells were treated with compounds: B070 (100 μM), B087 (50 μM) B176 (85 μM), B327 (75 μM) and A882 (10 μM), co-immunoFISH method was used. To investigate the co-localization, cells were observed by confocal microscopy, in three different laser channels, which corresponded to telomere PNA probe (green channel - AF488), TIN2 proteins (red channel - AF594) and nuclei (blue channel - DAPI) (Figure 40).

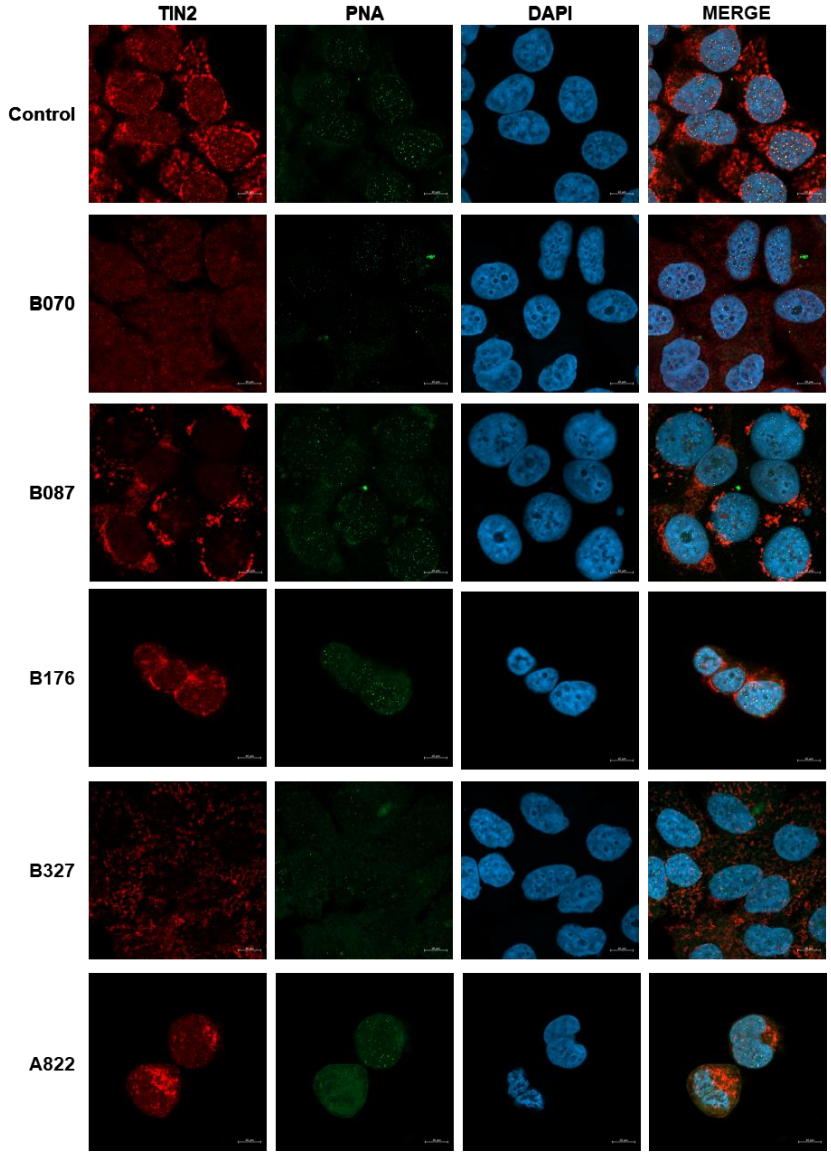

Figure 40. Co-localization of telomere (PNA) and TIN2 proteins. Representative immunostaining images of MCF7 cells showing co-localization between TIN2 protein (green) and telomere (red) proteins (control – untreated cells and cells after treatment with B070 (100 μM), B087 (50 μM), B176 (85 μM), B327 (75 μM) and A822 (10 μM) compounds. DNA was stained by DAPI (blue). Incubation time – 48 h. Scale bars correspond to 10 μm.

For quantification of protein co-localization after the treatment of compounds, Pearson's correlation coefficient (r) was used. The results show no significant change in correlation between telomeres and TIN2 protein after cell exposure to all compounds after 24 h and 48 h (Figure 41).

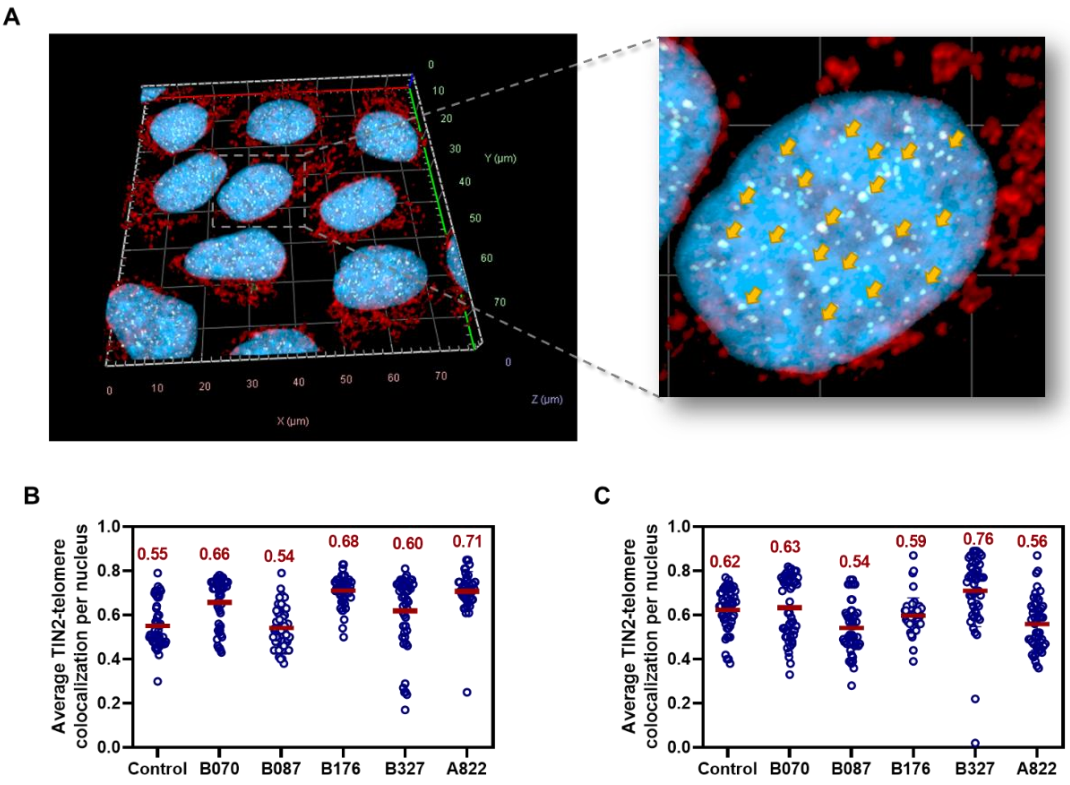

Figure 41. Co-localization of telomere (PNA) and TIN2 proteins. A - representative 3D immunostaining images of MCF7 cells showing co-localization between telomeres (green) and TIN2 (red) proteins in cells. DNA was stained by DAPI (blue). Incubation time – 48 h. Yellow arrows show telomere and protein localization. B, C - quantification of telomere and TIN2 protein co-localization in MCF7 cells - control (untreated cells) and after treatment with B070 (100 μM), B087 (50 μM), B176 (85 μM), B327 (75 μM) and A822 (10 μM) compounds with used Pearson's correlation coefficient (r). The plot shows the average number of telomere -TIN2 co-localization events per nucleus. All quantifications were carried out blindly. Each point on the plot represents a value obtained from one image (cells' nuclei). Mean values are indicated in red.

However, the TIN2 protein binds not only to the TRF1, TRF2, but also to the TPP1-POT1 complex, thereby bridging units being attached to double-stranded DNA and units being attached to single-stranded DNA. Therefore, lack of significant changes in the correlation after compound applications, seems to confirm that B327 and A822 compounds are inhibitors only when interfering with TIN2 protein binding to TRF1 or TRF2.

The Mitochondria Changes after Compound Application

Mitochondria play a crucial role in cancer cell viability and tumorigenesis [291]. Dysregulated energy supply is a hallmark of cancer, and recent studies have emphasized the importance of investigating mitochondria biology in cancers and targeting this organelle therapeutically [292]. TIN2, a protein involved in telomere maintenance, has also been found to regulate oxidative phosphorylation in mitochondria independently from its role in telomere maintenance. Depletion of TIN2 increases mitochondrial ATP production and oxygen consumption and inhibits ROS generation [293]. Therefore, targeting mitochondria may be a potential strategy for cancer therapy. The effects of compounds on mitochondrial morphology were investigated in MCF7 cells, and changes in mitochondrial morphology were observed after treatment with all compounds (Figure 42).

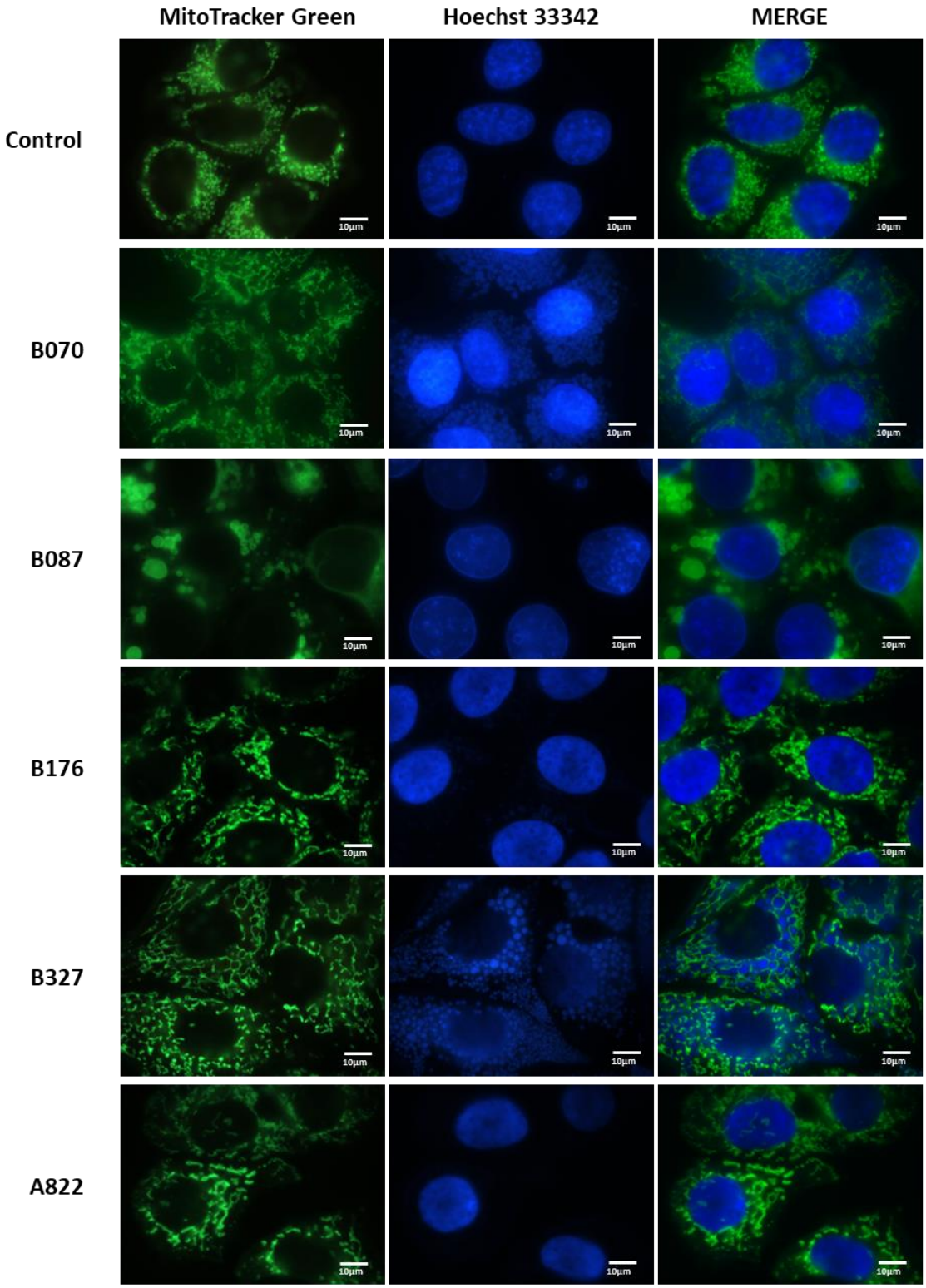

Figure 42. Representative image of mitochondrial morphology after MCF7 cells treatment with B070 (100 µM), B087 (50 µM), B176 (50 µM), B327 (75 µM) and A822 (10 µM) compounds. Cell nuclei were stained with Hoechst 33342. Incubation time – 48 h. Scale bars correspond to 10 µm.

Furthermore, the Western Blot was used to detect the expression of mitochondrial maker ATP5A1. The marker expression is strictly correlated with the number of mitochondria. The results show statistically significant differences in the number of mitochondria after MCF7 cells were treated with B070 and B327 compounds (Figure 43).

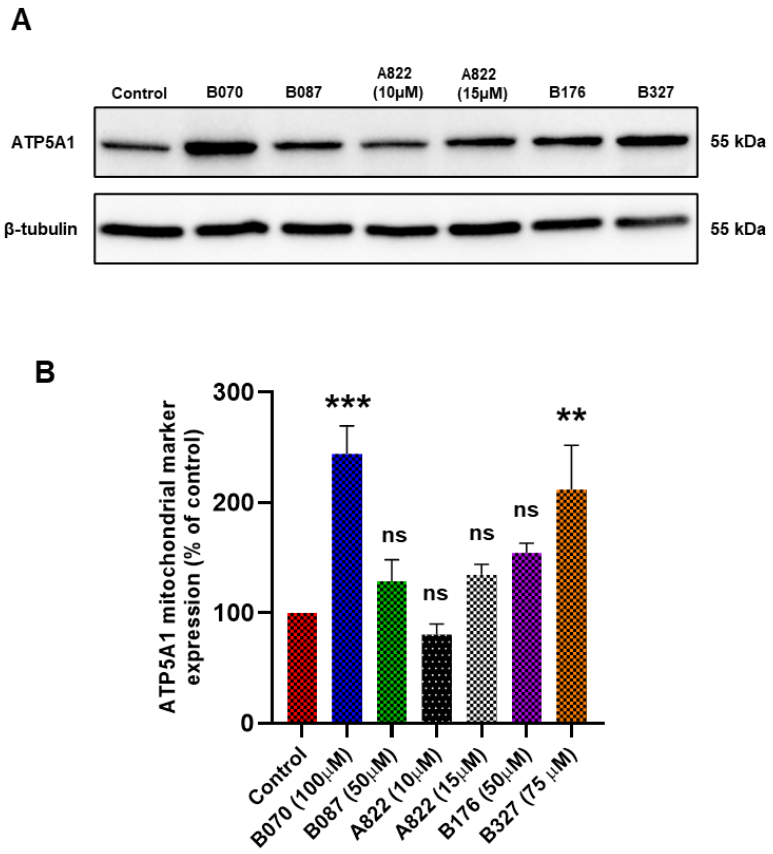

Figure 43. The comparison of the ATP5A1 mitochondrial marker expression level in MCF7 cells after treatment with compounds. Incubation time - 48 h. A - representative Western Blot analysis with ATP5A1 mitochondrial marker used. β-tubulin was an internal standard. B - quantification of ATP5A1 mitochondrial marker expression level for control. Data presented as standard error mean bar and asterisks denote statistical significance (*** - P<0.001, ** - P<0.01, * - P<0.05, ns - P>0.05) by ANOVA test.

Next, the ROS levels were investigated after treating cells with compounds (Figure 44). The results show that B070, B087 and A822 compounds induced the production of ROS after 3 h and 6 h. However, a significant decrease in ROS production was observed after 24 h cell incubation with B070 and A822 compounds. No increase in ROS levels was observed after the application of B176 and B327 compounds. ROS

are considered as an important off-target effect of drug use, however a small amount of ROS after compounds application might appear beneficial.

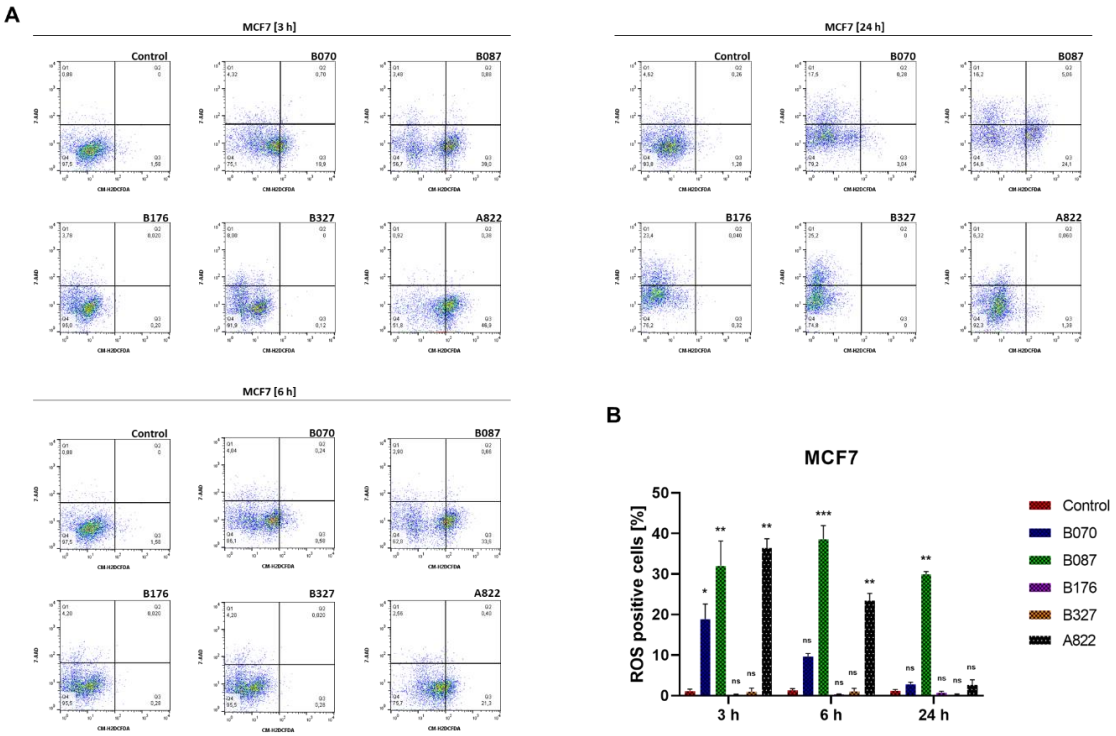

Figure 44. Compound-induced ROS generation over time in MCF7 cells. A - two-parameter dot plots of the cell apoptosis (7-AAD) and ROS generation (CM-H2DCFDA) in MCF7 cells population treated with B070 (100 μM), B087 (50 μM), B176 (50 μM), B327 (75 μM), A822 (15 μM) and untreated control for 3 h, 6 h, and 24 h. B- quantification of % of ROS-positive cells. Data presented as standard error mean bar and asterisks denote statistical significance (*** - P<0.001, ** - P<0.01, * - P<0.05, ns - P>0.05) by ANOVA test.

Thus, the results suggest that these compounds may have an effect on mitochondrial function. However, further studies are needed to explore the potential of these compounds as mitochondrial targeting agents for cancer therapy.

Results – part II

Ex vivo Cytotoxicity

To evaluate the toxic effects of the compound MTT assay was used. The percentage reduction in activity relative to control cells was assessed. The mean of the control was standardized and defined as 100% cell activity. The difference in cell viability between the reference compound (doxorubicin) and cells after treatment with tested compounds was analyzed using one-way ANOVA corrected by Tukey's test.

Based on the previous results within this study, selected 5 compounds (B070, B087, B176, B327 and A822) were used to analysis in the primary patient-derived non-tumor and tumor cell culture (PDC). Cell cultures were treated with different concentrations of tested compounds in the range 0.78-100 μM and doxorubicin in the range 0.01-12.5 μM for 72 h. As demonstrated in Table 9, the strongest cytotoxic effect was obtained after applying compounds: A822 for the primary patient-derived non-tumor (range of IC_{50}: 2.5-21 μM) and tumor cell culture (range of IC_{50}: 2.5-23 μM) and B327 for the primary patient-derived non-tumor (range of IC_{50}: 13-40 μM) and tumor cell culture (range of IC_{50}: 4.5-37 μM).

Table 9. IC_{50} values for compounds: B070, B087, B176, B327 and A822 tested in primary cell cultures derived from normal and cancer breast tissues. Doxorubicin was used as a cytotoxic reference drug. The data shown are means ± SEM. N – primary patient-derived non-tumor cell culture and T- primary patient-derived tumor cell culture.

IC_{50} (μM)							
Patient no.		**Compounds**					
		B070	**B087**	**B176**	**B327**	**A822**	**Doxorubicin**
P01	**N01**	27.85 ± 0.93	> 50	17.96	25.41 ± 0.46	5.73 ± 1.05	0.49 ± 0.07
	T01	31.37 ± 1.7	> 50	34.73 ± 0.55	30.10 ± 0,18	8.39 ± 0.68	0.56 ± 0.06
P02	**N02**	> 50	> 50	25.97 ± 0.61	39,06	12.07 ± 0.60	0.19 ± 0.05
	T02	25.94 ± 0.46	> 50	28.61 ± 1.37	21.72 ± 0.22	9.74	0.48 ± 0.05
P03	**N03**	33.65 ± 1.12	> 50	27.03 ± 1.66	21.90	8.54 ± 0.30	0.19 ± 0.07
	T03	26.39 ± 3.99	> 50	28.15 ± 1.98	21.47 ± 1.62	7.73 ± 0.92	0.19 ± 0.10
P04	**N04**	27.16 ± 1.09	> 50	29.04 ± 0.30	23.10 ± 1.67	8.61 ± 0.30	0.26 ± 0.13
	T04	25.93 ± 1.32	> 50	26.57	27.81 ± 3.08	7.36 ± 0.87	1.93 ± 0.06
P05	**N05**	3.12	> 50	18.37 ± 1.26	29.51 ± 1.95	-	0.30 ± 0.10
	T05	8.04 ± 0.01	> 50	21.56 ± 0.83	26.53 ± 0.69	-	0.39 ± 0.14
P06	**N06**	24.4 ± 2.25	> 50	30.37 ± 1.26	30.61 ± 1.95	-	0.28 ± 0.09

	T06	42.70 ± 1.60	> 50	54.72 ± 3.90	28.35 ± 1.38	-	0.15 ± 0.01
P07	**N07**	45.22 ± 1.37	> 50	41.20 ± 1.28	25.32 ± 2.37	17.23 ± 0.49	0.19 ± 0.09
	T07	57.77 ± 2.34	> 50	> 50	33.32 ± 0.22	18.46 ± 1.30	0.33 ± 0.03
P08	**N08**	21.44 ± 2.71	34.50 ± 4.53	15.56 ± 1.79	21.25 ± 1.43	8.19 ± 1.14	0.49 ± 0.07
	T08	24.70 ± 0.69	> 50	12.87 ± 1.54	22.47 ± 1.03	9.50 ± 1.41	0.56 ± 0.06
P09	**N09**	41.34 ± 2.57	> 50	27.44 ± 2.10	25.24 ± 1.55	15.41 ± 1.09	0.19 ± 0.07
	T09	> 50	> 50	> 50	25.62 ± 1.36	16.47 ± 0.24	0.23 ± 0.06
P10	**N10**	> 50	> 50	> 50	26.50 ± 1.66	20.31 ± 0.95	0.56 ± 0.12
	T10	> 50	> 50	> 50	35.11 ± 0.18	21.20 ± 0.92	1.52 ± 0.36
P11	**N11**	> 50	> 50	48.66 ± 3.87	39.71 ± 1.15	18.67 ± 0.74	0.84 ± 0.31
	T11	> 50	> 50	> 50	33.46 ± 2.10	17.08 ± 1.00	0.49 ± 0.11
P12	**N12**	15.29 ± 1.66	14.15 ± 1.90	15.00 ± 0.68	18.20 ± 0.89	4.57 ± 0.52	0.07 ± 0.01
	T12	> 50	> 50	40.53 ± 1.20	26.56 ± 2.21	16.07 ± 2.91	0.35 ± 0.07
P13	**N13**	46.15 ± 1.97	> 50	> 50	34.45 ± 1.62	16.46 ± 0.73	1.17 ± 0.34
	T13	44.77 ± 1.69	> 50	> 50	36.86 ± 4.14	17.22 ± 1.70	1.11 ± 0.32
P14	**N14**	> 50	> 50	> 50	34.59 ± 1.25	18.60 ± 0.22	0.50 ± 0.06

	T14	> 50	> 50	> 50	34.51 ± 1.43	22.59 ± 0.44	0.24 ± 0.04
P15	**N15**	35.93 ± 1.60	> 50	35.24 ± 1.75	20.59 ± 1.65	17.36 ± 1.76	0.13 ± 0.01
	T15	40.01 ± 2.08	> 50	37.81 ± 0.99	29.91 ± 2.40	14.56 ± 1.32	0.42 ± 0.10
P16	**N16**	17.73 ± 1.27	26.57 ± 6.33	18.39 ± 0.18	17.08 ± 1.22	5.90 ± 0.44	0.17 ± 0.02
	T16	11.14 ± 2.71	> 50	14.24 ± 2.16	11.66 ± 0.58	6.52 ± 0.72	0.12 ± 0.09
P17	**N17**	13.96 ± 3.09	> 50	6.70 ± 2.72	18.56 ± 1.44	2.54 ± 0.75	0.06 ± 0.01
	T17	4.32 ± 1.53	> 50	4.12 ± 0.66	18.99 ± 0.83	3.58 ± 1.31	0.08 ± 0.01
P18	**N18**	9.43 ± 1.57	> 50	12.5 ± 0.10	12.38 ± 0.32	13.72 ± 0.57	0.06 ± 0.01
	T18	12.67 ± 1.38	> 50	22.12 ± 2.27	18.26 ± 0.57	10.76 ± 2.02	0.08 ± 0.02
P19	**N19**	29.92 ± 3.06	> 50	36.05 ± 1.52	29.57 ± 1.59	20.04 ± 1.12	0.18 ± 0.06
	T19	29.71 ± 3.03	> 50	38.43 ± 1.99	33.16 ± 0.48	20.85 ± 1.72	0.35 ± 0.11
P20	**N20**	18.87 ± 1.97	> 50	26.24 ± 3.60	18.29 ± 1.42	3.71 ± 0.92	0.09 ± 0.02
	T20	40.04 ± 1.49	> 50	37.78 ± 1.93	32.99 ± 1.05	15.62 ± 0.71	0.29 ± 0.04
P21	**N21**	22.93 ± 1.28	> 50	> 50	28.11 ± 1.33	8.94 ± 1.33	0.23 ± 0.04
	T21	3.75 ± 0.28	> 50	2.45 ± 1.11	4.42 ± 1.95	2.41 ± 0.91	0.07 ± 0.01

Tukey's test is a post-hoc test commonly used in one-way ANOVA to compare all pairs of means to determine which are significantly different. In this case, the test was used to analyze the difference in cell viability between different compounds (B070, B087, B176, B327, and A822) and the reference compound (doxorubicin) in primary patient-derived non-tumor and tumor cell culture (PDC). The results of the analysis showed that there were no statistically significant differences between A822 treatment and doxorubicin in both non-tumor and tumor PDC cell cultures (Figure 45). This means that the effect of A822 on cell viability was similar to that of doxorubicin in these cell cultures. Overall, the analysis suggests that A822 may be a potential candidate for further investigation as an anti-cancer agent, as it had a similar effect on cell viability as doxorubicin, a commonly used chemotherapy drug.

A

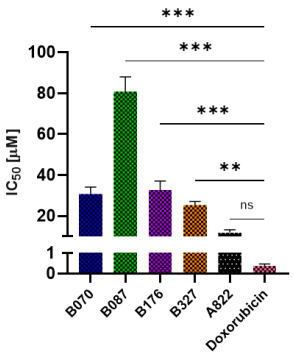

IC_{50} (µM)					
B070	B087	B176	B327	A822	Doxorubicin
34.97 ± 4.47	> 50	38.12 ± 4.89	26.39 ± 1.80	12.95 ± 1.40	0.53 ± 0.13

B

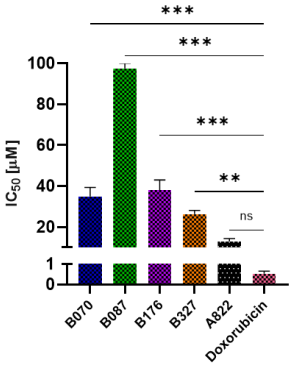

IC_{50} (µM)					
B070	B087	B176	B327	A822	Doxorubicin
30.70 ± 3.45	> 50	32.63 ± 4.39	25.26 ± 1.85	11.93 ± 1.38	0.37 ± 0.09

Figure 45. Comparison of the IC_{50} values of the cytotoxicity of TRF1 / TRF2-TIN2 protein interaction inhibitors and the significance of changes in IC_{50} values for inhibitors with the IC_{50} values for doxorubicin (*** - P<0.001, ** - P<0.01, * - P<0.05, ns - P>0.05, one-way ANOVA corrected by Tukey's test) in primary patient-derived non-tumor (A) and tumor (B) cell culture.

Disrupting Shelterin Complex with A822 and B327 Inhibitors: Effects on Telomere Function in Primary Patient-Derived Non-Tumor and Tumor Cell Cultures

The TIF (telomere dysfunction-induced foci) assay was performed on primary patient-derived non-tumor and tumor cell cultures (PDCs) to investigate the effect of A822 and B327 compounds, as the most promising, on telomere function. The A822 compound is an inhibitor that disrupts the binding between TRF1 and TIN2 proteins, two important components of the shelterin complex, which plays a crucial role in telomere maintenance and function. After treatment with A822 (10 μM), telomere fusion was observed in the PDCs, indicating that the inhibitor disrupted the normal function of the shelterin complex, leading to telomere dysfunction. Telomere fusion occurs when the ends of two or more chromosomes fuse together, which can result in chromosomal abnormalities and genomic instability. The B327 is an inhibitor that disrupts the binding between TRF2 and TIN2 proteins. After treatment with B327 (50 μM), both telomere fusion and anaphase bridges were observed in the PDCs. Anaphase bridges are structural aberrations that occur when chromosomes are not properly separated during cell division. This result suggests that the inhibitor not only disrupted the function of the shelterin complex but also affected the proper segregation of chromosomes during cell division, which can lead to genomic instability. Overall, these results suggest that both A822 and B327 compounds disrupted the normal function of the shelterin complex, leading to telomere dysfunction in PDCs (Figure 46).

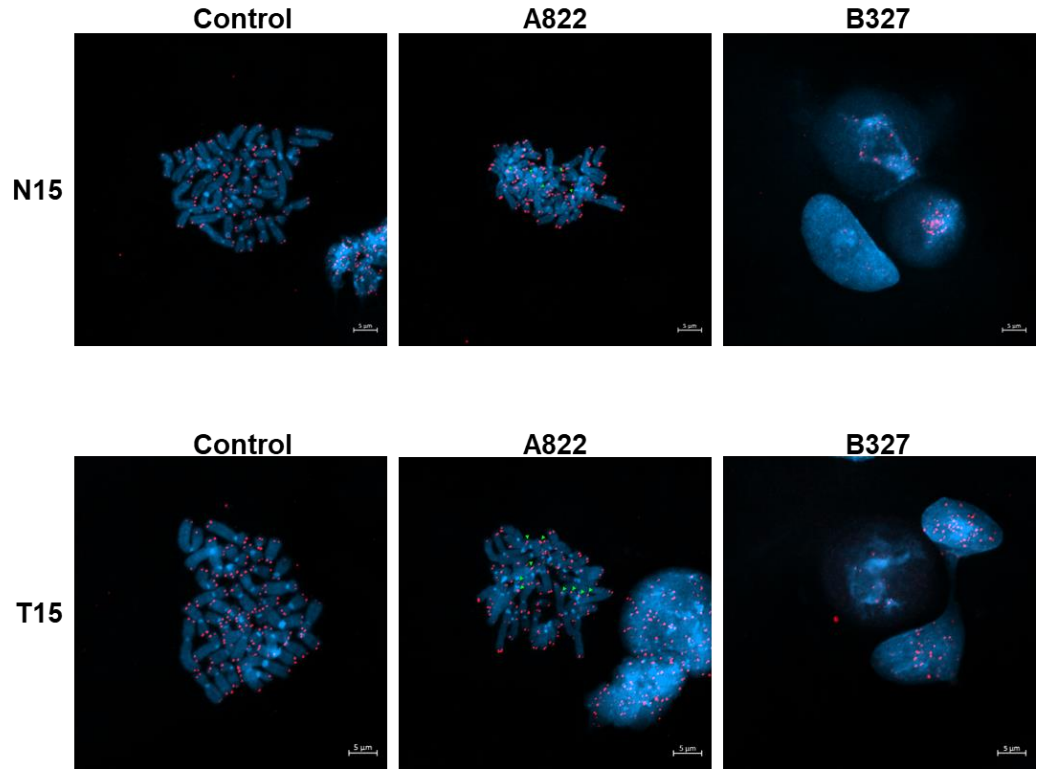

Figure 46. Representative image of telomere dysfunction in primary patient-derived non-tumor and tumor cell cultures after cell treatment with B327 (50 μM) and A822 (10 μM) compounds. Incubation time - 48 h. Meta-TIF assay samples were stained with DAPI (blue) and telomere PNA (red). Scale bars correspond to 5 μm.

Effects of Shelterin Complex-Targeting Compounds on Cell Cycle Progression in Primary Patient-Derived Non-Tumor and Tumor Cell Cultures

The results of the study showed that the tested compounds, including B070 (50 μM), B087 (50 μM), B176 (50 μM), B327 (50 μM), and A822 (10 μM), affected the cell cycle progression of primary patient-derived non-tumor and tumor cell cultures. Specifically, an increase in the sub-G1 population of cells was observed after treatment with B070 and B176, indicating cell death. Cell cycle arrest occurred at the G1 phase for primary patient-derived non-tumor cell cultures treated with B087, B176, and B327, while it occurred at the G1 phase for primary patient-derived tumor cell cultures treated with B327 only. Additionally, cell cycle arrest occurred at the G2 phase for primary patient-derived non-tumor cell culture treated with B070 and B176, while it occurred at the G2 phase for primary patient-derived tumor cell culture treated with B176. Furthermore, a decrease in the S-

phase population of cells was observed after treatment with B070, B176, B327, and A822 for primary patient-derived non-tumor cell culture after 24 h, and for primary patient-derived tumor cell culture after 48 h for B070, B087, B176, and B327. These results suggest that the tested compounds have an inhibitory effect on the cell cycle progression not only of the MCF7 cell line but also in primary patient-derived non-tumor and tumor cell cultures (Figure 47).

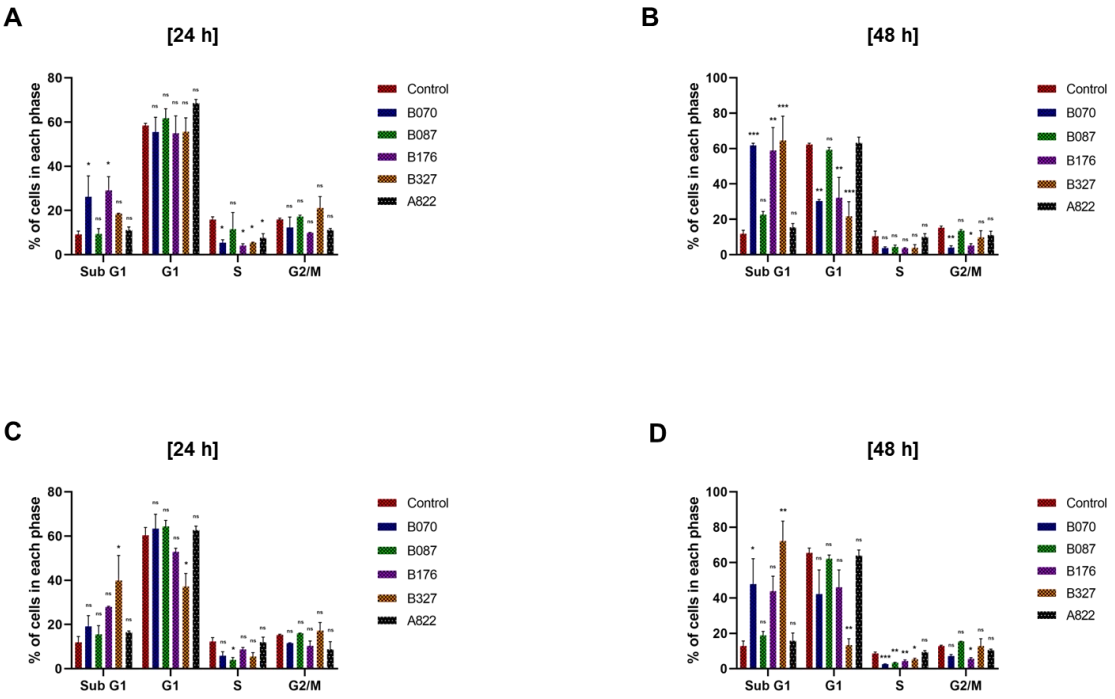

Figure 47. Flow cytometry analysis of cell cycle progression of primary patient-derived non-tumor and tumor cell cultures. A and B - quantification of % of cells in cell cycle each phase for primary patient-derived non-tumor cell culture treated with compounds and untreated control. C and D - quantification of % of cells in cell cycle each phase for primary patient-derived tumor cell culture treated with compounds and untreated control.

Compounds concentration: B070 (50 μM), B087 (50 μM), B176 (50 μM), B327 (50 μM), and A822 (10 μM).

Data presented as standard error mean bar and asterisks denote statistical significance (*** - P<0.001, ** - P<0.01, * - P<0.05, ns - P>0.05) by ANOVA test.

Effects of Shelterin Complex-Targeting on Mitochondrial Morphology and Function in Patient-Derived Non-Tumor and Tumor Cell Cultures

The profound mitochondrial morphology changes were detected after primary patient-derived non-tumor and tumor cell cultures were treated with compounds: B070 (50 μM), B087 (50 μM), B176 (50 μM), B327 (50 μM) and A822 (10 μM) for 48 h. The observed mitochondrial morphological changes that included enlargement and elongation suggestive of mitochondrial swelling after treatment with the compounds (Figure 48) suggest that in addition to their potential effects on telomeres these compounds affect he mitochondrial structure and possibly function. Mitochondria play a critical role in cellular energy production, metabolism and cell signaling, and alterations in mitochondrial morphology can be indicative of changes in these cellular processes. Therefore, the observed changes in mitochondrial morphology by these compounds may extent cellular targets for anticancer therapy beyond telomeres. However, further studies would be needed to confirm the specificity and biological relevance of the observed mitochondrial morphological changes and to investigate the potential therapeutic applications of these compounds.

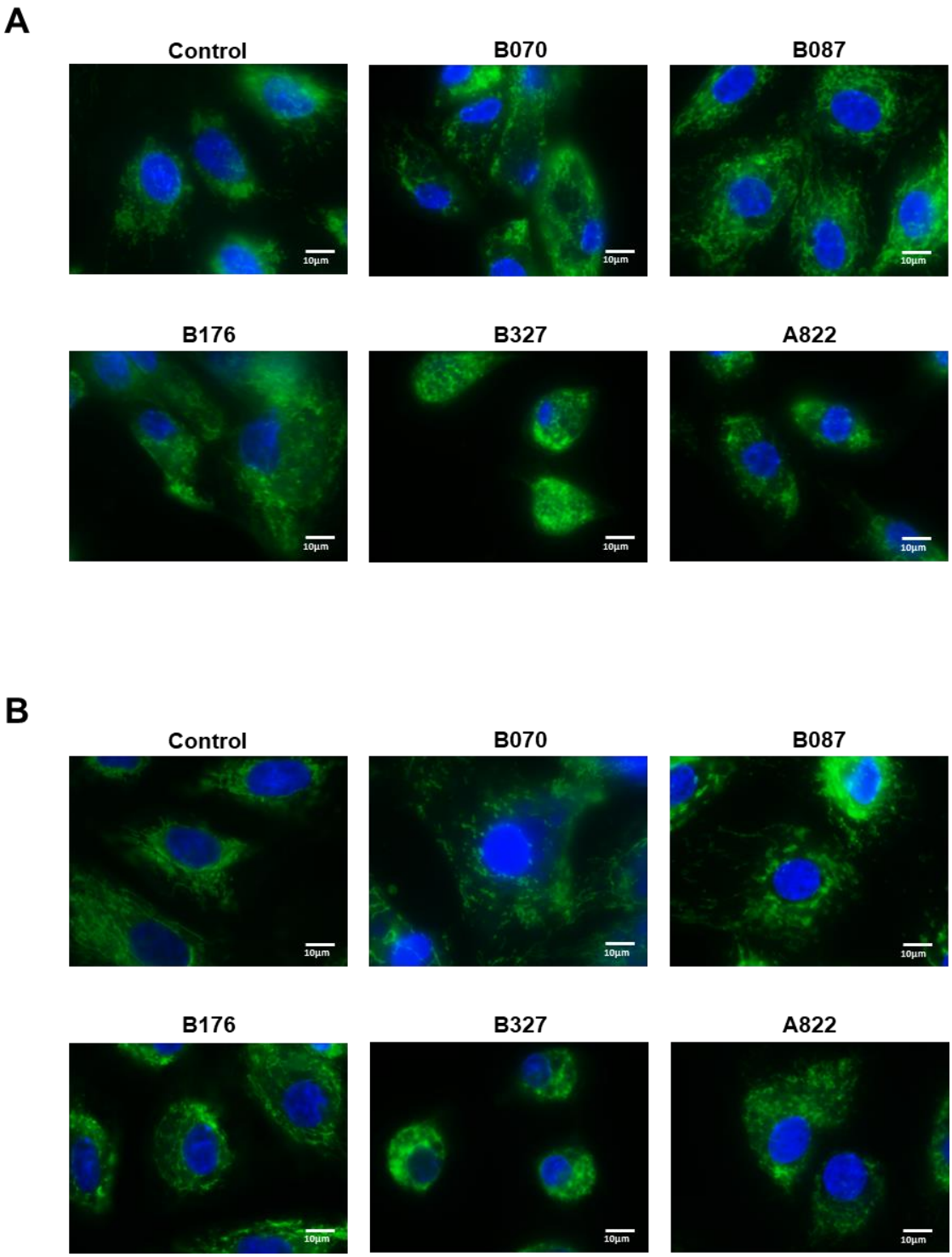

Figure 48. Representative image of mitochondrial morphology of primary patient-derived non-tumor (A) and tumor cell cultures (B) after treatment with B070 (50 μM), B087 (50 μM), B176 (50 μM), B327 (50 μM) and A822 (10 μM) compounds. Cell nuclei were stained with Hoechst 33342. Incubation time – 48 h. Scale bars correspond to 10 μm.

Effects of compounds on lipid droplets and their accumulation in primary patient-derived non-tumor and tumor cell cultures

The primary patient-derived non-tumor and tumor cell cultures were stained with Nile red (after 48 h incubation with compounds) to observe the lipid droplets. Importantly, all the tested compounds possessed their own fluorescent properties and upon excitation with UV light their emission (blue channel in Figure 49 and Figure 50) well co-localized with lipid droplets detected by Nile red (red channel in Figure 49 and Figure 50). The accumulation of the compounds within the lipid droplets indicates a potential role of these organelles in sequestering and storing these compounds within the cells. Lipid droplets that accumulated the compounds might serve as a depo compartment for the investigated compounds, thus prolonging the bio-availability of them when used as pharmaceutics. The observation of an increase in both the size and number of lipid droplets in the cells after treatment with the compounds (Figure 49 and Figure 50) suggests that these compounds may be affecting the regulation of lipid metabolism and storage within the cells.

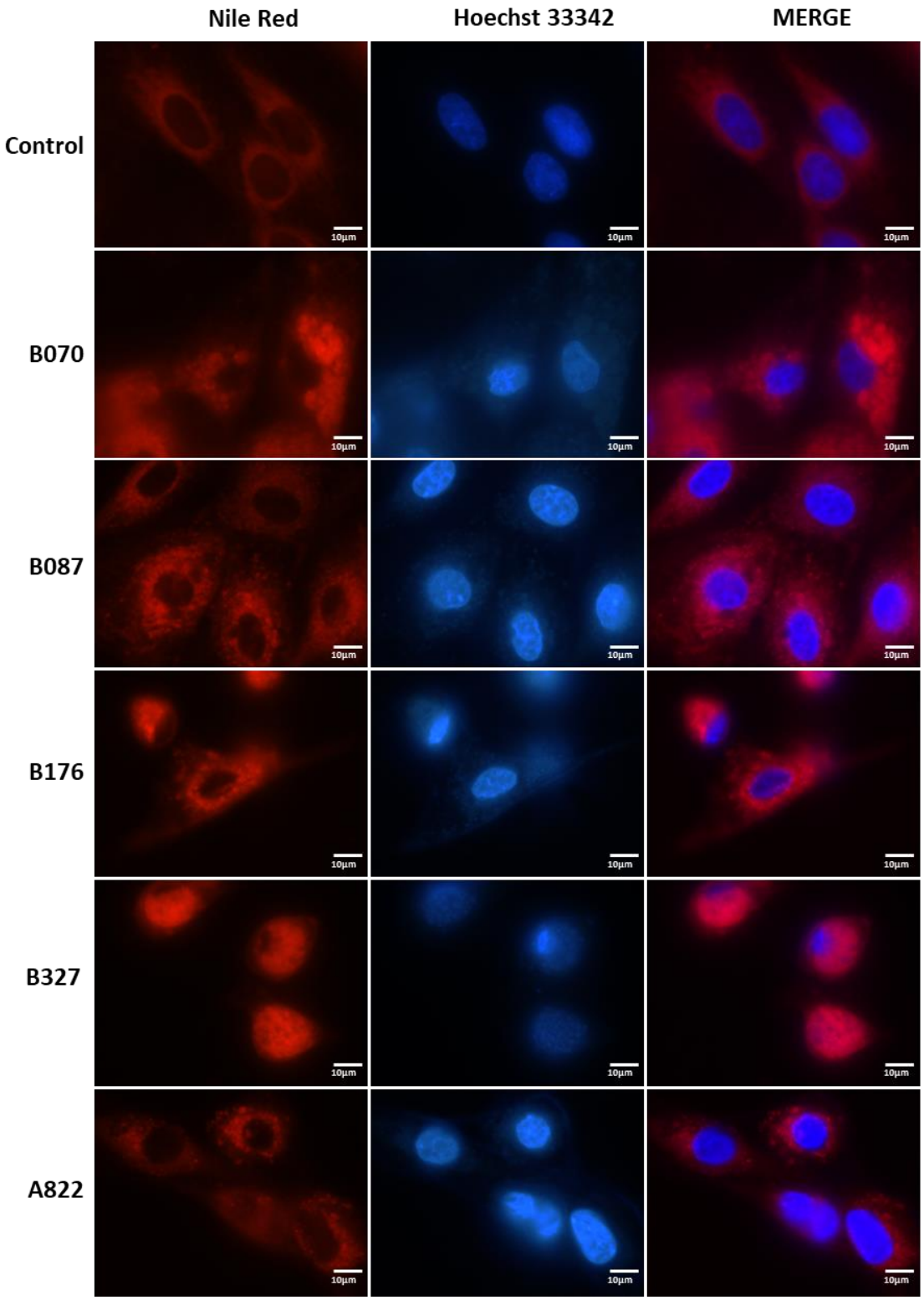

Figure 49. Representative image of compound accumulation (blue channel, extranuclear areas of cells) in lipid droplets (red channel) in patient-derived non-tumor cell cultures. Cell nuclei were stained with Hoechst 33342, (blue channel. nuclear areas of cells). Incubation time – 48 h. Scale bars correspond to 10 µm.

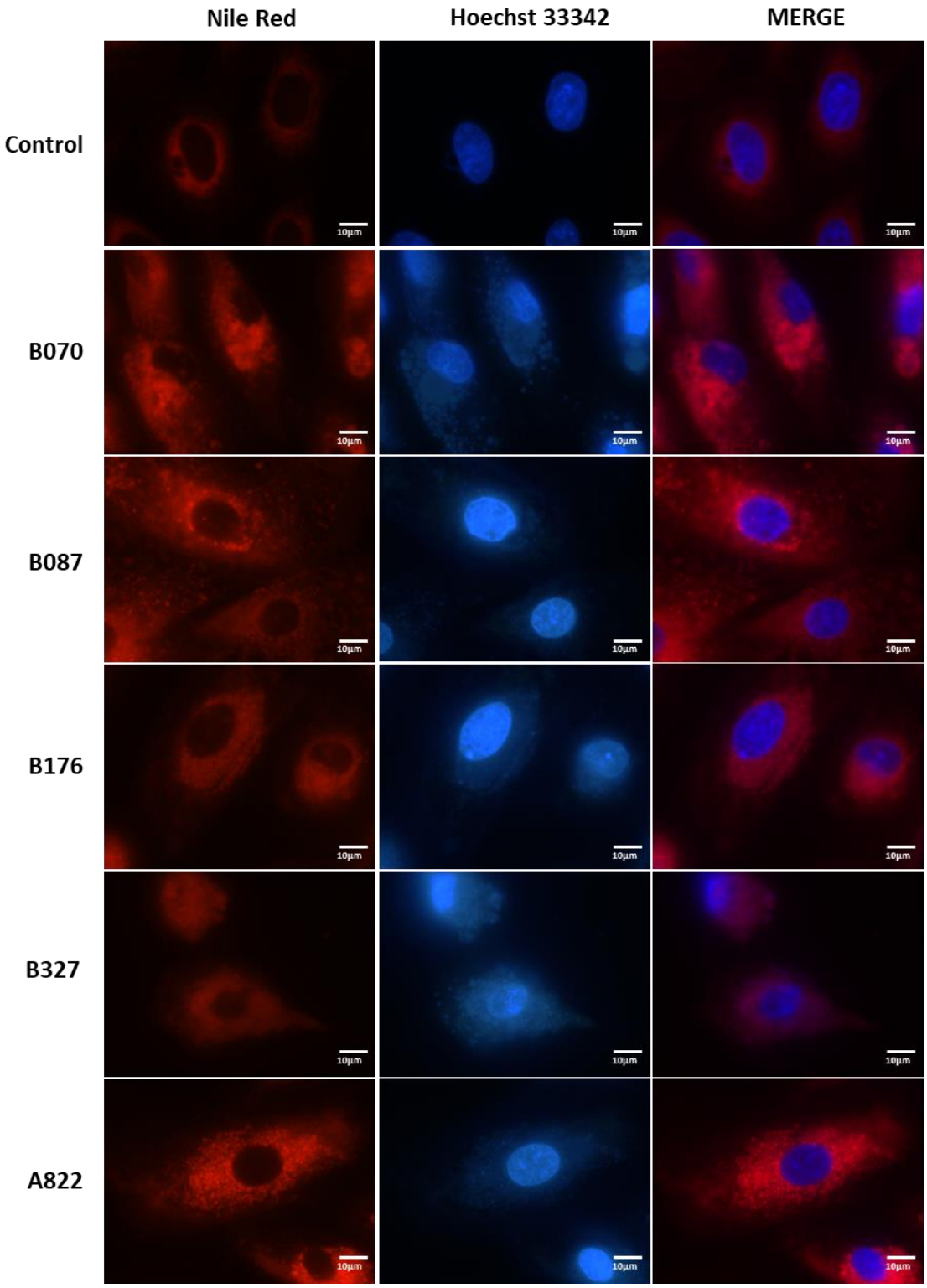

Figure 50. Representative image of compound accumulation (blue channel, extranuclear areas of cells) in lipid droplets (red channel) in patient-derived tumor cell cultures. Cell nuclei were stained with Hoechst 33342, (blue channel. nuclear areas of cells). Incubation time – 48 h. Scale bars correspond to 10 µm.

Effect of Compounds on Actin Filaments in Non-Tumor and Tumor Tissues

Phalloidin staining is a commonly used method to visualize actin filaments (F-actin, in contrast to monomeric actin) in cells and tissues. In this study, phalloidin staining was used to analyze the effect of different compounds (B070, B087, B176, B327, and A822) on actin filaments in both non-tumor and tumor parts of tissues, after partial enzymatic digestion of sampled tissue. After applying B070 and B327 compounds, some ring structures were observed around lipid droplets (identified by morphology, based on the previous experiment) (Figure 51). These structures are likely to be actin rings, which are known to be involved in the regulation of lipid droplet dynamics and metabolism, and organelles' trafficking. Actin rings are formed by the polymerization of actin filaments around the perimeter of lipid droplets, which may help to maintain their size and stability.

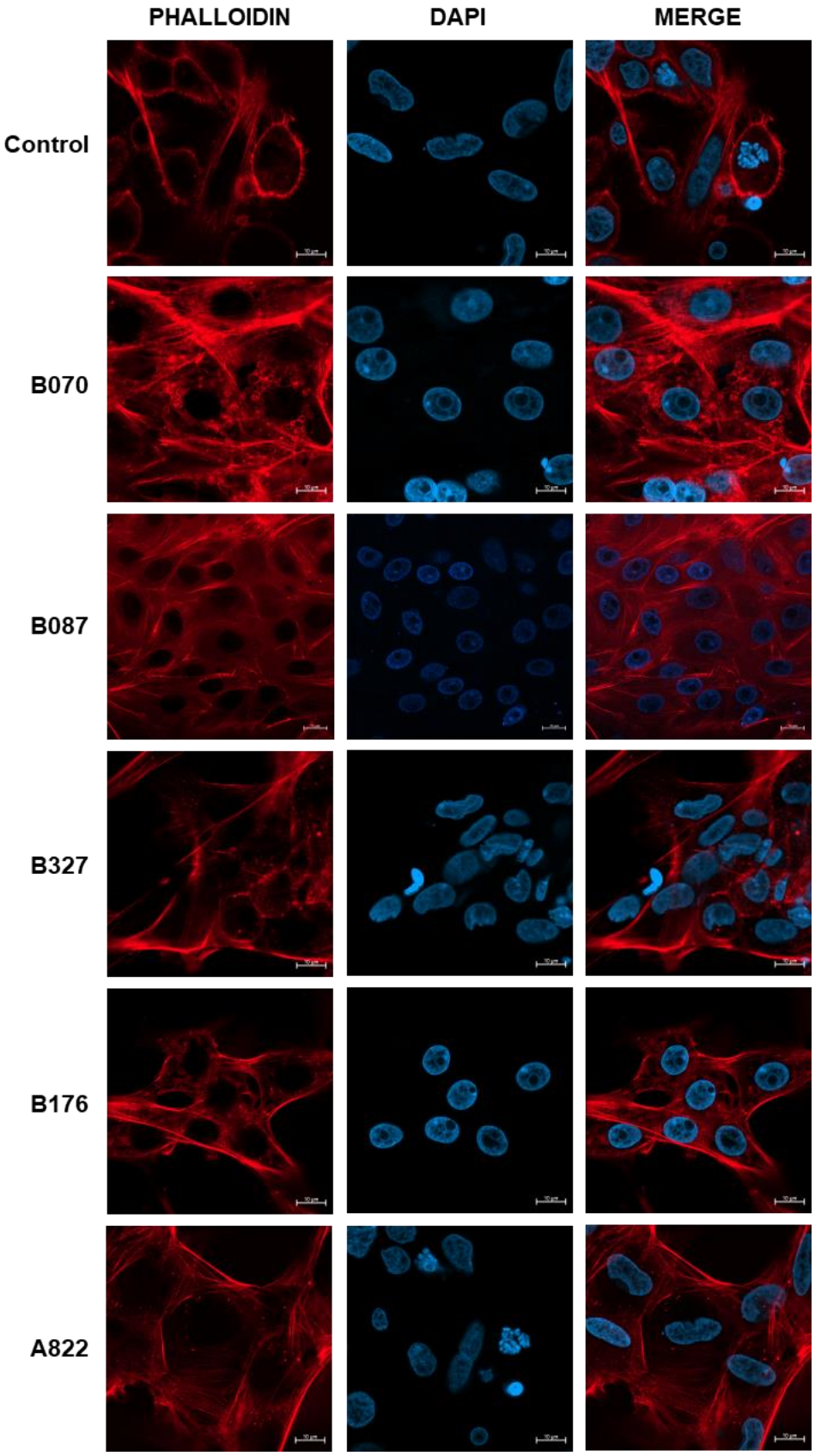

Figure 51. Representative image of microfilament staining in primary tumor tissues after cell treatment with B070, B087, B176 B327 (50 μM) and A822 (10 μM) compounds. F-actin (red channel). Incubation time - 48 h. Cell nuclei were stained with DAPI (blue channel, nuclear areas). Scale bars correspond to 10 μm.

The observation of actin rings after treatment with B070 and B327 compounds suggests that these compounds may have an effect on lipid droplet metabolism in non-tumor and tumor tissues. Further studies are needed to investigate the molecular mechanism underlying this effect and to determine the potential therapeutic implications of these findings. In summary, the results of the phalloidin staining analysis showed that treatment with B070 and B327 compounds resulted in the formation of actin rings around lipid droplets in both non-tumor and tumor tissues. This finding highlights the potential role of these compounds in regulating lipid metabolism and suggests a potential therapeutic target for cancer treatment.

Discussion and Conclusions

Breast cancer is not considered a single disease because of its genetic and histological complexity, and underlying variable response to therapy [294]. Over the past 10–15 years, treatment concepts have evolved to take this heterogeneity into account, with the emphasis being placed on more biologically-directed therapies and treatment de-escalation to reduce the adverse effects of the treatment [88]. The two major pillars of breast cancer management are locoregional treatment and systemic therapy. Initial locoregional treatment is defined as mastectomy, breast-conserving surgery without radiation therapy, and breast-conserving surgery with radiation therapy [295]. The systemic therapies used for breast cancer are chemotherapy, hormone therapy, and molecularly-targeted therapy [296]. However, despite improvements in the last decades in the treatment of this disease, the treatment of advanced breast cancer is still the main clinical problem.

The targeting of telomere maintenance mechanisms represents a promising therapeutic approach for various types of cancer since it is potential new molecular target which still have to be evaluated and explored. In somatic (i.e., non-immortalized) cells, telomeres shorten during iterative rounds of cell division [297]. To combat this event, cancer cells maintain their telomeres using one of two telomere maintenance mechanisms (TMMs): telomerase or alternative lengthening of telomeres (ALT) [298]. Telomerase is a reverse transcriptase enzyme composed of an RNA moiety (TERC, also known as TR) that provides a template for telomeric DNA synthesis and a protein moiety (TERT) that facilitates telomerase recruitment and carries out its polymerase activity [299]. In contrast, ALT relies upon homology-directed, recombination-dependent synthesis of nascent telomeric DNA [300]. ALT requires transient deprotection of telomeres coupled to activation of a DDR that is accompanied by telomere extension in a manner similar to break-induced DNA synthesis [301,302]. DDR activation occurs in

response to alterations in telomeric and subtelomeric chromatin structure that are brought about by the loss of the chromatin remodelers ATRX (explain abbreviations) and DAXX [301,303]. Notably, evidence of each of these mechanisms has been found in breast cancer and can be correlated with specific histologic subtypes or disease stages [16,304]. These findings support the idea that the plasticity inherent to TMM identity has far-reaching prognostic and therapeutic implications. Tumors driven by distinct TMMs may show sensitivity or resistance to specific treatments, which has a substantial impact on patient survival [298].

In this study, we investigated an alternative approach to target telomeres by targeting the telomere-protective TRF1-TIN2 and TRF2-TIN2 proteins binding complexes with which we expected to induce telomere uncapping in tumor cell, independently of its telomere length.

Firstly, the cytotoxic and anti-proliferative effects of the B070, B087, B176, B327 and A822 compounds selected previously in *in silico* studies were evaluated on human non-cancer and cancer cell populations. Results obtained from MTT assay showed that especially B327 and A822 compounds exhibited cytotoxicity against human cancer cells and induced cell cycle arrest. The cell cycle arrest may occur as a result of the dysfunctional telomeres and this causes entry into senescence (it prevents cell proliferation) or apoptosis [305]. The evaluation of the cell senescence showed statistically significantly induced SA-β-gal in MCF7 cells after B327 and A822 compounds application. The shelterin complex is critical for maintaining the t-loop and preventing the activation of the DDR that otherwise induces cellular senescence. Therefore, this observation supports the proposed mechanism of the action of the compounds consisting of the deregulation of the shelterin complex [306]. This observation is further supported by *in vitro* SPR assays indicating that B327 and A822 directly interact with TRF proteins and can bind to the same site as TIN2. Since telomere dysfunction also can lead to apoptosis, to detect this process after cell incubation with compounds the flow cytometry method was used. The result showed significantly increased necrotic cells after 6 h of MCF7 cell incubation with higher concentrations of B327 and A822 compounds. These two experiments proved the concentration-dependent induction of cell death after B327 and A822 application. Replicative senescence is considered to be protective against malignant transformation because

senescent cells are unable to divide, and eventually undergo apoptosis. Replicative senescence is driven by the shortening and dysfunction of telomeres [307]. The length of telomeric DNA is maintained by the enzyme telomerase, but it is the the shelterin complex that coordinates the regulation of telomerase activity at telomeres and ultimately helps define the set-point for telomere length, establishing telomere length homeostasis [308]. The quantitative polymerase chain reaction (qPCR) assay was used to directly compare the average telomere length in treated samples and untreated control. The results show a reduction in telomere length compared to the control after the cell was incubated with B327 and A822 compounds. Excessive telomere shortening due to a defect in the function of telomerase or any components of the shelterin may lead to end-to-end chromosomal fusion, increased HR, and genomic instability [128]. The metaphase-TIF assay confirmed that cell incubation with B327 and A822 compounds induced telomere fusions in samples from patients. Therefore, disrupting TRF1-TIN2 or TRF2-TIN2 interaction impacts both telomere length regulation and telomere cohesion. The TIN2 is the linchpin among the shelterin proteins, that bridges double-stranded (TRF1 and TRF2) and single-stranded telomeric DNA binding proteins (TPP1-POT1) [309]. To study TRF1-TIN2 and TRF2-TIN2 binding after the tested compounds' application, the co-immunofluorescence method and SPR assay were used. It was observed that the co-localization between TRF1 and TIN2 protein was significantly lower in MCF7 cells treated with A822, and the co-localization between TRF2 and TIN2 proteins was significantly lower in MCF7 cells treated with B327. These observations, combined with SPR analyses provided direct evidence that the A822 compound is an inhibitor of TRF1 - TIN2 proteins interaction and the B327 compound is an inhibitor of TRF2 - TIN2 proteins interaction. Additionally, by immunofluorescence staining of telomeric shelterin protein TIN2, followed by FISH for telomere DNA the co-localization between TIN2 protein and telomeres was analyzed. Strikingly, it was observed that the co-localization between TIN2 protein and telomeres was not significantly lower in MCF7 cells treated with compounds. The TIN2 protein binds not only to the TRF1, TRF2, but also to the TPP1-POT1 complex, thereby the bridging units attach to double-stranded DNA and other units attach to single-stranded DNA. Therefore, lack of significant changes in the correlation after compound applications, confirm that B327 and

A822 compounds are inhibitors interfering with the TRF1/TRF2 and TIN2 protein binding rather than telomere/TIN2 binding.

In addition to its role in telomere maintenance, TIN2 can also localize in the mitochondria, where it is post-translationally processed and can regulate oxidative phosphorylation [131]. Depletion of TIN2 increases mitochondrial ATP production and oxygen consumption, and inhibits ROS generation [293]. The statistically significant differences in the number of mitochondria after cells were treated with the B327 compound were observed. Furthermore, the results showed that the A822 compound induced the production of ROS after 3 h and 6 h I MCF7 cells. However, a significant decrease in ROS production was observed after 24 h cell incubation with the A822 compound, therefore the effect of A822 on ROS may be bi-phasic. Mitochondria functioning as a center for cellular metabolism provide intermediates critical for the synthesis of DNA, protein, and components essential for tumor cell growth [310]. Therefore, targeting altered mitochondrial dynamics and trafficking holds immense potential as a therapeutic strategy for cancer, given the reliance of cancer cells on these for their proliferation and metastasis [310].

Proliferation is an important part of cancer development and progression. Cell proliferation is the process by which a cell grows and divides to produce two daughter cells [311]. The clonogenic assay is a widely used method to study the ability (or its lack) of cells to 'infinitely' produce progeny. The result show, that all compounds efficiently suppressed cancer cell growth, two of them from doses as low as 7.5 μM (A822) and 20 μM (B327). Thus, the tested compounds effectively inhibited cell proliferation, an auspicious result in cancer treatment.

We propose that all compounds partition into the plasma membrane and then gain access to lipid droplets. How the compounds move from the plasma membrane, the first barrier for any drug to lipid droplets remains to be clarified but we speculate that this may occur at inter-organelle contact sites. Lipid droplets and other phase-separated organelles may function as reservoirs for drug-like small molecules in cells [312]. For example, a recent study found that the accumulation of a lipophilic antibiotic (bedaquiline) in lipid droplets enhances its antibacterial action against *Mycobacterium tuberculosis* [313]. Lipid droplets are

increased in several types of cancer cells [314,315], including clear cell renal cancer [316], prostate cancer [314] and breast cancer [315], and this increase has been correlated with tumor aggressiveness [317]. Nutrient deprivation, hypoxia and chemotherapy exposure, in addition to inflammatory stress, have been postulated to promote lipid droplet biogenesis in cancer cells [312]. Therefore, lipid droplets appear a useful adjunct in anticancer treatment by lipophilic compounds. Cancer types with increased lipid droplet number may be particularly vulnerable to drugs like B070, B087, B176, B327 and A822 that also exploit a lipid droplet-based mechanism of drug's toxicity.

In summary, I demonstrated here, that interfering with TRF1 - TIN2 and TRF2 - TIN2 proteins binding was an effective target in breast cancer. These observations are of potential clinical relevance, as the treatment of BC is complex and despite it is constantly evolving with a large number of ongoing clinical trials on emerging therapies, there is still a large number of therapy failures. Indeed, the BC molecular subtype determines the personalized therapeutic approach, such as targeted treatments like endocrine therapy for HR+ BC or anti-HER2 therapy for HER2+ BC [318]. These therapies have demonstrated their safety and efficacy in treating BC over the years. However, it is essential to go beyond these conventional treatments since not all patients benefited from personalized treatment. One of the major challenges in BC treatment is finding effective therapies to treat TNBC patients since conventional targeted therapies cannot be administered for this specific BC subtype, stigmatized by the worst survival outcomes. Another important issue in BC treatment is the acquisition of treatment resistance [318]. This is a common phenomenon for either endocrine therapy, anti-HER2 therapy, and chemotherapy. Since the stability of telomeres contributes to the replication immortality in cancer cells, thus targeting telomere stability by interfering with the telomere protection may provide a newer approach to the treatment of cancer. Targeting shelterin components for cancer therapy emerged a few years ago. The POT1 is targeted by a berberine derivative (Sysu-00692) which disrupts interaction POT1 with telomeric DNA [319]. The TRF2 is targeted by gemcitabine, which acts via incorporation into DNA in place of cytosine and consequently inhibits DNA replication and promotes telomere loss through TRF2 stabilization [320]. Recently, two novel compounds (ETP-47228 and ETP-47037)

have been identified that abrogate the function of one of the important telomeres uncapping proteins, TRF1 [152]. Hence, targeting the shelterin proteins proved to be successful approach in combating cancer.

The compounds used in this study should at current stage be regarded as model compounds to treat breast and other cancers. Further studies are expected to further specify their activity on one side and to expand this new class of drugs by synthesis of new derivatives on other side. Such approach is typical in medicinal chemistry as the presented compounds were found as hits in high-throughput *in silico* studies and therefore as the new class of potential pharmaceutics may significantly benefit from enriching their number and thus broadening of pharmacokinetic spectrum. Thus, the presented work is a first step towards extensive preclinical studies in the pipeline to drug development since the most promising candidates as new-lead anticancer therapeutics already underwent the procedure of patenting.

In summary:

In this work, a telomere as an emerging anticancer target was spottedand explored, a novel strategy involving telomeric processing was elaborated, new candidates for telomere shelterin interference selected by high-throughput library screen were tested at cellular and molecular levels and the new-lead molecules were identified and proposed for further preclinical evaluation, with a patent procedure initiated accordingly. Breast cancer was chosen for tissue-level assays of anticancer activity for the chosen compounds for its significance for human survival and accessibility of large number of clinical peri-operative samples.

References

1. Bray, F., Laversanne, M., Weiderpass, E. & Soerjomataram, I. The ever-increasing importance of cancer as a leading cause of premature death worldwide. *Cancer* **127**, 3029–3030 (2021).

2. Sung, H. *et al.* Global Cancer Statistics 2020: GLOBOCAN Estimates of Incidence and Mortality Worldwide for 36 Cancers in 185 Countries. *CA Cancer J Clin* **71**, 209–249 (2021).

3. Omran, A. R. The Epidemiologic Transition: A Theory of the Epidemiology of Population Change. *The Milbank Memorial Fund Quarterly* **49**, 509–538 (1971).

4. Gersten, O. & Wilmoth, J. R. The Cancer Transition in Japan since 1951. *Demographic Research* **7**, 271–306 (2002).

5. Hanahan, D. & Weinberg, R. A. The Hallmarks of Cancer. *Cell* **100**, 57–70 (2000).

6. Hanahan, D. & Weinberg, R. A. Hallmarks of cancer: The next generation. *Cell* **144**, 646–674 (2011).

7. Hanahan, D. Hallmarks of Cancer: New Dimensions. *Cancer Discovery* **12**, 31–46 (2022).

8. Cooper, G. M. The Development and Causes of Cancer. (2000).

9. Blackburn, K. B. Benign tumors: 5 common questions. *MD Anderson Cancer Center* https://www.mdanderson.org/cancerwise/what-are-benign-tumors-and-four-more-questions.h00-159536589.html.

10. Low, K. C. & Tergaonkar, V. Telomerase: central regulator of all of the hallmarks of cancer. *Trends Biochem Sci* **38**, 426–434 (2013).

11. Hayflick, L. The limited in vitro lifetime of human diploid cell strains. *Experimental Cell Research* **37**, 614–636 (1965).

12. Shay, J. W. & Bacchetti, S. A survey of telomerase activity in human cancer. *European Journal of Cancer* **33**, 787–791 (1997).

13. Dilley, R. L. & Greenberg, R. A. ALTernative Telomere Maintenance and Cancer. *Trends Cancer* **1**, 145–156 (2015).

14. De Vitis, M., Berardinelli, F. & Sgura, A. Telomere Length Maintenance in Cancer: At the Crossroad between Telomerase and Alternative Lengthening of Telomeres (ALT). *Int J Mol Sci* **19**, 606 (2018).

15. Cacchione, S., Biroccio, A. & Rizzo, A. Emerging roles of telomeric chromatin alterations in cancer. *Journal of Experimental & Clinical Cancer Research* **38**, 21 (2019).

16. Heaphy, C. M. *et al.* Prevalence of the alternative lengthening of telomeres telomere maintenance mechanism in human cancer subtypes. *Am J Pathol* **179**, 1608–1615 (2011).

17. Henson, J. D. & Reddel, R. R. Assaying and investigating Alternative Lengthening of Telomeres activity in human cells and cancers. *FEBS Lett* **584**, 3800–3811 (2010).

18. Zhang, J.-M., Genois, M.-M., Ouyang, J., Lan, L. & Zou, L. Alternative lengthening of telomeres is a self-perpetuating process in ALT-associated PML bodies. *Molecular Cell* **81**, 1027-1042.e4 (2021).

19. Sobinoff, A. P. *et al.* BLM and SLX4 play opposing roles in recombination-dependent replication at human telomeres. *EMBO J* **36**, 2907–2919 (2017).

20. Dilley, R. L. *et al.* Break-induced telomere synthesis underlies alternative telomere maintenance. *Nature* **539**, 54–58 (2016).

21. Lu, R. & Pickett, H. A. Telomeric replication stress: the beginning and the end for alternative lengthening of telomeres cancers. *Open Biology* **12**, 220011 (2022).

22. Wright, W. E. & Shay, J. W. Time, telomeres and tumours: is cellular senescence more than an anticancer mechanism? *Trends in Cell Biology* **5**, 293–297 (1995).

23. Kipling, D. *et al.* Telomere-dependent senescence. *Nat Biotechnol* **17**, 313–314 (1999).

24. Yaswen, P. *et al.* Therapeutic targeting of replicative immortality. *Seminars in Cancer Biology* **35**, S104–S128 (2015).

25. Bilsland, A. E., Cairney, C. J. & Keith, W. N. Targeting the telomere and shelterin complex for cancer therapy: current views and future perspectives. *J Cell Mol Med* **15**, 179–186 (2011).

26. Gorgoulis, V. *et al.* Cellular Senescence: Defining a Path Forward. *Cell* **179**, 813–827 (2019).

27. Birch, J. & Gil, J. Senescence and the SASP: many therapeutic avenues. *Genes Dev* **34**, 1565–1576 (2020).

28. Faget, D. V., Ren, Q. & Stewart, S. A. Unmasking senescence: context-dependent effects of SASP in cancer. *Nat Rev Cancer* **19**, 439–453 (2019).

29. He, S. & Sharpless, N. E. Senescence in Health and Disease. *Cell* **169**, 1000–1011 (2017).

30. Marabitti, V. *et al.* R-Loop-Associated Genomic Instability and Implication of WRN and WRNIP1. *Int J Mol Sci* **23**, 1547 (2022).

31. Aguilera, A. & García-Muse, T. Causes of Genome Instability. *Annual Review of Genetics* **47**, 1–32 (2013).

32. Lawrence, K. S., Chau, T. & Engebrecht, J. DNA Damage Response and Spindle Assembly Checkpoint Function throughout the Cell Cycle to Ensure Genomic Integrity. *PLoS Genet* **11**, e1005150 (2015).

33. Brambati, A., Colosio, A., Zardoni, L., Galanti, L. & Liberi, G. Replication and transcription on a collision course: eukaryotic regulation mechanisms and implications for DNA stability. *Front Genet* **6**, 166 (2015).

34. Christensen, S. *et al.* 5-Fluorouracil treatment induces characteristic T>G mutations in human cancer. *Nat Commun* **10**, 4571 (2019).

35. The impact of mitotic errors on cell proliferation and tumorigenesis. http://genesdev.cshlp.org/content/32/9-10/620.long.

36. Comaills, V. *et al.* Genomic Instability Is Induced by Persistent Proliferation of Cells Undergoing Epithelial-to-Mesenchymal Transition. *Cell Rep* **17**, 2632–2647 (2016).

37. Wang, Y. *et al.* Temporal DNA-PK activation drives genomic instability and therapy resistance in glioma stem cells. *JCI Insight* **3**, e98096.

38. Tumor aneuploidy correlates with markers of immune evasion and with reduced response to immunotherapy | Science. https://www.science.org/doi/10.1126/science.aaf8399.

39. Chen, M., Linstra, R. & van Vugt, M. A. T. M. Genomic instability, inflammatory signaling and response to cancer immunotherapy. *Biochimica et Biophysica Acta (BBA) - Reviews on Cancer* **1877**, 188661 (2022).

40. Alhmoud, J. F., Woolley, J. F., Al Moustafa, A.-E. & Malki, M. I. DNA Damage/Repair Management in Cancers. *Cancers* **12**, 1050 (2020).

41. Srinivas, U. S., Tan, B. W. Q., Vellayappan, B. A. & Jeyasekharan, A. D. ROS and the DNA damage response in cancer. *Redox Biology* **25**, 101084 (2019).

42. Terradas, M., Martín, M., Tusell, L. & Genescà, A. Genetic activities in micronuclei: Is the DNA entrapped in micronuclei lost for the cell? *Mutation Research/Reviews in Mutation Research* **705**, 60–67 (2010).

43. Drews, R. M. *et al.* A pan-cancer compendium of chromosomal instability. *Nature* **606**, 976–983 (2022).

44. Sansregret, L., Vanhaesebroeck, B. & Swanton, C. Determinants and clinical implications of chromosomal instability in cancer. *Nat Rev Clin Oncol* **15**, 139–150 (2018).

45. Dahal, S., Dubey, S. & Raghavan, S. C. Homologous recombination-mediated repair of DNA double-strand breaks operates in mammalian mitochondria. *Cell. Mol. Life Sci.* **75**, 1641–1655 (2018).

46. Shokolenko, I. N., Wilson, G. L. & Alexeyev, M. F. Persistent damage induces mitochondrial DNA degradation. *DNA Repair* **12**, 488–499 (2013).

47. Bonora, M. *et al.* Mitochondrial Control of Genomic Instability in Cancer. *Cancers (Basel)* **13**, 1914 (2021).

48. Saman, H., Raza, S. S., Uddin, S. & Rasul, K. Inducing Angiogenesis, a Key Step in Cancer Vascularization, and Treatment Approaches. *Cancers (Basel)* **12**, 1172 (2020).

49. Kopec, M. & Abramczyk, H. The role of pro- and antiangiogenic factors in angiogenesis process by Raman spectroscopy. *Spectrochimica Acta Part A: Molecular and Biomolecular Spectroscopy* **268**, 120667 (2022).

50. Zheng, W. *et al.* Multi-omics analysis of tumor angiogenesis characteristics and potential epigenetic regulation mechanisms in renal clear cell carcinoma. *Cell Communication and Signaling* **19**, 39 (2021).

51. Lee, S. G. *et al.* Endothelial angiogenic activity and adipose angiogenesis is controlled by extracellular matrix protein TGFBI. *Sci Rep* **11**, 9644 (2021).

52. Nishida, N., Yano, H., Nishida, T., Kamura, T. & Kojiro, M. Angiogenesis in Cancer. *Vasc Health Risk Manag* **2**, 213–219 (2006).

53. Ravi, R. *et al.* Regulation of tumor angiogenesis by p53-induced degradation of hypoxia-inducible factor 1α. *Genes Dev* **14**, 34–44 (2000).

54. de Mas, I. M. *et al.* Cancer cell metabolism as new targets for novel designed therapies. *Future Medicinal Chemistry* **6**, 1791–1810 (2014).

55. Dong, Y., Tu, R., Liu, H. & Qing, G. Regulation of cancer cell metabolism: oncogenic MYC in the driver's seat. *Sig Transduct Target Ther* **5**, 1–11 (2020).

56. DeBerardinis, R. J. *et al.* Beyond aerobic glycolysis: Transformed cells can engage in glutamine metabolism that exceeds the requirement for protein and nucleotide synthesis. *Proceedings of the National Academy of Sciences* **104**, 19345–19350 (2007).

57. Min, H.-Y. & Lee, H.-Y. Oncogene-Driven Metabolic Alterations in Cancer. *Biomol Ther (Seoul)* **26**, 45–56 (2018).

58. Eberlin, L. S. *et al.* Alteration of the lipid profile in lymphomas induced by MYC overexpression. *Proc Natl Acad Sci U S A* **111**, 10450–10455 (2014).

59. Morrish, F., Neretti, N., Sedivy, J. M. & Hockenbery, D. M. The oncogene c-Myc coordinates regulation of metabolic networks to enable rapid cell cycle entry. *Cell Cycle* **7**, 1054–1066 (2008).

60. Fares, J., Fares, M. Y., Khachfe, H. H., Salhab, H. A. & Fares, Y. Molecular principles of metastasis: a hallmark of cancer revisited. *Sig Transduct Target Ther* **5**, 1–17 (2020).

61. Tahtamouni, L., Ahram, M., Koblinski, J. & Rolfo, C. Molecular Regulation of Cancer Cell Migration, Invasion, and Metastasis. *Analytical Cellular Pathology* **2019**, 1–2 (2019).

62. Martin, T. A., Ye, L., Sanders, A. J., Lane, J. & Jiang, W. G. *Cancer Invasion and Metastasis: Molecular and Cellular Perspective*. *Madame Curie Bioscience Database [Internet]* (Landes Bioscience, 2013).

63. Folkman, J. & Shing, Y. Angiogenesis. *Journal of Biological Chemistry* **267**, 10931–10934 (1992).

64. Folkman, J. Fighting cancer by attacking its blood supply. *Sci Am* **275**, 150–154 (1996).

65. Jiang, W. G. *et al.* Tissue invasion and metastasis: Molecular, biological and clinical perspectives. *Seminars in Cancer Biology* **35**, S244–S275 (2015).

66. Dissemination and growth of cancer cells in metastatic sites | Nature Reviews Cancer. https://www.nature.com/articles/nrc865.

67. Greten, F. R. & Grivennikov, S. I. Inflammation and Cancer: Triggers, Mechanisms and Consequences. *Immunity* **51**, 27–41 (2019).

68. Medzhitov, R. Origin and physiological roles of inflammation. *Nature* **454**, 428–435 (2008).

69. Singh, N. *et al.* Inflammation and Cancer. *Ann Afr Med* **18**, 121–126 (2019).

70. Grivennikov, S. I., Greten, F. R. & Karin, M. Immunity, Inflammation, and Cancer. *Cell* **140**, 883–899 (2010).

71. Nakamura, K. & Smyth, M. J. Myeloid immunosuppression and immune checkpoints in the tumor microenvironment. *Cell Mol Immunol* **17**, 1–12 (2020).

72. Thomas, S. *et al.* The Host Microbiome Regulates and Maintains Human Health: A Primer and Perspective for Non-Microbiologists. *Cancer Res* **77**, 1783–1812 (2017).

73. Sepich-Poore, G. D. *et al.* The microbiome and human cancer. *Science* **371**, eabc4552 (2021).

74. Lythgoe, M. P., Mullish, B. H., Frampton, A. E. & Krell, J. Polymorphic microbes: a new emerging hallmark of cancer. *Trends in Microbiology* **30**, 1131–1134 (2022).

75. Brücher, B. L. D. M. & Jamall, I. S. Somatic Mutation Theory - Why it's Wrong for Most Cancers. *Cell Physiol Biochem* **38**, 1663–1680 (2016).

76. Baylin, S. B. & Jones, P. A. A decade of exploring the cancer epigenome — biological and translational implications. *Nat Rev Cancer* **11**, 726–734 (2011).

77. Feinberg, A. P., Koldobskiy, M. A. & Göndör, A. Epigenetic modulators, modifiers and mediators in cancer aetiology and progression. *Nat Rev Genet* **17**, 284–299 (2016).

78. Comet, I., Riising, E. M., Leblanc, B. & Helin, K. Maintaining cell identity: PRC2-mediated regulation of transcription and cancer. *Nat Rev Cancer* **16**, 803–810 (2016).

79. The molecular hallmarks of epigenetic control | Nature Reviews Genetics. https://www.nature.com/articles/nrg.2016.59.

80. Feinberg, A. P. Phenotypic plasticity and the epigenetics of human disease. *Nature* **447**, 433–440 (2007).

81. Epigenetic plasticity and the hallmarks of cancer | Science. https://www.science.org/doi/10.1126/science.aal2380.

82. Darwiche, N. Epigenetic mechanisms and the hallmarks of cancer: an intimate affair. *Am J Cancer Res* **10**, 1954–1978 (2020).

83. Wang, F., Du, H., Li, B., Luo, Z. & Zhu, L. Unlocking phenotypic plasticity provides novel insights for immunity and personalized therapy in lung adenocarcinoma. *Front Genet* **13**, 941567 (2022).

84. Lakhtakia, R. A Brief History of Breast Cancer. *Sultan Qaboos Univ Med J* **14**, e166–e169 (2014).

85. Lyons: Medicine an illustrated History. Harry N Abrams - Google Scholar. https://scholar.google.com/scholar_lookup?title=Medicine+-+An+illustrated+history&author=AS+Lyons&author=RJ+Petrucelli&publication_year=1978&.

86. Didkowska, J., Wojciechowska, U., Michalek, I. M. & Caetano dos Santos, F. L. Cancer incidence and mortality in Poland in 2019. *Sci Rep* **12**, 10875 (2022).

87. Chen, Y. *et al.* Three-dimensional bioprinting adipose tissue and mammary Organoids feasible for artificial breast structure regeneration. *Materials & Design* **200**, 109467 (2021).

88. Harbeck, N. *et al.* Breast cancer. *Nat Rev Dis Primers* **5**, 1–31 (2019).

89. Invasive Breast Cancer (IDC/ILC). https://www.cancer.org/cancer/breast-cancer/about/types-of-breast-cancer/invasive-breast-cancer.html.

90. IARC Publications Website - WHO Classification of Tumours. https://publications.iarc.fr/Book-And-Report-Series/Who-Classification-Of-Tumours.

91. Gjerde, J. *et al.* Associations between tamoxifen, estrogens, and FSH serum levels during steady state tamoxifen treatment of postmenopausal women with breast cancer. *BMC Cancer* **10**, 313 (2010).

92. Koh, J. & Kim, M. J. Introduction of a New Staging System of Breast Cancer for Radiologists: An Emphasis on the Prognostic Stage. *Korean J Radiol* **20**, 69–82 (2019).

93. Dowsett, M. *et al.* In vivo measurement of aromatase inhibition by letrozole (CGS 20267) in postmenopausal patients with breast cancer. *Clin Cancer Res* **1**, 1511–1515 (1995).

94. Influence of Letrozole and Anastrozole on Total Body Aromatization and Plasma Estrogen Levels in Postmenopausal Breast Cancer Patients Evaluated in a Randomized, Cross-Over Study | Journal of Clinical Oncology. https://ascopubs.org/doi/10.1200/JCO.2002.20.3.751?url_ver=Z39.88-2003&rfr_id=ori:rid:crossref.org&rfr_dat=cr_pub%20%200pubmed.

95. Staging & Grade - Breast Pathology | Johns Hopkins Pathology. https://pathology.jhu.edu/breast/staging-grade.

96. Nielsen, T. O. *et al.* Immunohistochemical and Clinical Characterization of the Basal-Like Subtype of Invasive Breast Carcinoma. *Clinical Cancer Research* **10**, 5367–5374 (2004).

97. Perou, C. M. *et al.* Molecular portraits of human breast tumours. *Nature* **406**, 747–752 (2000).

98. McCormack, V. A. *et al.* Breast cancer receptor status and stage at diagnosis in over 1,200 consecutive public hospital patients in Soweto, South Africa: a case series. *Breast Cancer Res* **15**, R84 (2013).

99. Zhang, M. H., Man, H. T., Zhao, X. D., Dong, N. & Ma, S. L. Estrogen receptor-positive breast cancer molecular signatures and therapeutic potentials (Review). *Biomed Rep* **2**, 41–52 (2014).

100. Miah, S. *et al.* Estrogen receptor signaling regulates the expression of the breast tumor kinase in breast cancer cells. *BMC Cancer* **19**, 78 (2019).

101. Hicks, D. G. & Lester, S. C. Hormone Receptors (ER/PR). in *Diagnostic Pathology: Breast (Second Edition)* (eds. Hicks, D. G. & Lester, S. C.) 430–439 (Elsevier, 2016). doi:10.1016/B978-0-323-37712-6.50067-3.

102. Vaz-Luis, I., Winer, E. P. & Lin, N. U. Human epidermal growth factor receptor-2-positive breast cancer: does estrogen receptor status define two distinct subtypes? *Ann Oncol* **24**, 283–291 (2013).

103. Iqbal, N. & Iqbal, N. Human Epidermal Growth Factor Receptor 2 (HER2) in Cancers: Overexpression and Therapeutic Implications. *Molecular Biology International* **2014**, e852748 (2014).

104. Krishnamurti, U., Hammers, J. L., Atem, F. D., Storto, P. D. & Silverman, J. F. Poor prognostic significance of unamplified chromosome 17 polysomy in invasive breast carcinoma. *Modern Pathology* **22**, 1044–1048 (2009).

105. Haroon, S. *et al.* Ki67 index in breast cancer: correlation with other prognostic markers and potential in pakistani patients. *Asian Pac J Cancer Prev* **14**, 4353–4358 (2013).

106. Orrantia-Borunda, E., Anchondo-Nuñez, P., Acuña-Aguilar, L. E., Gómez-Valles, F. O. & Ramírez-Valdespino, C. A. Subtypes of Breast Cancer. in *Breast Cancer* (ed. Mayrovitz, H. N.) (Exon Publications, 2022).

107. Prat, A. *et al.* Clinical implications of the intrinsic molecular subtypes of breast cancer. *Breast* **24 Suppl 2**, S26-35 (2015).

108. Koboldt, D. C. *et al.* Comprehensive molecular portraits of human breast tumours. *Nature* **490**, 61–70 (2012).

109. Parker, J. S. *et al.* Supervised risk predictor of breast cancer based on intrinsic subtypes. *J Clin Oncol* **27**, 1160–1167 (2009).

110. Caan, B. J. *et al.* Intrinsic subtypes from the PAM50 gene expression assay in a population-based breast cancer survivor cohort: prognostication of short- and long-term outcomes. *Cancer Epidemiol Biomarkers Prev* **23**, 725–734 (2014).

111. Coates, A. S. *et al.* Tailoring therapies--improving the management of early breast cancer: St Gallen International Expert Consensus on the Primary Therapy of Early Breast Cancer 2015. *Ann Oncol* **26**, 1533–1546 (2015).

112. Kensler, K. H. *et al.* PAM50 Molecular Intrinsic Subtypes in the Nurses' Health Study Cohorts. *Cancer Epidemiol Biomarkers Prev* **28**, 798–806 (2019).

113. Prat, A. *et al.* Phenotypic and molecular characterization of the claudin-low intrinsic subtype of breast cancer. *Breast Cancer Res* **12**, R68 (2010).

114. Sabatier, R. *et al.* Claudin-low breast cancers: clinical, pathological, molecular and prognostic characterization. *Mol Cancer* **13**, 228 (2014).

115. Lehmann-Che, J. *et al.* Molecular apocrine breast cancers are aggressive estrogen receptor negative tumors overexpressing either HER2 or GCDFP15. *Breast Cancer Res* **15**, R37 (2013).

116. Hu, Z. *et al.* The molecular portraits of breast tumors are conserved across microarray platforms. *BMC Genomics* **7**, 96 (2006).

117. *AJCC Cancer Staging Manual*.

118. Maughan, K. L., Lutterbie, M. A. & Ham, P. S. Treatment of Breast Cancer. *afp* **81**, 1339–1346 (2010).

119. Loibl, S., Poortmans, P., Morrow, M., Denkert, C. & Curigliano, G. Breast cancer. *The Lancet* **397**, 1750–1769 (2021).

120. Rossiello, F., Jurk, D., Passos, J. F. & d'Adda di Fagagna, F. Telomere dysfunction in ageing and age-related diseases. *Nat Cell Biol* **24**, 135–147 (2022).

121. Fan, H.-C. *et al.* Telomeres and Cancer. *Life (Basel)* **11**, 1405 (2021).

122. de Lange, T. How telomeres solve the end-protection problem. *Science* **326**, 948–952 (2009).

123. Bonnell, E., Pasquier, E. & Wellinger, R. J. Telomere Replication: Solving Multiple End Replication Problems. *Front Cell Dev Biol* **9**, 668171 (2021).

124. Lansdorp, P. M. Major cutbacks at chromosome ends. *Trends Biochem Sci* **30**, 388–395 (2005).

125. Lundblad, V. Telomere end processing: unexpected complexity at the end game. *Genes Dev* **26**, 1123–1127 (2012).

126. Gong, J. G. *et al.* The tyrosine kinase c-Abl regulates p73 in apoptotic response to cisplatin-induced DNA damage. *Nature* **399**, 806–809 (1999).

127. Stiewe, T. & Pützer, B. M. p73 in apoptosis. *Apoptosis* **6**, 447–452 (2001).

128. Mir, S. M. *et al.* Shelterin Complex at Telomeres: Implications in Ageing. *Clin Interv Aging* **15**, 827–839 (2020).

129. Team 2, H. J. Telomere, telomere length, function & telomere structure. *Health Jade* https://healthjade.com/telomere/ (2019).

130. de Lange, T. Shelterin: the protein complex that shapes and safeguards human telomeres. *Genes Dev* **19**, 2100–2110 (2005).

131. Chen, L.-Y., Liu, D. & Songyang, Z. Telomere maintenance through spatial control of telomeric proteins. *Mol Cell Biol* **27**, 5898–5909 (2007).

132. Patel, T. N., Vasan, R., Gupta, D., Patel, J. & Trivedi, M. Shelterin proteins and cancer. *Asian Pac J Cancer Prev* **16**, 3085–3090 (2015).

133. Campisi, J., Kim, S. H., Lim, C. S. & Rubio, M. Cellular senescence, cancer and aging: the telomere connection. *Exp Gerontol* **36**, 1619–1637 (2001).

134. Garton, M. & Laughton, C. A Comprehensive Model for the Recognition of Human Telomeres by TRF1. *Journal of Molecular Biology* **425**, 2910–2921 (2013).

135. Xin, H., Liu, D. & Songyang, Z. The telosome/shelterin complex and its functions. *Genome Biology* **9**, 232 (2008).

136. Diotti, R. & Loayza, D. Shelterin complex and associated factors at human telomeres. *Nucleus* **2**, 119–135 (2011).

137. Hu, C. *et al.* Structural and functional analyses of the mammalian TIN2-TPP1-TRF2 telomeric complex. *Cell Res* **27**, 1485–1502 (2017).

138. van Steensel, B., Smogorzewska, A. & de Lange, T. TRF2 protects human telomeres from end-to-end fusions. *Cell* **92**, 401–413 (1998).

139. Nakamura, M., Zhou, X. Z., Kishi, S. & Lu, K. P. Involvement of the telomeric protein Pin2/TRF1 in the regulation of the mitotic spindle. *FEBS Lett* **514**, 193–198 (2002).

140. Zhou, X. Z., Perrem, K. & Lu, K. P. Role of Pin2/TRF1 in telomere maintenance and cell cycle control. *J Cell Biochem* **89**, 19–37 (2003).

141. Canudas, S. *et al.* Protein requirements for sister telomere association in human cells. *EMBO J* **26**, 4867–4878 (2007).

142. Lin, J. *et al.* Functional interplay between SA1 and TRF1 in telomeric DNA binding and DNA-DNA pairing. *Nucleic Acids Res* **44**, 6363–6376 (2016).

143. Tan, R. *et al.* Nek7 Protects Telomeres from Oxidative DNA Damage by Phosphorylation and Stabilization of TRF1. *Mol Cell* **65**, 818-831.e5 (2017).

144. Sun, L. *et al.* WRN is recruited to damaged telomeres via its RQC domain and tankyrase1-mediated poly-ADP-ribosylation of TRF1. *Nucleic Acids Res* **45**, 3844–3859 (2017).

145. Lee, Y. W., Arora, R., Wischnewski, H. & Azzalin, C. M. TRF1 participates in chromosome end protection by averting TRF2-dependent telomeric R loops. *Nat Struct Mol Biol* **25**, 147–153 (2018).

146. Li, X. *et al.* Dynamics of TRF1 organizing a single human telomere. *Nucleic Acids Research* **49**, 760–775 (2021).

147. Ohki, R. & Ishikawa, F. Telomere-bound TRF1 and TRF2 stall the replication fork at telomeric repeats. *Nucleic Acids Res* **32**, 1627–1637 (2004).

148. Zimmermann, M., Kibe, T., Kabir, S. & de Lange, T. TRF1 negotiates TTAGGG repeat-associated replication problems by recruiting the BLM helicase and the TPP1/POT1 repressor of ATR signaling. *Genes Dev* **28**, 2477–2491 (2014).

149. Sfeir, A. *et al.* Mammalian telomeres resemble fragile sites and require TRF1 for efficient replication. *Cell* **138**, 90–103 (2009).

150. Pal, D., Sharma, U., Singh, S. K., Kakkar, N. & Prasad, R. Over-expression of telomere binding factors (TRF1 & TRF2) in renal cell carcinoma and their inhibition by using SiRNA induce apoptosis, reduce cell proliferation and migration invitro. *PLoS One* **10**, e0115651 (2015).

151. Hu, H., Zhang, Y., Zou, M., Yang, S. & Liang, X.-Q. Expression of TRF1, TRF2, TIN2, TERT, KU70, and BRCA1 proteins is associated with telomere shortening and may contribute to multistage carcinogenesis of gastric cancer. *J Cancer Res Clin Oncol* **136**, 1407–1414 (2010).

152. Bejarano, L. *et al.* Inhibition of TRF1 Telomere Protein Impairs Tumor Initiation and Progression in Glioblastoma Mouse Models and Patient-Derived Xenografts. *Cancer Cell* **32**, 590-607.e4 (2017).

153. Martínez, P. & Blasco, M. A. Role of shelterin in cancer and aging. *Aging Cell* **9**, 653–666 (2010).

154. Liu, F. *et al.* Expression of hPOT1 in HeLa cells and the probability of gene variation of hpot1 Exon14 in endometrial cancer are much higher than in other cancers. *Asian Pac J Cancer Prev* **13**, 5659–5663 (2012).

155. Stewart, J. A., Chaiken, M. F., Wang, F. & Price, C. M. Maintaining the end: roles of telomere proteins in end-protection, telomere replication and length regulation. *Mutat Res* **730**, 12–19 (2012).

156. Rai, R., Chen, Y., Lei, M. & Chang, S. TRF2-RAP1 is required to protect telomeres from engaging in homologous recombination-mediated deletions and fusions. *Nat Commun* **7**, 10881 (2016).

157. Celli, G. B. & de Lange, T. DNA processing is not required for ATM-mediated telomere damage response after TRF2 deletion. *Nat Cell Biol* **7**, 712–718 (2005).

158. Muñoz, P., Blanco, R., Flores, J. M. & Blasco, M. A. XPF nuclease-dependent telomere loss and increased DNA damage in mice overexpressing TRF2 result in premature aging and cancer. *Nat Genet* **37**, 1063–1071 (2005).

159. Nakane, H. *et al.* High incidence of ultraviolet-B-or chemical-carcinogen-induced skin tumours in mice lacking the xeroderma pigmentosum group A gene. *Nature* **377**, 165–168 (1995).

160. Sands, A. T., Abuin, A., Sanchez, A., Conti, C. J. & Bradley, A. High susceptibility to ultraviolet-induced carcinogenesis in mice lacking XPC. *Nature* **377**, 162–165 (1995).

161. Liu, D. *et al.* PTOP interacts with POT1 and regulates its localization to telomeres. *Nat Cell Biol* **6**, 673–680 (2004).

162. Sullivan, L. B., Santos, J. H. & Chandel, N. S. Mitochondria and telomeres: the promiscuous roles of TIN2. *Mol Cell* **47**, 823–824 (2012).

163. Okamoto, K., Iwano, T., Tachibana, M. & Shinkai, Y. Distinct roles of TRF1 in the regulation of telomere structure and lengthening. *J Biol Chem* **283**, 23981–23988 (2008).

164. Ye, J. Z.-S. & de Lange, T. TIN2 is a tankyrase 1 PARP modulator in the TRF1 telomere length control complex. *Nat Genet* **36**, 618–623 (2004).

165. Kim, S. H., Kaminker, P. & Campisi, J. TIN2, a new regulator of telomere length in human cells. *Nat Genet* **23**, 405–412 (1999).

166. Chiang, Y. J., Kim, S.-H., Tessarollo, L., Campisi, J. & Hodes, R. J. Telomere-associated protein TIN2 is essential for early embryonic development through a telomerase-independent pathway. *Mol Cell Biol* **24**, 6631–6634 (2004).

167. Karlseder, J. *et al.* Targeted deletion reveals an essential function for the telomere length regulator Trf1. *Mol Cell Biol* **23**, 6533–6541 (2003).

168. Yamada, M. *et al.* Down-regulation of TRF1, TRF2 and TIN2 genes is important to maintain telomeric DNA for gastric cancers. *Anticancer Res* **22**, 3303–3307 (2002).

169. Bellon, M. *et al.* Increased expression of telomere length regulating factors TRF1, TRF2 and TIN2 in patients with adult T-cell leukemia. *Int J Cancer* **119**, 2090–2097 (2006).

170. Oh, B.-K., Kim, Y.-J., Park, C. & Park, Y. N. Up-regulation of telomere-binding proteins, TRF1, TRF2, and TIN2 is related to telomere shortening during human multistep hepatocarcinogenesis. *Am J Pathol* **166**, 73–80 (2005).

171. Martínez, P., Gómez-López, G., Pisano, D. G., Flores, J. M. & Blasco, M. A. A genetic interaction between RAP1 and telomerase reveals an unanticipated role for RAP1 in telomere maintenance. *Aging Cell* **15**, 1113–1125 (2016).

172. Janoušková, E. *et al.* Human Rap1 modulates TRF2 attraction to telomeric DNA. *Nucleic Acids Res* **43**, 2691–2700 (2015).

173. Kabir, S., Hockemeyer, D. & de Lange, T. TALEN gene knockouts reveal no requirement for the conserved human shelterin protein Rap1 in telomere protection and length regulation. *Cell Rep* **9**, 1273–1280 (2014).

174. Martinez, P. *et al.* Mammalian Rap1 controls telomere function and gene expression through binding to telomeric and extratelomeric sites. *Nat Cell Biol* **12**, 768–780 (2010).

175. Martínez, P. *et al.* RAP1 protects from obesity through its extratelomeric role regulating gene expression. *Cell Rep* **3**, 2059–2074 (2013).

176. Teo, H. *et al.* Telomere-independent Rap1 is an IKK adaptor and regulates NF-kappaB-dependent gene expression. *Nat Cell Biol* **12**, 758–767 (2010).

177. Yang, Y. *et al.* Repressor activator protein 1-promoted colorectal cell migration is associated with the regulation of Vimentin. *Tumour Biol* **39**, 1010428317695034 (2017).

178. Ye, J. Z.-S. *et al.* POT1-interacting protein PIP1: a telomere length regulator that recruits POT1 to the TIN2/TRF1 complex. *Genes Dev* **18**, 1649–1654 (2004).

179. Kibe, T., Osawa, G. A., Keegan, C. E. & de Lange, T. Telomere protection by TPP1 is mediated by POT1a and POT1b. *Mol Cell Biol* **30**, 1059–1066 (2010).

180. Zhong, F. L. *et al.* TPP1 OB-fold domain controls telomere maintenance by recruiting telomerase to chromosome ends. *Cell* **150**, 481–494 (2012).

181. Xin, H. *et al.* TPP1 is a homologue of ciliate TEBP-beta and interacts with POT1 to recruit telomerase. *Nature* **445**, 559–562 (2007).

182. Zhang, Y. *et al.* Phosphorylation of TPP1 regulates cell cycle-dependent telomerase recruitment. *Proc Natl Acad Sci U S A* **110**, 5457–5462 (2013).

183. Chen, C. *et al.* Structural insights into POT1-TPP1 interaction and POT1 C-terminal mutations in human cancer. *Nat Commun* **8**, 14929 (2017).

184. Else, T. *et al.* Tpp1/Acd maintains genomic stability through a complex role in telomere protection. *Chromosome Res* **15**, 1001–1013 (2007).

185. Martínez, P. *et al.* Increased telomere fragility and fusions resulting from TRF1 deficiency lead to degenerative pathologies and increased cancer in mice. *Genes Dev* **23**, 2060–2075 (2009).

186. Stout, G. J. & Blasco, M. A. Genetic dissection of the mechanisms underlying telomere-associated diseases: impact of the TRF2 telomeric protein on mouse epidermal stem cells. *Dis Model Mech* **2**, 139–156 (2009).

187. Denchi, E. L. & de Lange, T. Protection of telomeres through independent control of ATM and ATR by TRF2 and POT1. *Nature* **448**, 1068–1071 (2007).

188. Loayza, D. & De Lange, T. POT1 as a terminal transducer of TRF1 telomere length control. *Nature* **423**, 1013–1018 (2003).

189. Lee, J. Y., Okumus, B., Kim, D. S. & Ha, T. Extreme conformational diversity in human telomeric DNA. *Proc Natl Acad Sci U S A* **102**, 18938–18943 (2005).

190. Baumann, P. & Price, C. Pot1 and telomere maintenance. *FEBS Lett* **584**, 3779–3784 (2010).

191. Hockemeyer, D., Daniels, J.-P., Takai, H. & de Lange, T. Recent expansion of the telomeric complex in rodents: Two distinct POT1 proteins protect mouse telomeres. *Cell* **126**, 63–77 (2006).

192. Wu, L. *et al.* Pot1 deficiency initiates DNA damage checkpoint activation and aberrant homologous recombination at telomeres. *Cell* **126**, 49–62 (2006).

193. Nathan, V. *et al.* A rare missense variant in protection of telomeres 1 (POT1) predisposes to a range of haematological malignancies. *Br J Haematol* **192**, e57–e60 (2021).

194. Lee, O.-H. *et al.* Genome-wide YFP fluorescence complementation screen identifies new regulators for telomere signaling in human cells. *Mol Cell Proteomics* **10**, M110.001628 (2011).

195. Poonepalli, A. *et al.* Telomere-mediated genomic instability and the clinico-pathological parameters in breast cancer. *Genes Chromosomes Cancer* **47**, 1098–1109 (2008).

196. Kishi, S., Wulf, G., Nakamura, M. & Lu, K. P. Telomeric protein Pin2/TRF1 induces mitotic entry and apoptosis in cells with short telomeres and is down-regulated in human breast tumors. *Oncogene* **20**, 1497–1508 (2001).

197. Heng, J. *et al.* Integrated analysis of promoter methylation and expression of telomere related genes in breast cancer. *Oncotarget* **8**, 25442–25454 (2017).

198. Dinami, R. *et al.* miR-155 drives telomere fragility in human breast cancer by targeting TRF1. *Cancer Res* **74**, 4145–4156 (2014).

199. Gao, R., Singh, R., Kaul, Z., Kaul, S. C. & Wadhwa, R. Targeting of DNA Damage Signaling Pathway Induced Senescence and Reduced Migration of Cancer cells. *J Gerontol A Biol Sci Med Sci* **70**, 701–713 (2015).

200. Diehl, M. C. *et al.* Elevated TRF2 in advanced breast cancers with short telomeres. *Breast Cancer Res Treat* **127**, 623–630 (2011).

201. Zhang, Y. *et al.* Rap1-mediated nuclear factor-kappaB (NF-κB) activity regulates the paracrine capacity of mesenchymal stem cells in heart repair following infarction. *Cell Death Discov* **1**, 15007 (2015).

202. Lantuejoul, S. *et al.* Telomere maintenance and DNA damage responses during lung carcinogenesis. *Clin Cancer Res* **16**, 2979–2988 (2010).

203. El Maï, M. *et al.* The Telomeric Protein TRF2 Regulates Angiogenesis by Binding and Activating the PDGFRβ Promoter. *Cell Rep* **9**, 1047–1060 (2014).

204. Raynaud, C. M. *et al.* Telomere shortening is correlated with the DNA damage response and telomeric protein down-regulation in colorectal preneoplastic lesions. *Ann Oncol* **19**, 1875–1881 (2008).

205. Kojima, K. *et al.* Telomerase activation without shortening of telomeric 3'-overhang is a poor prognostic factor in human colorectal cancer. *Cancer Sci* **102**, 330–335 (2011).

206. Akincilar, S. C., Chan, C. H. T., Ng, Q. F., Fidan, K. & Tergaonkar, V. Non-canonical roles of canonical telomere binding proteins in cancers. *Cell. Mol. Life Sci.* **78**, 4235–4257 (2021).

207. Ding, Y. *et al.* Rap1 deficiency-provoked paracrine dysfunction impairs immunosuppressive potency of mesenchymal stem cells in allograft rejection of heart transplantation. *Cell Death Dis* **9**, 386 (2018).

208. Salhab, M., Jiang, W. G., Newbold, R. F. & Mokbel, K. The expression of gene transcripts of telomere-associated genes in human breast cancer: correlation with clinico-pathological parameters and clinical outcome. *Breast Cancer Res Treat* **109**, 35–46 (2008).

209. Garcia-Aranda, C. *et al.* Correlations of telomere length, telomerase activity, and telomeric-repeat binding factor 1 expression in colorectal carcinoma. *Cancer* **106**, 541–551 (2006).

210. Kim, S.-H. *et al.* Androgen receptor interacts with telomeric proteins in prostate cancer cells. *J Biol Chem* **285**, 10472–10476 (2010).

211. Matsutani, N. *et al.* Expression of telomeric repeat binding factor 1 and 2 and TRF1-interacting nuclear protein 2 in human gastric carcinomas. *Int J Oncol* **19**, 507–512 (2001).

212. Zhao, Y. *et al.* Pontin, a new mutant p53-binding protein, promotes gain-of-function of mutant p53. *Cell Death Differ* **22**, 1824–1836 (2015).

213. Ferrandon, S. *et al.* Telomere profiling: toward glioblastoma personalized medicine. *Mol Neurobiol* **47**, 64–76 (2013).

214. Fujii, K. *et al.* Protection of telomeres 1 protein levels are associated with telomere length in gastric cancer. *Int J Mol Med* **21**, 599–604 (2008).

215. Lee, J.-E., Oh, B.-K., Choi, J. & Park, Y. N. Telomeric 3' overhangs in chronic HBV-related hepatitis and hepatocellular carcinoma. *Int J Cancer* **123**, 264–272 (2008).

216. Igarashi, M. *et al.* Interferon can block telomere erosion and in rare cases result in hepatocellular carcinoma development with telomeric repeat binding factor 1 overexpression in chronic hepatitis C. *Clin Cancer Res* **9**, 5264–5270 (2003).

217. Yokota, T. *et al.* Telomere length variation and maintenance in hepatocarcinogenesis. *Cancer* **98**, 110–118 (2003).

218. Kim, H. *et al.* Telomere length, TERT and shelterin complex proteins in hepatocellular carcinomas expressing 'stemness'-related markers. *J Hepatol* **59**, 746–752 (2013).

219. Zhao, Y. *et al.* The transcription factor RFX5 is a transcriptional activator of the TPP1 gene in hepatocellular carcinoma. *Oncol Rep* **37**, 289–296 (2017).

220. La Torre, D. *et al.* Telomere length modulation in human astroglial brain tumors. *PLoS One* **8**, e64296 (2013).

221. Bai, Y. *et al.* Molecular targeting of TRF2 suppresses the growth and tumorigenesis of glioblastoma stem cells. *Glia* **62**, 1687–1698 (2014).

222. Ohyashiki, J. H. *et al.* Impaired telomere regulation mechanism by TRF1 (telomere-binding protein), but not TRF2 expression, in acute leukemia cells. *Int J Oncol* **18**, 593–598 (2001).

223. Poncet, D. *et al.* Changes in the expression of telomere maintenance genes suggest global telomere dysfunction in B-chronic lymphocytic leukemia. *Blood* **111**, 2388–2391 (2008).

224. Véronèse, L. *et al.* Telomeres and chromosomal instability in chronic lymphocytic leukemia. *Leukemia* **27**, 490–493 (2013).

225. Guièze, R. *et al.* Telomere status in chronic lymphocytic leukemia with TP53 disruption. *Oncotarget* **7**, 56976–56985 (2016).

226. Augereau, A. *et al.* Telomeric damage in early stage of chronic lymphocytic leukemia correlates with shelterin dysregulation. *Blood* **118**, 1316–1322 (2011).

227. Hoxha, M. *et al.* Relevance of telomere/telomerase system impairment in early stage chronic lymphocytic leukemia. *Genes Chromosomes Cancer* **53**, 612–621 (2014).

228. Campbell, L. J. *et al.* hTERT, the catalytic component of telomerase, is downregulated in the haematopoietic stem cells of patients with chronic myeloid leukaemia. *Leukemia* **20**, 671–679 (2006).

229. Nakanishi, K. *et al.* Expression of mRNAs for telomeric repeat binding factor (TRF)-1 and TRF2 in atypical adenomatous hyperplasia and adenocarcinoma of the lung. *Clin Cancer Res* **9**, 1105–1111 (2003).

230. Hu, J., Sun, L., Zhang, C. & Zhou, X. Expression of telomeric repeat binding factor 1 in non-small cell lung cancer. *J Surg Oncol* **93**, 62–67 (2006).

231. Lin, X., Gu, J., Lu, C., Spitz, M. R. & Wu, X. Expression of telomere-associated genes as prognostic markers for overall survival in patients with non-small cell lung cancer. *Clin Cancer Res* **12**, 5720–5725 (2006).

232. Frías, C. *et al.* Telomere shortening is associated with poor prognosis and telomerase activity correlates with DNA repair impairment in non-small cell lung cancer. *Lung Cancer* **60**, 416–425 (2008).

233. Yajima, T. *et al.* Telomerase reverse transcriptase and telomeric-repeat binding factor protein 1 as regulators of telomerase activity in pancreatic cancer cells. *Br J Cancer* **85**, 752–757 (2001).

234. Roy, S. *et al.* p38 MAPK pathway and its interaction with TRF2 in cisplatin induced chemotherapeutic response in head and neck cancer. *Oncogenesis* **7**, 53 (2018).

235. Knecht, H. & Mai, S. LMP1 and Dynamic Progressive Telomere Dysfunction: A Major Culprit in EBV-Associated Hodgkin's Lymphoma. *Viruses* **9**, 164 (2017).

236. Lajoie, V. *et al.* LMP1 mediates multinuclearity through downregulation of shelterin proteins and formation of telomeric aggregates. *Blood* **125**, 2101–2110 (2015).

237. Cantara, S. *et al.* Lack of mutations of the telomerase RNA component in familial papillary thyroid cancer with short telomeres. *Thyroid* **22**, 363–368 (2012).

238. Vega, F. *et al.* Splenic marginal zone lymphomas are characterized by loss of interstitial regions of chromosome 7q, 7q31.32 and 7q36.2 that include the protection of telomere 1 (POT1) and sonic hedgehog (SHH) genes. *Br J Haematol* **142**, 216–226 (2008).

239. Panero, J. *et al.* Altered mRNA expression of telomere-associated genes in monoclonal gammopathy of undetermined significance and multiple myeloma. *Mol Med* **16**, 471–478 (2010).

240. MARHUENDA, M. A. B. *et al.* Modulation of trf1 for brain cancer treatment. (2022).

241. Bejarano, L. *et al.* Multiple cancer pathways regulate telomere protection. *EMBO Molecular Medicine* **11**, e10292 (2019).

242. Du, G.-J. *et al.* Epigallocatechin Gallate (EGCG) Is the Most Effective Cancer Chemopreventive Polyphenol in Green Tea. *Nutrients* **4**, 1679–1691 (2012).

243. Chen, B.-H., Hsieh, C.-H., Tsai, S.-Y., Wang, C.-Y. & Wang, C.-C. Anticancer effects of epigallocatechin-3-gallate nanoemulsion on lung cancer cells through the activation of AMP-activated protein kinase signaling pathway. *Sci Rep* **10**, 5163 (2020).

244. Rady, I., Mohamed, H., Rady, M., Siddiqui, I. A. & Mukhtar, H. Cancer preventive and therapeutic effects of EGCG, the major polyphenol in green tea. *Egyptian Journal of Basic and Applied Sciences* **5**, 1–23 (2018).

245. Udroiu, I., Marinaccio, J. & Sgura, A. Epigallocatechin-3-gallate induces telomere shortening and clastogenic damage in glioblastoma cells. *Environmental and Molecular Mutagenesis* **60**, 683–692 (2019).

246. Tan, A. R. & Swain, S. M. Review of flavopiridol, a cyclin-dependent kinase inhibitor, as breast cancer therapy. *Semin Oncol* **29**, 77–85 (2002).

247. Bhari, V. K., Kumar, D., Kumar, S. & Mishra, R. Shelterin complex gene: Prognosis and therapeutic vulnerability in cancer. *Biochem Biophys Rep* **26**, 100937 (2021).

248. Seimiya, H. Crossroads of telomere biology and anticancer drug discovery. *Cancer Science* **111**, 3089–3099 (2020).

249. Fragkiadaki, P. *et al.* Telomerase inhibitors and activators in aging and cancer: A systematic review. *Molecular Medicine Reports* **25**, 1–11 (2022).

250. Mender, I., Gryaznov, S., Dikmen, Z. G., Wright, W. E. & Shay, J. W. Induction of Telomere Dysfunction Mediated By the Telomerase Substrate Precursor 6-Thio-2'-Deoxyguanosine. *Cancer discovery* **5**, 82 (2015).

251. El Maï, M. *et al.* A Novel Screen for Expression Regulators of the Telomeric Protein TRF2 Identified Small Molecules That Impair TRF2 Dependent Immunosuppression and Tumor Growth. *Cancers (Basel)* **13**, 2998 (2021).

252. Rassart, E., Desmarais, F., Najyb, O., Bergeron, K.-F. & Mounier, C. Apolipoprotein D. *Gene* **756**, 144874 (2020).

253. Di Maro, S. *et al.* Shading the TRF2 recruiting function: a new horizon in drug development. *J Am Chem Soc* **136**, 16708–16711 (2014).

254. Cheng, Y. *et al.* Arsenic trioxide inhibits glioma cell growth through induction of telomerase displacement and telomere dysfunction. *Oncotarget* **7**, 12682–12692 (2016).

255. Rizzo, A. *et al.* SIRT6 interacts with TRF2 and promotes its degradation in response to DNA damage. *Nucleic Acids Res* **45**, 1820–1834 (2017).

256. Wang, M. *et al.* Curcusone C induces telomeric DNA-damage response in cancer cells through inhibition of telomeric repeat factor 2. *Biochim Biophys Acta Proteins Proteom* **1865**, 1372–1382 (2017).

257. Gurung, R. L., Lim, S. N., Low, G. K. M. & Hande, M. P. MST-312 Alters Telomere Dynamics, Gene Expression Profiles and Growth in Human Breast Cancer Cells. *J Nutrigenet Nutrigenomics* **7**, 283–298 (2014).

258. Zahler, A. M., Williamson, J. R., Cech, T. R. & Prescott, D. M. Inhibition of telomerase by G-quartet DNA structures. *Nature* **350**, 718–720 (1991).

259. Salvati, E. *et al.* Telomere damage induced by the G-quadruplex ligand RHPS4 has an antitumor effect. *J Clin Invest* **117**, 3236–3247 (2007).

260. Biroccio, A. *et al.* TRF2 inhibition triggers apoptosis and reduces tumourigenicity of human melanoma cells. *Eur J Cancer* **42**, 1881–1888 (2006).

261. Wang, J. *et al.* Sirtinol, a class III HDAC inhibitor, induces apoptotic and autophagic cell death in MCF-7 human breast cancer cells. *Int J Oncol* **41**, 1101–1109 (2012).

262. Altschuler, S. E., Croy, J. E. & Wuttke, D. S. A small molecule inhibitor of Pot1 binding to telomeric DNA. *Biochemistry* **51**, 7833–7845 (2012).

263. Amir, M. *et al.* Virtual high-throughput screening of natural compounds in-search of potential inhibitors for protection of telomeres 1 (POT1). *J Biomol Struct Dyn* **38**, 4625–4634 (2020).

264. Dratwa, M. *et al.* Relationship between Telomere Length, TERT Genetic Variability and TERT, TP53, SP1, MYC Gene Co-Expression in the Clinicopathological Profile of Breast Cancer. *Int J Mol Sci* **23**, 5164 (2022).

265. Franken, N. A. P., Rodermond, H. M., Stap, J., Haveman, J. & van Bree, C. Clonogenic assay of cells in vitro. *Nat Protoc* **1**, 2315–2319 (2006).

266. Puck, T. T., Marcus, P. I. & Cieciura, S. J. CLONAL GROWTH OF MAMMALIAN CELLS IN VITRO : GROWTH CHARACTERISTICS OF COLONIES FROM SINGLE HELA CELLS WITH AND WITHOUT A 'FEEDER' LAYER. *Journal of Experimental Medicine* **103**, 273–284 (1956).

267. Zimmermann, M. & Meyer, N. Annexin V/7-AAD staining in keratinocytes. *Methods in molecular biology (Clifton, N.J.)* **740**, 57–63 (2011).

268. Lee, S. & Lee, J. S. Cellular senescence: a promising strategy for cancer therapy. *BMB reports* **52**, 35–41 (2019).

269. Campisi, J., Andersen, J. K., Kapahi, P. & Melov, S. Cellular senescence: A link between cancer and age-related degenerative disease? *Seminars in Cancer Biology* **21**, 354–359 (2011).

270. Dimri, G. P. *et al.* A biomarker that identifies senescent human cells in culture and in aging skin in vivo. *Proceedings of the National Academy of Sciences* **92**, 9363–9367 (1995).

271. Debacq-Chainiaux, F., Erusalimsky, J. D., Campisi, J. & Toussaint, O. Protocols to detect senescence-associated beta-galactosidase (SA-betagal) activity, a biomarker of senescent cells in culture and in vivo. *Nature protocols* **4**, 1798–1806 (2009).

272. de Mera-Rodríguez, J. A. *et al.* Is Senescence-Associated β-Galactosidase a Reliable in vivo Marker of Cellular Senescence During Embryonic Development? *Frontiers in Cell and Developmental Biology* **9**, 36 (2021).

273. Thomé, M. P. *et al.* Ratiometric analysis of Acridine Orange staining in the study of acidic organelles and autophagy. *Journal of Cell Science* **129**, 4622–4632 (2016).

274. Mallela, S. K. *et al.* Detection and Quantification of Lipid Droplets in Differentiated Human Podocytes. *Methods in molecular biology (Clifton, N.J.)* **1996**, 199 (2019).

275. Stenvall, A., Larsson, E., Holmqvist, B., Strand, S. E. & Jönsson, B. A. Quantitative γ-H2AX immunofluorescence method for DNA double-strand break analysis in testis and liver after intravenous administration of 111InCl3. *EJNMMI Research* **10**, 1–12 (2020).

276. Hamer, G. *et al.* DNA double-strand breaks and gamma-H2AX signaling in the testis. *Biology of reproduction* **68**, 628–634 (2003).

277. Vasireddy, R. S. *et al.* Evaluation of the Spatial Distribution of γH2AX following Ionizing Radiation. *JoVE (Journal of Visualized Experiments)* e2203 (2010) doi:10.3791/2203.

278. Relative Human Telomere Length Quantification qPCR Assay Kit (RHTLQ).

279. Hu, L. *et al.* Fluorescence in situ hybridization (FISH): an increasingly demanded tool for biomarker research and personalized medicine. *Biomarker Research* **2**, 3 (2014).

280. Sorvina, A. *et al.* Mitochondrial imaging in live or fixed tissues using a luminescent iridium complex. *Scientific Reports 2018 8:1* **8**, 1–8 (2018).

281. Kumari, S., Badana, A. K., Murali Mohan, G., Shailender, G. & Malla, R. R. Reactive Oxygen Species: A Key Constituent in Cancer Survival. *Biomarker insights* **13**, (2018).

282. Galadari, S., Rahman, A., Pallichankandy, S. & Thayyullathil, F. Reactive oxygen species and cancer paradox: To promote or to suppress? *Free radical biology & medicine* **104**, 144–164 (2017).

283. Snezhkina, A. V. *et al.* ROS Generation and Antioxidant Defense Systems in Normal and Malignant Cells. *Oxidative Medicine and Cellular Longevity* **2019**, (2019).

284. Phalloidin staining protocol | Abcam. https://www.abcam.com/protocols/phalloidin-staining-protocol.

285. Sato, A., Hiramoto, A., Kim, H.-S. & Wataya, Y. Anticancer Strategy Targeting Cell Death Regulators: Switching the Mechanism of Anticancer Floxuridine-Induced Cell Death from Necrosis to Apoptosis. *International Journal of Molecular Sciences* **21**, 5876 (2020).

286. Mallela, S. K. *et al.* Detection and Quantification of Lipid Droplets in Differentiated Human Podocytes. *Methods Mol Biol* **1996**, 199–206 (2019).

287. Welte, M. A. Expanding roles for lipid droplets. *Curr Biol* **25**, R470-481 (2015).

288. Sławińska, N. & Krupa, R. Molecular Aspects of Senescence and Organismal Ageing—DNA Damage Response, Telomeres, Inflammation and Chromatin. *Int J Mol Sci* **22**, 590 (2021).

289. Sarandi, E. *et al.* Telomeres and Telomerase. in *Reference Module in Biomedical Sciences* (Elsevier, 2022). doi:10.1016/B978-0-12-824315-2.00091-9.

290. Lin, J. & Epel, E. Stress and telomere shortening: Insights from cellular mechanisms. *Ageing Res Rev* **73**, 101507 (2022).

291. Weinberg, F. *et al.* Mitochondrial metabolism and ROS generation are essential for Kras-mediated tumorigenicity. *Proc Natl Acad Sci U S A* **107**, 8788–8793 (2010).

292. Liu, Y. & Shi, Y. Mitochondria as a target in cancer treatment. *MedComm (2020)* **1**, 129–139 (2020).

293. Chen, L.-Y. *et al.* Mitochondrial Localization of Telomeric Protein TIN2 Links Telomere Regulation to Metabolic Control. *Molecular cell* **47**, 839 (2012).

294. Testa, U., Castelli, G. & Pelosi, E. Breast Cancer: A Molecularly Heterogenous Disease Needing Subtype-Specific Treatments. *Medical Sciences* **8**, (2020).

295. Ozanne, E. M. *et al.* Locoregional Treatment of Breast Cancer in Women With and Without Preoperative MRI. *Am J Surg* **213**, 132-139.e2 (2017).

296. Teven, C. M., Schmid, D. B., Sisco, M., Ward, J. & Howard, M. A. Systemic Therapy for Early-Stage Breast Cancer: What the Plastic Surgeon Should Know. *Eplasty* **17**, e7 (2017).

297. Khodadadi, E. *et al.* Shelterin complex at telomeres: Roles in cancers. *Gene Reports* **23**, 101174 (2021).

298. Robinson, N. J., Taylor, D. J. & Schiemann, W. P. Stem cells, immortality, and the evolution of metastatic properties in breast cancer: telomere maintenance mechanisms and metastatic evolution. *Journal of Cancer Metastasis and Treatment* **5**, 39 (2019).

299. Schmidt, J. C. & Cech, T. R. Human telomerase: biogenesis, trafficking, recruitment, and activation. *Genes Dev* **29**, 1095–1105 (2015).

300. Cho, N. W., Dilley, R. L., Lampson, M. A. & Greenberg, R. A. Interchromosomal homology searches drive directional ALT telomere movement and synapsis. *Cell* **159**, 108–121 (2014).

301. Heaphy, C. M. *et al.* Altered telomeres in tumors with ATRX and DAXX mutations. *Science* **333**, 425 (2011).

302. Cesare, A. J. *et al.* Spontaneous occurrence of telomeric DNA damage response in the absence of chromosome fusions. *Nat Struct Mol Biol* **16**, 1244–1251 (2009).

303. Lovejoy, C. A. *et al.* Loss of ATRX, genome instability, and an altered DNA damage response are hallmarks of the alternative lengthening of telomeres pathway. *PLoS Genet* **8**, e1002772 (2012).

304. Subhawong, A. P. *et al.* The alternative lengthening of telomeres phenotype in breast carcinoma is associated with HER-2 overexpression. *Mod Pathol* **22**, 1423–1431 (2009).

305. Kumari, R. & Jat, P. Mechanisms of Cellular Senescence: Cell Cycle Arrest and Senescence Associated Secretory Phenotype. *Front Cell Dev Biol* **9**, 645593 (2021).

306. Liu, Y., Bloom, S. I. & Donato, A. J. The role of senescence, telomere dysfunction and shelterin in vascular aging. *Microcirculation* **26**, e12487 (2019).

307. Fyhrquist, F., Saijonmaa, O. & Strandberg, T. The roles of senescence and telomere shortening in cardiovascular disease. *Nat Rev Cardiol* **10**, 274–283 (2013).

308. Srinivas, N., Rachakonda, S. & Kumar, R. Telomeres and Telomere Length: A General Overview. *Cancers (Basel)* **12**, 558 (2020).

309. Pan, H. *et al.* Structure, dynamics, and regulation of TRF1-TIN2-mediated trans- and cis-interactions on telomeric DNA. *J Biol Chem* **297**, 101080 (2021).

310. Ghosh, P., Vidal, C., Dey, S. & Zhang, L. Mitochondria Targeting as an Effective Strategy for Cancer Therapy. *Int J Mol Sci* **21**, 3363 (2020).

311. Tannock, I. F. & Gordon Steel, G. Cell proliferation, drug distribution and therapeutic effects in relation to the vascular system of solid tumours. *Br J Cancer* **128**, 413–418 (2023).

312. Dubey, R. *et al.* Lipid droplets can promote drug accumulation and activation. *Nat Chem Biol* **16**, 206–213 (2020).

313. Greenwood, D. J. *et al.* Subcellular antibiotic visualization reveals a dynamic drug reservoir in infected macrophages. *Science* **364**, 1279–1282 (2019).

314. Hager, M. H., Solomon, K. R. & Freeman, M. R. The role of cholesterol in prostate cancer. *Curr Opin Clin Nutr Metab Care* **9**, 379–385 (2006).

315. Aboumrad, M. H., Horn, R. C. & Fine, G. Lipid-secreting mammary carcinoma. Report of a case associated with Paget's disease of the nipple. *Cancer* **16**, 521–525 (1963).

316. Sundelin, J. P. *et al.* Increased expression of the very low-density lipoprotein receptor mediates lipid accumulation in clear-cell renal cell carcinoma. *PLoS One* **7**, e48694 (2012).

317. Ramos, C. V. & Taylor, H. B. Lipid-rich carcinoma of the breast. A clinicopathologic analysis of 13 examples. *Cancer* **33**, 812–819 (1974).

318. Burguin, A., Diorio, C. & Durocher, F. Breast Cancer Treatments: Updates and New Challenges. *Journal of Personalized Medicine* **11**, 808 (2021).

319. Xiao, N. *et al.* Interaction of Berberine derivative with protein POT1 affect telomere function in cancer cells. *Biochem Biophys Res Commun* **419**, 567–572 (2012).

320. Su, C.-H. *et al.* Gemcitabine causes telomere attrition by stabilizing TRF2. *European Journal of Cancer* **48**, 3465–3474 (2012).